

UNIVERSITE JOSEPH FOURIER – GRENOBLE I

Discipline : Sciences de la Planète

Mémoire pour l'obtention du diplôme

HABILITATION A DIRIGER DES RECHERCHES

**Contribution à l'étude de la variabilité pluviométrique en
Afrique de l'Ouest : interactions ondes-convection-pluie**

Arona DIEDHIOU

Soutenance souhaitée entre le 23 Novembre et le 4 Décembre 2009

Merci de donner vos disponibilités sur ce lien :

<http://www.doodle.com/tqhrygewnxuqek2z>

Rapports à rendre SVP au plus tard le 16 octobre 2009

Proposition de Jury

Michel Fily	Professeur à l'Université Joseph Fourier	Examinateur
Bernard Fontaine	Directeur de Recherche au CNRS/CRC	Rapporteur externe
Jean François Royer	Ingénieur de la Météorologie (Meteo-France)	Rapporteur externe
Jacques Verron	Directeur de Recherche au CNRS/LEGI	Rapporteur interne
Thierry Lebel	Directeur de Recherche à l'IRD/LTHE	Examinateur
Jean Luc Redelsperger	Directeur de Recherche au CNRS/CNRM	Examinateur

Table des matières

1) Curriculum vitae.....	4
2) Productions scientifiques	6
a. Liste des publications dans des revues de rang A.....	6
b. Principales publications dans revues de rang B.....	7
c. Contributions à la rédaction des documents suivants :	7
d. Liste des principales communications (congrès, colloques) avec publication des actes.....	8
e. Liste des séminaires scientifiques, réunions d'information et communication	10
3) Présentation des travaux de recherche antérieurs.....	12
3.1 Activités de recherche	12
a. Intérêt scientifique et cadre général	12
b. Perturbations synoptiques, systèmes convectifs et précipitations en Afrique de l'Ouest	19
c. Ondes d'est africaines et activité cyclonique sur l'Atlantique	25
d. Quelques références bibliographiques sur le sujet :	36
3.2) Implication dans les programmes nationaux et internationaux	39
a. Implication au Programme National d'Etude de la Dynamique du Climat (PNEDC)	39
b. Implication au Programme National Atmosphère et Océan Multi-échelles (PATOM).....	39
c. Depuis 2003 : Coordination du programme international AMMA	39
d. Coordination de l'initiative africaine dans le Programme AMMA	40
e. Implication dans les programmes internationaux de l'OMM en Afrique	40
f. Coordination du FSP RIPLECSA sur les interactions climat-écosystèmes – sociétés.....	40
3.3) Participation à la formation.....	41
a. Contribution encadrement et formation doctorale	41
b. Contribution encadrement et formation niveau Maîtrise, DEA, Master	41
c. Activités d'enseignement	42
3.4) Collaborations scientifiques avec l'Afrique et l'Amérique Latine	43
a. Organisation de manifestations (colloques, séminaires, ateliers)	43
b. Codirections de thèse	43
c. Encadrement d'étudiants et d'élèves ingénieurs	43
d. Collaborations avec les institutions du Sud	44
4) Implication dans le Programme International AMMA	46
a) Bilan du réseau AMMANET et de l'initiative africaine dans le programme AMMA.....	46
b) Le Centre principal des Opérations AMMA au Niger (AOC-AMMA).....	48
5) Perspectives de recherche.....	54
5.1) Thèmes de recherches en cours et à initier pour le prochain quadriennal	54
a) Système de mousson et interactions ondes-convection – pluie	54
b) Influence des facteurs de l'atmosphère et des surfaces continentales.....	55
c) Régionalisation du changement climatique en Afrique de l'Ouest	57
d) Variabilité multi-échelles de la convection sur l'Amérique Latine	58
5.2 Implication au LTHE et stratégie de mise en œuvre	59
6) Sélection d'articles	61

1) Curriculum vitae

Arona DIEDHIOU

LTHE/ENSHMG (UR 012 ; UMR 5564)
BP : 53, 38041 Grenoble Cedex 9
Tél : + 33 4 76 82 50 57
Fax : + 33 4 76 82 50 04

Né le 31 Décembre 1969

Marié 3 enfants

Nationalité : Sénégalaise

Email: arona.diedhiou@inpg.fr

Fonction

Chargé de Recherches de l'IRD (Institut de Recherche pour le Développement)

Unité de Recherche : Laboratoire des Transferts en Hydrologie et Environnement (LTHE ; Grenoble)

Unité Mixte de Recherche CNRS, INPG, IRD, Université de Grenoble

Grade : CR2 depuis mars 1999 ; CR1 depuis Mars 2003

Résumé des compétences : Climatologue et Physicien de l'atmosphère

> Depuis 2007 : Laboratoire des Transferts en Hydrologie et Environnement ; LTHE (Grenoble)

Expertise : Détermination de la variabilité et du changement climatique et pluviométrique, de la grande échelle à la mésoéchelle, à partir de réanalyses américaines et européennes, de données observées et de sorties de modèles de circulation générale et régionale.

Chef de Projet FSP RIPIECSA : Le Ministère français des Affaires Etrangères a délégué à l'IRD dans sa fonction d'Agence Inter-organismes de Recherche pour le Développement (AIRD), la mise en œuvre du FSP RIPIECSA (Recherche Interdisciplinaire et Participative sur les Interactions entre les Ecosystèmes, le Climat et les Sociétés d'Afrique de l'Ouest), projet de 3,5 millions d'Euros pour une durée de 4 ans (2007 - 2010). RIPIECSA soutient 25 projets en Afrique de l'Ouest sur les interactions sociétés-écosystèmes-climat.

> 2003-2007 : En poste à la Représentation IRD au Niger.

- Coordination et mise en œuvre du programme international AMMA (Analyse Multidisciplinaire de la Mousson Africaine et ses impacts) comme Responsable du Centre des Opérations.
- Coordination de l'initiative africaine dans le programme AMMA, création d'un réseau (AMMANET) et contribution à l'élaboration d'un plan scientifique AMMA-Afrique.

> 1999-2003 : Chercheur au Laboratoire des Transferts en Hydrologie et Environnement.

- Etude des perturbations atmosphériques et de leurs interactions avec les systèmes nuageux et la pluie en Afrique de l'Ouest et sur l'Atlantique tropical.
- Dynamique des systèmes nuageux sur l'Amérique Latine (programme CAPES-COFECUB) : séjours au Brésil (CTA/Sao José Dos Campos ; FUNCEME/Fortaleza).

> 1999 : Recrutement comme chercheur à l'IRD et affectation au LTHE (Grenoble)

> 1996-1998: Thèse de doctorat d'Université (Université Paris XII)

> 1994-1995: Centre National de Recherche Météorologique (METEO-France ; Toulouse)

Stage de fin d'études de Mastère puis Contrat CDC (Equipe Unité Dynamique du Climat /UDC) : Etude de validation et de sensibilité du modèle ARPEGE sur l'Afrique aux variations des conditions de surfaces continentales (impact d'une déforestation au Sahel et rôle des océans).

Formation

1995-1998: Thèse de doctorat d'Université (Université Paris XII) effectuée au Laboratoire de Météorologie Dynamique du CNRS, Ecole Polytechnique, Palaiseau, France. Sujet : Etude des régimes d'ondes d'Est et de leurs interactions avec la convection en Afrique de l'Ouest et sur l'Atlantique tropical.

1992-1994: Mastère Spécialisé de Météorologie Tropicale, Ecole Nationale de la Météorologie (17 mois, Toulouse; FRANCE) Mémoire : Etude numérique de l'influence des conditions de surface sur le cycle hydrologique en Afrique de l'Ouest (effectué au CNRM/Météo-France).

1991-1992 : Diplôme d'Etudes Approfondies en Astrophysique, Géophysique et Techniques Spatiales (Option: Dynamique de la biosphère continentale). Université Paul Sabatier (Toulouse III ; FRANCE). Mémoire : Evaluation des données NOAA/AVHRR pour le suivi du fonctionnement de la végétation au Sahel.

1990-1991: Maîtrise de Physique Appliquée. Options : Physico-chimie de l'océan et de l'atmosphère, Micro-ondes et Optoélectronique. Université Paris VI, (FRANCE). Mémoire : Interpolation spatiale à partir d'un semis irrégulier de points: Application à la variabilité pluviométrique au Sahel.

1987-1990: DEUG A puis Licence de Physique. Université Paris VI (FRANCE)

1987 : Baccalauréat Série C ; Cours Secondaires Sacré Coeur ; Dakar, (SENEGAL)

Responsabilités scientifiques

Encadrement, Enseignement et Formation (voir pages suivantes pour plus d'informations)

- Co-directeur de deux thèses INPG (Institut National Polytechnique de Grenoble) soutenues en 2006 sur les cyclones tropicaux (Mr Christophe LAVAYSSE) et sur la mousson africaine (Mr Moctar CAMARA).
- Une Codirection de thèse en cours (2008-2010) sur la représentation du cycle de vie des systèmes convectifs dans les modèles (Mr Youssouph SANE).
- Seize (16) encadrements d'étudiants et d'élèves ingénieurs en France et au Niger depuis 1999.

Responsabilité au sein du programme international AMMA

- Membre du Bureau Exécutif AMMA-International (composé de 5 personnes)
- Membre du Comité Scientifique AMMA-International et du Comité AMMA-France
- Responsable du Centre Opérationnel Principal AMMA (AOC-AMMA) au Niger
- Leader du Deliverable 7.1c/AMMA-Europe (Thematic Priority : Global change and Ecosystems)

Animation de réseaux scientifiques

- Co-président du Comité AMMA-Afrique sur la mousson africaine et ses impacts jusqu'en 2009
- Coordinateur du Plan Scientifique AMMA-Afrique (PIAF) jusqu'en 2009
- Membre du Bureau Exécutif AMMA-Afrique

Publications, prix et distinctions

Publications, conférences et communications (voir liste jointe)

- 21 publications de rangs A et 12 de rang B (voir liste jointe).
- Plusieurs articles et conférences sur la mousson africaine et ses impacts pour le « grand public » en Afrique et en Europe (voir liste des publications jointe).

Prix et distinctions :

- Diedhiou A., J. Ronchail , N. Dessay., L.A.T. Machado, H. Laurent., J-F. Royer, 2002. Climate Change over South America in relation with the Increase of Global Greenhouse Gases: a numerical study. XII Congresso Brasileiro de Meteorologia., Iguassu Falls, Brasil. (Awarded: Prix du meilleur travail présenté oralement dans la session "Variabilité et changement climatique").

2) Productions scientifiques

a. Liste des publications dans des revues de rang A

1. **Diedhiou** A. and J. F. Mahfouf, **1996**. Comparative influence of Land and Sea surfaces on the Sahelian drought: a numerical study. *Annales Geophysicae*, 14 : 115-130.
2. **Diedhiou** A., S. Janicot, A. Viltard, P. de Felice, H. Laurent, **1998a** : Evidence of two regimes of easterly waves over West Africa and the tropical Atlantic. *Geophys. Res. Lett.*, 25 : 2805-2808.
3. **Diedhiou**, A., S. Janicot, A. Viltard, P. de Félice, and H. Laurent, **1998b**: A fast eastern waves in West Africa troposphere. *Meteor. And Atmos. Physics*, 69, 39-47.
4. **Diedhiou** A., S. Janicot, A. Viltard, P. De Felice, H. Laurent, **1999**. Easterly waves regimes and associated convection over West Africa and the tropical Atlantic : results from the NCEP/NCAR and ECMWF reanalyses. *Climate. Dynamics*, 15, 795-822.
5. **Diedhiou**, A., S. Janicot, A. Viltard, P. de Félice, **2001**: Composite patterns of easterly waves disturbances over West Africa and the tropical Atlantic. *Climate. Dynamic*, 18, 241-253.
6. **Diedhiou**, A., S. Janicot, A. Viltard and P. de Félice, **2002a**: Energetics of easterly waves disturbances over West Africa and the tropical Atlantic. *Climate Dynamic*, 18, 487-500.
7. Redelsperger J.L., Diongue A., **Diedhiou** A., Ceron J.P., Diop M., Gueremy J.F., Lafore J.P., **2002b**: Multiscale description of a Sahelian synoptic weather system representative of West African monsoon. *Quart. Journ. Roy. Meteor. Soc.*, 128 : 122S-1257.
8. Mathon V., A. **Diedhiou**, H. Laurent, **2002c**: Relationship between easterly waves and mesoscale convective systems over the Sahel. *Geophys. Res. Lett.*, vol. 29 (8) : 57/1-4.
9. Jenkins G. S., Kamga A., Garba A., **Diedhiou** A., Morris V., Joseph E., **2002d**: Investigating the West African Climate System using Global/Regional Climate models. *Bull. of Americ. Met. Soc.*, 83/4, 583-595.
10. Jenkins G. S., A. Kamga, G. Adamou, A. **Diedhiou**, V Morris, E. Joseph, **2002e**: Summary of the Workshop on Modeling the West African Climate System with Global and Regional Scale Climate Models: Relevance to Understanding Climate Variability, Land-Use, and Climate Change, *Bull. of Americ. Met. Soc.*, 583-595.
11. Sultan B., S. Janicot, et al. **Diedhiou**, **2003a**. The West African monsoon dynamics, Part I : Intraseasonal variability. *Journal of Climate*, 16, 3389-3406
12. Lebel, T.; **Diedhiou**, A.; Laurent, H. **2003b**: Seasonal cycle and interannual variability of the Sahelian rainfall at hydrological scales. *Journal of Geophysical Research*. Vol. 108; D8. 8389.
13. Dessay, N.; Laurent, H.; Machado, L. A. T.; Shimabukuro, Y. E; **Diedhiou**, A.; Ronchail, J. **2004** : Comparative study of 1982-1983 and 1997-1998 El Niño events over different types of vegetation in South America. *International Journal of Remote Sensing*. Vol., 25; 4063-4077.
14. Ali A., A. Amani, A. **Diedhiou**, T. Lebel, **2005**. Rainfall estimation in the Sahel. Part 2: Evaluation of Raingauge Networks in the CILSS Countries and Objective Intercomparison of Rainfall Products. *J. of Applied Meteor.*, 44(11) pp. 1707-1722.
15. Lavaysse C, A. **Diedhiou**, Laurent H, Lebel T, **2006** African Easterly Waves and convective activity in wet and dry sequences of the West African Monsoon. *Climate Dynamics* 27(2-3): 319.
16. Redelsperger, J.L., Thorncroft, C., **Diedhiou** A., Lebel, T., Parker, D.J. and J. Polcher, **2006**: African Monsoon Multidisciplinary Analysis (AMMA): An International Research Project and Field Campaign. Published in *BAMS*, Volume 87, Issue 12 (December 2006), pp. 1739–1746.
17. Bedou M., Konare A., Sanda I-S., Assamoi S. and **Diedhiou** A., **2007**: Hygroscopic properties of aerosols in the Sahel: preliminary results. *Scientific Research and Essays*, Vol. 2 (6), pp. 177-183.
18. Parker D., Fink A., Janicot S., Ngamini J.-B., Douglas M., Afiesimama E., Agusti-Panareda A., Beljaars A., Dide F., **Diedhiou** A., Lebel T., Polcher J., Redelsperger J.-L., Thorncroft C. and Wilson G., **2008**. The AMMA radiosonde program and its implications for the future of atmospheric monitoring over Africa. *Bulletin of the American Meteorological Society*, 89 : 1015-1027.
19. Lebel T., Parker D.J., Flamant C., Bourles B., Marticorena M., Mougin E., Peugeot C., **Diedhiou** A., Haywood J.M., Ngamini J.B., Polcher J., Redelsperger J.-L. and Thorncroft C.D., **2009**. The AMMA field campaigns : Multiscale and multidisciplinary observations in the West African region. *QJRMS*, Accepted.
20. Descroix, L., Mahé, G., Favreau, G., Galle, S., Gautier, E., Olivry, J.-C., Albergel, J., Amogu, O., Cappelaere, B. et al.(**Diedhiou** A.), **2009**. Spatio-Temporal Variability of Hydrological Regimes Around the Boundaries between Sahelian and Sudanian Areas of West Africa: A Synthesis. *Journal of Hydrology*, doi: 10.1016/j.jhydrol.2008.12.012, in press.
21. **Diedhiou** A., L. A. Machado, H. Laurent, **2009**. Mean Kinematic of Synoptic Easterly Disturbances over the Atlantic. *Advances on Atmospheric Research*. do 10.1007/s00376-009-9092-5; in press.

b. Principales publications dans revues de rang B

1. Bigot S., Brou Yao T., **Diedhiou A.**, Laganier R., **1999**. Détection des feux de végétation en Côte d'Ivoire à partir des données AVHRR et ATSR : relations avec le NDVI et les précipitations. *Publications de l'Association Internationale de Climatologie*, n°12, p.209-218,
2. **Diedhiou A.**, H. Laurent, T. Lebel, and A. Amani, **2003**. Multiscale View of the Sahelian Rainfall Regimes. *CLIVAR Exchanges*. No. 27. 24-26.
3. Thierry L., L. Le Barbe, A. **Diedhiou** and A. Amani, **2003**. A revised scheme of the West African Monsoon Seasonal Cycle. *CLIVAR Exchanges*. Online version. No. 27.
4. **Diedhiou A.**, Abdallah Nassor, Abou Amani, Lekan Oyebande, Amadou Gaye Adamou Garba, Delphin Ochou **2003**: AMMANET: Building the African Participation to AMMA. *CLIVAR Exchanges*. No. 27.Vol8 N° 2/3 Page 55.
5. Ward N., Cook K., **Diedhiou A.**, Fontaine B., Giannini A., Kamga A., Lamb P.J., Ben M. A., Nassor A. and Thorncroft C., **2004** : «Seasonal-to-Decadal Predictability and Prediction of West African Climate» , *CLIVAR Exchanges*, 9, 3, 14-20.
6. Bigot S.; Brou, T.Y.; Oszwald, Y.; **Diedhiou A.**, **2005** : Facteurs de la variabilité pluviométrique en Côte d'Ivoire et relations avec certaines modifications environnementales. *Sécheresse* ; 16(1) ; 5-13.
7. Bigot S., I. Zin and **Diedhiou A.**, **2005** : Apport de données de HRV de Spot pour l'étude des variations phénologiques dans le bassin de l'Ouémé (Bénin) ; *Télédétection*, Vol. : 4, No. : 4 ; Page(s) 339-353
8. Redelsperger J.L., A. **Diedhiou**, C. Flamant, S. Janicot, et al. **2006** :AMMA, une étude multidisciplinaire de la mousson ouest-africaine, *La Météorologie*, No 54, pp. 22-32.
9. Gaye, A. T., and A. **Diedhiou**; **2006** : African contribution to AMMA. GEWEX News 16(1): 6-7.
10. Redelsperger J.-L., C. Thorncroft, A. **Diedhiou**, T. Lebel, D. Parker, and J. Polcher; **2006**: AMMA and its first international conference address the West African monsoon. GEWEX news 16(1): 5-6.
11. Lebel, T. D. J. Parker, B. Bourles, A. **Diedhiou**, A. Gaye, J. Polcher, J.-L. Redelsperger, C. D. Thorncroft, **2007**: The AMMA field campaigns in 2005 and 2006. GEWEX News.
12. Janicot, S., F. Mounier and A. **Diedhiou** **2008** : Les ondes atmosphériques d'échelle synoptique dans la mousson d'Afrique de l'Ouest et Centrale : ondes d'Est et ondes de Kelvin. *Sécheresse* ; 19 (1), p. 13-22.

c. Contributions à la rédaction des documents suivants :

1. **Système Mondial d'Observation du Climat : Un Plan d'Action pour l'Afrique Occidentale et Centrale.** OMM/SMOC; WMO/GCOS report. May 2004.
2. **African Climate Report (consulté et remercié dans le texte):** A report commissioned by the UK Government to review African climate science, policy and options for action. ; Contact: Dougie Brew, DFID; Richard Washington, University of Oxford. December 2004.
3. **Programme international AMMA sur la mousson Africaine (2004):** Contribution au Plan d'Implémentation AMMA-France, au Plan Scientifique International AMMA-International et au Plan d'Implémentation AMMA-Afrique (PIAF).
4. **RADAGAST (Radiative Atmospheric Divergence using Arm mobile facility, GERB data and AMMA Stations).** A proposal to the ARM Climate Research Facility (ACRF) by Anthony Slingo, Environmental Systems Science Centre, University of Reading, UK. Subrnitted June 2004 to the US Dept. of Energy and funded in 2005 for a full year (2006) deployment of the AMF in Niamey in the frame of AMMA international program.
5. **African Climate Change: Taking the Shorter Route (consulté et remercié dans le texte):** A view, commissioned by the British Government, on the interrelationships between climate variability and development across Africa, the link to managing climate change, and related current and future resource needs within the continent. Richard Washington et al, Bulletin American Meteorol Society; October 2005.
6. **THORPEX-Africa (2007):** Programme de l'Organisation Mondiale de la Météorologie (OMM) sur la prévision des événements extrêmes en Afrique. Contribution à la rédaction du plan d'implémentation et du plan scientifique pour le volet Système d'Observation

d. Liste des principales communications (congrès, colloques) avec publication des actes

- Diedhiou A. and Mahfouf J.F., 1996: The influence of surface conditions on rainfall in the Sahel., Proceed. of the 2nd Int. Conf. of African Met. Soc.(SMA), Casab anca, **Maroc**.
- Diedhiou A., Mathon V., Laurent H., Janicot S., 1998: Suivi de systèmes convectifs dans un flux d'Est perturbé en Afrique de l'Ouest. Conférence Internationale sur la variabilité des Ressources en Eau en Afrique de l'Ouest au XXème siècle, vol. 2, p. 57-63, Abidjan, **Côte d'Ivoire**.
- Diedhiou A., Laurent H. Janicot S., Viltard A., 1998: Approche composite de la variabilité synoptique en Afrique de l'Ouest et relation avec les précipitations. Conférence Internationale sur la variabilité des ressources en eau en Afrique de l'Ouest au XXème siècle, vol. 1, p. 3-10, Abidjan, **Côte d'Ivoire**.
- Diedhiou A., Janicot S., Viltard A., De Felice P., Laurent H., 1998: Different regimes of easterly waves over West Africa and tropical Atlantic (1979-1995). XXIII General Assembly of European Geophysical Society, Nice, 20-24 Avril 1998. Annales Geophysicae, 1998, vol. 16, Part. II, p. C 688, Nice, **France**.
- Diedhiou A., Janicot S., 1999: Variability of synoptic disturbances over West Africa and tropical Atlantic in ECMWF and NCEP/NCAR reanalyses : on easterly waves, rainfall and convection. XXIV General Assembly of European Geophysical Society,. Annales Geophysicae 0129-41, Tropical climate variability, La Haye, **Hollande**.
- Janicot S., and Diedhiou A.,1999: Evidence of a 6-9 day easterly wave regime over West Africa and the tropical application to gate. Proc. of the 23rd Conference on Hurricanes and Tropical Meteorology, AMS Publ. 1999, 115-119, Dallas, **USA**.
- Diedhiou A., 1999: Relations entre ondes d'est d'échelle synoptique et régime pluviométriques en Afrique de l'Ouest. Séminaire CATCH (Couplage entre l'Atmosphère Tropicale et le Cycle Hydrologique)/PNRH, Ecole de Physique des Houches, **France**.
- Diedhiou A., Janicot S., 1999: Variability of synoptic disturbances over West Africa : preliminary result of energetic study. International Workshop West African Monsoon Variability and Predictability (WAMAP), Dakar, **Sénégal**.
- Diedhiou A., Lebel T., 2000: Comparative study of rainfall events variability over Sahel and Guinea Coast. XXV General Assembly of European Geophysical Society, Session Océans & Atmosphères : OA32.1. Résumés in CD ROM, 2000, vol. 2, Nice, **France**
- Diedhiou A.,2000. GCM simulations of the mean state of West Africa in the WAMP Project. Workshop on modeling the West African Climate system with Global and Regional scale climate models, Howard University, Washington DC, **USA**.
- Diedhiou A., Janicot S., Laurent H., 2000: Variability of the Monsoon layer and rainfall over West Africa. XXV General Assembly of European Geophysical Society, Session Océans & Atmosphères : OA32.1. Résumés in CD ROM 2000, Nice, **France**.
- Lebel T., Sacher W., Cras A., Balme M., Diedhiou A., 2001: EPSAT-Niger : 10 years of fine scale observation of rainfall variability in the Sahel. XXVI General Assembly of European Geophysical Society, Session Océans et Atmosphère : OA26-1. Résumés in CD ROM 2001, vol. 3, Nice, **France**.
- Moufouma-Okia W., Gallée H., Brasseur O., Lebel T., Diedhiou A., 2001: Simulation of climate over west africa using a regional climate model : sensitivity studies. XXVI General Assembly of European Geophysical Society, Session Océans & Atmosphère : OA26-1 (poster OA054). Résumés in CD ROM 2001, vol. 3, Nice, **France**.
- Diedhiou A., Lebel T., Diongue A. 2001: Synoptic context associated to COPT and Hapex-Sahel Mesoscale Convective Systems. XXVI General Assembly of European Geophysical Society. Session Océans & Atmosphere : OA26-1. Résumés in CD ROM 2001, vol. 3, Nice, **France**.
- Diedhiou A., Lavaysse C., 2001: Rainfall variability and rainfall over Sahel : the concept of wet and dry waves. XXVI General Assembly of European Geophysical Society. Session Oceans & Atmosphere : OA26-1. 2001, Résumés in CD ROM 2001, vol. 3, Nice, **France**.
- Gallée H., Brasseur O., Moufouma-Okia W., Messager G., Diedhiou A., P. Marbaix, Lebel T. Une simulation de haute résolution du climat de l'Afrique de l'Ouest. Atelier sur le couplage des modèles atmosphériques et hydrologiques. CR : 115-118 (Poster), Toulouse, **France**.
- Afouda A., Angulo-Jaramillo R., Bouchez J.M., Braud I., Cazenave F., Depraetere C., Diedhiou A., Galle S., Gallée H., Gohoungossou, Gosset M., Haverkamp R., Le Barbe L., Lebel Th., Reggiani P., 2001: Couplage de l'atmosphère et du cycle hydrologique continental en zone tropical : le projet CATCH. Atelier sur le Couplage des Modèles Atmosphériques et Hydrologiques. Session 1 : Inventaire des besoins en termes d'échelles et de bassin. CR : 27-31., Toulouse, **France**.
- Ramel R., Diedhiou A., Gallée H., Lebel Th., Moufouma-Okia W., 2002: Validation of a regional climate model over western africa. XXVII General Assembly of European Geophysical Society, Session Océans & Atmosphères : OA23.01. Résumés in CD ROM, vol. 4, Nice, **France**.

- Diedhiou A., Royer J.F., Poccard I., Lebel T., 2002:** Impact of greenhouse warning on the variability of african easterly waves. XXVII General Assembly of European Geophysical Society. Session Océans & Atmosphères :OA23.01. Résumés in CD ROM, vol. 4, Nice, France.
- Diedhiou A., Laurent H., Lebel T., Lavaysse C., 2002:** Rainfall variability and convection in African easterly wave regime. 25th Conference on Hurricanes and Tropical Meteorologie, AMS Publ. San Diego, Californie, USA
- Moufouma-Okia W., Gallée H., Brasseur O., Messager C., Ramel R., Lebel T., **Diedhiou A.**, 2002: The Seasonal variability of the West African rainfall in the nested regional climate model MAR : Sensitivity to ECMWF Reanalysis. International NCCR Climate Summer School, Grindelwald, Suisse.
- Diedhiou A., J-F Royer, I. Poccard, T Lebel. 2002.** Impact of Greenhouse Warming on the variability of easterly waves, rainfall and convection over West Africa ; Proceedings of AMS, P1.53, 25th Conference on Hurricanes and Tropical Meteorology, San Diego, CA, USA.
- Diedhiou A., J. Ronchail , N. Dessay., L.A.T. Machado, H. Laurent., J-F. Royer, 2002.** Climate Change over South America in relation with the Increase of Global Greenhouse Gases: a numerical study. XII Congresso Brasileiro de Meteorologia, Iguassu Falls, Brasil. (*Awarded: Prix du meilleur travail présenté oralement dans la session "Variabilité et changement climatique"*).
- Hall N. and A. **Diedhiou**, 2003: African easterly waves: Dynamical stability and possible precursors, 14th Symposium on Global Change and Climate Variations, P3.13; The 83rd Annual AMS Meeting. Long Beach, Californie, USA.
- Kahan D. S., Y. Xue, S. D. Prince, A. **Diedhiou**, and P. J. Lamb, 2003: Simulated surface hydrology and energy balance of West Africa using SSIB with observed precipitation and satellite-derived vegetation. 17TH Conference on Hydrology., P1.4; 83rd Annual AMS Meeting., Long Beach, Californie, USA.
- Lavaysse C., A.**Diedhiou**, T.Lebel, J.Y. Grandpeix, H.Laurent, 2003: Wet and dry convective events over Sahel:Diagnostic and numerical studies. EGS-AGU-EUG Joint Assembly, Nice, France.
- Bigot S., I. ZIN and A. **Diedhiou**, 2004: Apport de données SPOT multirésolution pour l'étude des variations phénologiques dans le bassin de l'Ouémé (Nord-Bénin). Réseau Télédétection de l'Agence Universitaire de la Francophonie Journées Scientifiques d'Ottawa. Canada.
- Bigot S., Oswald J., Brou Yao T., **Diedhiou A.**, Konare A., Fofana M., Assamoi P. 2004 : Le suivi des variations climatiques et écologiques en Afrique de l'Ouest : le rôle de la station géophysique et écologique de Lamto (Côte d'Ivoire). 17e Colloque International de l'Association Internationale de Climatologie « Climat, mémoire du temps » Mémorial de Caen, France
- Lavaysse C., A. **Diedhiou**, H. Laurent and T. Lebel, 2005 : Waves and Convection in Wet and Dry sequences of the West African Monsoon. Geophys. Res. Abs., Vol. 7, 07715, European Geosciences Union, Vienna, Austria.
- Adamou G., El Mahaman I. S., Itoua.E..N., **Diedhiou A.**, Gaye A.T, et G. Jenkins., 2005: Utilisation des données MSG dans des études de cas des perturbations (poussières, orages et lignes de grains) observées à Niamey en 2004. 1st International AMMA Conference; Dakar, Sénégal
- Camara M., A. **Diedhiou**, A. T. Gaye., 2005. African Easterly Waves and Cyclonic activity over the eastern Atlantic: Composite and case studies. 1st International AMMA Conference ; Dakar, Sénégal
- Descroix, L., Amogu, O., Le Breton, E., Alzouma, I., Mamadou, I., Besnier, A-L., **Diedhiou, A.**, Lebel, T., 2005. Silting up of Niger river channel in Niger : a consequence of land use changes. VIIème Assemblée Scientifique de l'AISH, Foz de Iguaçu, Brésil.
- Bailleul, C., Descroix, L., Lebel, T., **Diedhiou, A.**, Cappelaere, B., Gérard, B., Traoré, S., Laurent, J-P., Morel, J., Gignoux, J., Boulain, N., Rabanit, M., Bousquet, S., Boubkraoui, S., Alassane, H., Koné, A., 2005. Feed back surface/atmosphère : et l'échelle locale ?. 1ère Conférence Internationale AMMA ; Dakar 27/11-2/12/2005, Sénégal.
- Diedhiou A. et al. (colleagues of AMMA-TT1 group), 2006:** "Atmospheric sounding (EOP, SOP & IOP modes)". Conference AMMA-International: "SOP debriefing and preparation of process studies"; France, Toulouse.
- Redelsperger J.L., C.D. Thorncroft, A. **Diedhiou**, T. Lebel, D.J. Parker, J. Polcher, 2007 : AMMA: An international research project and field campaign, Geophys. Res. Abs.Vol. 9, 11547, EGU, Vienna, Austria.
- Kamga A. F. , A. Diongue Niang, E. Afiesimama, A. **Diedhiou**, B. L. Lamptey, O. Ndiaye, M. Kamara, and R. Roehrig. 2008. "Towards the development of a revised THORPEX AFRICA science plan". Symposium on Linkages among Societal Benefits, Prediction Systems and Process Studies for 1-14 day Weather Forecasts. The 88th Annual Meeting of American Meteorological Society (20-24 January 2008). New Orleans; USA.
- Diogue A., Afiesimama E., **Diedhiou A.**, Kamga F., Lamptey B., Ndiaye O., 2008: "THORPEX-Africa: A programme to Mitigate the Effects of Natural Disasters for the Benefit of the African Society ". Science with Africa, UNECA International Conference; 3-7 March 2008, Addis Ababa, Ethiopia

- Diedhiou A. and Bricout A, 2009:** The RIPIECSA program: A. Support to Interdisciplinary and Participatory Research on Interactions between Ecosystems, Climates and Societies in West Africa; International Workshop of Experts on Global Environmental Change (including Climate Change and Adaptation) in sub-Saharan Africa. ICSU-RoA Meeting; 9 – 11 February 2009; Pretoria, **South Africa**
- Ruti P.M., M.B. Barmou Batoure, A. **Diedhiou**, A. Dell'aquila, **2009** ; Seasonal error in the seasonal forecast over West Africa from European multi-model ensemble system. 3rd AMMA International Conference; Ouagadougou; **Burkina –Faso**.
- T.E. N'Datchoh, A. Konaré, A. **Diedhiou**, F. Solmon **2009**; Effet de la variabilité climatique sur le régime des feux en Afrique de l'Ouest. 3rd AMMA International Conference; Ouagadougou; **Burkina –Faso**.
- A. Diongue Niang, A. Kamga, E. Afiesimama, A. Babu, A. **Diedhiou**, B. Lamptey, A. Mokssit, F. Opijeh, E. Poolman, J. Caughey, D. Parsons, **2009**. WWRP/THORPEX-Africa ; 3rd AMMA International Conference; Ouagadougou; **Burkina –Faso**.
- L. Descroix, B Ibrahim; K Souleye Yero; A **Diedhiou**; **2009**; Vegetation pattern and rain fields in the Sahel. 3rd AMMA International Conference; Ouagadougou; **Burkina –Faso**.
- Y. Sane, M Bonazzola, F Hourdin, A Diongue-Niang, A. **Diedhiou**; **2009**; Diurnal cycle of precipitation at Dakar in the model LMDZ. 3rd AMMA International Conference; Ouagadougou; **Burkina –Faso**.
- K. Abdou, D.J Parker, B Brooks, N Kalthoff, A. **Diedhiou**, T. Lebel; **2009**; Diurnal cycle of lower boundary layer wind in the West African monsoon. 3rd AMMA International Conference; Ouagadougou; **Burkina –Faso**.
- S. Silue, A. Konaré, A. **Diedhiou**, V. Yoboue, P. Assamoi; **2009**; Sahelian dust: responses to main mode of variability in Atlantic, Pacific and Indian Oceans and their impacts on the deep convection in the Sahel. 3rd AMMA International Conference; Ouagadougou; **Burkina –Faso**.

e. Liste des séminaires scientifiques, réunions d'information et communication

- Diedhiou A. 1998 :** "Etude des perturbations synoptiques en Afrique de l'Ouest". LTHE, Grenoble, France.(Contact: Dr. Thierry Lebel).
- Diedhiou A. 1999:** "Identification of two regimes of easterly waves over West Africa and the tropical Atlantic from NCEP/NCAR and ECMWF reanalyses", NOAA, Climate Prediction Center, Maryland, USA. (contact: Dr. Wassila Thiaw).
- Diedhiou A. 1999:** "Easterly waves and rainfall variability over West Africa". Dept. of Atmospheric and Oceanic Sciences. McGill University., Montreal, Canada. (contact: Dr. Nick Hall).
- Diedhiou A., 1999 :** "Variabilité synoptique sur l'Afrique de l'Ouest et relations avec la convection et la pluie." Laboratoire de Physique de l'Atmosphère, UCAD/ESP, Dakar, Sénégal. (contact: Dr. Amadou Gaye).
- Diedhiou A. 2001:**"African easterly waves characteristics over the Atlantic Ocean" CPTEC (Centro de Previsão de Tempo e Estudos Climáticos), Cachoeira Paulista, SP, Brasil. (contact: Dr Luiz. A. Machado and Dr. H. Laurent).
- Diedhiou A.. 2001 :** "Mousson Africaine et Variabilité des ondes d'est ", EAMAC/ASECNA, Niamey, Niger. (contact: Dr. Adamou Garba).
- Diedhiou A. 2002;** "West African monsoon variability, African easterly waves and relationship with convection and rainfall". Department of Geography, University of California (UCLA), Los Angeles, CA, USA. (contact: Dr. Yongang Xue).
- Diedhiou A. 2002 ;**"Wet and dry convective systems and African easterly waves", Department of Earth and Atmospheric Sciences, University at Albany, SUNY Albany, New York, USA. (contact: Dr. Chris Thorncroft)
- Diedhiou A. 2002 :** "Kinematic of synoptic atlantic disturbances". Instituto de Astronomia, Geofísica e Ciências Atmosféricas, Universidade de São Paulo, Brasil. (Contact: Dr. Ascencão).
- Diedhiou A. 2002 :** "Variability of atlantic disturbances and convection over South America". FUNCEME, Fundação Cearense de Meteorologia e Recursos Hídricos – Fortaleza, Brasil. (contact: Dr. Antonio G. Ferreira and Dr. Jacques Servain).
- Diedhiou A. et Daniel Roux. 2003 :** « Analyse Multidisciplinaire de la Mousson Africaine (Projet AMMA) » Atelier Régional SMOC (Système Mondiale d'Observation du Climat) pour l'Afrique de l'Occidentale et Centrale. Organisé par l'OMM. Niamey, Niger 27-29 March 2003

Depuis 2003: Implication (100%) dans la mise en œuvre du programme International AMMA sur la Mousson Africaine

Depuis Novembre 2006 : Chef de Projet du FSP RIPIECSA (AIRD/MAEE) sur les interactions Climat-Ecosystèmes-Sociétés

- Co-organisateur des réunions d'informations AMMA avec les différents comités nationaux en Afrique. Plusieurs séries de conférences sur AMMA et sur l'initiative africaine dans ce programme ont été faites au Niger et dans la sous-région devant des ministres, des journalistes, des étudiants.... Interview sur AMMA aux radios (RFI, radios nationales) et passages à la télévision (TV5, Journaux Télévisés TF1, France 2, France 24, AITV, télévisions nationales africaines, etc.) et citation dans la presse écrite africaine (au Niger, au Mali, au Sénégal) et européenne (Le Monde, Le Figaro, SPORE).
- Plusieurs conférences en Afrique de l'Ouest sur le projet FSP RIPIECSA, plusieurs interviews sur la problématique des changements climatiques en Afrique et sur l'expertise africaine dans ce domaine avec passages à la radio (RFI, radios nationales africaines, etc.) et passages à la télévision (TV5, AITV, télévisions nationales africaines, etc.).

Diedhiou A. 2005 : "Building the African involvement in AMMA International Program". NEPAD Workshop on Water Sciences and Technology Development; 9-12 Mai 2005, Nairobi Kenya.

Diedhiou A. 2005: « Le montage de projet et la mobilisation des ressources ». Atelier Climat-Santé co-organisé par l'ACMAD et l'OMM : « Informations climatiques : prévention et lutte contre les épidémies de paludisme et de méningites en Afrique de l'Ouest » ; Niger ; Niamey, 23-25 Novembre 2005

Diedhiou A. 2007: Présentation 1: « Les réseaux scientifiques et centres d'excellence en Afrique de l'Ouest et leur implication dans les changements climatiques ». Présentation 2 : « AMMA-Afrique : la composante africaine du programme International AMMA ». Conférence Internationale sur la réduction de la vulnérabilité des systèmes naturels, économiques et sociaux de l'Afrique de l'Ouest face aux changements climatiques (Organisé par ONU/CEA et CILSS ; Burkina Faso ; Ouagadougou, du 24 au 27 Janvier 2007).

Diedhiou A. 2007: « L'initiative africaine dans le programme AMMA » OMM / WMO RA1 seminar (invited expert) ; Burkina Faso ; Ouagadougou, 12-13 Février 2007.

Diedhiou A. 2007: "Endorsement of newly implemented meteorological Infrastructure in West Africa". Atelier "Sahel Conference 2007: Improving Lives by Understanding Weather " Session : AMMA and Beyond: Potential collaborations with West African institutions, universities and scientists in the U.S. and the world and the WMO programs. Co-organisé par le CILSS, UCAR et le programme SAGAA (Burkina Faso ; Ouagadougou ; 2 - 6 April 2007).

Diedhiou A. 2007 : « Présentation du FSP RIPIECSA » ; Atelier du Programme « Desert Margin Program » sur la lutte contre la désertification et la dégradation des sols ; Burkina Faso ; Ouagadougou, 22-24 Mai 2007.

Diedhiou A. 2007 : Conférencier invité. « le FSP RIPIECSA » 4^{ème} séminaire des correspondants « Environnement » des ambassades de France (Ministère des Affaires Etrangères et Européennes). 2-3 juillet 2007, Paris, France

Diedhiou A. 2007 : Conférencier invité. « Changements climatiques en Afrique: La nécessaire concertation entre chercheurs des sciences physiques et des sciences sociales et implication de la société civile». Journées de la Coopération Internationale et du Développement (Ministère des Affaires Etrangères et Européennes), Atelier Climat. 17 juillet 2007 ; Paris, France.

Diedhiou A., 2008 : Conférence Scientifique Méditerranéenne ; « Vers un Espace Méditerranéen de la Science » ; Gouvernance, Rôle des divers acteurs et acceptabilité sociale : le FSP RIPIECSA et le lien avec l'Afrique Sub-saharienne. Rencontre organisée par le Groupe Inter-académique pour le Développement, l'Institut de France (Académie des Sciences) avec le soutien du Ministère des Affaires étrangères et européennes et de « l'Union pour la Méditerranée » ; 24-26 Juin 2008; Paris ; France.

- **Invitation à participer à deux documentaires scientifiques télévisés** (sur les changements climatiques et ses impacts ainsi que sur l'émergence d'une expertise dans ce domaine) :
 - La calebasse et le pluviomètre (2007), sur le programme AMMA
 - Le fleuve Niger en danger (2008) pour la conférence des ministres du Bassin du fleuve Niger

3) Présentation des travaux de recherche antérieurs

3.1 Activités de recherche

a. Intérêt scientifique et cadre général

Sous les tropiques en général et en Afrique de l'Ouest en particulier, la pluie résulte de trois phénomènes étroitement imbriqués : le flux de mousson, en relation avec la circulation générale, les conditions de surfaces continentales et océaniques (les gradients méridiens d'énergies en surface à l'échelle régionale) et la convection de méso-échelle. La compréhension des processus de surface continentale en termes d'interactions entre l'atmosphère et la surface constitue un défi majeur pour l'étude des changements climatiques, mais à l'heure actuelle, la modélisation ne permet pas encore d'obtenir un consensus sur le rôle relatif des divers processus de surface.

Le Barbé et Lebel (1997) ont montré que la réduction et la variabilité des précipitations au Sahel sont fortement associées à la variation du nombre d'événements pluviométriques. Ces événements sont d'origine convective, les plus importants étant les systèmes convectifs de méso-échelle qui apportent 90% du total pluviométrique (Laurent et al., 1998). En effet, la fréquence de ces systèmes précipitants (plus que leurs caractéristiques) semble sensible aux processus de surface continentaux dans des modèles de circulation générale (Polcher, 1995). Mais s'il existe, en première approximation, une bonne relation entre les événements pluvieux ainsi définis et les systèmes convectifs observés par satellite, la question des liens entre variabilité interannuelle des précipitations et systèmes convectifs reste toujours ouverte.

Ces systèmes convectifs de méso-échelle interagissent avec les ondes d'échelle synoptique (les ondes d'Est, Diedhiou et al., 1999, 2001) et avec les fluctuations du flux de mousson qui modulent les caractéristiques du flux de vapeur d'eau d'origine océanique sur le continent. Les mécanismes qui régissent ces interactions sont actuellement mal compris. Il importe donc d'approfondir nos connaissances sur les variations des événements convectifs et des phénomènes atmosphériques associés en Afrique de l'ouest. Plusieurs échelles de temps et d'espace doivent être considérées, depuis la méso-échelle (heure/100 km), l'organisation synoptique (jour/1000 km) jusqu'aux échelles saisonnière et inter-annuelle (mois/10000 km).

Ma recherche à l'IRD concerne l'étude de la relation onde - convection - pluie aux échelles spatio-temporelles caractéristiques. Ainsi, depuis plusieurs années, un axe de recherche sur l'étude des systèmes convectifs de méso-échelle et leur interaction avec les perturbations atmosphériques d'échelle synoptique s'est développé au LTHE. En effet, le système convectif de méso-échelle apparaît aujourd'hui comme un élément essentiel à la compréhension du climat des régions Sahéliennes : il est la clef entre le forçage de grande échelle et les précipitations locales. Pour comprendre et modéliser l'impact du climat sur les ressources en eau, en régions tropicales, il apparaît indispensable d'étudier les caractéristiques et les propriétés de ces systèmes convectifs ainsi que leur interaction avec la circulation générale atmosphérique et leur impact pluviométrique.

Membre de l'équipe ASP/LTHE dans le projet ATIRE (UR012), je contribue à l'étude du cycle de l'eau dans l'atmosphère et de sa variabilité sur les surfaces continentales, de la grande échelle à la méso-échelle à partir de réanalyses américaines et européennes, de données observées et de sorties de modèles de circulation générale, régionale et de méso-échelle.

Jusqu'en 2003, ma recherche à l'IRD fut soutenue et financée par les programmes nationaux PNEDC (coordonné par Dr. Bernard Fontaine du CRC/Dijon puis Dr Serge Janicot du LMD), PATOM (coordonné par Dr. Jean-Philippe Lafore, CNRM). En effet, elle se situe à l'interface des différentes échelles et je proposais chaque année un projet dans ces programmes autour de la variabilité multi-échelles de la convection et de ses interactions avec la pluie en Afrique de l'Ouest (aux échelles interannuelles, intrasaisonnières et en liaison avec les conditions de surface). Mes projets dérivaient des travaux déjà engagés dans les projets européens WAMP (West African Monsoon Project) et PROMISE (Predictability and variability of Monsoons, and the agricultural and hydrological impacts of climate change). Ils étaient toujours conformes aux recommandations de CLIVAR/TAV (Tropical Atlantic Variability) et CLIVAR/VACS (Variability of the African Climate System).

Depuis 2003, ma recherche est fortement impliquée dans le Programme international AMMA sur la mousson africaine et l'investigation des phénomènes physiques sous-jacents et leur modélisation prévue dans ce cadre répondent à certains des objectifs scientifiques prioritaires qui ont été définis et présentés dans le Plan Scientifique International (AMMA-ISP).

Nous avons d'abord abordé l'étude des perturbations synoptiques en Afrique de l'Ouest et sur l'Atlantique tropical. L'objectif est de mieux cerner les caractéristiques de ces ondes et de contribuer à la compréhension des liens entre ces perturbations synoptiques et les précipitations. Nous avons utilisé principalement les réanalyses NCEP/NCAR¹ et à titre de comparaison ou de validation, nous discutons des mêmes résultats obtenus avec les réanalyses du CEPMMT². Pour l'étude des interactions avec la convection, nous utilisons les précipitations observées disponibles à l'IRD³, l'OLR⁴ fourni par la NOAA⁵ et la nébulosité issue du projet ISCCP⁶. Nous avons établi, par différentes méthodes statistiques, l'existence de deux régimes d'ondes d'Est, différents à l'échelle synoptique et liés aux instabilités de l'AEJ (Jet d'Est Africain, situé entre 600 et 700 hPa): un régime d'onde entre 3 et 5 jours et un autre, plus intermittent, entre 6 et 9 jours (Diedhiou et al. 1998a, 1998b, 1999, 2001, 2002a).

Le régime d'onde 3-5 jours (figure 1) présente des caractéristiques identiques à celles de l'onde d'Est classique bien étudiée en Afrique de l'Ouest et sur l'Atlantique tropical. Les ondes 3-5 jours apparaissent, en moyenne, autour de 20°E et se propagent vers l'Ouest jusqu'aux Caraïbes. Elles suivent deux axes sur le continent (à 5°N et à 15°N), de part et d'autre de l'AEJ, qui convergent sur l'océan, pour ne suivre qu'un seul axe, autour de 17.5°N. Lorsque cette onde est active au Nord de l'AEJ, elle présente une forte extension méridienne avec deux cellules de part et d'autre de ce jet. Elle a une longueur d'onde moyenne de 2500 km avec une vitesse de phase d'environ 7-8° longitude par jour (8-9 m/s). En général, elle présente une périodicité entre 4 et 5 jours. Lorsqu'elle est active au Sud de l'AEJ, autour de 5°N, sa période moyenne est de 3-4 jours. Dans cette région, elle présente une longueur d'onde moyenne de 4500 km, une vitesse de phase de 10-12° longitude par jour soit environ 12 m/s. Lorsqu'elle arrive sur l'océan, sa trajectoire remonte progressivement vers le Nord, pour se fondre avec l'axe Nord, sur l'Atlantique; l'onde retrouve alors les caractéristiques cinématiques présentées ci-dessus. Ce gradient méridien de longueur d'onde et de vitesse des ondes 3-5 jours a été trouvé dans les réanalyses du NCEP/NCAR et du CEPMMT. Nous avons suggéré que cette différence, pouvait être liée au gradient méridien de vent zonal, plus faible au Sud de l'AEJ.

Le régime d'onde 6-9 jours (figure 2) est très actif au Nord de l'AEJ entre 17.5dgN et 25dgN; il est caractérisé par de fortes circulations anticycloniques entre deux talwegs. Ces ondes ont une longueur d'onde d'environ 4500-5000 km et une vitesse de phase, vers l'Ouest, de 8-9° longitude par jour, soit de 7-8 m/s. Le développement et la propagation vers l'Ouest de larges circulations anticycloniques en relation avec les anticyclones de Libye et des Açores constituent les particularités de ce régime. Ces ondes modulent fortement la composante zonale de l'AEJ. Des études de cas ont montré que le passage d'un régime d'ondes à l'autre se fait de façon continue et ont révélé que la phase I de GATE, considérée comme une phase de faible activité des ondes 3-5 jours, était une période de forte activité du régime 6-9 jours.

La variabilité des ondes d'est 3-5-jours et 6-9-jours sur l'Afrique de l'Ouest et leurs interactions avec la convection et les précipitations ont pu être établi à l'aide des réanalyses américaines du NCEP/NCAR (Diedhiou et al., 1998a, 1998b, 1999). Une première climatologie a permis de mieux différencier les caractéristiques de ces deux perturbations sur le continent et sur l'océan (Diedhiou et al. 2001) et une seconde a fait la synthèse des différentes conversions énergétiques associées (Diedhiou et al. 2002a). Ces deux régimes d'ondes résultent d'une combinaison d'instabilités barotropes et barocliniques de l'AEJ et leurs structures composites horizontales et verticales présentent beaucoup de similarités. Cependant, quelques différences fondamentales existent.

En régime 3-5 jours, au Nord de l'AEJ, les plus fortes modulations sont localisées dans les basses couches, autour de 900 hPa, et sont liées à la prédominance des conversions barocliniques d'énergie. La convection, au passage de cette onde, est principalement modulée par le transport horizontal d'humidité et est forte à l'arrière du talweg de l'onde, dans le flux de Sud. Lorsqu'elles sont actives au Sud, dans la zone de convergence (autour de 5°N), ces ondes sont surtout maintenues par des conversions barotropes d'énergie

¹ National Center for Environmental Prediction/National Center for Atmospheric Research

² Centre Européen de Prévisions Météorologiques à Moyen Terme

³ Institut de Recherche pour le Développement, ex ORSTOM

⁴ Outgoing Longwave Radiation, rayonnement ondes-longues sortant au sommet de l'atmosphère

⁵ National Oceanic and Atmospheric Administration

⁶ International Satellite Clouds Climatology Project

avec un maximum au niveau de l'AEJ. Le maximum de modulation de la convection profonde, dans la zone de convergence, est localisé dans et à l'avant du talweg de l'onde, dans le flux de Nord. Sur l'océan (autour de 17.5°N), à l'Ouest de 30°W, cette onde est très développée au niveau de l'AEJ et présente sous ce jet, un noyau froid, dans son talweg. Elle est maintenue essentiellement par des conversions barotropes d'énergie. Dans les basses couches, la convection est localisée dans le talweg. Au-dessus du jet, elle est localisée à l'arrière du talweg, dans le flux de Sud.

En régime 6-9 jours, ces ondes sont maintenues par des conversions barotropes (700 hPa) et baroclines (autour de 900 hPa) d'énergie sur le continent; sur l'océan, les conversions d'énergie sont essentiellement barotropes avec un maximum à 700 hPa. Au Nord de l'AEJ, comme dans la zone de convergence au Sud, et contrairement aux ondes 3-5 jours, la convection profonde est renforcée à l'arrière du talweg de l'onde, dans le flux de Sud, par l'advection méridienne d'humidité et par la convergence du vent zonal dans l'AEJ. L'anomalie de précipitations présente une structure fortement zonale.

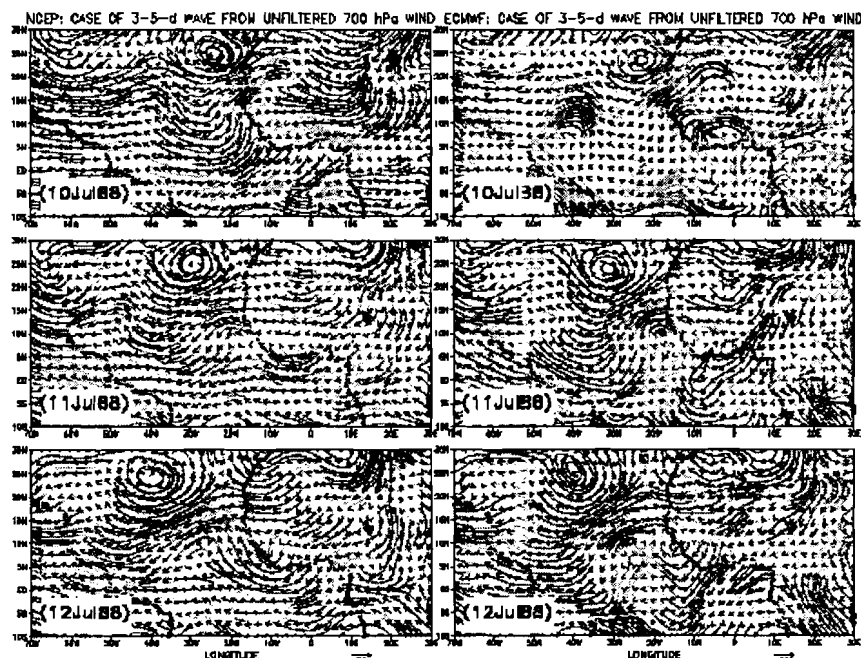


Figure 1 : Séquence de 3 jours d'un régime d'onde 3-5 jours dans les réanalyses NCEP/NCAR et ECMWF

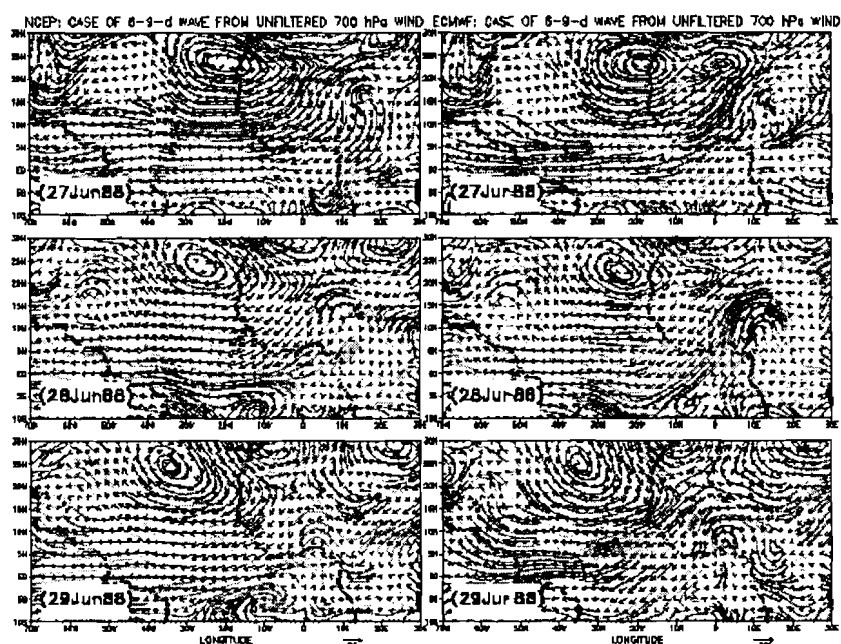


Figure 2 : Séquence de 3 jours d'un régime d'onde 6-9 jours dans les réanalyses NCEP/NCAR et ECMWF

Les résultats de l'étude sur les échanges d'énergie entre ces deux régimes d'ondes et le courant de base (l'AEJ), ont montré que les sens des différentes conversions d'énergie sont identiques pour les deux perturbations. La principale différence entre ces deux régimes d'ondes réside dans la quantité d'énergie potentielle zonale disponible qui est nettement plus élevée en régime 6-9 jours sur le continent. La hausse de l'énergie dans ce réservoir est cohérente avec le renforcement de la circulation anticyclonique au Nord, lors de la mise en place du régime 6-9 jours. Certaines fluctuations de l'AEJ sur le continent se traduisent par des talwegs, distants d'environ 2000-3000 km et dont la structure est identique à celle d'une onde 3-5 jours. C'est la configuration la plus courante. Le régime 6-9 jours pourrait résulter d'une interaction entre ces fluctuations du jet et celles liées à la circulation anticyclonique au Nord, sur le continent.

Les précipitations en région sahélienne étant à 80% d'origine convective, nous illustrons sur la figure 3 comment ces systèmes convectifs de méso-échelle suivis et classées à partir du canal infrarouge de METEOSAT à l'IRD / LTHE évoluent dans une perturbation atmosphérique d'échelle synoptique. Pour caractériser ces perturbations, nous avons utilisé les réanalyses américaines du NCEP/NCAR. Sur la figure ci-dessous, nous présentons une séquence (du 23 Juin 1989 à 00 heures au 24 Juin 1989 à 18 heures) du champ de vent filtré entre 3 et 10 jours à 700 hPa (lignes de courant) à laquelle nous superposons les clusters (pavés en couleur) obtenus par seuillage de la température de brillance METEOSAT à -20°C, -40°C et à -60°C. Malheureusement, la fenêtre METEOSAT est limitée en longitude (de -20°W à 20°E); il nous est donc impossible de suivre ces systèmes convectifs sur l'océan.

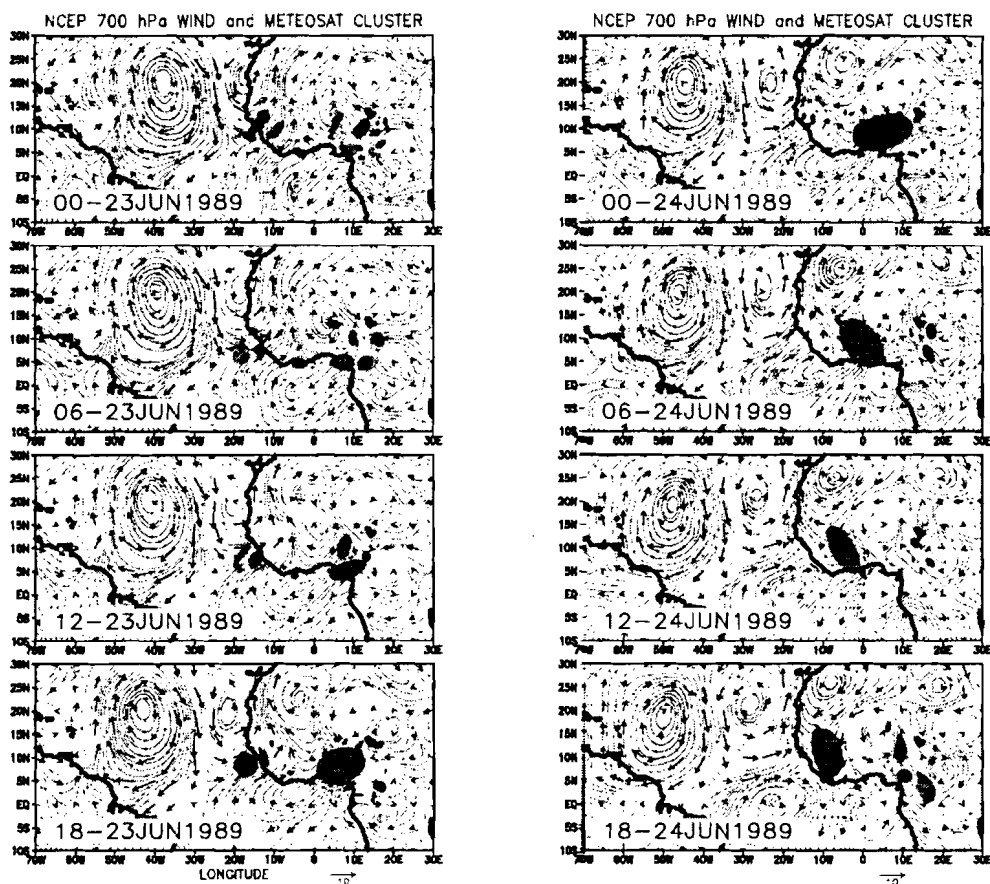


Figure 3 : Passage d'une onde 6-9 jours suivi d'une onde 3-5 jours le 23-24 Juin 1989: lignes de flux du vent non filtré à 700 hPa; Les ellipsoïdes sur ces figures représentent les clusters obtenus au 3 seuils de températures -20° C, -40° C et -60° C de METEOSAT.

La séquence que nous présentons ici traduit, à travers les lignes de courant, le passage d'une perturbation de périodicité 6-9 jours suivie à l'arrière par une perturbation de périodicité 3-5 jours. Le suivi de la propagation vers l'Ouest de ces ondes devient aisément en suivant les positions successives des centres des tourbillons cyclonique et anticyclonique. Le 23 Juin à 00 heures, nous avons entre 5° W et 15° W c'est à dire dans et à l'arrière du talweg de l'onde 6-9 jours, un ensemble de clusters de petite taille qui se déplacent vers l'Ouest avec la perturbation; nous pouvons ainsi les suivre jusqu'au 23 Juin à 18 heures tout en notant qu'ils sont toujours dans le même secteur de l'onde 6-9 jours, là où nous avons un flux de vent de

Sud. Le 23 Juin à 00 heures, nous observons dans et à l'avant du talweg de l'onde 3-5 jours arrivant derrière l'onde 6-9 jours, un ensemble de petit clusters qui s'organisent (entre 10° E et 20° E). Tout en restant dans ce même secteur d'onde, ces clusters vont se propager vers l'Ouest avec l'onde en s'agglomérant de plus en plus. Cette propagation peut être visible jusqu'au 24 Juin à 18 heures avec un gros cluster centré autour de 10° W. Nous avions noté plus haut qu'après le passage de la perturbation 6-9 jours, nous entrions dans une séquence d'onde 3-5 jours la deuxième onde 3-5 jours présentant un talweg visible autour de 30° E dès le 24 Juin à 00 heures. Six heures après, le talweg de cette seconde perturbation 3-5 jours est à 25° E et en Afrique Centrale au Sud du Lac Tchad, apparaissent de petits clusters entre ces deux talwegs. Ces clusters vont rester dans ce flux tout en se propageant vers l'Ouest avec ces ondes en s'organisant de plus en plus.

Pour introduire la complexité de l'interaction onde-convection-pluie, la figure 4 montre l'évolution de Juin à Septembre pour une année humide (1988, Fig. 4a), une année normale (1989, Fig. 4b) et une année sèche (1984, fig. 4c), des différents régimes d'ondes représentés en ombragé coloré par le module de l'analyse en ondelettes sur le vent méridien à 700 hPa (Torrence et Compo 1999). Dessus, nous superposons l'OLR observé par la NOAA pour suivre en une première approximation la convection (ligne noire pleine) et les précipitations quotidiennes IRD observées au point de grille de Niamey par l'IRD (ligne noire discontinue).

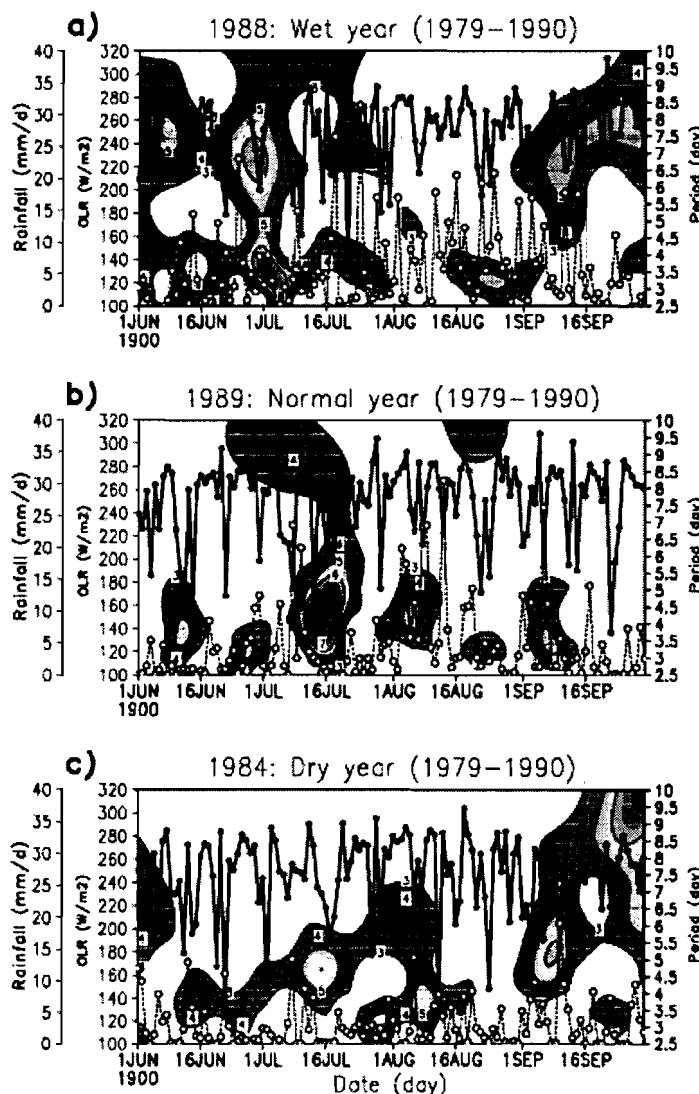


Figure 4: Evolution de Juin à Septembre des différents régimes d'onde au dessus de Niamey et relation avec la convection et les précipitations : Evolution du module de la transformée en ondelette du vent méridien à 700 hPa (couleur), NOAA OLR (ligne noire continue) et précipitations journalières observées par l'IRD (ligne noire discontinue) pour l'année la plus humide : 1988 (a), une année normale : 1989 (b), et l'année la plus sèche : 1984 (c) de la période 1979-1990.

L'analyse en ondelettes confirme que la période de la plupart des perturbations sur le Sahel se situe entre 3 et 5 jours. Le maximum de la 6-9-jours bande période est associé à un autre régime d'onde qui se produit principalement au début et à la fin de la saison des pluies saison (Diedhiou et al. 1999). Si l'on considère tous les jours concernés par une 3-5-jours d'onde régime, nous constatons qu'il est difficile, en utilisant le nombre d'ondes par an, de distinguer une année humide (1988) et une année sèche (1984) sur le Sahel. En effet, ces trois années sont affectées également par le même nombre d'ondes 3-5-jours

En 1989 (Fig.4b), nous observons autour du 1^{er}-10 Août et autour du 7 Septembre 1989 que ces ondes sont associées à des nuages à sommet froid (OLR <220W/m²; forte convection) et de fortes précipitations. C'est le cas idéal d'interactions onde-convection-pluie et qui motive les études sur la dynamique des ondes pour la prévision du temps.

Cependant, les régimes d'ondes autour du 8-16 Juin et autour du 21 août 1989 sont associés à des événements fortement convectifs (OLR entre 180 et 200 W/m² pour le premier cas et à moins de 160 W/m² pour la seconde) mais pas assez de précipitations observées à la surface. Comme le module de l'ondelette est positivement corrélé à la variance de l'onde, cela signifie que l'activité des ondes, estimée à partir des fluctuations de la composante méridienne du vent, n'est pas un bon indicateur de la variabilité des précipitations. Il peut y avoir une onde (condition de large échelle favorable), une forte convection et pourtant pas de pluie en surface.

Le régime d'ondes autour du 16 Juillet 1989 n'est pas associé à de la convection ni à de la pluie en surface. Cela signifie que les ondes peuvent se produire sans convection. Le fort module de l'ondelette associé à ce régime d'onde est un bon exemple de la non-corrélation entre la variance de l'onde et les précipitations et suggère que la dynamique n'est pas suffisante pour expliquer les précipitations. Le 14 août 1989, nous observons une forte convection (OLR moins de 170 W/m²) et de fortes précipitations (jusqu'à 15 mm / jour), ce qui signifie que la convection peut se produire sans onde.

Cette illustration explique en partie pourquoi, à l'échelle interannuelle, les corrélations sont mauvaises et toute la difficulté de prévoir le temps, d'estimer les précipitations par satellite ou de faire le lien entre système convectif vu par satellite et événement pluvieux.

L'étude de la relation entre la variabilité synoptique et les systèmes convectifs de méso-échelle en Afrique de l'Ouest a impliqué la collaboration entre le LTHE et le CNRM (METEO-France) et le LMD (CNRS). Une étude comparative de l'activité synoptique associée aux systèmes convectifs durant HAPEX-SAHEL (1992) et COPT (21-24 Juin 1981) a permis de comprendre en quoi certains systèmes HAPEX-SAHEL au Nord pouvaient être différents des systèmes convectifs se propageant plus au sud, en région guinéenne (Diedhiou A., Lebel T., Diongue A. 2001; Synoptic context associated to COPT and Hapex-Sahel Mesoscale Convective Systems. XXVI General Assembly of European Geophysical Society. Session Océans & Atmosphère : 0A26-1. Résumés in CD ROM 2001, vol. 3, Nice, France).

Les caractéristiques de la ligne de grains du 22 Août 1992 durant l'expérience HAPEX-SAHEL ont pu être étudiées et une restitution de ses propriétés sur plusieurs échelles spatio-temporelles a été faite Redelsperger et al. (2002). Les échelles interannuelle et intrasaisonnière, l'échelle synoptique ainsi que le cycle de vie associé à cette perturbation ont pu être étudiés afin d'en faire un cas de référence pouvant servir aux études numériques multi-échelles avec la mise en place de la modélisation emboîtée des modèles de climat aux modèles méso-échelles.

Comme en présence d'ondes (convergence à l'échelle synoptique et donc situation favorable à une convection profonde), on pouvait avoir un système convectif mais, celui-ci peut générer ou pas de la pluie en surface. Mathon and al., 2002 ont objectivement démontré que le nombre d'ondes d'est ne jouent pas un rôle majeur à l'échelle interannuelle sur la variabilité des systèmes convectifs organisés. L'étude de la relation entre la variabilité des ondes et des systèmes convectifs a permis de décrire l'environnement synoptique associé aux événements convectifs humides et secs (associés ou non à de la pluie en région sahélienne). Une étude numérique utilisant le modèle uni-cyclone du LMD/CNRS forcé par les réanalyses du NCEP/NCAR a permis de restituer sur la maille de Niamey (Niger) le profil vertical associé à ces deux types de systèmes convectifs. La distribution des précipitations sur la verticale est différente de même que les profils thermodynamiques associés. Beaucoup plus que les flux de masse ascendants, ce sont les descentes précipitantes qui dans les deux cas présentent des profils significativement différents : les précipitations s'évaporent avant qu'elles n'arrivent en surface. Il est difficile de savoir à ce stade qu'elle a été le rôle de la couche limite, des conditions de surface, celui de la grande échelle. Cependant, il était impossible de faire la part entre la thermodynamique intrinsèque au système et son environnement (Lavaysse C., A. Diedhiou, T. Lebel, J.Y. Grandpeix, H. Laurent, 2003: Wet and dry convective events over

Sahel: Diagnostic and numerical studies. EGS-AGU-EUG Joint Assembly, Nice, France). D'où, l'idée et la nécessité de se placer d'abord dans l'intrasaisonnier et de revoir cette relation onde – système convectifs – événement pluvieux à cette échelle.

b. Perturbations synoptiques, systèmes convectifs et précipitations en Afrique de l'Ouest

Le lien entre les ondes d'est africaines et la convection ou avec la pluie a été étudié plusieurs fois. A l'aide d'un modèle simplifié, Thorncroft and Hoskins (1994a), Thorncroft and Hoskins (1994b) et Mass (1979) ont étudié comment les ondes pouvaient moduler la convection. Ces simulations ont permis de montrer l'impact des tourbillons positifs à l'avant du talweg, du cisaillement de vent, de l'humidité, de l'AEJ et de certaines caractéristiques de la couche limite. En effet, Miller and Lindzen (1992) notent à partir de plusieurs simulations qu'en l'absence de cisaillement de vents lié à l'AEJ, la convergence d'humidité atteint les plus basses couches sans être atténuée, mais les valeurs restent trop faibles pour générer des ascendances. A l'inverse, un cisaillement trop fort va diminuer l'impact des ondes trop rapidement. Ainsi, avec un cisaillement optimum, une onde peut générer une forte convergence d'humidité et donc des précipitations organisées à condition d'être à une certaine distance de la source d'humidité. Ces résultats ont été confirmés par Fink and Reiner (2003) avec les réanalyses NCEP/NCAR de 1998 et 1999 en Afrique de l'Ouest. Ils trouvent que près de 42% sont associées aux ondes durant ces deux années et que cet impact est maximum au cœur de la saison avec 68% vers la côte sénégalaise. Pendant la campagne GATE, Reeves et al., (1979) montrent qu'au cours de la phase III (Août et Septembre 1974), une grande partie des précipitations côtières était liée au ondes.

Bien que l'onde corresponde à un environnement favorable à la convection, elle ne paraît pas être une condition suffisante. Taleb and Druyan (2003), Mathon et al. (2002) et Lebel et al. (2003) ont trouvé de faibles corrélations entre la variabilité interannuelle du cumul de pluie et celle du nombre d'ondes d'est. Par ailleurs, Gu et al. (2003) n'arrivent pas à faire le lien entre la variabilité interannuelle des pluies certaines propriétés des ondes. De même, Fink and Reiner (2003) ne trouvent pas de différences particulières dans les caractéristiques des systèmes convectifs (durée de vie, intensité), qu'ils soient associés ou non à des ondes.

Il est difficile donc de voir quel est le rôle des ondes d'est sur l'organisation de la convection et surtout sur la variabilité pluviométrique aux différentes échelles. Ces incertitudes peuvent être causées par les effets très différents des secteurs de l'onde. Burpee (1974), Fink and Reiner (2003) et Mathon et al. (2002) ont observé que la position de la convection dans les différents secteurs de l'onde dépendait de la latitude de l'axe de propagation de la perturbation. A l'échelle interannuelle, Druyan and Hall (1996) trouvent une variabilité de la position de la convection dans le champ de vent perturbé, avec un basculement du pic des précipitations de l'arrière du talweg en 1987 (année sèche) à un pic à l'avant du talweg en 1988 (année humide).

Dans le cadre de sa thèse de l'Université Joseph Fourier de Grenoble soutenue en 2006 et que j'ai codirigée, M. Christophe Lavaysse a mené une étude au LTHE pour comprendre l'influence du flux de mousson sur les interactions onde - convection - pluie en Afrique de l'Ouest.

Le travail de M. Christophe Lavaysse propose une étude détaillée des relations entre les ondes d'Est, la convection et les précipitations durant la mousson Ouest africaine. Cette étude sur 23 années (1968-1990) constitue une contribution majeure à la connaissance de la variabilité du flux de mousson ouest-africaine. Christophe Lavaysse a proposé méthode objective de détection des ondes d'Est africaines et a élaboré un indice de leur activité, basées sur une décomposition en ondelettes. La pertinence de l'approche est illustrée par une étude originale du cycle saisonnier de l'activité des ondes, ainsi que la variation de cette activité suivant la latitude et le niveau d'altitude considéré.

De même, les principaux modes de variabilités des précipitations et de l'activité convective sur le Sahel sont analysés dans cette thèse. Cette étude a permis de caractériser plusieurs régimes d'activité pour la convection et les précipitations observées et d'extraire le signal saisonnier. Cette classification préalable sera exploitée par la suite pour caractériser les relations Ondes – Convection – Pluie. En particulier, les relations ondes – convection – pluie sont étudiées en fonction du secteur considéré de l'onde en utilisant les outils et classifications précédemment introduits. Des analyses composites révèlent la structure de l'onde pour différents champs essentiels (pluie, tourbillon potentiel, température, divergence, vitesse verticale) et sa sensibilité à l'indice d'activité de l'onde. Enfin, l'étude des interactions onde – convection – pluie en fonction du mode de variabilité intrasaisonnier dans la gamme 10-85 jours a été abordée (Lavaysse et al.

2006). L'analyse composite de séquences humides et sèches donne une bonne idée du cycle de vie des systèmes convectifs. De tels événements sont au centre des préoccupations du projet AMMA.

En effet, en étudiant les fluctuations intra-saisonnieres de la convection en Afrique de l'Ouest, Sultan et al. (2003) et Sultan et Janicot (2003) montrent qu'elles s'expriment dans deux bandes de fréquences distinctes entre 10 et 25 jours, et entre 30 et 40 jours. Une analyse composite basée sur des indices pluviométriques régionaux sur le Sahel met en évidence que le signal le plus fort se traduit par des phases de renforcement et d'affaiblissement de la mousson appartenant à un signal quasi-périodique à 15 jours. Cette modulation de la convection est cohérente avec la dynamique atmosphérique dans les basses couches qui montre une propagation vers l'Ouest de larges circulations cycloniques et anticycloniques sur le Sahel s'associant avec des anomalies d'advection d'humidité à l'échelle intrasaisonnière. Pour mieux caractériser ce qu'on peut appeler des phases de renforcement ou d'affaiblissement de la mousson ouest-africaine, des analyses composites ont été réalisées à l'échelle intrasaisonnière, sur les 23 ans de la période 1968-1990, à la fois pour les précipitations et le champ de vent à 925 hPa, ceci afin de mettre éventuellement en évidence une organisation atmosphérique à l'échelle régionale.

Sur la figure 5, Janicot et Sultan (2001) représentent les séries chronologiques d'un indice régional de précipitations sur le Sahel, du 1er Juin au 30 Septembre de chaque année, ont été filtrées entre 10 et 60 jours. Ils ont retenu les dates (nommées t_0) où cet indice de précipitations est maximum (minimum) et supérieur à 130% (inférieur à 70%) du signal saisonnier filtré pour définir les séquences humides (sèches). Sur la période Juin- Septembre 1968-1990, on obtient en moyenne 3.9 séquences humides et 4.5 séquences sèches. Ils ont calculé ensuite la moyenne de cet indice, de $t_0 - 10$ jours à $t_0 + 10$ jours, séparément pour les séquences humides et sèches. Les deux séries composites sont présentées sur la figure 5a. La modulation de la précipitation moyenne régionale de ces séquences est forte, et relativement symétrique, montant jusqu'à 180% pour les séquences humides et descendant jusqu'à 60% pour les séquences sèches (soit un rapport proche de 2 et 0.5 respectivement). Ces fortes valeurs (exprimées en %) résultent en partie des fluctuations de précipitations à 15°Nord, où le rapport au signal saisonnier peut être élevé.

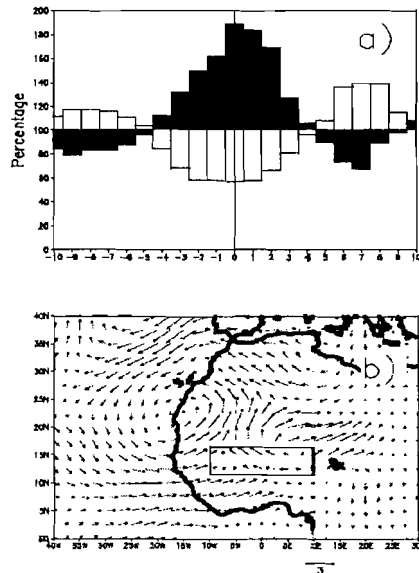


Figure 5 : Extrait de Janicot et Sultan (2001) : (a) Séquence composite humide (barres noires) et sèche (barres blanches) de l'indice de précipitations quotidiennes moyennées sur $10^{\circ}\text{W}-10^{\circ}\text{E}/12.5^{\circ}\text{N}-15^{\circ}\text{N}$, sur la période Juin-Septembre 1968-1990. Ces valeurs (%) représentent le rapport du signal brut où la variabilité inférieure à 10 jours est éliminée, sur le signal saisonnier (variabilité supérieure à 60 jours). (b) Champ de vent à 925 hPa correspondant pour 10, filtré 10-60-jours, calculé comme la différence entre séquence composite humide et séquence composite sèche. Le rectangle représente la zone de l'indice pluviométrique.

La question abordée par Christophe Lavaysse dans cette partie est de savoir quelles influences vont avoir les séquences de renforcement ou d'atténuation du flux de mousson sur l'activité convective et quels impacts auront ces ondes dans ces environnements plus ou moins favorables à la convection.

Dans ce qui suit, nous présenterons les résultats de cette étude sur l'évolution des interactions onde-convection-pluie seulement durant la phase active (séquences humide/renforcement et sèche/atténuation) du flux de mousson. Les résultats durant les périodes et dehors de ces phases actives (humides ou

sèches) sont disponibles dans son document de thèse (Lavaysse 2006) ; mais bien que ne présentant pas de modulations importantes dans la bande 10-60 jours, ces périodes inactives du flux de mousson peuvent toute fois enregistrer des précipitations importantes issues de convections locales ou de lignes de grains dont les durées de vie sont bien inférieures à 10 jours.

Les travaux de Christophe Lavaysse montrent que la répartition du nombre de jours dans chaque séquence (humide ou sèche) est assez constante chaque année et ne peut être liée à la variabilité interannuelle du cumul de pluie (figure 6). Cependant, le nombre de jours dans les séquences sèches est supérieur au nombre de jours dans les séquences humides alors que le cumul de pluie est supérieur dans les séquences humides que dans les séquences sèches. Ces cumuls ne présentent pas de lien avec les cumuls annuels de précipitations mais les précipitations moyennes journalières (4,25 mm/jour et 2,5mm/jour respectivement dans les séquences humides et sèches) apparaissent bien corrélées au cumul annuel des précipitations.

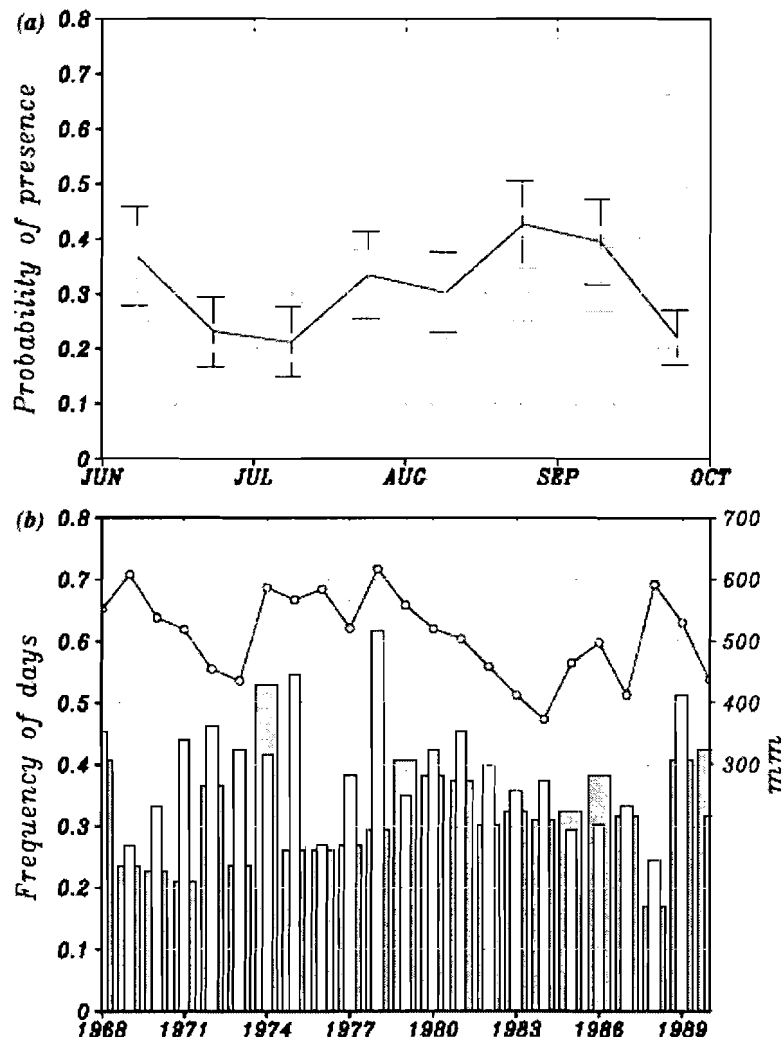


Figure 6 : a) Distribution intrasaisonnière des jours dans les séquences humides (courbe noire) et dans les séquences sèches (courbes grises) de Juin à Septembre avec les intervalles de confiance associés (significativité à 80 %). b) Fréquence traduisant le nombre de jours par an (du 1er Juin au 30 Septembre de 1968 à 1990) dans les séquences humides (barres grisées) et sèches (barres claires). Le cumul annuel de pluie est représenté par la courbe noire (en mm).

Les ondes sont plus courantes dans les séquences humides que dans les séquences sèches et tendent à augmenter les précipitations journalières moyennes (figure 7, Tables 1, 2, et 3). La contribution des ondes dans les différentes séquences correspond en moyenne respectivement à 42% et à 29% du cumul des séquences humides et sèches. L'activité des ondes montre une sensible augmentation (diminution) dans les deux types de séquences (humides et sèches) du flux de mousson au cours des années humides (sèches).

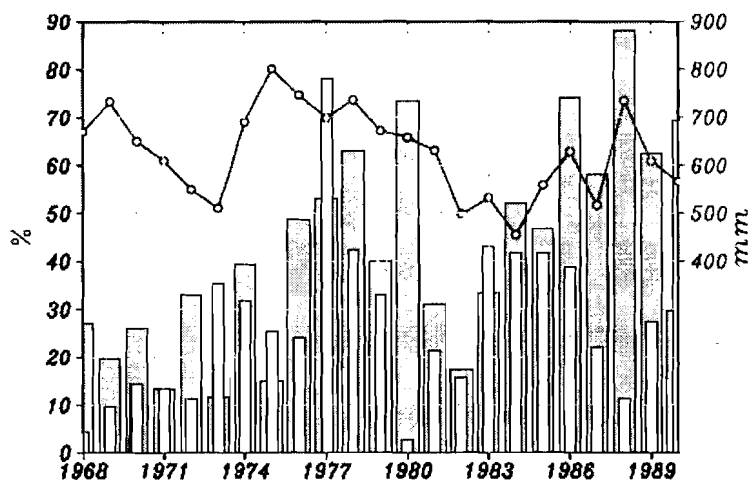


Figure 7 : Contribution (%) des jours associés aux ondes au cumul de pluie dans chaque séquence de 1968 à 1990 au point de grille de Niamey.

Table 1 Probability of presence (total number) of days with or without AEWs, in different intraseasonal sequence between 1 June and 30 September

Sequence	Days with AEWs	Without AEW	Total
Wet sequence	12.4 (351)	18.3 (518)	30.7 (869)
Dry sequence	10.2 (288)	27.0 (763)	37.2 (1051)
Inactive sequence	11.8 (334)	20.3 (575)	32.1 (909)
Total	34.4 (973)	65.6 (1856)	100.0 (2829)

Table 2 Distribution in % of days in each sequence associated or not with AEWs, between 1 June and 30 September

Sequence	Days with AEWs	Without AEW	Total
Wet sequence	40	60	100
Dry sequence	27	73	100
Inactive sequence	37	63	100
Total	34	66	100

Table 3 Distribution of mean daily rainfall (in mm) associated or not with AEWs in each sequences between 1 June and 30 September

Sequence	Days with AEWs	Without AEW	Total
Wet sequence	6.46	5.96	6.16
Dry sequence	3.04	2.72	2.81
Inactive sequence	4.88	4.61	4.71
Total	4.91	4.21	4.45

La figure 8 montre que l'activité convective est renforcée durant les séquences humides ; ceci est dû au nombre de jours de forte convection, deux fois plus importante en séquence humide qu'en séquence sèche. Les travaux de Christophe Lavaysse suggèrent que la différence de cumul annuel entre les séquences humides et sèches peut être liée à l'augmentation du nombre d'événements convectifs. En présence d'un fort événement convectif, les précipitations associées peuvent présenter une forte variabilité suivant qu'elles se produisent en séquence humide ou sèche avec un rapport allant de 1.5 à 2 entre ces deux séquences.

Donc les différences constatées entre les cumuls dans les deux séquences sont dues à la fois à une différence du nombre de systèmes convectifs mais aussi à l'efficacité pluviométrique moyenne de ces systèmes convectifs dans chaque séquence.

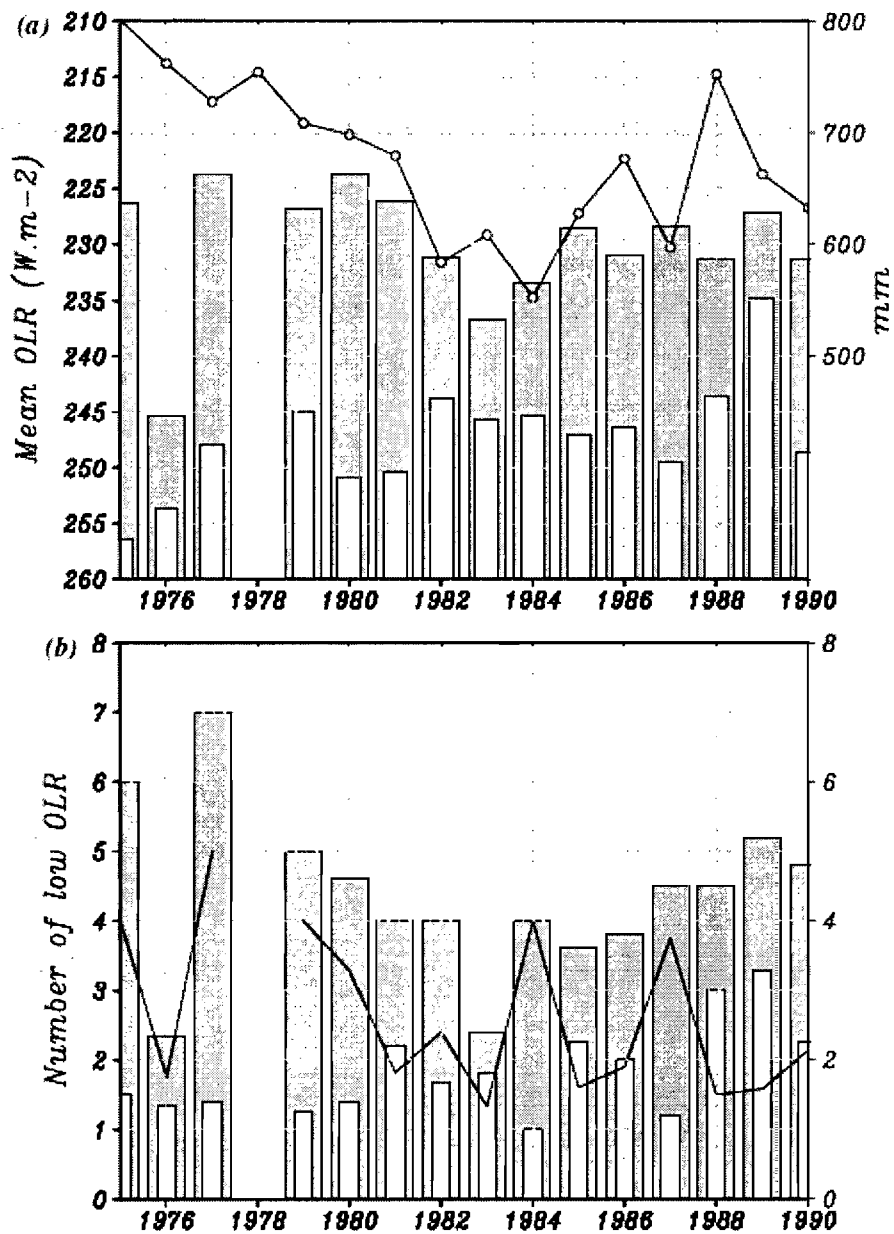


Figure : a) Moyenne de OLR (W.m^{-2}) de 1975 à 1990 : dans les séquences humides (barres sombres) et dans les séquences sèches (barres claires) ; la courbe représente cumul annuel de pluie (mm) sur le point de grille de Niamey. B) Nombre de forts événements convectifs ($\text{OLR} < 225 \text{ W.m}^{-2}$) dans les séquences humides (barres sombres) et dans les séquences sèches (barres claires) ; la courbe représente le rapport entre ce nombre de forts événements et le nombre total se systèmes dans chaque séquence.

L'importance de ces événements convectifs a pu être vérifiée avec la contribution des jours qui représente 34% (14%) du nombre de jour total alors que la contribution des précipitations sur le cumul atteint 55% (31%) dans les séquences humides (sèches).

Enfin, une étude composite sur une période de 21 jours (entre D_0-10 et D_0+10) a été faite sur la maille de Niamey pour les séquences humides et sèches (figure 9). Celle-ci a montré que l'environnement grande échelle apparaissait plus favorable à la convection lors des séquences humides, avec conjointement une

diminution du gradient méridien de PV, une augmentation de l'activité ondulatoire moyenne, une diminution du cisaillement dans les basses et les hautes couches. Ainsi, l'augmentation de la convection à D_0-5 est accompagnée d'une augmentation des précipitations journalières qui persiste jusqu'à D_0+5 . A 700 hPa, le Jet d'Est Africain (AEJ) s'affaiblit durant les séquences humides alors que le Jet d'Est Tropical (TEJ) se renforce en cohérence avec l'augmentation de la divergence dans les hautes couches suite à une forte activité convective associée à une baisse du cisaillement vertical du vent zonal.

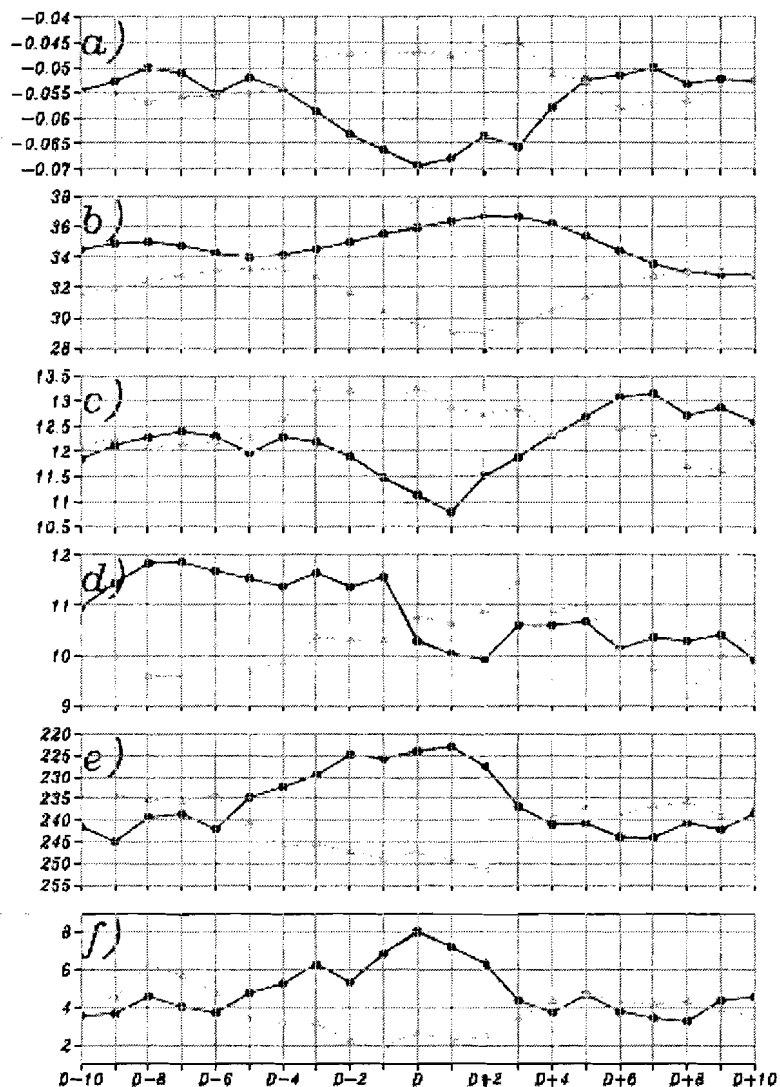


Figure 9 : Etude composite au dessus point de grille de Niamey entre les jours D_0-10 et D_0+10 , D_0 étant le jour l'indice de précipitations défini par Janicot et Sultan (2001) est maximum (minimum) pour les séquences humides en trait noir (sèches, en trait gris). a) gradient méridien du tourbillon potentiel d'ertel à 700 hPa (en PVU) ; b) moyenne dans la bande 3-5 jours du module de la transformée en ondelette du vent méridien à 700hPa (en $m^2.s^{-2}$) ; c) cisaillement du vent zonal entre 700 hPa et 925 hPa (en $m.s^{-1}$) ; d) cisaillement du vent zonal entre 925 hPa et 200 hPa (en $m.s^{-1}$) ; e) OLR (convection) en $W.m^{-2}$ sur un axe des ordonnées renversé ; f) précipitation moyenne observée sur Niamey (en mm).

c. Ondes d'est africaines et activité cyclonique sur l'Atlantique

Les Ondes d'Est Africaines ont été très tôt étudiées en raison de leur capacité à engendrer des cyclones sur l'Atlantique Nord (Carlson 1969). Ces ondes sont les principaux précurseurs de l'activité cyclonique sur l'Atlantique (Avila et Pasch 1992). Landsea (1993) a montré que 60% des cyclones de l'océan Atlantique sont initiés par des perturbations synoptiques d'origines africaines et que 85% des ouragans intenses tirent leur origine de ces ondes d'est (Figure 10). De même, Landsea et Gray (1992) ont montré que les années sèches (humides) au Sahel correspondent à une forte (faible) activité cyclonique. Ces auteurs ont émis l'hypothèse que ce contraste résulterait de la différence de nombre d'ondes au cours de ces deux phases : les années humides au Sahel sont caractérisées par la propagation d'ondes d'est actives et intenses contrairement aux années sèches durant lesquelles il y a une faible activité ondulatoire tant en fréquence qu'en intensité.



Figure 10: Andrew (1992) vu par le satellite GOES s'approchant de la Floride

Avila et al. (2000) ont trouvé qu'en moyenne 61 ondes d'est naissent par an sur le continent et traversent les côtes ouest africaines. Sur cette même période, ces auteurs notent que les ondes d'est africaines ont été les précurseurs de 62% des cyclones qui se sont déclenchés dans l'Atlantique. Ce résultat montre que le rôle des ondes d'est ne se limite pas uniquement à moduler la pluviométrie journalière au Sahel ; elles influencent aussi la convection humide sur l'océan ainsi que sur l'activité cyclonique qui s'y déroule.

Cependant, on connaît très peu les mécanismes physiques mettant en relation ondes d'est africaines et cyclones. Deux aspects de la variabilité des ondes d'est ont été plus particulièrement étudiés. A propos de la fréquence de ces ondes, il est plausible de penser que si le nombre d'ondes d'est augmente, le nombre de cyclones augmente. Il est tout aussi plausible de penser que des ondes d'intensité plus importante donnent plus fréquemment naissance à des cyclones. Cependant, sur de longues séries, il apparaît d'une part que la relation entre nombre d'ondes et nombre de cyclones n'est pas directe et d'autre part, très peu d'études ont abordé la relations ondes-cyclones du point de vue de l'activité des ondes parce qu'il est difficile de savoir ce qu'on entend par intensité d'une onde d'est, sachant que la structure de ce type d'onde est particulièrement compliquée. En effet, ces ondes peuvent avoir plusieurs centres, avec un vortex maximum à la fois au Sud de l'AEJ autour de 600-700 hPa dans la zone pluvieuse mais aussi autour de 850 hPa, au nord du jet (Pytharoulis et al 1999). Du fait de cette structure compliquée, il semble que la modification de structure de l'onde puisse aussi avoir une influence sur la naissance des cyclones.

Une étude réalisée par Thorncroft et Hodges (2001) sur les années 1979 à 1998 tend à montrer qu'il existe une certaine corrélation entre le nombre d'ondes d'est comptabilisées et le nombre de cyclones observés.

En effet, nous remarquons sur la figure 11 de très fortes corrélations certaines années (en particulier en 85-86 et pour la période 94-98), même si d'autres années sont marquées par une corrélation négative.

Cependant et de toute évidence, la corrélation n'est pas assez forte pour expliquer entièrement le phénomène de cyclogenèse. Ce résultat montre que l'hypothèse de Landsea liant la variabilité de l'activité cyclonique sur l'Atlantique à celle des ondes d'est africaines est intéressante mais n'est pas suffisante pour expliquer toute la variabilité interannuelle de l'activité cyclonique dans l'Atlantique Nord parce que la circulation de large échelle au-dessus de l'océan Atlantique joue un rôle non négligeable dans le déclenchement de l'activité cyclonique (Goldenberg et Shapiro, 1996). L'activité cyclonique est par exemple influencée par la température de surface de l'océan, la pression au niveau de la mer, le cisaillement vertical du vent, etc.

Durant la saison cyclonique 2002, Pasch et al (2004) ont d'ailleurs montré qu'un seul des 10 cyclones qui ont pris naissance sur l'atlantique était associé à des OEA. Avila et al (2000) ont aussi montré que bien que le nombre d'ondes soit presque constant d'une année à l'autre, la fraction d'ondes qui se développent en cyclones présente une variabilité interannuelle non négligeable.

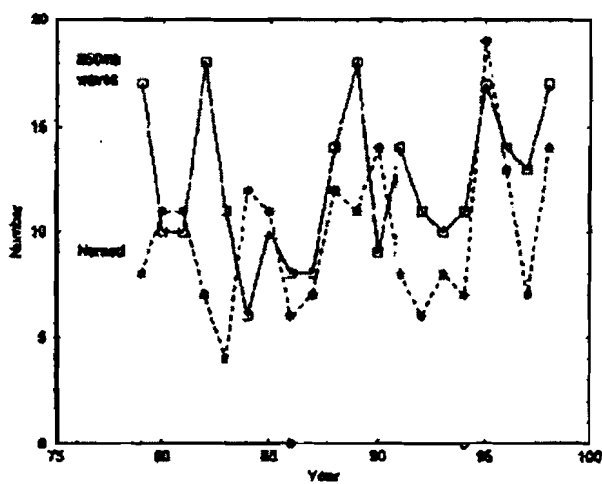


Figure 11: Relation entre Nombre d'ondes et Nombre de cyclones (Thorncroft and Hodges ; 2001)

Dans le cadre de la thèse de Moctar Camara soutenue en 2006, nous avons apporté notre contribution à la compréhension des liens qui existent entre l'activité cyclonique dans l'Atlantique tropicale Nord et les principaux caractéristiques du climat ouest africain de l'échelle interannuelle à l'échelle intrasaisonnière.

La thèse de Moctar Camara trouve son originalité dans le fait qu'elle apporte une contribution à la compréhension des facteurs qui précède la cyclogenèse sur l'Atlantique. On ne s'intéresse pas véritablement à ce qui se passe sur l'Atlantique, après la cyclogenèse, mais plutôt à ce qui se passe au dessus du continent Africain avant une cyclogenèse. On s'attachera à tester et à relever les incertitudes liées aux différentes hypothèses émises dans le passé pour relier l'activité cyclonique sur l'Atlantique au climat africain et en particulier, on précisera le rôle des ondes d'est Africaines. Considérant le chapitre précédent sur la complexité des interactions ondes-convection-pluie en Afrique de l'Ouest et avec des conditions de large échelle favorables sur l'Atlantique, le résultat principal de cette thèse est de montrer objectivement que, sur l'Afrique de l'Ouest, ce n'est pas tant le nombre d'onde d'est, ni leur fréquence qui va être déterminant dans la cyclogenèse, mais c'est surtout l'activité des ondes qui va contribuer à expliquer la récente hausse de l'activité cyclonique observée de 1995 sur l'Atlantique, et cela, sans lien direct avec la pluviométrie sur le continent.

Dans la première partie de cette thèse, après avoir présenté les principales caractéristiques du climat ouest Africain et effectué une étude bibliographique sur la cyclogenèse dans l'Atlantique, Moctar Camara a passé en revue les conditions favorables à la cyclogenèse dans l'Atlantique et les facteurs qui influencent cette cyclogenèse dans l'Atlantique Nord. Ensuite, il a effectué une classification des cyclones en fonction de leur

zone de naissance, de leur jour de déclenchement ainsi que de leur de leur durée de vie et enfin, il a étudié les conditions de large échelle qui existent en Afrique de l'ouest et sur l'Atlantique Nord avant le déclenchement d'une activité cyclonique sur l'Atlantique.

La saison cyclonique officielle dans l'océan Atlantique démarre du 1er juin au 30 novembre. A la fin de chaque saison cyclonique, le centre américain des ouragans (National Hurricane Center ; NHC) établit des cartes où sont répertoriées des informations sur chaque cyclone qui s'est produit (durée de vie, date de déclenchement, position et intensité du cyclone toutes les 6 heures, pression minimale, vitesse maximale, etc.), ainsi que les éventuels dommages matériels ou humains qu'il a occasionnés. Les forces et faiblesses de cette base de données peuvent être obtenues dans Landsea et al (1993). La classification de Moctar Camara s'est appuyée sur ces informations fournies par le NHC. Les deux cartes ci-dessous illustrent les produits fournies synthétiques fournis par le NHC pour deux années, 1998 et 2004 (Figures 12).

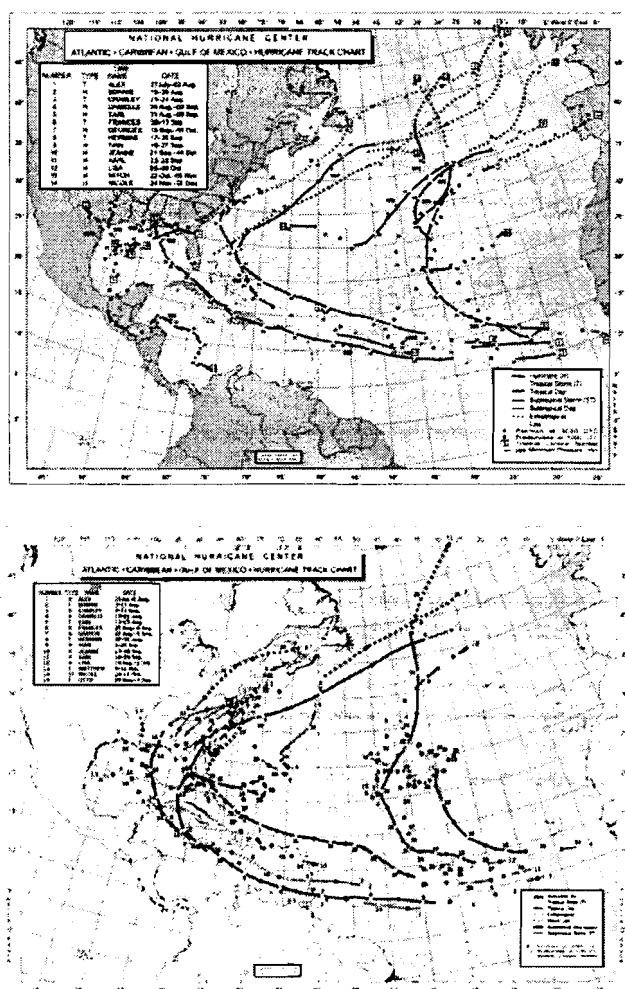


Figure 12 : Tableau synthétique de l'activité des cyclones sur l'Atlantique tropicale en 1998 (en haut) et en 2004 (en bas). La couleur verte indique le stade où le cyclone est dépression tropicale, jaune pour tempête tropicale, rouge pour ouragan. Source NHC.

A partir de l'ensemble des cartes du NHC, on représente sur la figure 13, les zones de naissances des cyclones et des intenses ouragans. Dans le cas des cyclones, nous remarquons la présence de deux axes de naissance préférentielle. Le premier est centré vers 12.5°N et s'étend des côtes ouest africaines à la longitude 100°W. Le second axe est centré vers 25°N et présente une forte densité entre 60°W et 100°W.

Le premier axe correspond bien à la trace du maximum de tourbillon relatif à 850 hPa (figure 14) suggérant que les cyclones nés dans cette zone ont pour origine les perturbations africaines. Tandis que la trajectoire Nord semble plutôt liée aux perturbations des latitudes tempérées, des dépressions froides d'altitudes et parfois, perturbations barocliniques des latitudes subtropicales (Hess 1995).

Le lien entre ondes d'est et cyclones intenses est aussi visible sur la figure 13 qui représente en cercle ouvert les cyclones non associés à des perturbations africaines et en cercles pleins ceux associés à des ondes d'est africaines. Les ouragans intenses sont générés en majeure partie par les ondes d'est africaines. Les cyclones, les ouragans et les ouragans intenses qui sont nés à l'ouest de 60°W sont généralement de courte durée de vie, tandis que ceux qui prennent naissance aux larges des côtes ouest africaines et initiés par des ondes d'est africaines semblent être de longue durée de vie.

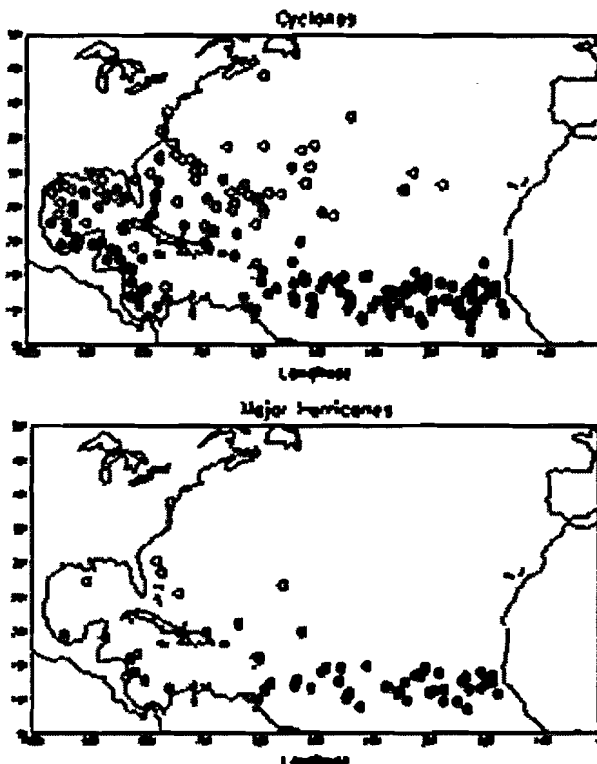


Figure 13 : zone de naissances des cyclones (haut) et des ouragans majeurs ou intenses (bas). Les cercles pleins correspondent aux cyclones associés à des ondes d'est Africaines alors que les cercles couverts ne sont pas associés (en première approximation) à des perturbations synoptiques en provenance d'Afrique.

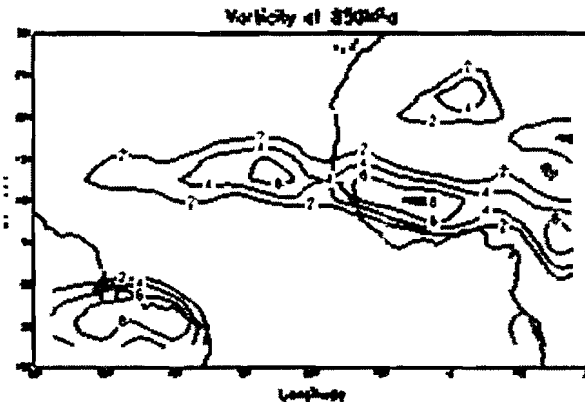


Figure 14 : Tourbillon relatif à 850 hPa (moyenne sur la période 1989-1994)

La question qui est posée dans le cadre de cette thèse est de savoir sur l'Afrique de l'Ouest (sur le continent) quelle est la différence entre une onde d'est qui irrite un cyclone sur l'Atlantique et une autre qui n'entraîne pas de cyclogenèse sur l'Atlantique.

Pour répondre à cette question, une étude composite est menée ; chaque composite est composé de 48 cas d'ondes d'est africaines. Le tracking du maximum de vorticité relative à 850hPa accompagnant l'onde associée à un cyclone est résumé sur la figure 15 pour la période 1989-1994. Ces trajectoires ont été obtenues en suivant les maximums de vorticité relative du trajet des ondes d'est associées à des cyclones les jours de déclenchement de ces derniers. Ces ondes d'est sont ensuite suivies en retour sur le continent

africain jusqu'à ce que le maximum de vorticité relative soit inférieur au seuil de $0.5 \cdot 10^{-5} \text{ s}^{-1}$. Un tel seuil a été précédemment utilisé par Thorncroft et Hodges (2001) pour faire un tracking des ondes d'est. Seuls les cyclones qui se sont déclenchés sur la période 1989-1994 sont représentés dans le but de rendre cette figure plus lisible.

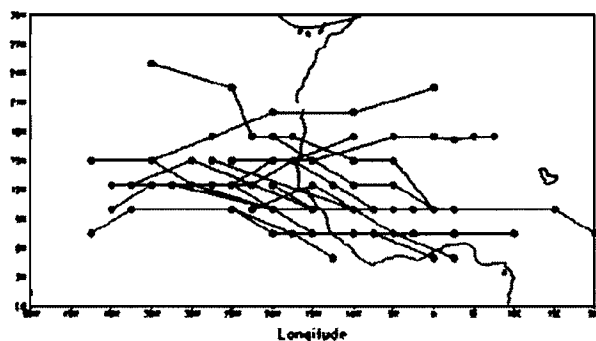


Figure 15 : Trajectoire des OEA associées à des cyclones sur la période 1989-1994. Les jours de naissance des cyclones sont obtenus à partir des cartes de la NHC.

Par ailleurs, une analyse en ondelette du vent méridien à 700 hPa pour le composite des ondes d'est associées à des cyclones a été effectuée pour appréhender toutes les échelles de fréquence qui interviennent au cours de la saison.

La figure 16 présente la moyenne du module de l'analyse en ondelette du vent méridien à 700 hPa dans la bande 3-5 jours pour les 48 cyclones retenus dans cette étude sur la période 1989-2003 et qui sont nés sur l'Atlantique Est. Cette moyenne a été faite aux larges des côtes ouest africaines (30°W - 15°W , 5°N - 15°N). La bande de latitude 5°N - 15°N ne prend en compte que l'axe sud de propagation des ondes d'est. Le trait vertical représente le jour moyen de naissance des cyclones selon les archives du centre américain des ouragans (NHC). Le module de la transformée en ondelette du vent méridien à 700 hPa croît et atteint son maximum le jour moyen de naissance des cyclones, suggérant que l'activité ondulatoire atteint un maximum le jour de la cyclogenèse. La courbe décroît aussitôt après le jour de déclenchement moyen des cyclones.

Modulus of wavelet analysis(Cyclonic AEWs)

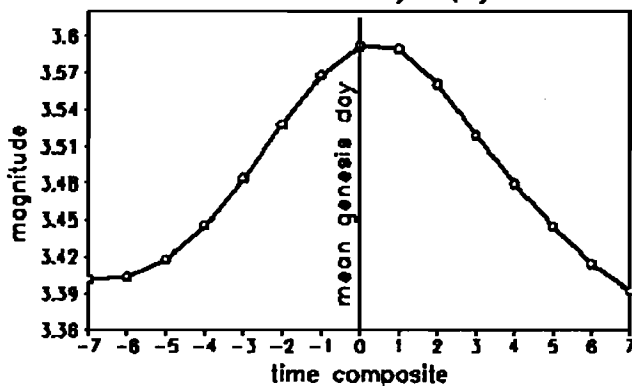


Figure 16 : Cumul du module de la transformée en ondelette du vent méridien à 700 hPa dans la bande 3-5 jours dans le cas des ondes d'est associées à des cyclones. T = 0 correspond au jour moyen de naissance des cyclones.

Sur la figure 17, le module de la transformée en ondelette du vent méridien à 700 hPa a été aussi tracée pour la saison cyclonique 1995 sur le même domaine (30°W - 15°W , 5°N - 15°N). Les traits représentent les jours de déclenchement des cyclones en 1995 ; année de très forte activité cyclonique. En effet au cours de cette année 19 cyclones sont nés et plus de 90% d'entre eux étaient associés à des ondes d'est Africaines. À l'exception de Pablo (4 octobre), tous les autres cyclones qui sont nés dans ce domaine (Felix : 8-22 août; Humberto : 22 août – 1er Septembre ; Luis 27 août – 11 septembre ; et Noel 11 septembre – 16 octobre) sont associées à la présence d'une forte énergie dans la bande 3-5 jours, suggérant la présence d'une forte activité ondulatoire dans la bande 3-5 jours. Ces cyclones sont aussi caractérisés par leur longue durée de vie (supérieure à 9 jours). Par contre, le cyclone Pablo est caractérisé par la présence d'un

régime 6-9 jours et d'une courte durée de vie. Ce résultat confirme que c'est l'activité des ondes qui va être prépondérante dans la cyclogenèse et non, le nombre d'onde d'est, même si des périodes de forte activité ondulatoire peuvent ne pas être associées à une cyclogenèse (autour du 1^{er} Août).

Modulus of wavelet analysis in 1995

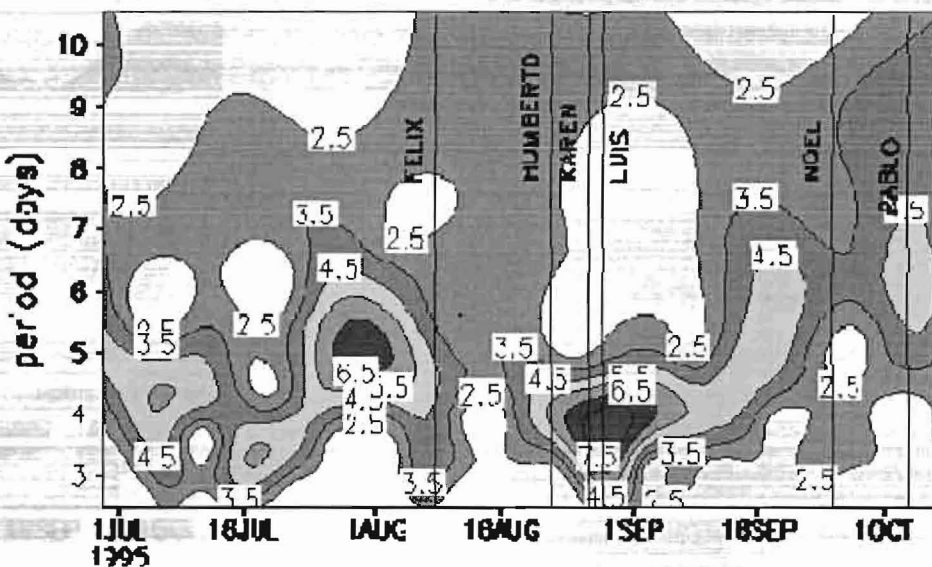


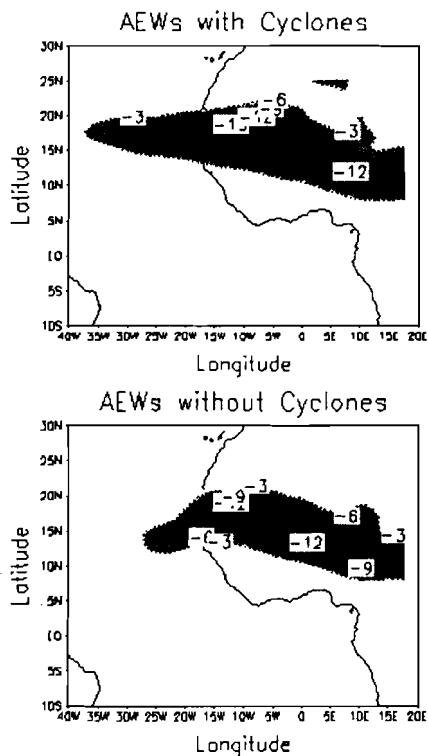
Figure 17 : Module de la transformée en ondelette du vent méridien à 700 hPa sur le domaine (30°W- 15°W, 5°N- 15°N) pour la saison cyclonique 1995 (haut). Les traits représentent les jours de naissance des cyclones. Cumul du module de la transformée en ondelette du vent méridien à 700 hPa dans la bande 3-5 jours dans le cas des OEA associées à des cyclones. T = 0 correspond au jour moyen de naissance des cyclones.

La figure 18a représente le gradient méridien de PV à 315°K. On remarque que les ondes d'est associées à des cyclones présentent les valeurs négatives les plus fortes avec des pointes à $15 \cdot 10^{-14} \text{ K m s}^{-1} \text{ Kg}^{-1}$ contre $-12 \cdot 10^{-14} \text{ K m s}^{-1} \text{ Kg}^{-1}$ pour les ondes non associées des cyclones. Ces zones négatives sont celles où se développent les instabilités barocliniques et barotropes nécessaires à la croissance des ondes. Ces zones d'instabilités se prolongent plus loin sur l'océan dans le cas des ondes associées à des cyclones. Donc à priori on pourrait dire que les ondes associées à des cyclones sont plus actives en amplitude que celles non associées à des cyclones. Ces résultats sont cohérents avec les études de Landsea and Gray (1992) qui ont émis l'hypothèse qu'à l'échelle interannuelle, une active saison cyclonique est caractérisée par la propagation du continent vers l'océan d'ondes de fortes amplitudes.

La figure 18b représente le tourbillon relatif à 850 hPa. Les ondes associées à des cyclones ont les plus fortes valeurs positives de tourbillon relatif à 850 hPa aussi bien sur le continent ($9 \cdot 10^{-6} \text{ s}^{-1}$) que sur l'océan. Ce résultat est cohérent avec les conclusions de l'analyse du gradient méridien de PV. Les ondes associées à des cyclones ont une plus forte amplitude. Ces ondes de forte amplitude sont probablement plus aptes à déclencher une activité cyclonique sur l'océan (Emmanuel 1989 ; Thorncroft and Hodges 2001).

On note par ailleurs la présence de valeurs positives de tourbillon relatif sur le désert du Sahara suggérant la présence à ce niveau de la convection sèche en relation avec la « heat low » (dépression saharienne de basse couche). Cette convection ne montre pas de différence systématique entre les deux types d'ondes. Ce résultat suggère que la « heat low » n'a pas un impact direct sur la cyclogénèse, mais cela reste à être confirmé.

a) Gradient méridiien de PV



b) Tourbillon relatif 850hPa

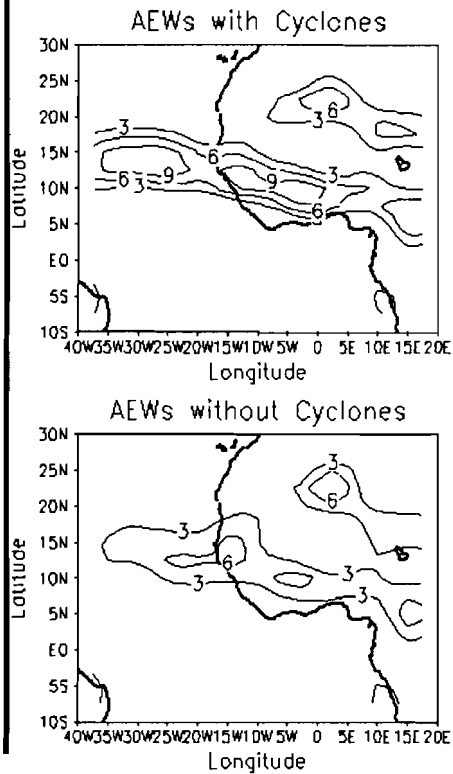


Figure 18 : (a) Gradient méridiien de PV sur l'isentrope (ligne d'égal température potentielle) 315K pour les OEA associées à des cyclones (haut) et pour les OEA non associées à des cyclones (bas). Seules les valeurs négatives ont été tracées. L'unité est : 10-14 K m s⁻¹ Kg⁻¹. (b) Tourbillon relatif à 850 hPa dans le cas des OEA associées à des cyclones (haut) et des OEA non associées à des cyclones (bas). Seules les valeurs positives ont été tracées. L'unité est : 10-6 s⁻¹.

Dans la suite, la variabilité interannuelle de l'activité cyclonique a été étudiée afin de mettre en évidence les différences entre une période inactive (1991-1994) et une période active (1998-2001) du point de vue de l'activité cyclonique sur l'Atlantique. Plus particulièrement, les structures des ondes d'est durant ces deux périodes contrastées sont présentées ici. Nous tenterons par la suite de montrer en quoi les ondes d'est pourraient contribuer à expliquer la récente hausse de l'activité cyclonique observée depuis 1995.

La variance du vent méridien à 700 hPa filtré entre 3 et 5 jours en Mai-Juin-Juillet (MJJ, période avant la saison cyclonique) et en Août-Septembre-Octobre (ASO, saison cyclonique) est représentée sur la figure 19.

En période de forte activité cyclonique sur l'Atlantique, l'activité des ondes d'est est forte sur l'Afrique et sur l'océan Atlantique dès MJJ. Durant ASO, la variance du vent méridien à 700 hPa filtré entre 3 et 5 jours présente pour les deux périodes les 3 maxima qui sont les trajectoires préférentielles des ondes d'est sur l'Afrique et sur l'Atlantique : 2 maxima se trouvent à l'ouest de 20°W sur le Sahel et le Golfe de Guinée ; Ces deux trajectoires vont converger sur l'océan autour de 20°N correspondant à la troisième trajectoire des ondes sur l'Atlantique.

Les années de forte activité cyclonique sur l'Atlantique sont caractérisées par la présence d'une forte activité ondulatoire (forte variance) sur les deux trajectoires africaines (Sahel et Golfe de Guinée) et une décroissance d'activité sur la trajectoire océanique. La décroissance de la variance sur la trajectoire océanique pourrait être expliquée par la transformation en cyclones d'un grand nombre d'intenses ondes d'est.

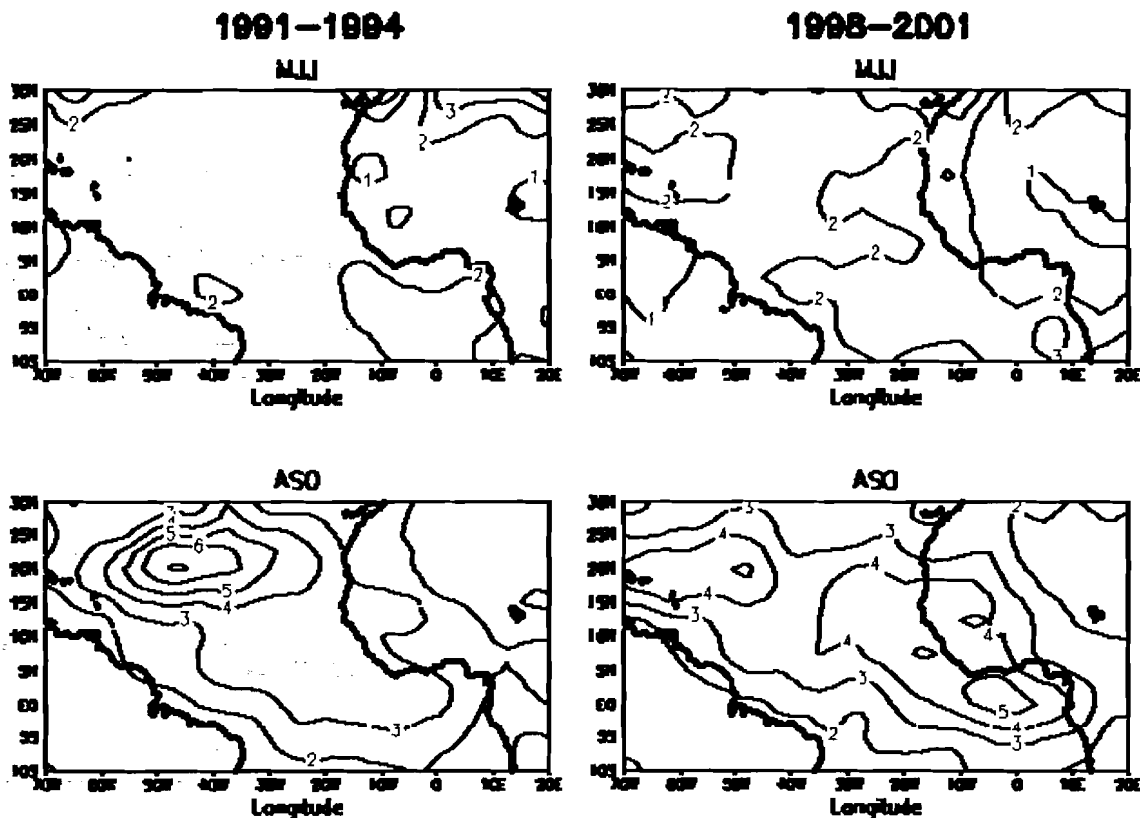


Figure 19 : Variance du vent méridien à 700 hPa filtré entre 3 et 5 jours durant MJJ (haut) et ASO (bas) pour la période active (droite) et la période inactive (gauche). L'unité est : n2.s-2.

Plus précisément, cette décroissance de la variance du vent méridien filtré entre 3 et 5 jours sur l'océan semble être liée à la diminution du nombre d'ondes d'est de forte amplitude. En effet, un calcul du nombre d'ondes de forte amplitude sur trois points de grille dans les zones où se trouvent les maxima de variance (0°W - 5°N pour la trajectoire Sud, 20°W - 15°N pour la trajectoire Nord et 40°W - 15°N pour la trajectoire océanique) a été mené. Les ondes d'est ont été détectées en considérant que les fortes fluctuations du vent méridien filtré entre 3 et 5 jours durant 3 jours consécutifs correspondent au passage d'une onde (Diedhiou et al 1999). Ces résultats sont récapitulés sur la table 4.

	Position	$(0^{\circ}\text{W}$ - $5^{\circ}\text{N})$	$(20^{\circ}\text{W}$ - $15^{\circ}\text{N})$	$(40^{\circ}\text{W}$ - $15^{\circ}\text{N})$
Période	Trajectoire Sud	Trajetoire Nord	Trajetoire océanique	
Active (1998-2001)	64	53	44	
Inactive (1991-1994)	49	48	48	

Table 4 : Nombre d'intenses Ondes d'Est Africaines (OEAs) sur 3 points de grille (0°W - 5°N , 20°W - 15°N , 40°W - 15°N) représentant respectivement les trajectoires Sud, Nord et Océanique des OEAs sur l'Afrique et l'Atlantique Nord.

Cette table montre que le nombre d'ondes d'est est plus élevé au dessus des deux trajectoires continentales (Est de 20°W) ; tandis que sur l'océan, ce nombre est plus faible en période de forte activité cyclonique. Ce résultat est ainsi cohérent avec la transformation sur l'océan d'un grand nombre d'onde d'est de forte amplitude en cyclones en période active.

Partant des hypothèses précédentes sur un lien potentiel entre la pluviométrie au Sahel et l'activité cyclonique sur l'Atlantique, nous représentons sur la figure 20, l'index pluviométrique de Lamb. Lamb (2003) a calculé son index en utilisant la moyenne de Avril à Octobre de 20 stations pluviométriques qui se situent entre les latitudes 11°N- 18°N et à l'ouest de 10°E sur la période 1950-2001. Les deux séquences (périodes sèches et humides) qui caractérisent le changement de la pluviométrie au Sahel apparaissent avec une rupture autour de 1970.

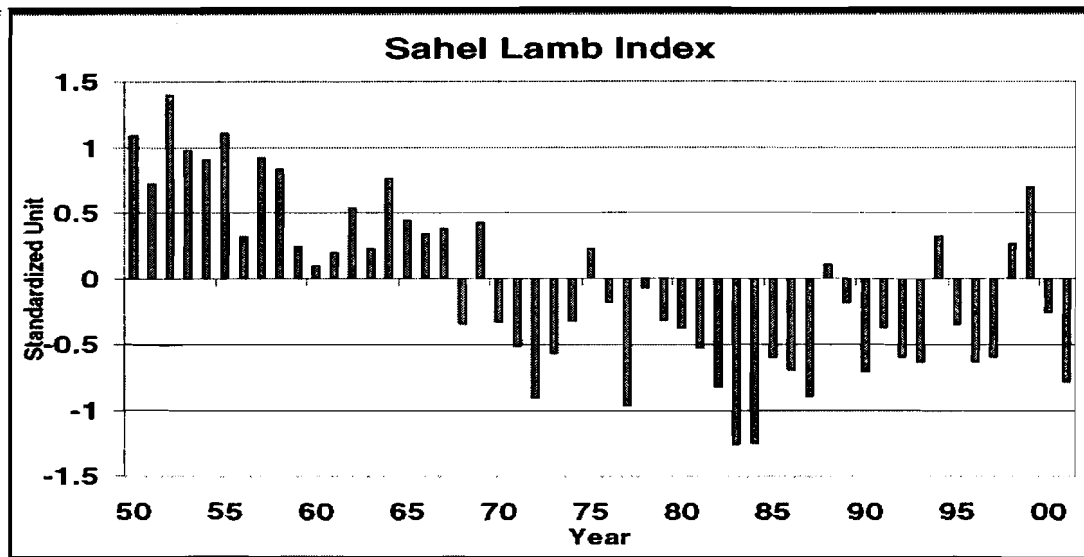


Figure 20 : Index sahélien de Lamb sur la période 1950-2001.

Pour caractériser l'activité d'une saison cyclonique, la NOAA utilise 4 paramètres à savoir le nombre de tempêtes tropicales, le nombre d'ouragans, le nombre d'intenses ouragans et l'ACE (Accumulated Cyclone Energy). L'ACE de la NOAA est calculé en tenant compte du nombre, de la durée de vie et de l'intensité des cyclones (tempêtes, ouragans et ouragans intenses). Pour chaque cyclone, on calcule l'ACE en sommant les carrés des maximums de vitesse de vent soutenus durant toutes les 6 heures lorsque ce système est au stade de tempête tropicale et d'ouragan. L'ACE saisonnier est ainsi obtenu en sommant les ACE de tous les cyclones qui se sont déclenchés au cours de la saison. Durant les années de forte activité cyclonique, les cyclones qui prennent naissance au niveau de la MDR et qui deviennent plus tard des ouragans et intenses ouragans constituent la fraction la plus importante de l'ACE (Goldenberg and Shapiro 1996). L'indice d'ACE est le pourcentage d'ACE par rapport à la valeur médiane de la période 1951-2000 qui est de $23,18 \cdot 10^4 \text{ m}^2 \text{s}^{-2}$ (soit 87,5 kts² ; kts = noeuds).

Une saison cyclonique est active (au dessus de la normale) lorsque son indice d'ACE est très supérieur à 117% de la médiane ou légèrement supérieure à 117% de la médiane avec au moins 2 des 3 paramètres restants (nombre de tempêtes, nombre d'ouragans et nombre d'ouragans intenses) supérieures à leur moyenne à long terme. Une saison cyclonique est normale lorsque son index d'ACE est compris entre 75% et 117% de la médiane ou que cet index est légèrement supérieur à 117% avec 1 des 3 autres paramètres supérieurs à la moyenne à long terme. Une saison inactive (en dessous de la normale) a un index d'ACE inférieur à 75% de la médiane.

Sur la figure 21, le nombre de cyclones présente bien des fluctuations interannuelles ponctuées par des périodes de hausse (1950-1970) et de diminution (1970-1994) de l'activité cyclonique, en phase avec les hypothèses de Landsea and Gray (1992).

Cependant, au cours de la période récente (1995-2004), excepté la saison cyclonique 1997, l'activité cyclonique annuelle est au-dessus de la moyenne en considérant le nombre de cyclones, d'ouragans et d'ouragans intenses. Ces mêmes tendances sont notées pour l'ACE avec cependant, la présence d'une activité en dessous de la moyenne pour l'année 2002. Généralement, nous notons une tendance à la hausse de l'activité cyclonique durant la période récente (1995 à nos jours), sans lien direct en première approximation avec la pluviométrie au Sahel. D'ailleurs, sur les deux séries, on note que les années humides ne correspondent pas forcément à une forte activité des ouragans intenses de même que les

années sèches ne sont pas toujours associées à une faible activité cyclonique. A titre d'exemple, 1995 fut une année sèche tandis qu'on y a noté une forte activité cyclonique et surtout celle des ouragans majeurs.

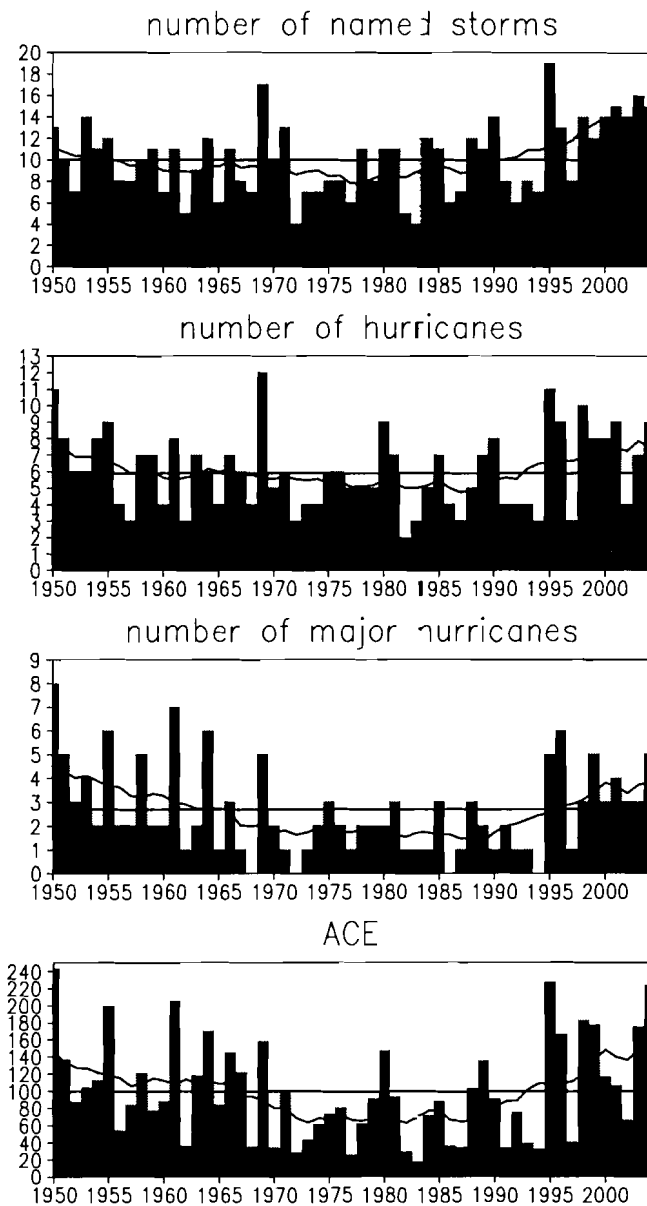


Figure 21 : De haut en bas, Nombre de cyclones, Nombre d'ouragans, nombre d'ouragans intenses et indice de l'énergie accumulée par les cyclones (ACE) sur la période 1950-2004. Le trait horizontal représente la moyenne de la série temporelle 1950-2004. La courbe représente une moyenne glissante sur 10 ans de cette série.

La table 5 montre le nombre de cyclones et l'index ACE sur les périodes 1970-1994 et 1995-2004. Comparée à la période 1970-1994, on note une augmentation des nombres de tempêtes, ouragans et ouragans intenses, de l'indice d'ACE, en somme de l'activité cyclonique au cours de la période récente ; la hausse la plus significative étant ceux du nombre d'ouragans intenses et de l'indice d'ACE. Par ailleurs, la période récente est marquée par une légère augmentation de la fraction de cyclones (0.70) qui prend naissance dans la zone tropicale (0°N - 25°N) ; cette fraction est de 0.64 pour la période 1970-1994. Plusieurs paramètres ont été analysés et ceux qui pourrait expliquer la forte activité cyclonique de cette récente période sont : la SST, le cisaillement vertical du vent entre les basses couches et les hautes couches de l'atmosphère, le flux de mousson Ouest Africain.

Nombre de cyclones Période	Tempêtes	Ouragans	Ouragans intenses	ACE
1970-1994	10,14	5,77	2,17	64,76
1995-2004	13,77	8,62	4	147,9

Table 5 : Nombre de cyclones (tempêtes baptisées, ouragans et ouragans intenses) sur les périodes 1970-1994 et 1995-2004.

Après avoir testé les hypothèses émises dans le passé pour expliquer la récente hausse de l'activité cyclonique depuis 1995 (réchauffement des eaux de l'Atlantique Nord, faible cisaillement vertical de vent entre les basses couches et les hautes couches de l'atmosphère), Moctar Camara précise durant cette thèse que cette récente hausse est aussi liée à une augmentation de l'activité des ondes d'est africaines le long de leur trajectoire Sud (en Afrique et sur l'Atlantique Est). Il confirme par ailleurs qu'il n'y a pas de lien direct avec le nombre d'onde d'est et que les ondes le long de l'axe Nord ont peu d'impact sur la cyclogenèse.

Cela est illustré sur la figure 22 ci-dessous où l'activité ondulatoire sur l'axe Sud des ondes d'est africaines montre une phase décroissante de 1970 à 1990 puis une phase croissante qui devient plus prononcée à partir de 1995. Sur la période antérieure à 1995, on note quelques séquences de forte activité ondulatoire (1977-1980 et 1988 et 1990) qui correspondent à une forte activité cyclonique surtout celle des ouragans intenses. Sur l'océan, la variance du vent méridien à 700 hPa filtrée entre 3 et 5 jours montre des caractéristiques opposées à la boîte continentale. On remarque une augmentation de l'activité ondulatoire jusqu'aux années 90 et ensuite, on note la présence d'une phase décroissante qui est compatible avec la probable transformation d'un grand nombre d'intenses ondes d'est en cyclones sur la période récente (1995-2004). Ces résultats mettent en évidence une fois de plus le rôle primordial que jouent les ondes d'est africaines le long de l'axe Sud dans l'initiation des ouragans majeurs sur l'Atlantique Nord.

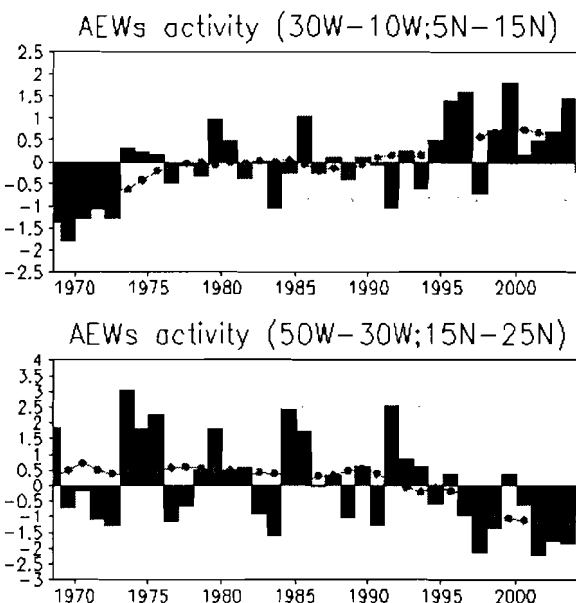


Figure 22 : Anomalie moyenne sur les trajectoires Sud (haut), océanique (bas) de la variance du vent méridien à 700 hPa filtré entre 3 et 5 jours. Les domaines Sud et océaniques considérés sont respectivement ($20^{\circ}W$ - $10^{\circ}E$, $0^{\circ}S$ - $10^{\circ}N$) et ($45^{\circ}W$ - $25^{\circ}W$, $15^{\circ}N$ - $20^{\circ}N$). La moyenne est faite par rapport à la climatologie 1980-2000 durant août -septembre -octobre (ASO) de 1968 à 2004. La courbe représente une moyenne glissante sur 10 ans.

d. Quelques références bibliographiques sur le sujet :

Les articles ci – dessous n'ont pas été tous explicitement cités dans ce document mais ont servi pour les différentes études et ont été cités dans les différents articles référencés dans la liste des publications;

- Ali, A., T. Lebel, Amani, A. 2003: Scale invariance of Sahelian rainfields. *J. of Hydrometeo.*, 4(6), 996-1011
- Ali A., A. Amani, A. Diedhiou, T. Lebel, 2005. Rainfall estimation in the Sahel. Part 2: Evaluation of Raingauge Networks in the CILSS Countries and Objective Intercomparison of Rainfall Products. *J. of Applied Meteor.*, 44(11) pp. 1707–1722.
- Avila, L. A.; R. J. Pasch, and J. Jiing, 2000 : Atlantic tropical systems of 1996 and 1997 : Years of contrasts. *Bull. Amer. Met. Soc.*, 128, 3695-3709.
- Avila, L. A., and R. J. Pasch, 1992 : Atlantic tropical systems cf 1991. *Mon. Wea. Rev.*, 120, 2688-2696.
- Avila, L. A., and R. J. Pasch, 1995 : Atlantic tropical systems cf 1993. *Mon. Wea. Rev.*, 123, pp.887-896.
- Barmou B MB; 1996. Analyse des impacts climatiques sur la dynamique de l'environnement dans l'arrondissement de Bouza au Niger. Mémoire de maîtrise, UNB-Cotonou (Bénin); 86p.
- Burpee, R.W., 1972: The origin and structure of easterly waves in the lower troposphere in North Africa. *J. Atmos. Sci.*, 29, 77-90.
- Burpee, R.W., 1974: Characteristics of North African easterly waves during the summers of 1968 and 1969. *J. Atmos. Sci.*, 31, 1556-1570.
- Burpee, R.W., 1975: Some features of synoptic-scale waves based on a compositing analysis of GATE data. *Mon. Wea. Rev.*, 103, 921-925.
- Cadet, L. D. And N. O. Nhli., 1987 : Water vapour transport over Africa and the Atlantic ocean during summer of 1979, *Quart. J. Roy. Meteor. Soc.*, 113, 581-602.
- Carlson, T.N., 1969: Some remarks on African disturbances and their progress over the tropical Atlantic. *Mon. Wea. Rev.*, 97, 716-726.
- Charney, J. G., and M. E. Stern, 1962 : On the stability of internal baroclinic jets in a rotating atmosphere. *J. Atmos. Sci.*, 19, 159-172.
- Charney J. G., 1975. Dynamics of deserts and drought in the Sahel. *Quart. J. Roy. Met. Soc.*, 101, 193-202.
- Chen, Y.L. and Y. Ogura, 1982: Modulation of convective activity by large-scale flow pattern observed during GATE. *J. Atmos. Sci.*, 39, 1260-1279
- Davis, C. A., and K. Emanuel , 1991 : Potential Vorticity Diagnostics of Cyclogenesis. *Bull. Amer. Meteor. Soc.*, 119, 1929-1953.
- DeMaria, M. J.A. Knaff, and B.H. Connell, 2001: A Tropical Cyclone Genesis Parameter for the Tropical Atlantic. *Weather Forecast.*, 16, 219-233.
- Dhonner G., 1974 : Traité de météorologie tropicale. Météo-France, 151p.
- Dickinson, M., and J. Molinari, 2000 : Climatology of sign reversal of the meridional Potential Vorticity gradient over Africa and Australia. *Mon. Wea. Rev.*, 128, 3890-3900. Diedhiou A., S. Janicot, A. Viltard, P. de Felice, H. Laurent, 1998a : Evidence of two regimes of easterly waves over West Africa and the tropical Atlantic. *Geophys Res. Let.*, 25 : 2805-2808.
- Diedhiou A., S. Janicot, A. Viltard, P. De Felice, H. Laurent, 1999. Easterly waves regimes and associated convection over West Africa and the tropical Atlantic : results from the NCEP/NCAR and ECMWF reanalyses. *Climate. Dynamics.*, 15, 795-822.
- Diedhiou, A., S. Janicot, A. Viltard; P. de Félice, 2001: Composite patterns of easterly waves disturbances over West Africa and the tropical Atlantic. *Climate. Dynamic.*, 18, 241-253.
- Diedhiou, A., S. Janicot, A. Viltard and P. de Félice, 2002a: Energetics of easterly waves disturbances over West Africa and the tropical Atlantic. *Climate Dynamic.*, 18, 487-500.
- Diedhiou A., Royer J.F., Poccard I., Lebel T. (2002) :Impact of greenhouse warning on the variability of african easterly waves. XXVII General Assembly of European Geophysical Society (Nice, 21-26/04/02). Session Océans & Atmosphères :OA23.01.Résumés in CD ROM ISSN 1029-7006, vol. 4).
- Diongue A., J.-P Lafore, J.-L.Redelsperger and R. Roca, 2002: "Numerical study of a sahelian synoptic weather system: Initiation and mature stage of convection and its interactions with the large scale dynamics", *Quart. J. R. Met. Soc.*, 128, 1899-1927
- Douville H., F. ; Chauvin, J.F. Royer, D. Salas y Méria, S. Tyteca, 2002 : Sensitivity of the hydrological cycles to increasing amounts of greenhouse gases and aerosols. *Climate Dynamics.*, 20, 45-68.
- Duvel, J.P., 1989: Convection over tropical Africa and the Atlantic ocean during northern summer. Part I: Interannual and diurnal variations. *Mon. Wea. Rev.*, 117, 2782-2799.
- Duvel, J.P., 1990: Convection over tropical Africa and the Atlantic ocean during northern summer. Part II: Modulations by easterly waves. *Mon. Wea. Rev.*, 118, 1855-1868.

- Emanuel, K.A., 1991: A scheme for representing cumulus convection in large-scale models. *J. Atmos. Sci.*, 48, 2313-2335.
- Emanuel, K.A., 1993: The Representation of Cumulus Convection in Numerical Models. (Editor, with D.J. Raymond) *Meteor. Mono.* 24, No. 46, Amer. Meteor. Soc., Boston, 246 pp.
- Fontaine B., Janicot S. and Moron V. 1995: Rainfall anomaly patterns and wind field signals over West Africa in August (1958-1989), *J. Climate*, 8, 1503-1510.
- Gray, W. M., 1979 : Hurricanes : their formation, structure and likely role in the tropical circulation. *Meteorology over the tropical oceans*. Royal Meteorological Society, Bracknell, England, D. B. Shaw, ED., pp. 155-218.
- Gray, W.M, 1984a : Atlantic seasonal hurricane frequency : Part I. El Nino and 30 mb Quasi-Biennial Oscillation influences. *Mon. Wea. Rev.*, 112, 1649-1668.
- Gray, W.M, and C.W. Landsea, 1992 : African rainfall as a precursor of hurricane-related destruction on the U.S. East Coast. *Bull. Amer. Meteor. Soc.*, 73, 1352-1364.
- Grist, J. P, 2002: Easterly waves over Africa. Part I: the seasonal cycle and contrasts between wet and dry years. *Mon. Wea. Rev.*, 130, 197-211.
- Grist, J. P, S. E. Nicholson, and A. I. Barcilon, 2002: Easterly waves over Africa. Part II: observed and modeled contrasts between wet and dry years. *Mon. Wea. Rev.*, 130, 212-225.
- Grueber and Krueger, 1984: The status of the NOAA outgoing longwave radiation data set. *Bull. AM. Meteorol. Soc.*, 65, 958-962.
- Hodges, K. I., and C. D. Thorncroft, 1997 ; Distribution and statistics of African mesoscale convective weather systems based on the ISCCP Meteosat imagery. *Mon. Wea. Rev.*, 125, 2821-2837.
- Ioannou P. and R.S. Lindzen (1986): Baroclinic instability in the presence of barotropic jets. *J. Atmos. Sci.*, 43, 2999-3014
- Janicot S. et B. Sultan (2001), Intra-seasonal modulation of convection in the West African monsoon, *Geophysical Research Letter*, 28, 3, 523-526
- Kalnay, E. M. Kanamitsu, R. Kistler, W. Collins, and al. ,1996 : The NCEP/NCAR 40 year reanalysis project. *Bull. Amer. Meteor. Soc.*, 77, 437-471.
- Karyampudi, V. M., and H. F. Pierce, 2002: Synoptic-scale influence of the Saharan air layer on tropical cyclogenesis over the eastern Atlantic. *Mon. Wea. Rev.*, 130, 3100-3128.
- Karyampudi, V. M., and H. F. Pierce, 2002: Synoptic-scale influence of the Saharan air layer on tropical cyclogenesis over the eastern Atlantic. *Mon. Wea. Rev.*, 130, 3100-3128.
- Lafore, J.P and M. W. Moncrieff, 1989 : A numerical investigation of organization and interaction of the convective and mesoscale regions of squall line. *J. Atmos. Sci.*, 46, 521-544.
- Lamb, P. J., 1983 : West African water vapor variations between recent contrasting subsaharan rainy seasons. *Tellus*, Ser. A, 35, 198-212.
- Lamb, P.J., 1985 : Rainfall in Subsaharian West Africa during 1941-83. *Z. Gletscher Glazialgeol.*, 21, 131-139.
- Landsea, C.W., and W.M. Gray, 1992 : The strong association between Western Sahelian monsoon rainfall and intense Atlantic hurricanes. *J. Climate*, 5, 435-453.
- Landsea, C. W., 1993 : A climatology of intense (or major) Atlantic hurricanes . *Mon. Wea. Rev.*, 121, 1703-1713.
- Landsea, C. W.,G.D. Bell, W.M. Gray, and S.B. Goldenberg, 1998 : The extremely active 1995 Atlantic hurricane season : Environmental conditions and verification of seasonal forecasts. *Mon. Wea. Rev.*, 126, 1174-1193.
- Lau, K.-H., and N.-C. Lau, 1990 : Observed structure and propagation characteristics of tropical cyclone summertime disturbances. *Mon. Wea. Rev.*, 118, 1888-1913.
- Laurent H., N. D'Amato and T. Lebel, 1998 : How important is the contribution of the Mesoscale Convective Complexes to the Sahelian rainfall ? *Phys. Chem. Earth*, 23, 629-633.
- Lavaysse C, A. Diedhiou, Laurent H, Lebel T, 2006 African Easterly Waves and convective activity in wet and dry sequences of the West African Monsoon. *Climate Dynamics* 27(2-3): 319.
- Le Barbé, L., and T. Lebel, 1997: Rainfall climatology of the HAPEX-Sahel region during the years 1950-1990. *J. Hydrol.* 188-189, 43-73.
- Le Barbé, L. ; T. Lebel, and D. Tapsoba, 2002, Rainfall variability in West Africa during the years 1950-1990, *J. Climate*, 15(2), 187-202.
- Lebel, T.; Diedhiou, A.; Laurent, H. 2003b: Seasonal cycle and interannual variability of the Sahelian rainfall at hydrological scales. *Journal of Geophysical Research*. Vol. 108; D8. 8389
- Hourdin F, Musat I, Bony S, Braconnot P, Codron F, Dufresne J, Fairhead L, Filiberti M, Friedlingstein P, Grandpeix J (2006) The LMDZ4 general circulation model: climate performance and sensitivity to parametrized physics with emphasis on tropical convection. *Climate Dynamics* 27(7-8): 787-813.
- Mass, C., 1979 : A linear primitive equation model of African wave disturbances. *J. Atmos. Sci.*, 36, 2075-2092.

- Mathon, V., and H. Laurent, Life cycle of the Sahelian mesoscale convective cloud systems, *Quart. J. Roy. Meteor. Soc.*, 127, 377-406, 2001.
- Mathon V., H. Laurent and T. Lebel, 2002a: Mesoscale convective system rainfall in the Sahel. *J. Applied Meteo.*, 41, 1081-1092.
- Mathon V., A. Diedhiou, H. Laurent, 2002c: Relationship between easterly waves and mesoscale convective systems over the Sahel. *Geophys. Res. Lett.*, vol. 29 (8) : 571-4.
- Maynard, K. ; J.F. Royer, F. Chauvin, 2002 : Impact of greer house warming on the West African summer monsoon. *Climate Dynamics*, vol 19, pp 499-514.
- Miller, R. and R.S. Lindzen (1992) Organization of rainfall by an unstable jet with application to African waves. *J. Atmos. Sci.*, 49, 1523-1540
- Norquist, D.C., E.E. Recker and R.J. Reed, 1977: The energetics of African wave disturbances as observed during Phase III of GATE. *Mon. Wea. Rev.*, 105, 334-342.
- Philippon, N. et Fontaine, B. (2002).The relationship between the sahelian and previous 2and guinean rainy season :a monsoon regulation by soil wetness ? *Annales Geophysicae*, 20575, 582.
- Pytharoulis, I. And C. D. Thorncroft, 1999 : The low-level structure of African Easterly Waves in 1995. *Mon. Wea. Rev.*, 127, 2266-2280.
- Redelsperger J.L., Diongue A., Diedhiou A., Ceron J.P., Diop M., Gueremy J.F., Lafore J.P., 2002b: Multiscale description of a Sahelian synoptic weather system representative of West African monsoon. *Quart. Journ. Roy. Meteor. Soc.*,128 : 1229-1257.
- Redelsperger, J.L., Thorncroft, C., Diedhiou, A., Lebel, T., Parker, D.J. and J. Polcher, 2006: African Monsoon Multidisciplinary Analysis (AMMA): An International Research Project and Field Campaign. Published in *BAMS*, Volume 87, Issue 12 (December 2006) , pp. 1739-1746.
- Reed, R.J. and E.E. Recker, 1971: Structures and properties of synoptic-scale wave disturbances in the equatorial western Pacific. *J. Atmos. Sci.*, 28, 1117-1133.
- Reed, R.J., D.C. Norquist and E.E. Recker, 1977: The structure and properties of African wave disturbances as observed during Phase III of GATE. *Mon. Wea. Rev.*, 105, 317-333.
- Reed, R.J., E. Klinder and A. Hollingsworth, 1988: The structure and characteristics of African easterly wave disturbances determined from ECMWF operational analysis/forecast system. *Meteorol. Atmos. Phys.*, 38, 22-33.
- Rowell D.P., Folland C.K., Maskell, K. and Ward M.N., 1995: Variability of summer rainfall over Tropical North Africa (1906-92): Observations and modelling, *Q. J. R. Meteorol. Soc.*, 121, 669-704.
- Shapiro, L. J. and S. B. Goldenberg, 1998: Atlantic Sea Surface Temperature and Tropical Cyclone Formation. *J. Climate*, 11, 578-590.
- Simmons, A. J., 1979 : A note on the instability of African Easterly Jet. *J. Atmos. Sci.*, 34, 1670-1674.
- Sultan, B., 2002 : Etude de la mise en place de la mousson en Afrique de l'ouest et de la variabilité intra saisonnière de la convection. Application à la sensibilité des rendements agricoles, thèse université Paris 7, 283pp.
- Sultan B., S. Janicot, et A. Diedhiou (2003a), The West African monsoon dynamics, Part I : Intra-seasonal variability, *Journal of Climate*, 16, 3389-3406.
- Sultan B. et S. Janicot (2003b), The West African monsoon dynamics, Part II : The "pre-onset" and the "onset" of the summer monsoon, *Journal of Climate*, 16, 3407-3427.
- Taleb, El Houssein, and Leonard M. Druyan, 2003: Relationships between rainfall and West African wave disturbances in station cbservations. *Int. J. Climatol.*, 23 (3), 305-313.
- Thompson, R.M., S.W. Payne, E.E. Recker and R.J. Reed, 1979: Structure and properties of synoptic-scale wave disturbances in the intertropical convergence zone of the eastern Atlantic. *J. Atmos. Sci.*, 36, 53-72.
- Thorncroft, C.D., 1995: An idealized study of African easterly waves. Part I: More realistic basic states. *Quart. J. Royal Meteorol. Soc.*, 121, 1589-1614.
- Thorncroft, C. D., and B. J. Hoskins, 1994a : An idealized study of African Easterly Waves. Part I: A linear view. *Quart. J. Roy. Meteor. Soc.*, 120, 953-982.
- Thorncroft, C. D., and B. J. Hoskins, 1994b: An idealized study of African easterly waves. Part II: A nonlinear view. *Quart. J. Roy. Meteor. Soc.*, 120, 893-1016.
- Thorncroft, C.D. and M. Blackburn, 1997: On maintenance of the African Easterly Jet. *Quart. J. Roy. Meteorol. Soc.* 125, 763-786.
- Thorncroft. C. D., and M. Blackburn, 1999 : Maintenance of the African Easterly Jet. *Quart. J. Roy. Meteor. Soc.*, 125, 763-786.
- Thorncroft, C., and K. Hodges , 2001 : African Easterly Wave Variability and Its relationship to Atlantic TC Activity. *J. Climate*, 14, 1166-1179.
- Torrance C and Compo, 1998: A practical guide to wavelet analysis. *Bull. Am. Meteorol. Soc.*, 79, 61-78.
- Xue, Y. and J. Shukla, 1993 : The influence of land surface properties on Sahel climate. Part I : Desertification. *J. Climate*, 6, 2232-2245.

3.2) Implication dans les programmes nationaux et internationaux

a. Implication au Programme National d'Etude de la Dynamique du Climat (PNEDC)

- **2000** : « Variabilité de la convection dans Eclat : échelles climatique, synoptique et meso-échelle » porté par Henri Laurent (LTHE) en partenariat avec le LMD/CNRS/IPSL et le CNRM/Meteo-France. Arona DIEDHIOU est en charge du volet « perturbations synoptiques » de ce projet.
- **2001** : « Variabilité de la convection dans Eclat : échelles climatique, synoptique et meso-échelle » porté par Arona DIEDHIOU (LTHE) en partenariat avec le LMD/CNRS/IPSL et le CNRM/Meteo-France.
- **2002-2004** : « Mécanismes multi-échelles de la variabilité de la ZCIT et de ses interactions avec les surfaces et sub-surfaces océaniques et continentales sur le domaine Atlantique tropical – Afrique » porté par Serge Janicot (LMD/CNRS/IPSL) en collaboration avec le LTHE, le CRC, le CNRM, le LEGOS, le LODYC. Dans ce programme, Arona DIEDHIOU au titre du LTHE étudiait les interactions ondes-convection-pluie en Afrique de l'Ouest.
- **2001-2003** : Le travail effectué au PNEDC m'a permis de m'impliquer dans le programme de coopération CAPES-COFECUB avec le Brésil intitulé « Convection et Précipitation en Amazonie » dont le responsable était Henri Laurent. En collaboration avec Luiz Machado (CPTEC) et Nadine Dessay (LTHE), j'ai participé à l'étude « dynamique des systèmes convectifs et végétation ». J'ai ainsi effectué des séjours scientifiques en 2001 et 2002 au CTA/IAE/ACA (Centre d'Etudes Spatiales) à San José do Campos (Sao Paulo), participé à une partie de la campagne LBA (radiosondages) et donné des conférences à l'Université de Sao Paulo et à la FUNCEME (Fortaleza).

b. Implication au Programme National Atmosphère et Océan Multi-échelles (PATOM)

- **2002-2004** : « Etude de la Dynamique Atmosphérique de la Mousson de l'Afrique de l'Ouest aux échelles intrasaisonnières » porté par Jean-Philippe Lafore (CNRM/METEO-France) en collaboration avec le CETP, le LTHE, le LA, et le LMD. Arona DIEDHIOU s'occupait ici du volet « organisation de la convection par les ondes ». Ce programme était en forte synergie avec le Programme PNEDC ci-dessus sur l'Afrique de l'Ouest.

c. Depuis 2003 : Coordination du programme international AMMA

- Membre du Bureau Exécutif AMMA-International
- Membre du Comité Scientifique AMMA-International (ISSC)
- Membre du Comité AMMA-France (CCMA)
- Responsable du Centre Opérationnel AMMA (AOC-AMMA)

Aspects scientifiques et opérationnels:

- Membre du WG 1.1 (La mousson africaine et le climat global) au niveau international et dans AMMA-France).
- Membre du TT1 (Task Team s'occupant du déploiement et du suivi des radiosondages, GPS, Pilots et VHF en Afrique).
- Membre du TT ARM (en charge du déploiement de la facilité ARM au Niger ; financement DoE/USA à Niamey, Niger).
- Membre du TT8 (Task Team en charge de la période intensive d'observations AMMA pendant le cœur de la saison des pluies ;
- Point focal pour le Centre des Opérations des équipes Ballons (Driftsondes et BSO) du Centre Nationale d'Etudes Spatiales-CNES) et AMMA-SCOUT.
- Leader du Deliverable 7.1c/AMMA-Europe (Thematic Priority : Global change and Ecosystems) sur le Centre des Opérations AMMA et sur le déploiement des instruments.

d. Coordination de l'initiative africaine dans le Programme AMMA

- Initiateur et co-fondateur du réseau AMMA-Afrique
- Co-président du Comité de coordination AMMA-Afrique jusqu'en 2009
- Coordinateur du Plan Scientifique AMMA-Afrique jusqu'en 2009
- Membre du Bureau Exécutif AMMA-Afrique
- Coordinateur du volet « mobilisation des ressources » pour le Plan AMMA-Afrique

e. Implication dans les programmes internationaux de l'OMM en Afrique

- Coordinateur du plan d'action régional pour l'Afrique de l'Ouest et l'Afrique central du GCOS/OMM (Système Mondial d'Observation du Climat ; 2004).
- Membre du Comité Régional THORPEX-Africa sur la prévision des événements extrêmes en Afrique. Contribution à la rédaction du plan d'implémentation et du plan scientifique pour le volet « Système d'Observation » ; 2007.

f. Coordination du FSP RIPIECSA sur les interactions climat-écosystèmes – sociétés.

- Chef de Projet du FSP RIPIECSA depuis Novembre 2006 : Le Ministère français des Affaires Etrangères a délégué à l'IRD dans sa fonction d'Agence Inter-organismes de Recherche pour le Développement (AIRD), la mise en œuvre du FSP RIPIECSA (Recherche Interdisciplinaire et Participative sur les Interactions entre les Ecosystèmes, le Climat et les Sociétés d'Afrique de l'Ouest), **RIPIECSA est un projet d'un montant de 3,5 millions d'Euros pour une durée de 4 ans (2007 - 2010).**
 - La finalité de RIPIECSA consiste à étayer scientifiquement les politiques nationales d'adaptation au changement climatique, susceptibles d'être adoptées par les gouvernements et acceptées la société civile. La méthodologie retenue est une **démarche scientifique interdisciplinaire et participative** :
 - **Interdisciplinaire**, afin de prendre en compte les multiples interactions entre le climat, l'écosystème et les sociétés au sein de zones ateliers,
 - **Participative**, afin d'associer à la réflexion aux côtés des scientifiques tous les acteurs sociaux.

Pour y parvenir, ce projet s'articule autour de 3 sous-objectifs :

- promouvoir des recherches interdisciplinaires, rapprocher les savoirs naturalistes locaux et la culture scientifique et inciter à la réflexion avec les gouvernements ;
- renforcer les capacités locales par les recherches en partenariat, l'organisation de forum de discussion, l'appui à la formation, aux mesures et à l'échange de données ;
- diffuser les recherches et leurs résultats

Un atelier de lancement s'est déroulé à Bamako au mois du 5 au 7 mars 2007. Il a réuni plus de 120 experts africains de différentes disciplines concernées, provenant de différents pays d'Afrique de l'Ouest et de France. Cet atelier a permis d'identifier les questions partagées entre les scientifiques d'une part et les décideurs et la société civile d'autre part. Il a été le lieu d'expression d'un questionnement scientifique autour de problématiques telles que la désertification, la gestion des ressources naturelles, la sécurité alimentaire, les impacts économiques et environnementaux du changement climatique, les stratégies d'adaptation, la santé, etc.

Sur cette base, seront lancés des projets de recherche proposés par des équipes des pays d'Afrique de l'Ouest dans le cadre de deux appels à proposition

- sur « projets ciolés » d'une part pour les recherches sur la variabilité climatique et les changements du climat. Ces études reposent sur des simulations numériques, des observations et enquêtes de terrain et sur la valorisation de données historiques ou anciennes.
- et sur « appel à propositions » pour les recherches sur les impacts sociaux et environnementaux ainsi que sur les stratégies d'adaptation. Certains projets de recherche favoriseront la participation de la société civile et des décideurs à leurs travaux, par une démarche participative.

Avec une équipe en Afrique (à la représentation IRD du Niger) de 4 personnes et un chargé de mission au siège de l'IRD auprès du DSF, RIPIECSA soutient 25 projets de recherche en Afrique de l'Ouest et du Centre avec des partenaires au Maghreb et en France.

3.3) Participation à la formation

a. Contribution encadrement et formation doctorale

1. Codirection thèse 2002-2005 (Financement IRD/DSF/BST) soutenue en 2006 : Moctar CAMARA, de nationalité sénégalaise, en cotutelle LPAOSF/ESP, Sénégal / LTHE/INPG, France sur la « Cyclogenèse dans l'Atlantique Nord en relation avec le système de mousson en Afrique de l'Ouest ». Codirecteurs : Thierry Lebel (DR IRD) et Arona Diedhiou (CR IRD)
2. Codirection thèse 2002-2005 (Financement Ministère) soutenue en 2006 : Christophe Lavaysse de nationalité française sur « l'étude des relations onde-convection-pluie et influence du flux de mousson ». Codirecteurs : Henri Laurent (DR IRD) et Arona Diedhiou (CR IRD)
3. Codirection thèse 2008-2010 (Financement IRD/DSF/BST) : Youssouf SANE, de nationalité sénégalaise sur la « Représentation du cycle de vie des systèmes convectifs avec le modèle LMDZ pendant la campagne AMMA 2006 ». Co - Direction avec Aida Diongue (ANAMS, Dakar, Sénégal), Arona Diedhiou (CR IRD ; LTHE, Grenoble, France) et Frédéric Hourdin (DR CNRS ; LMD/IPSL, Paris, France).
- Comité de Pilotage thèse 2007-2009 (Financement Ministère de la Recherche Côte d'Ivoire) : Mr S. Silué de nationalité ivoirienne sur le transport des poussières sahariennes et influences du flux de mousson et les téléconnexions avec l'ENSO, la SOI et la NAO». Codirecteurs : Paul Assamoi, Abdourahmane Konaré (Université Abidjan – Cocody)

b. Contribution encadrement et formation niveau Maîtrise, DEA, Master

1. 2000 : Encadrement DEA Sabine Diobo (30%) en Physique de l'Atmosphère, Université Abidjan-Cocody (Côte d'Ivoire). « Réduction de la visibilité en relation avec l'oscillation Nord Atlantique » avec Mr Abdourahmane Konaré. Collaboration avec l'IGT (Institut de Géographie Tropicale) et le LAPAMF (Laboratoire de Physique de l'Atmosphère et de mécanique des fluides).
2. 2000 : Nicolas Sabatier ; Stage Maîtrise des sciences de la Terre et de l'Univers. Sujet « caractérisation des différentes phases d'évolution du flux de mousson et le lien avec les régimes pluviométriques en Afrique de l'Ouest ».
3. 2001 : Encadrement Christophe Lavaysse ; Maîtrise de Physique de l'Université Joseph Fourier de Grenoble. Sujet : « Variabilité interannuelle des précipitations et de la nébulosité dans la région sahélienne : le concept des ondes humides et des ondes sèches ».
4. 2001 : Encadrement stage Véronique Guiné et Thibaud Renou ; Maîtrise des Sciences de la Terre et de l'Univers de l'Université Joseph Fourier de Grenoble. Sujet : « Variabilité pluviométrique et atmosphérique de l'Afrique de l'Ouest depuis 1950 ».
5. 2001 : Stage de deuxième année de Simon Kitous, élève ingénieur de l'ENSHMG (hydraulique de l'INPG de Grenoble). Sujet : « Impact du réchauffement global sur la pluie en Afrique de l'Ouest avec le modèle ARPEGE (Meteo-France) ».
6. 2002 : Encadrement stage de Marthe Bella-Medjo ; Maîtrise des Sciences de la Terre et de l'Univers de l'Université Joseph Fourier de Grenoble. Sujet : « variabilité pluviométrique en Afrique de l'Ouest et interactions avec les conditions de surface »
7. 2002 : Encadrement DEA Christophe Lavaysse ; École Doctorale Terre, Univers, Environnement. « Approches énergétique et numérique d'événements humides et secs en régime d'onde au Sahel : Etude de cas ».

8. **2003** : DEA Mécanique des milieux géophysiques et environnement ; Université Joseph Fourier ; Grenoble, France. **Jérôme CLARET**, ingénieur hydraulique ; INPG. « Le Rôle de la Végétation dans le Cycle de L'eau: Le cas du Mexique ». Co encadrements: Luc Descroix et Arona Diedhiou
9. **2003** : DEA Mécanique des milieux géophysiques et environnement ; Université Joseph Fourier ; Grenoble, France. **Thomas DESRUELLES**, ingénieur hydraulique ; INPG. « Impact du changement climatique sur la production de mil au Niger ».
10. **2004** : Encadrement Stage **Chloé-Mitard** : Elève 3^{ème} année IUP Environnement et Aménagement régional (université de Lille 1) sur L'accès à l'eau potable au Niger.
11. **2005** : Encadrement de stages d'élève ingénieurs en météorologie de l'EAMAC : Variabilité de l'intensité de la mousson en Afrique de l'Ouest et relations avec les pluies. (**Mme Esono Nuria-Mikue ASUMU** ; Guinée Equatoriale et **Mr Laurent BOUGMA** ; Burkina Faso)
12. **2006** : Encadrement de stage de techniciens supérieurs en agrométéorologie du Centre Régional AGRHYMET sur la variabilité des hyéogrammes à Niamey (Niger).
13. **2007** : Collaborations avec la Direction de la Météorologie Nationale : **Abdou Kassimou** ; ingénieur. Encadrement avec Doug Parker (Université de Leeds) sur l'exploration dynamique de la couche limite et variabilité des précipitations lors du passage des MCS sur le degré carré de Niamey. Mr Kassimou a effectué dans ce cadre un séjour en Angleterre pour exploiter les données de l'instrument SODAR déployé à Niamey dans le cadre de la campagne AMMA.
14. **2007** : Collaborations avec l'Université Abdou Moumouni de Niamey (Niger) : Encadrement d'un étudiant (**Mahamane Barmou Batoure**, titulaire d'un DEA) avec séjour à Rome (ENEA) chez Paolo Ruti de 6 mois (Janvier-Juin 2008) avec une bourse de la coopération italienne pour travailler sur la validation des modèles (ensemble) et la prévision saisonnière.
15. **2008** : Stage M2R "océan atmosphère hydrologie" de l'Université Joseph Fourier de Grenoble. **Aurélien Quiquet** sur « Etude de l'environnement et de l'efficacité pluviométrique des systèmes convectifs au dessus de Niamey pendant la campagne AMMA 2006 ».
16. **2009** : Stage M2R « Physique de l'Atmosphère et Mécanique des Fluides » de l'Université Abidjan – Cocody (Côte d'Ivoire). **Evelyne T. N'Datchoh** sur « Effet de la variabilité climatique sur le régime des feux en Afrique de l'Ouest ».

c. Activités d'enseignement

- **2001** : J'ai dispensé 21h de cours de météorologie tropicale pour la Maîtrise des Sciences de la Terre et de l'Univers de l'université Joseph Fourier de Grenoble (observatoire des sciences de l'univers de Grenoble ; OSUG).
 - **2003 et 2004** : Intervenant invité à l'EAMAC pour le volet « Les ondes d'Est africaines et la convection » pour les élèves ingénieurs en météorologie.
 - **2003** : Conférencier invité sur les interactions ondes-convection-pluies et le flux de mousson et sur le programme AMMA pour des étudiants de maîtrise – DEA de physique à l'Université de Niamey (Niger).
-

3.4) Collaborations scientifiques avec l'Afrique et l'Amérique Latine

a. Organisation de manifestations (colloques, séminaires, ateliers)

Pour toutes les réunions ci-dessous, je suis soit organisateur, soit membre du comité d'organisation, soit membre du comité scientifique, soit j'ai apporté un appui-conseil à la mise en œuvre.

- Réunions AMMA-Afrique / Comité de Coordination AMMA-Afrique (15-50 personnes) organisés en marge d'une réunion internationale : 2004 (Niger) ; 2005 (Sénégal) ; 2006 (Burkina- Faso) ; 2009 (Burkina Faso)
- Réunions AMMA-International (environ 200-300 personnes dont le tiers est africain) organisé alternativement en Europe et en Afrique (une réunion tous les deux ans, alternativement avec celles de AMMA-Afrique) (Dakar 2005; Sénégal puis Karlsruhe 2007, Allemagne ; Ouagadougou en 2009 ; Burkina Faso)
- Atelier THORPEX-Afrique : rédaction du plan scientifique et du plan d'implémentation (2006 : Ouagadougou, Burkina Faso ; 2007 : Dakar, Sénégal)
- Atelier de lancement du Projet FSP RIPIECSA (150 experts invités) organisé en 2007 à Bamako ; Mali
- Atelier de formation des porteurs de projets RIPIECSA Avril 2008 ; Dakar, Sénégal) et toutes les réunions RIPIECSA organisées au Niger, au Burkina, au Mali.

b. Codirections de thèse

- Codirection thèse 2002-2005 (Financement IRD/DSF/BST) soutenue en 2006 : Moctar CAMARA, de nationalité sénégalaise, en cotutelle LPAOSF/ESP, Sénégal / LTRE/INPG, France sur la « Cyclogenèse dans l'Atlantique Nord en relation avec le système de mousson en Afrique de l'Ouest ».
- Codirection thésitif 2008-2010 (Financement IRD/DSF/BST) : Youssouf SANE, de nationalité sénégalaise sur la « Représentation du cycle de vie des systèmes convectifs avec le modèle LMDZ pendant la campagne AMMA 2006 ». Co - Direction ANAMS, Dakar, Sénégal, le LTRE, Grenoble, France et le LMD/IPSL, Paris France.
- Comité de Pilotage thèse 2007-2009 (Financement Ministère de la Recherche Côte d'Ivoire) : Mr S. Silué de nationalité ivoirienne sur le transport des poussières sahariennes et influences du flux de mousson et les téléconnexions avec l'ENSO, la SOI et la NAO». Codirection : LAPA-MF, Université Abidjan Cocody et le LTRE, Grenoble, France.

c. Encadrement d'étudiants et d'élèves ingénieurs

- Membre de jury de soutenance de Mémoire de fin d'études d'élèves ingénieurs en météorologie de l'EAMAC (Ecole Africaine de Météorologie et d'Aviation Civile ; Niamey, Niger). 2004.
- Membre de jury de soutenance de Mémoire de fin d'études d'élèves ingénieurs en météorologie de l'AGRHYMET (Niamey, Niger). 2005.
- 17. Encadrement de stages d'élève ingénieurs en météorologie de l'EAMAC ; 2005 : Variabilité de l'intensité de la mousson en Afrique de l'Ouest et relations avec les pluies. (Mme Esono Nuria-Mikue ASUMU ; Guinée Equatoriale et Mr Laurent BOUGMA ; Burkina Faso)
- 18. Encadrement de stage de technicien supérieurs en agrométéorologie du Centre Régional AGRHYMET. 2006.
- 19. Co-Encadrement de stage M2R en physique de l'Atmosphère : Université Abidjan-Cocody (Côte d'Ivoire) sur la variabilité du climat et le régime des feux en zone de savane (Evelyne T. N'Datchoh).

d. Collaborations avec les institutions du Sud

- **Collaboration avec le Brésil (CPTEC et CTA) dans le cadre du programme de coopération CAPES-COFECUB avec le Brésil intitulé « Convection et Précipitation en Amazonie » dont le responsable était Henri Laurent.** En collaboration avec Luiz Machado (CPTEC) et Nadine Dessay (LTHE), j'ai participé à l'étude « dynamique des systèmes convectifs et végétation ». J'ai ainsi effectué des séjours scientifiques au CTA/IAE/ACA (Centre d'Etudes Spatiales) à San José do Campos (Sao Paulo), participé à une partie de la campagne LBA (radiosondages) et donné des conférences à l'Université de Sao Paulo et à la FUNCEME (Fortaleza).
 - **Diedhiou A., J. Ronchail , N. Dessay., L.A.T. Machado, H. Laurent., J-F. Royer, 2002.** Climate Change over South America in relation with the Increase of Global Greenhouse Gases: a numerical study. XII Congresso Brasileiro de Meteorologia., Iguassu Falls, Brasil. (Awarded: Prix du meilleur travail présenté oralement dans la session "Variabilité et changement climatique").
 - **Dessay, N.; Laurent, H.; Machado, L. A. T.; Shimabukuro, Y. E; Diedhiou, A.; Ronchail, J. 2004 :** Comparative study of 1982-1983 and 1997-1998 El Niño events over different types of vegetation in South America. International Journal of Remote Sensing. Vol., 25; 4063-4077.
 - **Diedhiou A., L. A. Machado, H. Laurent, 2009.** Mean Kinematic of Synoptic Easterly Disturbances over the Atlantic. Advances on Atmospheric Research. doi 10.1007/s00376-009-9092-5; in press.
- 20. **Collaborations avec la Direction de la Météorologie Nationale du Niger:** Abdou Kassimou ; ingénieur. Encadrement avec Doug Parker (Université de Leeds) sur l'exploration dynamique de la couche limite et variabilité des précipitations lors du passage des MCS sur le degré carré de Niamey. Mr Kassimou a effectué dans ce cadre un séjour en Angleterre en 2007 pour exploiter les données de l'instrument SODAR déployé à Niamey dans le cadre de la campagne AMMA.
 - **Kassimou Abdou, D.J.Parker, B Brooks, N Kalthoff, A. Diedhiou, T. Lebel; 2009;** Diurnal cycle of lower boundary layer wind in the West African monsoon. 3rd AMMA International Conference; Ouagadougou; Burkina –Faso.
- 21. **Collaborations avec la Direction de la Météorologie Nationale du Sénégal (ANAMS : Agence Nationale de la Météorologie du Sénégal) :** Collaborations avec Aida Diongue-Niang (i) dans le cadre de la mise en œuvre du programme THORPEX-AFFICA sur la variabilité et la prévisions des événements extrêmes en Afrique et (ii) dans le cadre d'une co-direction de la codirection de thèse de Y. Sané sur la représentation des systèmes convectifs en Afrique de l'Ouest dans les modèles.
 - **Diedhiou A., Lebel T., Diongue A. 2001;** Synoptic context associated to COPT and Hapex-Sahel Mesoscale Convective Systems. XXVI General Assembly of European Geophysical Society. Session Océans & Atmosphère : OA26-1, vol. 3, Nice, France
 - **Redelsperger J.L., Diongue A., Diedhiou A., Ceron J.P., Diop M., Gueremy J.F., Lafore J.P., 2002b;** Multiscale description of a Sahelian synoptic weather system representative of West African monsoon. Quart. Journ. Roy. Meteor. Soc., 128 : 1229-1257.
 - **A. Diongue-Niang, A. Kamga, E. Afiesimama, A. Babu, A. Diedhiou, B. Lamptey, A. Mokssit, F. Opijeh, E. Poolman, J. Caughey, D. Parsons, 2009.** WWRP/THORPEX-Africa ; 3rd AMMA International Conference; Ouagadougou; Burkina –Faso.
 - **Y. Sane, M Bonazzola, F Hourdin, A Diongue-Niang, A. Diedhiou; 2009;** Diurnal cycle of precipitation at Dakar in the model LMDZ. 3rd AMMA International Conference; Ouagadougou; Burkina –Faso.
- 22. **Collaborations avec l'Université Abdou Moumouni de Niamey (Niger) :**
 - Plusieurs séminaires effectués dans le cadre de AMMA-Niger
 - Encadrement d'un étudiant (Mahamane Barmou Batoure, titulaire d'un DEA) qui doit aller à Rome (ENEA) chez Paolo Ruti pour 6 mois (Janvier-Juin 2008) avec une bourse de la coopération italienne pour travailler sur la validation des modèles (ensemble) et la prévision saisonnières.
 - **Diedhiou A., Abdallah Nassor, Abou Amami, Lekan Oyebande, Amadou Gaye, Adamou Garba, Delphin Ochou (2003).** AMMANET: Building the African Participation to AMMA. CLIVAR Exchanges. No. 27.Vol8 N° 2/3 Page 55.
 - **Ward N., Cook K., Diedhiou A., Fontaine B., Giannini A., Kamga A., Lamb P.J., Ben M. A., Nassor A. and Thorncroft C., 2004 :** «Seasonal-to-Decadal Predictability and Prediction of West African Climate» , CLIVAR Exchanges, 9, 3, 14-20.

- Ruti P.M., M.B. Barmou Batoure, A. Diedhiou, A. Dell'aquila, 2009 ; Seasonal error in the seasonal forecast over West Africa from European multi-model ensemble system. 3rd AMMA International Conference; Ouagadougou; Burkina –Faso.
- L. Descroix, B Ibrahim; K Souley Yero; A Diedhiou; 2009; Vegetation pattern and rain fields in the Sahel. 3rd AMMA International Conference; Ouagadougou; Burkina –Faso.

23. Collaborations avec l'Université Abidjan Cocody (Côte d'Ivoire) :

- 1998-2000 : Fonds AUF pour travailler sur les téléconnexions et la végétation en Afrique de l'Ouest (porté par Sylvain Bigot, Université de Lille/LGMA et Telesphore Brou-Yao, Institut de Géographie Tropicale/CURAT).
- 2000-2001 : Encadrement DEA Sabine Diobo avec Mr Abdourahmane Konaré (LAPA ; Université Abidjan Cocody) sur le transport des poussières par les perturbations synoptiques, Oscillation Nord-Atlantique et variabilité et la visibilité.
 - Bigot S., Brou Yao T., Diedhiou A., Laganier R., 1999. Détection des feux de végétation en Côte d'Ivoire à partir des données AVHRR et ATSR : relations avec le NDVI et les précipitations. **Publications de l'Association Internationale de Climatologie**, n°12, p.209-218,
 - Bigot S., I. ZIN and A. Diedhiou, 2004: Apport de données SPOT multirésolution pour l'étude des variations phénologiques dans le bassin de l'Ouémé (Nord-Bénin). Réseau Télédétection de l'Agence Universitaire de la Francophonie Journées Scientifiques d'Ottawa. Canada.
 - Bigot S., Oszwald J., Brou Yao T., Diedhiou A., Konare A., Fofana M., Assamoi P. 2004 : Le suivi des variations climatiques et écologiques en Afrique de l'Ouest : le rôle de la station géophysique et écologique de Lamto (Côte d'Ivoire). 17e Colloque International de l'Association Internationale de Climatologie « Climat, mémoire du temps » Mémorial de Caen, France
 - Bigot, S.; Brou, T.Y.; Oszwald, Y.; Diedhiou, A., 2005 : Facteurs de la variabilité pluviométrique en Côte d'Ivoire et relations avec certaines modifications environnementales. **Sécheresse** ; 16(1) ; 5-13.
 - Bedou M., Konare A., Sanda I-S., Assamoi S. and Diedhiou A., 2007: Hygroscopic properties of aerosols in the Sahel: preliminary results. **Scientific Research and Essays**, Vol. 2 (6), pp. 177-183.
 - S. Silue,A. Konaré, A. Diedhiou, V. Yoboue, P. Assamoi; 2009; Sahelian dust: responses to main mode of variability in Atlantic, Pacific and Indian Oceans and their impacts on the deep convection in the Sahel3rd AMMA International Conference; Ouagadougou; Burkina –Faso.
 - T.E. N'Datchoh, A. Konaré, A. Diedhiou, F. Solmon 2009; Effet de la variabilité climatique sur le régime des feux en Afrique de l'Ouest. 3rd AMMA International Conference; Ouagadougou; Burkina –Faso.

24. Collaborations avec l'Université Cheikh Anta Diop de Dakar (Sénégal)

- Encadrement de thésards du LPAOSF/ESP (voir ci-dessus)
- Etude de la variabilité des perturbations synoptiques et sur la convection (collaborations avec le LPAOSF, Amadou Garba EAMAC et André Kamga, ACMAD)
 - Jenkins G. S., Kamga A., Garba A., Diedhiou A., Morris V., Joseph E., 2002d: Investigating the West African Climate System using Global/Regional Climate models. **Bull. of Americ. Met. Soc.**, 83/4, 583-595.
 - Jenkins G. S., A. Kamga, G. Adamou, A. Diedhiou, V. Morris, E. Joseph, 2002e: Summary of the Workshop on Modeling the West African Climate System with Global and Regional Scale Climate Models: Relevance to Understanding Climate Variability, Land-Use, and Climate Change, **Bull. of Americ. Met. Soc.**, 583-595.
 - Adamou G., El Mahaman I. S., Itoua.E. N., Diedhiou A., Gaye A.T, et G. Jenkins., 2005: Utilisation des données MSG dans des études de cas des perturbations (poussières, orages et lignes de grains) observées à Niamey en 2004. 1st International AMMA Conference ; Dakar, Sénégal
 - Camara M., A. Diedhiou, A. T. Gaye., 2005. African Easterly Waves and Cyclonic activity over the eastern Atlantic: Composite and case studies. 1st International AMMA Conference ; Dakar, Sénégal
 - Y. Sane, M Bonazzola, F Hourdin, A Diongue-Niang, A. Diedhiou; 2009; Diurnal cycle of precipitation at Dakar in the model LMDZ. 3rd AMMA International Conference; Ouagadougou; Burkina –Faso.

4) Implication dans le Programme International AMMA

Durant mon séjour au Niger (2003-2007), je me suis occupé de :

- la coordination de l'initiative africaine dans le programme AMMA, création d'un réseau (AMMANET) et contribution à l'élaboration d'un plan scientifique AMMA-Afrique.
- la coordination et mise en œuvre du programme international AMMA (Analyse Multidisciplinaire de la Mousson Africaine et ses impacts) comme Responsable du Centre des Opérations.

Dans cette partie, je fais une synthèse de mon bilan sur ces deux actions.

a) Bilan du réseau AMMANET et de l'initiative africaine dans le programme AMMA

Historique

C'est parce que le partenariat et la pluridisciplinarité s'inscrivent au cœur du programme international AMMA et que sa faisabilité et sa pérennité passent nécessairement par une implication effective des institutions et des scientifiques africains que, dès novembre 2001, un appel à contribution a été lancé auprès de scientifiques africains afin que s'engage une discussion commune sur les principales questions à traiter.

Cette initiative a été à l'origine de la 1ère réunion internationale fondatrice AMMA en février 2002 à Niamey où étaient présents une trentaine d'africains, et où le réseau de scientifiques africains AMMANET bénéficiant de l'appui des services météorologiques et hydrologiques, des universités et des centres régionaux tels que AGRHYMET et ACMAD a été créé avec un comité de coordination appelé CSAM et des points focaux dans les différents pays.

C'est en Novembre 2003 à Cotonou que s'est fait sentir la nécessité d'avoir un plan scientifique traduisant ce que les africains souhaitent faire, comment, où et quand dans le cadre de AMMA. Cette initiative, un an après la création du réseau AMMANET est motivée par un réel besoin des différents membres du réseau de prendre part activement à la mise en œuvre du programme AMMA et de s'afficher comme composante à part entière du programme travaillant en étroite synergie avec les autres parties (France, Europe, UK, USA).

Dans une première phase, un appel à propositions de « fiche de projet synthétique » a été lancé aux scientifiques de la sous-région afin d'identifier les préoccupations scientifiques et les différentes expertises. Ensuite, conformément aux recommandations du Comité Scientifique International (ISSC), ces fiches ont été regroupées en groupes de travail identiques à ceux du programme AMMA-International et un leader a été choisi pour fédérer les initiatives et les différentes propositions détaillées dans chaque thématique.

Un an après Cotonou, en Novembre 2004 à Niamey, avec l'appui financier de l'IRD et l'appui logistique de l'ACMAD, le CSAM s'est réuni pour la première fois et s'est efforcé en une semaine de travail de regrouper les projets dans les différentes thématiques et de fournir un ensemble de 5 documents constituant la première version du Plan d'Implémentation Africain (PIAF). AMMANET devenait ainsi AMMA-Afrique.

Le PIAF a été réalisé sur la base d'une centaine de propositions détaillées émanant de divers laboratoires d'universités et d'institutions de recherche africaines. À la différence des autres composantes européenne et américaine du programme international AMMA, le PIAF se singularise par son imposante contribution à la thématique sur les « impacts et les applications » mais également sur le volet « démonstration ». De plus, le volet « Formation et Renforcement des Capacités » dans le PIAF vise à prendre en compte les problèmes et les besoins exprimés par les universités, les services nationaux hydrométéorologiques.

Jusqu'en 2005, le PIAF a fédéré 36 institutions africaines autour de 89 projets de recherches allant de 3 à 5 ans aux échelles régionale et locale soit près de 200 enseignants et chercheurs, 40 ingénieurs et techniciens et 72 étudiants (Maîtrise, DEA et doctorants). Cependant, les chercheurs, ingénieurs, techniciens, étudiants africains n'ont cessé de marquer leur intérêt pour le programme AMMA mais malheureusement peu de projets du PIAF furent financés ou mis en œuvre faute de moyens, à la différence des projets du programme AMMA-International qui sont financés soit par l'Union Européenne ou via des consortiums nationaux. Fin 2005, seul 5 centres (ACMAD, AGHRYMET, ASECNA, 2IE(EIER), CERMES) ont pu être financés dans le cadre de leur participation à la mise en œuvre de la composante européenne de AMMA (Consortium AMMA-EU).

Face à l'approche de la SOP 2006 (campagne d'observations intensives) et pour répondre aux remarques de l'ISSC sur le PIAF, il était indispensable de réunir le CSAM, les coordinateurs des Comités Nationaux et certains leaders de projets pour améliorer le PIAF. S'appuyant sur un financement IRD et sur un financement INSU, le CSAM a pu organiser son premier colloque **AMMA-Afrique du 10 au 12 Mai 2006 à Ouagadougou au Burkina Faso**. Les questions scientifiques, les calendriers d'activités, la formation seront les principaux points à analyser ainsi que le rôle de AMMA-Afrique dans la mise en œuvre de la campagne d'observations à venir.

C'est ainsi que pendant la SOP 2006, AMMA-Afrique a contribué activement au déploiement des instruments AMMA sur le terrain et à la bonne mise en œuvre des opérations. Du point de vue opérationnel, le Centre des Opérations AMMA (AOC) au Niger s'est appuyé sur des structures africaines. Comme contribution aux opérations, beaucoup d'institutions ont apporté un soutien aux opérations sous forme de locaux, d'équipements, de ressources humaines et d'appui logistique au Burkina, au Mali, au Sénégal et en Guinée. Par ailleurs, 18 prévisionnistes mis à la disposition de l'AOC par les Services Météorologiques Nationaux ou par l'ASECNA et provenant de 12 pays de l'Afrique de l'Ouest et du Centre ont participé durant 4 mois (du 1er juin au 30 septembre) à la cellule de prévisions mise en œuvre à l'ACMAD avec le soutien de Météo-France et de l'Organisation Mondiale de la Météorologie.

Depuis 2007, des intentions pour soutenir la mise en œuvre du PIAF ont émergé et des initiatives ont permis l'extension du réseau AMMA-Afrique à d'autres disciplines et à d'autres institutions africaines. Parmi celles-ci, on peut citer :

- L'Europe (Initiative AMMA-EU / AMMA-TTC) : **1.2 millions d'euros (2007-2009)** pour des recherches sur les impacts des changements du climat sur l'agriculture, la ressource en eau et la santé. Financement du volet « Impact » du Plan AMMA-Afrique et consolidation du plan AMMA-EU dans cette thématique. Les africains impliqués dans AMMA-TTC sont membres du consortium AMMA-EU.
- Le « Fonds de Solidarité Prioritaire » RIPIECSA : **3.5 millions d'euros (2007-2010)** pour des recherches interdisciplinaires sur les interactions climat-écosystèmes-sociétés. RIPIECSA est un projet du Ministère Français des Affaires Etrangères et Européennes confié à l'IRID (Agence Inter-Etablissements de Recherche pour le Développement) pour sa mise en œuvre.

Un Bilan positif pour AMMA-Afrique

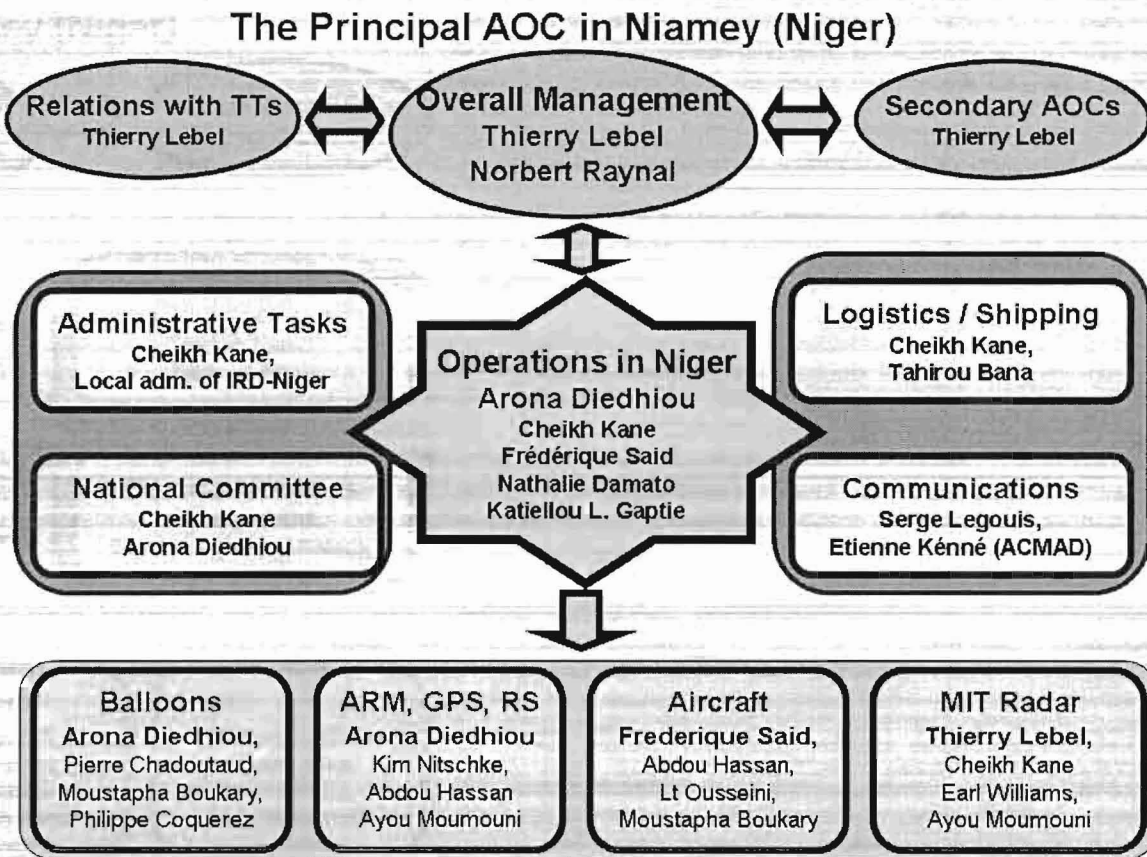
- Participation de AMMA-Afrique aux opérations AMMA. Les écoles de terrain sur les observatoires de recherche ORE (Mali, Niger, Benin), au Burkina Faso, Guinée Conakry et au Sénégal (SOP) ont permis l'implication d'une vingtaine d'ingénieurs, techniciens des services opérationnels hydrologique et météorologiques nationaux.
- Europe/AMMA-TTC : Soutien à 17 institutions de recherche et service opérationnels nationaux africains pour la période 2007-2010 pour des études sur les impacts.
- FSP RIPIECSA : 56 institutions africaines impliquées dans des recherches interdisciplinaires sur les interactions climat-écosystèmes-sociétés et sur un total de 25 projets soutenus, 17 projets sont directement issus de la communauté AMMA-Afrique.
- Formation : 67 étudiants africains sont en cours de thèses et 27 étudiants africains ont soutenus leur thèse dans le cadre de AMMA et de RIPIECSA.

Rappel de la composition des membres du CSAM jusqu'en Juillet 2009

- Amadou Gaye, UCAD, Sénégal (co-chair)
- Arona Diedhiou, IRD, Niger (co-chair)
- Ernest Afiesimana, NIMET, Nigeria
- Abel Afouda, UNB, Bénin
- Abou Amani, AGRHYMET, Niger
- Lassine Diarra, IER, Mali
- Isabelle Jeanne, CERMES, Niger
- André Kamga, ACMAD, Niger
- Harouna Karambiri, EIER, Burkina
- Abé Delfin Ochou, LAPA Côte d'Ivoire
- Lekan Oyebande, Université Lagos, Nigeria
- Luc Sigha, CRH, Cameroun
- Seydou Traoré, AGRHYMET, Niger

(ii) Supporting the operations

The support to the deployment of instruments and the operations was organised as depicted in the diagram below.



ii-a) Before the SOP : support to the deployment of instruments

The AMMA Operation Center (AOC) was in charge of coordinating and supervising the instrument deployment before the SOP. This consists in:

- Considering the requests for logistical support formulated by AMMA scientific teams, from summaries produced by Task Teams.
- Proposing responses to these requests following standardised procedures, following a preliminary endorsement by the Task Team Managers and the ICIG.

Each instrument PI had to fill in an "instrument form" and a "logistic form" to be sure that the instrument was properly taken into account by the AMMA Operation Center (AOC). In several cases, a recce field trip was needed. Then, if the AOC knew details sufficiently in advance, it could set up the needed assistance (vehicles, logistical support, contacts with authorities) as listed in the logistic form. At the end of the recce mission, an overall debriefing was organised on site to evaluate what was fulfilled and what remained to be done and a final report on the visit was written.

Moreover, the AOC provided information on the partnership between African and non-African scientists in AMMA, particularly with respect to the instrument deployment and to the AMMA training and capacity building programs. It was – and remains – indeed an AMMA rule that, prior to the deployment of any instrument in AMMA, a contact point and a scientific collaboration should have been identified in the country of deployment. Information had to be given on this topic in the instrument form and the AOC was committed to help the PIs in making contact with potential African collaborators. The involvement of young scientists and students in AMMA was especially sought. Communication activities were also performed to inform

people or pupils in some primary and secondary schools. Conferences and site visits also contributed to build and enhance the partnership.

To achieve its mission, the AOC organised its work according to groups of instruments as shown in the figure above; this was made possible by working in close collaborations with the local institutions and with the National AMMA committee. As the AOC had to handle sophisticated devices like aircraft, balloons, radar, etc, it was important to formalize and to work inside a well defined institutional framework. Since two years ago, an important work was done with the Niger authorities to help on obtaining clearances both for the deployment of the instruments and for the operations. Thus, the AOC-Niger operated under the label of the Niger Ministry of research with the help of its Office of Logistical and Administrative Supports to Scientific Operations (hereafter BALAOS).

For any request concerning an instrument or the operations, the BALAOS who worked in close collaboration with the AOC informed the ministry who sent personally a letter to his colleague of the concerned ministry (Army, Transport, Communications, Foreign office or Security, etc) asking him to achieve the task as soon as possible due to the importance that the Niger government give to AMMA. Such kind of relationships with the authorities means take time to explain what we wanted to do and why it was important for the country. It means also to work in close collaboration with the local partners to achieve the AOC mission.

ii-b) The AOC in SOP mode : support to the operations

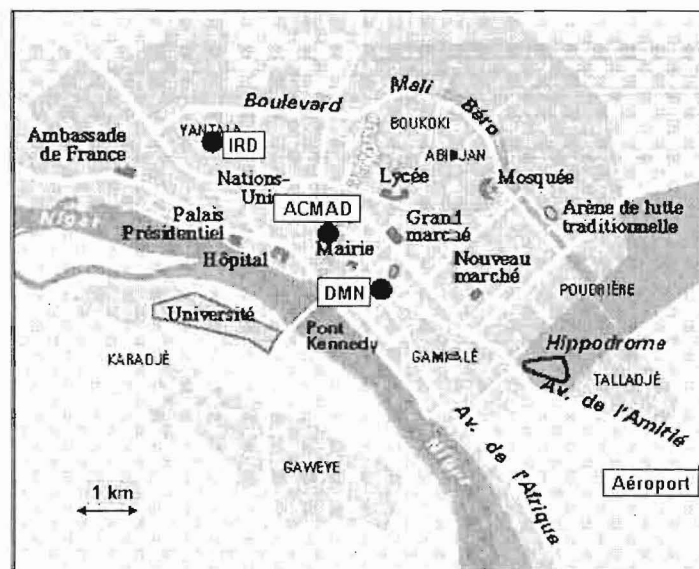
During SOP operations, the main AOC of Niamey assumed the following functions:

- Daily support to the SOP coordination.
- Daily support for the teams working in Niger.
- Daily support to the scientific secretary and to the operational forecasting team.
- Overall logistical coordination

After working hours (on holidays and during week-ends) a member of the AOC team was on duty. This person was available at any time in case of emergency or for any other problem. A calendar to know who to call was distributed. The AOC was also structured to manage tasks related to transportation, clearance, financial issues, telephone, hotel and health.

(iii) Buildings

The AMMA campaign took advantage of the support offered by various local organisations, which each provided buildings of various sizes: ACMAD, DMN, IRD, the Civil and military airports (see map below). On the other hand, the complexity of the operations to be coordinated required a centralised functional organization with a single briefing location easily accessible to the ground and aircraft teams. Because of its location close to the main hotels used by the AMMA teams and of the availability of a villa, it was decided that the SOP operational headquarter would be located at the DMN; this advanced site housed the briefing room and was connected to the three other sites (ACMAD, Airport) by a fast Internet connection.



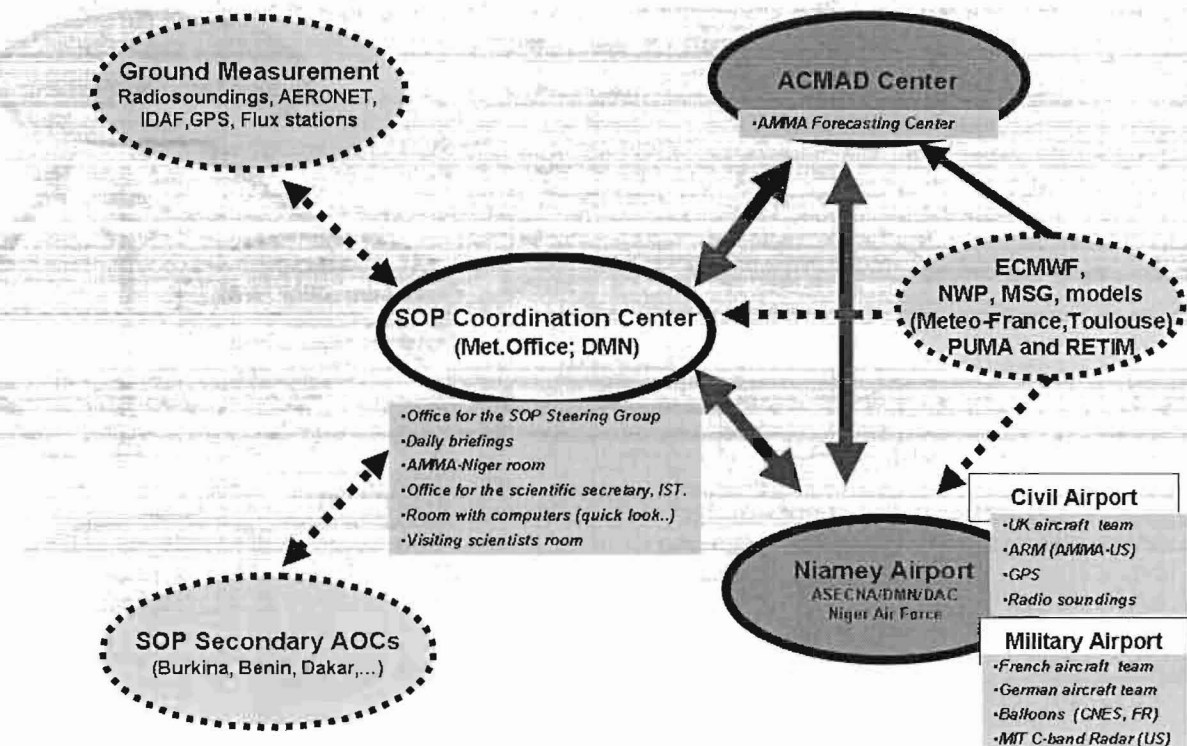
Locations of the AOC sites in Niamey

The local institutions provided the following office and operation space:

- ASECNA and the civil airport provided office space and technical rooms for scientists, aircraft technicians and crews (around 120m²).
- The Niger Air Force (military airport) lent their large hangar where three of the research aircraft as well as the SCOUT and CNES balloons team could be sheltered. Moreover, they continuously offered their assistance for logistical issues.
- ACMAD provided a large meeting room to organise the forecasting activity, which involved African meteorologists coming from various meteorological services of the region.
- DMN (Direction de la Météorologie Nationale du Niger) offered an entire villa with a large meeting room used for the daily SOP briefings, and several offices for the scientific secretariat and for scientists; this villa had been inhabited for several years and required an heavy rebuilding program in order to be used as the nervous centre of the SOP operations;

All these offices needed to be completely refurbished and equipped with air conditioning. For most of them, the electricity or power supply needed to be significantly upgraded and secured. At the military airport, the number of offices was not sufficient to shelter all the teams operating there. It took 8 months to define a scheme allowing to supply the needed office and technical space and to carry out the associated refurbishing of the existing spaces and building of new spaces.

The AMMA Operation Center in Niger :



(iv) Communications

Good communications (especially Internet) between the AOC sites and the outside world for accessing numerical weather forecasting products and satellite data was a key requirement of AMMA.

As explained below, the existing facilities needed a drastic improvement. A request for funding the corresponding work and equipment was submitted to AMMA-EU who contributed 110 k€ for this task. The additional source of funding and effort for implementation was given by Meteo-France with a support of ACMAD.

iv-a) The status of communications in Niamey before AMMA

The means of telecommunication available in Niamey vary in technology and reliability. The historical (and recently privatised) operator's main offer for data transfer is based on specialised links (LS) with flows of 64kbit/s and 128kbit/s. In addition, the outdated nature of the network is such that frequent cuts or malfunctioning occur.

It therefore appeared out of question for the AOC telecommunications network to rely on this network. Furthermore, the state of the local installations did not satisfy the AMMA needs in term of speed and amount of data to be transmitted between the various AOCs and scientific teams based in Niamey.

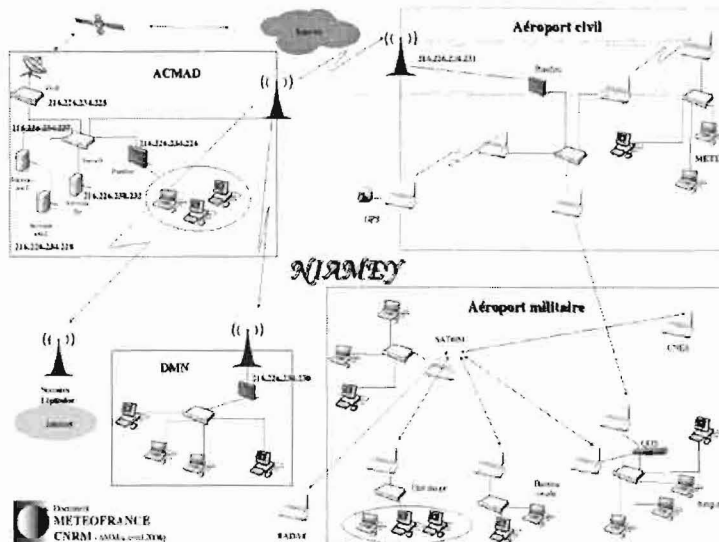
Alternatives existed, based on radio transmissions by satellite for Internet access, coupled with Local Radio Loops (11Mbits/s) between the AOC transmission centers. This solution had already been implemented in Niamey by the bank agencies for the Internet and by ACMAD and ASECNA/DMN for data exchange between the airport and ACMAD.

iv-b) Network setup for AMMA in Niamey

The proposed type of Internet access for the AOC was via satellite (VSAT or Geolink) 684/384 KB (download/upload). Inter-site connections was of the theoretical 11 Mb/s (1 Mb/s real) local radio loop type, thereby connecting the main centres: ACMAD, the civil and military airports and DMN.

The structure installed for the AOC by the Meteo-France engineers is schematized in the figure below. It provided the following functions during all the SOPs:

- A protected operational network for the AMMA AOC, providing data exchange between AOC's four geographical sites, integrating the server that houses AMMA's Internet site and offering a printing service for all the participants in AMMA connected by the network.
- A network for receiving scientific visitors, allowing them free Internet access for their laptops (WIFI or RJ45), free access to AMMA Intranet, data exchange and document printing.



iv-c) Overall assessment of operation

All the objectives have been achieved following the AMMA-EU DOW. For the decision making cycle, it was implemented a network system with possibility to receive satellite images, quicklooks and meteorological products and a communication system to be able to maintain contact with the various AOC sites in Niger and in the region.

Thus, it was important to maintain and to monitor 24h/24 and 7day/day the internet connexions between the airports, the SOP Coordination Center and ACMAD (where all the meteorological products from the major European and American forecasting centres and the satellite images are received). These products were needed at the DMN to plan the oncoming operations or to propose a strategy of coordination between the different instruments and for the future missions. At the airports, necessity to have direct access on radar images from the MIT for the nowcasting needs was requested and also implemented.

Moreover, full-Internet access was available in the different sites of the AOC-Niamey to make Internet accessible to both scientists and operational teams in an efficient and sustainable manner.

In conclusion, this mission was accomplished in working in close collaboration with the local partners to create a networking infrastructure in a town where quite none had existed. To secure the operations, this operational network has been installed with its own clean power source, back-up generator, servers and routers for provision of Internet service for around 350 scientists and instrument operators.

iv-d) Future of this network beyond AMMA

Capacity building in the domains of climate monitoring, data archiving and analysis are the main fallbacks expected from AMMA by the operational met and hydrological services who are strongly involved in the project.

Building the AOC is not only an operation tailored to the AMMA scientific needs. It involves an important training component as well as an application component, which are part of the overall AMMA commitment to research for development. Partnership and multidisciplinarity are at the core of AMMA. The feasibility and long term benefits of AMMA require an effective participation and involvement of African scientists and institutions. This rule was applied to the AOC as well as to the other AMMA components. New computing and communications equipments acquired for the different partners will stay on site after AMMA.

More generally, the communication infrastructure that was setup for the AOC will significantly contribute to facilitate the cooperation in the domain of science and technology between the various regional research and application centres, the operational national service, and the universities. This will greatly improve the capacity of these institutions in term of data analysis, archiving and diffusion. In particular, this will facilitate the sending of synoptic data and quality controlled messages on the GTS. Last, but not least, the training associated with this deployment of new equipment will contribute to the increase the capacity building in the domain of data analysis.

To finish, at international level, scientists agree to recognize that the AOC web server based at Toulouse (Meteo-France) with a mirror at ACMAD with several meteorological products and satellite data is unique and is a useful scientific tool which will serve all scientists working in the region.

The overall assessment of the AOC work was very positive, as shown from the letters sent by various teams to the ICIG or the IGB, acknowledging that without the support of the AOC their deployment would not have been possible. This success was made possible thanks to a good coordination and collaboration between IRD and METEO-France and to the overall good collaboration spirit between the various teams that participated to the SOP.

5) Perspectives de recherche

5.1) Thèmes de recherches en cours et à initier pour le prochain quadriennal

Cette partie présente d'une part, les thèmes de recherche à poursuivre ainsi que ceux à initier pour le prochain quadriennal et d'autre part, l'implication au LTHE et la stratégie de mise en œuvre avec les axes prioritaires. Elle se décompose en trois parties :

a) Thèmes de recherche en cours et à poursuivre:

- i. Système de mousson et interactions ondes-convection – pluie dans un contexte de variabilité et de changement du climat en Afrique de l'Ouest
- *Variabilité multi-échelles de la convection en Afrique de l'Ouest et sur l'Atlantique tropicale*
 - *Représentation du cycle de vie des systèmes convectifs avec le modèle LMDZ pendant la campagne AMMA 2006.*

b) Thèmes à initier :

- ii. Facteurs de l'atmosphère et des surfaces continentales influençant le régime pluviométrique en Afrique de l'Ouest
- iii. Régionalisation du changement climatique en Afrique de l'Ouest
- iv. Variabilité multi-échelles de la convection sur l'Amérique Latine

c) Implication au LTHE et stratégie de mise en œuvre

a) Système de mousson et interactions ondes-convection – pluie dans un contexte de variabilité et de changement du climat en Afrique de l'Ouest

Le Barbé et Lebel (1997) ont montré que la réduction et la variabilité des précipitations au Sahel sont fortement associées à la variation du nombre d'événements pluviométriques. Ces événements sont d'origine convective, les plus importants étant les systèmes convectifs de méso-échelle qui apportent 90% du total pluviométrique (Laurent et al., 1998 ; Mathon et Laurent, 2001 ; Mathon et al., 2002a). Le système convectif de méso-échelle apparaît donc comme un élément essentiel à la compréhension du climat des régions Sahéliennes: il est la clef entre le forçage de grande échelle et les précipitations locales.

Mais s'il existe, en première approximation, une bonne relation entre les événements pluvieux ainsi définis et les systèmes convectifs observés par satellite, la question des liens entre variabilité interannuelle des précipitations et systèmes convectifs reste toujours ouverte (Lebel et al. 2003).

Ces systèmes convectifs de méso-échelle interagissent avec les ondes d'échelle synoptique (les ondes d'Est, Diedhiou et al., 1999, 2001) et avec les fluctuations du flux de mousson qui modulent les caractéristiques du flux de vapeur d'eau d'origine océanique sur le continent. Les mécanismes qui régissent ces interactions sont actuellement mal compris (Mathon et al., 2002b ; Lavaysse et al., 2006). Il importe donc d'approfondir nos connaissances sur les variations des événements convectifs et des phénomènes atmosphériques associés en Afrique de l'ouest.

Les travaux en cours concernent l'étude de la relation onde - convection - pluie aux échelles spatio-temporelle caractéristiques et s'articulent autour de deux axes :

- a. *Variabilité multi-échelles de la convection en Afrique de l'Ouest et sur l'Atlantique tropicale*
- b. *Représentation du cycle de vie des systèmes convectifs avec le modèle LMDZ pendant la campagne AMMA 2006 (thèse IRD Youssouph Sané au LMD)*

a) Variabilité multi-échelles de la convection en Afrique de l'Ouest et sur l'Atlantique tropicale

L'objectif ici est de mieux comprendre la dynamique de ces systèmes pluviogènes et leurs interactions avec la circulation de plus grande échelle, en particulier avec les différents régimes d'ondes d'Est, la dépression thermique saharienne, le flux de mousson qui modulent différemment la pluviométrie quotidienne, et qui sont, avec les systèmes convectifs, les "objets" météorologiques principaux sur cette région.

Notre contribution se décline en trois axes de recherches :

- a. *Etude comparative de l'environnement synoptique associé aux MCS arrivant sur le degré carré de Niamey et sur l'Ouémé et caractérisation de la pluie associée (intensité, durée et forme des hyéogrammes).*
- b. *Etude de l'influence comparée des ondes d'est, du flux de mousson et de la dépression thermique saharienne sur l'efficacité pluviométrique des MCS.*
- c. *Etude climatologique et multi-échelles de la variabilité et de l'occurrence des situations des dry spells en zone sahélienne.*

b) Représentation du cycle de vie des systèmes convectifs avec le modèle LMDZ pendant la campagne AMMA 2006

(Thèse IRD de Youssouph Sané au LMD avec Arona Diedhiou et Aida Diongue co-directeurs et Frédéric Hourdin, Directeur de thèse) :

Si beaucoup de progrès ont été réalisés ces dernières années pour que les modèles soient capables de représenter de façon relativement correcte les caractéristiques moyennes du système de mousson, très peu en revanche ont été évalués dans leur capacité à représenter de façon réaliste le système convectif de méso-échelle.

La bonne représentation de ces systèmes est pourtant un enjeu à deux titres : d'abord parce que l'organisation en systèmes conditionne la distribution spatio-temporelle locale des pluies, et que la bonne représentation de cette distribution est essentielle pour les études d'impact sur l'agriculture et pour les études de couplage/forçage avec l'hydrologie.

Ce travail mené en partie dans le cadre de la thèse de Youssouph Sané s'attaquera donc à la difficile question de la représentation des systèmes convectifs organisés dans les modèles de climat avec pour but ultime de simuler correctement le cycle annuel de l'eau sur l'Afrique de l'Ouest avec le modèle LMDZ.

- a. *Le premier objectif de la thèse est d'effectuer une « réanalyse » de la campagne de mesures du programme AMMA. Pour ce faire, le modèle sera d'abord configuré en mode prévision (avec un guidage aux bords par les prévisions du CEPMMT ou de NCEP) pour modéliser des cas d'événements convectifs. En plus de ce guidage par des champs dynamiques, on utilisera une nouvelle formulation du déclenchement de la convection qui devrait permettre d'initialiser les systèmes au bon endroit afin d'obtenir des pluies simulées en phase avec les observations, en utilisant les observations infrarouges des satellites géostationnaires.*
- b. *Le deuxième objectif consiste à étudier d'une part l'environnement dynamique dans lequel se déclenchent et se développent ces systèmes convectifs, particulièrement leurs interactions avec les ondes d'est synoptiques et d'autre part, de caractériser les conditions de surface associées. Dans ce dernier volet, des simulations « en mode climatique » (sans guidage) seront réalisées pour la saison 2006 et comparées avec les observations issues d'AMMA.*

b) Facteurs de l'atmosphère et des surfaces continentales influençant le régime pluviométrique en Afrique de l'Ouest

En Afrique de l'Ouest, la pluie dépend de trois phénomènes étroitement imbriqués : le système de mousson, en relation avec la circulation générale, les conditions de surfaces continentales et océaniques (les gradients méridiens d'énergies en surface à l'échelle régionale) et la convection de mésoéchelle. Si Le

Barbé et Lebel (1997) ont montré que la variabilité interannuelle des précipitations en Afrique de l'Ouest s'explique principalement par une variation du nombre des événements pluvieux, et semble peu liée à la variation du cumul moyen de précipitations par événement, la fréquence de ces systèmes précipitants (plus que leurs caractéristiques) semble par contre plus sensible aux processus de surface continentaux dans des modèles de circulation générale (Polcher, 1995).

En effet, Les rétroactions entre la surface et le système de mousson s'opèrent à travers la couche limite atmosphérique qui alimente en énergie les MCS et contribuent à influencer les propriétés de ces MCS durant toute leurs cycles de vie.

Mais même si des rétroactions positives entre les pluies et l'humidité du sol ont été mises en évidence à grande échelle (Bounoua and Krishnamurti, 1993 ; Koster et al. 2004) et à méso-échelle (Taylor and Lebel ; 1998) suggérant la complexité des phénomènes de différentes échelles intervenant sur l'efficacité pluviométrique de ces MCS, comprendre la variabilité du régime pluviométrique en Afrique de l'Ouest nécessite surtout de suivre l'occurrence des MCS et d'identifier les facteurs influant sur leur cycle de vie en précisant le rôle potentiel joué par les structures synoptiques et les conditions de surface sur leur efficacité pluviométrique.

Par ailleurs, les ondes d'Est ne semblent pas jouer un rôle sur le degré d'organisation de ces systèmes (Mathon et al., 2002). Elles semblent en revanche avoir un effet sur l'efficacité pluviométrique des SCM et modifier la modulation diurne de la pluie associée à ces systèmes. Une étude menée au LTHE sur les interactions onde - convection - pluie en Afrique de l'Ouest a montré que ce lien n'est pas direct ; en présence d'onde (convergence à l'échelle synoptique et donc situation favorable à une convection profonde), on pouvait avoir un système convectif mais, celui ci peut générer ou pas de la pluie en surface (Lavaysse et al., 2003 ; Fink et Reiner 2003). C'est ce qui explique en partie pourquoi, à l'échelle interannuelle, les corrélations sont mauvaises et toute la difficulté de prévoir le temps, d'estimer les précipitations par satellite ou de faire le lien entre système convectif vu par satellite et événement pluvieux. D'ailleurs, il a aussi été établi que le nombre d'ondes d'est ne jouent pas un rôle majeur à l'échelle interannuelle sur la variabilité des systèmes convectifs (Lebel et al., 2003). D'où, l'idée et la nécessité de se placer d'abord dans l'intrasaisonner et de revoir cette relation onde – système convectifs – événement pluvieux à cette échelle pour savoir qu'elle est le rôle de la couche limite, des conditions de surface et celui de la grande échelle.

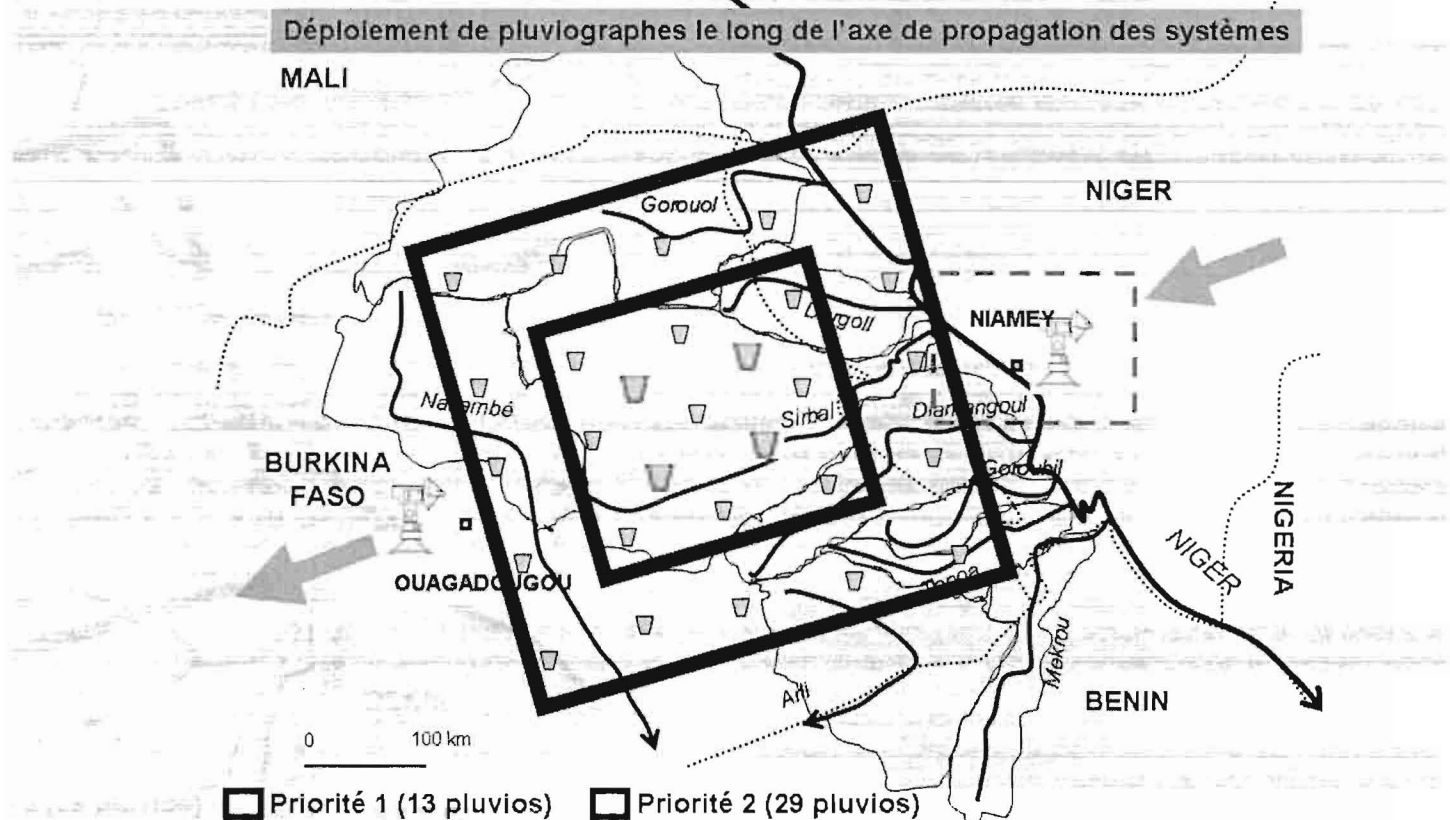
L'objectif de cette proposition est de caractériser les facteurs de l'environnement synoptique et des conditions de surface influençant le régime pluviométrique associé aux systèmes convectifs durant leur cycle de vie à l'échelle régionale. Plus particulièrement, par rapport à l'ORE, il s'agit d'étudier, à l'échelle intrasaisonnière et de façon rétrospective à l'échelle interannuelle sur un axe Niamey-Ouaga :

- (i) d'une part, l'influence comparée du flux de mousson, des ondes d'est et de la dépression thermique ouest - africaine sur l'efficacité pluviométrique associée à chaque système convectif.
- (ii) et d'autre part, de façon diagnostique, le rôle des conditions de surface (NDVI, albédo, rugosité, ETP) sur la genèse, l'occurrence, la trajectoire et l'efficacité pluviométrique des systèmes. Il s'agit aussi de mener des études de sensibilité avec un modèle climatique régional pour étudier le rôle potentiel des conditions de surface (albédo, rugosité, humidité du sol, ETR) sur le cycle de vie des MCS : genèse, occurrence (dry spells et persistance), trajectoire, environnement synoptique et efficacité pluviométrique

En complément de cette étude et dans la perspective des futures missions satellitaires (SMOS et MEGHA-TROPIQUES), nous envisageons de proposer le Projet VESPA (Variabilité et Efficacité des Systèmes Précipitants en Afrique) afin d'étudier le rôle de l'humidité des sols et mieux caractériser l'efficacité pluviométrique des systèmes convectifs durant leur cycle de vie. Il s'agit en perspectives de profiter de SMOS et de MEGHA-TROPIQUES pour compléter les études précédentes par des études de cas et des études composites à l'échelle régionale. VESPA devrait contribuer à atteindre les objectifs suivants :

- o Revue des conditions de surfaces associées aux zones de genèse des systèmes.
- o Peut-on lier efficacité pluviométrique des MCS et environnement synoptique ?
- o Peut-on lier efficacité pluviométrique des MCS et conditions de surface ?
- o Peut-on lier trajectoire des MCS et conditions de surface ?

Pour cela, la stratégie d'observation doit aussi intégrer une vue plus régionale et tenir compte de la faible densité de pluviographes à l'heure actuelle. Il faut donc renforcer le système d'observation au sol par un déploiement du réseau de pluviographes entre Niamey et Ouagadougou (cf figure) avec 13 pluviographes (en Priorité 1 ; ou 29 pluviographes en Priorité 2). L'orientation du réseau pluviométrique est conçue dès le départ pour prendre en compte la direction moyenne d'arrivée des lignes de grains.



Pluviographes à installer le long de l'axe Niamey-Ouaga avec deux options

Au-delà des aspects suivi de l'efficacité pluviométrique des systèmes convectifs et étude de la variabilité spatiale de la pluie, ce nouveau réseau, s'il est endossé de façon concertée et cohérente entre les équipes HCLIM et (HGB-IBIS), contribuera à l'exercice de calibration/validation des futurs missions satellitaires (SMOS et Megha-tropique) et servira aussi de site de validation de modèles régionaux. Par ailleurs, beaucoup d'études ont été menées sur la réponse des hydro-systèmes en zone de sédiment et nous disposons de beaucoup de données sur les bassins endoréiques. La zone proposée dans le cadre de ce projet a l'intérêt d'explorer de nouvelles questions sur la variabilité de la ressource en eau en zone de socle et plus généralement, dans les bassins exoréiques comme la Sirba pour lesquels nous savons peu de choses. Enfin, l'instrumentation prévue est en forte synergie avec le réseau déployé par les collègues de HSM au Nord du Burkina -Faso et en particulier dans le Nakambé en étroite collaboration avec les partenaires de 2IE (Institut International d'Ingénierie pour l'eau et l'Environnement).

c) Régionalisation du changement climatique en Afrique de l'Ouest

La compréhension de l'évolution climatique de notre planète et de ses impacts constitue un des grands enjeux de la recherche du XXI^e siècle. En zone intertropicale, cette évolution du climat a un impact global (c'est la source chaude du climat de la planète). A l'échelle régionale, en Afrique de l'Ouest, cette variabilité s'est traduite par une période de sécheresse prolongée de près de 30 ans ayant eu des conséquences majeures sur les économies et sur les populations des états concernés.

En effet, dans son rapport sur les impacts probables du changement climatique, le GIEC prédit que les effets du changement climatique frapperont tout particulièrement les communautés les plus pauvres et les plus démunies face à la multiplication et à l'aggravation des phénomènes météorologiques et estime qu'il

faut s'attendre à une réduction générale du rendement agricole dans la plupart des régions tropicales et subtropicales, à une baisse des ressources en eau dans les régions - notamment subtropicales - souffrant déjà de pénuries chroniques. L'Afrique comme la plupart des régions en développement serait particulièrement vulnérable aux impacts potentiels de changements climatique.

Les modèles sont cohérents quand il s'agit de simuler la répartition des changements de température ou de précipitation sur de très grande échelle d'espace (tropiques, moyennes et hautes latitudes, continents par rapport aux océans). Cependant, à l'échelle d'une région particulière, les différences sont notables. La plus grande disparité entre les modèles se retrouve sur l'amplitude et la répartition géographique des précipitations et cela provient du caractère de très petite échelle des événements pluvieux, difficiles à représenter dans les modèles climatiques. Or il se trouve que le régime pluviométrique en Afrique de l'Ouest est expliqué à plus de 80 % par des systèmes convectifs de méso-échelle. Une difficulté supplémentaire survient lorsque l'on veut prévoir les conséquences potentielles d'un changement climatique. Pour que ces prévisions aient un sens et puissent déboucher sur des mesures d'adaptation, celles-ci doivent être évaluées à des échelles d'espace au moins régionales, voire locales.

Ces incertitudes sur le futur du climat en Afrique de l'Ouest (y compris dans le 4ème et dernier rapport du GIEC) constituent une préoccupation majeure clairement exprimée dans le rapport de la conférence internationale pour la « réduction de la vulnérabilité des systèmes naturels, économiques et sociaux en Afrique de l'ouest, face aux changements climatiques », organisée par la Commission Economique pour l'Afrique des Nations unies à Ouagadougou, du 24 au 27 Janvier 2007.

Notre contribution comporte deux objectifs :

- a. *Une évaluation approfondie des simulations issues de plusieurs modèles pour mieux préciser les incertitudes sur le régime pluviométrique en Afrique de l'Ouest.*
- b. *Une régionalisation de ces scénarios sur des sites pilotes (ORE AMMA-CATCH) en utilisant les techniques de désagrégation (downscaling) préalablement évaluées sur l'Afrique de l'Ouest.*

Notre ambition est de proposer des indicateurs fiables et significatifs de l'évolution du régime pluviométrique à l'échelle régionale et locale pour pouvoir faire un suivi et prévoir sa variabilité dans le futur, en fonction des différents scénarios climatiques. Il s'agit de proposer de façon objective, aux échelles régionales et locales, des différentes scénarios possibles d'évolution du régime pluviométrique pour permettre des études d'impact et des stratégies d'adaptation appropriées. In fine, le croisement de différentes sources de données devraient aboutir à des résultats utiles pour permettre des études d'impact sur la ressource en eau et sur l'agriculture.

d) Variabilité multi-échelles de la convection sur l'Amérique Latine

Ce projet rentre dans la continuité des travaux initiés au LTHE par Henri Laurent dans le cadre d'une collaboration avec le Brésil (Luiz Machado ; CPTEC). Toujours en collaboration avec le CPTEC, il est prévu d'étudier le comportement de la Zone de Convergence Inter-tropical (ZCIT) et de la Zone de Convergence de l'Atlantique Sud (ZCAS) sur le domaine Atlantique tropical – Amérique Latine dans leurs fluctuations allant des échelles intra-saisonnière à interannuelle, et à travers la variabilité liée aux Systèmes Convectifs de Méso-échelle et à leurs interactions avec les conditions de surface océaniques et continentales (Dessay et al, 2004 ; Machado and Laurent (2004)).

Plus particulièrement,

- a. à l'échelle intrasaisonnière, on étudiera les interactions entre les MCS et leur environnement atmosphérique sur différents zones géographiques et on fera une étude comparative avec la variabilité de la convection en Afrique de l'Ouest.
- b. Ensuite, on investiguera les téléconnexions potentielles entre l'Afrique de l'Ouest et l'Amérique Latine (propagation des Ondes d'est Africaines sur l'Amérique Latine et comment ils organisent la convection sur le Nord-Est Brésilien).

5.2 Implication au LTHE et stratégie de mise en œuvre

Notre projet s'intègre pleinement dans la prospective de l'équipe HCLIM du LTHE dont l'ambition est de comprendre les processus associés à la genèse et au cycle de vie des systèmes convectifs ainsi que la pluie en analysant leur lien avec la dynamique atmosphérique de grande échelle et les processus de surface. Notre projet s'appuie sur la synergie entre observations in-situ et satellites d'une part et modélisation d'autre part pour aborder la question des interactions ondes-convection-pluie :

- En particulier, nous utiliserons les précipitations observées dans les différents sites de méso-échelle de l'ORE AMMA-CATCH porté par le LTHE. De même dans le cadre du projet sur le suivi de l'efficacité pluviométrique des systèmes convectifs que nous proposons ici, nous envisageons un renforcement du système d'observation au sol par un déploiement du réseau de pluviographes entre Niamey et Ouagadougou, axe de propagation des lignes de grains. Ce nouveau réseau, s'il est endossé de façon concertée et cohérente entre les équipes HCLIM et (HGP-IBIS), contribuera :
 - à l'exercice de calibration/validation de futures missions satellitaires (SMOS et Megha-Tropique) dans lequel le LTHE est impliqué
 - aux études sur la réponse des hydro-systèmes et sur la variabilité de la ressource en eau en zone de socle et dans les bassins exoréiques, comme posées dans la prospective (HGP-IBIS).
- Pour la convection, nous utiliserons aussi l'observation par satellite : le suivi des systèmes convectifs se fera en première approximation avec l'OLR de la NOAA et plus finement avec les sorties du logiciel de tracking ISIS-RDT développé par METEO-France à partir des données du satellite Meteosat Seconde Génération (MSG). De même, les futures missions satellitaires à venir (Megha-Tropique et SMOS), dans lesquelles le LTHE est impliquée pour les exercices de calibration/validation, seront une opportunité pour aborder la problématique de la variabilité de l'efficacité pluviométrique des systèmes convectifs durant leur cycle de vie avec le projet VESPA et la méthodologie pourra être transférée sur la Méditerranée dans le cadre de HyMeX.
- Pour la dynamique atmosphérique, les réanalyses américaines et européennes ainsi que les scénarios du GIEC pour la grande échelle seront utilisées en complément avec les sorties de modélisation atmosphérique régionale, avec le modèle WRF implanté au CRC (Université de Bourgogne ; Dijon) pour des études de sensibilité aux conditions de surface et avec le modèle LMDZ de l'IPSL (sensibilité de la variabilité de la convection et de la pluie au guidage et au déclenchement).

Plus généralement, les outils d'analyse développés ici peuvent être indifféremment utilisés pour l'étude de la convection tropicale (Afrique de l'Ouest – Brésil) et tempérée (Bassin Méditerranéen et Alpes), permettant ainsi des transferts d'expertises d'un « chantier » à l'autre.

- En priorité 1, il importe de profiter du jeu de données acquises durant le programme AMMA et de consolider la ressource humaine pour poursuivre les thèmes de recherche en cours sur le système de mousson et les interactions ondes-convection – pluie dans un contexte de variabilité et de changement du climat en Afrique de l'Ouest. La thèse en cours au LMD sur la représentation des systèmes convectifs dans les modèles contribuera aux études menées au LTHE sur la réponse des hydro-systèmes à la variabilité temporelle et spatiale du forçage par les précipitations. En effet, un des résultats attendus de cette thèse dans laquelle plusieurs simulations guidées seront réalisées est de comprendre où, quand et comment (quantité) il pleut ; quel est l'effet de la variabilité atmosphérique sur les systèmes convectifs et la pluie et enfin, quels sont les processus de l'atmosphère qui sont associés au déclenchement et à l'initiation de la convection. Cette dernière problématique est très complémentaire à celle posée en interne dans la prospective de l'équipe HCLIM qui s'attache à comprendre quels sont les processus de convection qui sont à l'origine de la répartition spatio-temporelle de la pluie.
- En priorité 1, la proposition « Facteurs de l'atmosphère et des surfaces continentales influençant le régime pluviométrique en Afrique de l'Ouest » doit être considérée comme une action transversale s'appuyant pour sa mise en œuvre sur les ressources humaines et l'expertise des deux équipes. Ainsi, ce projet renforcera la collaboration et les interactions entre les équipes HCLIM et HGP-IBIS,

- Enfin, certaines parties de cette prospective (priorité 2) sont en cours d'élaboration et pour leur mise en œuvre, les stratégies suivantes seront proposées :
 - Chaires croisées avec l'Université d'Abidjan Cocody avec comme propositions d'axes de recherche pour des échanges bilatéraux et Demande de bourse de thèse DSF/IRD pour un étudiant de l'université Abdou Moumouni de Niamey sur la « Régionalisation du changement climatique en Afrique de l'Ouest et contributions aux études d'impact sur la ressource en eau et sur l'agriculture ».
 - Bourses d'échanges scientifiques (ESCD/IRD) avec le Brésil (Luis Machado, CPTEC) : le thème scientifique commun : interactions ondes – convection – pluie et ondes – convection – végétation dans un contexte de variabilité et de changement du climat.

Plus généralement, la prospective présentée ici permettra de renforcer notre partenariat au niveau local avec l'OSUG (notamment le LGGE) dans le domaine de la régionalisation du Climat, au niveau national avec le CRC/Dijon, le CNRM/Toulouse, l'IPSL/Paris sur l'étude de la variabilité du régime pluviométrique et de la physique de l'atmosphère et enfin, au niveau international (Brésil, Afrique) autour de l'étude du climat régional et de la variabilité de la convection et de la pluie (Université de Dakar (LPAOSF), Université de Abidjan Cocody (LAPA-MF), Université Abdou Moumouni de Niamey (Dept. De Physique), CPTEC (Brésil)).

8) Sélection d'articles

1. **Diedhiou** A., S. Janicot, A. Viltard, P. De Felice, H. Laurent, **1999**. Easterly waves regimes and associated convection over West Africa and the tropical Atlantic : results from the NCEP/NCAR and ECMWF reanalyses. *Climate. Dynamics.*, 15, 795-822.
2. Redelsperger J.L., Diongue A., **Diedhiou** A., Ceron J.P., Diop M., Gueremy J.F., Lafore J.P., **2002b**: Multiscale description of a Sahelian synoptic weather system representative of West African monsoon. *Quart. Journ. Roy. Meteor. Soc.*, 128 : 1229-1257.
3. Mathon V., A. **Diedhiou**, H. Laurent, **2002c**: Relationship between easterly waves and mesoscale convective systems over the Sahel. *Geophys. Res. Lett.*, vol. 29 (8) : 57/1-4.
4. Sultan B., S. Janicot, et A. **Diedhiou**, **2003a**. The West African monsoon dynamics, Part I : Intraseasonal variability. *Journal of Climate*, 16, 3389-3406
5. Lebel, T.; **Diedhiou**, A.; Laurent, H. **2003b**: Seasonal cycle and interannual variability of the Sahelian rainfall at hydrological scales. *Journal of Geophysical Research*. Vol. 108; D8. 8389.
6. Ali A.; A. Amani; A. **Diedhiou**; T. Lebel, **2005**. Rainfall estimation in the Sahel. Part 2: Evaluation of Raingauge Networks in the CILSS Countries and Objective Intercomparison of Rainfall Products. *J. of Applied Meteor.*, 44(11) pp. 1707–1722.
7. Redelsperger, J.L., Thorncroft, C., **Diedhiou**, A., Lebel, T., Parker, D.J. and J. Polcher, **2006**: African Monsoon Multidisciplinary Analysis (AMMA): An International Research Project and Field Campaign. Published in *BAMS*, Volume 87, Issue 12 (December 2006) , pp. 1739–1746.

A. Diedhiou · S. Janicot · A. Viltard · P. de Felice
H. Laurent

Easterly wave regimes and associated convection over West Africa and tropical Atlantic: results from the NCEP/NCAR and ECMWF reanalyses

Received: 28 May 1998 / Accepted: 2 May 1999

Abstract NCEP/NCAR and ECMWF daily reanalyses are used to investigate the synoptic variability of easterly waves over West Africa and tropical Atlantic at 700 hPa in northern summer between 1979–1995 (1979–1993 for ECMWF). Spectral analysis of the meridional wind component at 700 hPa highlighted two main periodicity bands, between 3 and 5 days, and 6 and 9 days. The 3–5-day easterly wave regime has already been widely investigated, but only on shorter datasets. These waves grow both north and south of the African Easterly Jet (AEJ). The two main tracks, noted over West Africa at 5°N and 15°N, converge over the Atlantic on latitude 17.5°N. These waves are more active in August–September than in June–July. Their average wavelength/phase speed varies from about 3000 km/8 m s⁻¹ north of the jet to 5000 km/12 m s⁻¹ south of the jet. Rainfall, convection and monsoon flux are significantly modulated by these waves, convection in the Inter-Tropical Convergence Zone (ITCZ) being enhanced in the trough and ahead of it, with a wide meridional extension. Compared to the 3–5-day waves, the 6–9-day regime is intermittent and the corresponding wind field pattern has both similar and contrasting characteristics. The only main track is located north of the AEJ along 17.5°N both over West Africa and the Atlantic. The mean wavelength is higher, about 5000 km long, and the average phase speed is about

7 m s⁻¹. Then the wind field perturbation is mostly evident at the AEJ latitude and north of it. The perturbation structure is similar to that of 3–5-days in the north except that the more developed circulation centers, moving more to the north, lead to a large modulation of the jet zonal wind component. South of the AEJ, the wind field perturbation is weaker and quite different. The zonal wind core of the jet appears to be an almost symmetric axis in the 6–9-day wind field pattern, a clockwise circulation north of the AEJ being associated with a counter-clockwise circulation south of the jet, and vice versa. These 6–9-day easterly waves also affect significantly rainfall, convection and monsoon flux but in a different way, inducing large zonal convective bands in the ITCZ, mostly in the trough and behind it. As opposed to the 3–5-day wave regime, these rainfall anomalies are associated with anomalies of opposite sign over the Guinea coast and the Sahelian regions. Over the continent, these waves are more active in June–July, and in August–September over the ocean. GATE phase I gave an example of such an active 6–9-day wave pattern. Considered as a sequence of weak easterly wave activity, this phase was also a sequence of high 6–9-day easterly wave activity. We suggest that the 6–9-day regime results from an interaction between the 3–5-day easterly wave regime (maintained by the barotropic/baroclinic instability of the AEJ), and the development of strong anticyclonic circulations, north of the jet over West Africa, and both north and south of the jet over the Atlantic, significantly affecting the jet zonal wind component. The permanent subtropical anticyclones (Azores, Libya, St Helena) could help initiation and maintenance of such regime over West Africa and tropical Atlantic. Based on an a priori period-band criterion, our synoptic classification has enabled us to point out two statistical and meteorological easterly wave regimes over West Africa and tropical Atlantic. NCEP/NCAR and ECMWF reanalyses are in good agreement, the main difference being a more developed easterly wave activity in the

A. Diedhiou
Laboratoire de Meteorologie Dynamique du CNRS,
Ecole Polytechnique, Palaiseau, France

S. Janicot (✉)
METEO-FRANCE, Laboratoire de Meteorologie Dynamique du
CNRS, Ecole Polytechnique, Palaiseau, France
E-mail: janicot@lmd.ens.fr

A. Viltard · P. de Felice
Universite Paris XII, Laboratoire de Meteorologie Dynamique du
CNRS, Ecole Polytechnique, Palaiseau, France

H. Laurent
Institut de Recherche pour le Developpement, Montpellier, France

NCEP/NCAR reanalyses, especially for the 3–5-day regime over the Atlantic.

1 Introduction

Easterly waves have been identified as fundamental features of synoptic weather systems over West Africa and tropical Atlantic during northern summer. They are westward travelling waves originating west of 20°E, through barotropic and baroclinic conversions of energy from the African Easterly Jet (AEJ), located at 600 hPa (Burpee 1972; Rennick 1976, 1981; Simmons 1977; Reed et al. 1977; Norquist et al. 1977; Walker and Rowntree 1977; Thompson et al. 1979; Mass 1979; Kwon 1989; Thorncroft and Hoskins 1994a, b; Paradis et al. 1995; Thorncroft 1995). These waves' kinematic characteristics have been described in studies dealing with operational radiosounding networks (Carlson 1969a, b; Burpee 1972, 1974), forecast model analyses (Reed et al. 1988a, b; Duvel 1990), and, particularly the intensive observational program of the GARP Atlantic Tropical Experiment (GATE) made during summer 1974 (Burpee 1975; Reed et al. 1977; Norquist et al. 1977; Thompson et al. 1979; Albignat and Reed 1980; Chen and Ogura 1982). Typically African easterly waves occur both on the equatorward and poleward sides of the AEJ, with a greater amplitude at the jet level towards the equator and a greater amplitude at low levels poleward. Their wavelength varies between 2000 km and 4000 km at a westward speed of about 8 m s^{-1} , leading to spectral periodicities of between 3 and 5 days. The two preferential tracks observed over West Africa north and south of the AEJ converge into one track, located north of the jet over the tropical Atlantic (Reed et al. 1988a, b). Observations suggest also that the interaction between easterly waves and convection is different north and south of the AEJ (Burpee 1974; Duvel 1990). On the equatorward side of the jet, convective heating is located in the trough and ahead of it, while on the poleward side of the jet the convection is located mostly in the southerly moist winds behind the trough. Easterly waves south of the jet are also characterized by a southwest-northeast horizontal tilt indicating barotropic energy conversions and either by the absence of vertical tilt (in phase III of GATE; Reed et al. 1977) expressing the great influence of convective heating, or the existence of a vertical tilt opposed to the vertical wind shear (in summers 1968 and 1969; Burpee 1974) indicating the significant role of baroclinic conversions of energy and the weak interaction with deep convection. North of the jet, easterly waves are characterized by wide baroclinic energy conversion expressed by the opposition of the vertical tilt to the vertical wind shear.

Another periodic signal of between 6 and 9 days, has also been detected over West Africa and tropical Atlantic, on wind components in the middle and lower

troposphere, on sea level pressure, precipitable water, cloud cover, using station and radiosounding data as well as ECMWF analyses and satellite data (Cadet and Houston 1984; Cadet and Nnoli 1987; de Felice et al. 1990, 1993; Viltard et al. 1997; Viltard et al. 1998; Pytharoulis and Thorncroft 1999). Based on a small dataset, de Felice et al. (1990, 1993) and Viltard et al. (1997) showed that it corresponds to a westward propagating signal with a wavelength of about 6000 km and a velocity of about 8.5° longitude per day. The strongest modulation was noticed on the zonal wind component of the AEJ at 12.5°N. Viltard et al. (1998) also showed that rainfall over West Africa can be significantly altered in this band period.

As part of the West African Monsoon Project (WAMP), this work aims to investigate the long-term wind field patterns at 700 hPa associated with the 6–9-day signal and to compare it to the 3–5-day wave pattern. (More information concerning WAMP can be found on the web site <http://www.reading.ac.uk/~swsthcri/tropical.html>.) Previous studies addressing the question of easterly waves over West Africa and tropical Atlantic presented results computed over short periods like the phase III of GATE (30 August–19 September, 1974), which was often used and may be considered as a reference, especially following work by Reed et al. (1977, 1988a, b) and Norquist et al. (1977) or for particular years (see Burpee 1972, 1974, 1975; Carlson 1969a, b; Duvel 1989, 1990; Reed et al. 1977, 1988a, b; de Felice et al. 1990, 1993; Viltard et al. 1997, 1998). For the first time, the initiation of different reanalysis projects offers the opportunity to establish easterly wave climatology and interannual variability in a long-term period based on homogeneous datasets. Towards this goal, we used the National Centers for Environmental Prediction/National Center for Atmospheric Research (NCEP/NCAR) reanalyses for the period 1979–95 and the European Center for Medium-Range Weather Forecasts reanalyses (ERA) for the period 1979–93. Since there has been some discussion in previous papers about the occurrence of different kinds of easterly waves (3–5-day periods and 6–9-day periods), we will reconsider the whole issue. The reference variable in our analysis is the meridional component of the wind at 700 hPa. We chose to use such a pressure level instead of the 850 hPa level, also often used, to be outside the monsoon layer even when near the Guinea coast. (An index to define the top of the monsoon layer, used by Lamb 1983, or Janicot 1992, is the pressure level where the zonal component of the wind shifts from west to east; at 850 hPa the mean wind can have a westerly component over West Africa.) We also preferred to use the wind meridional component instead of its relative vorticity, firstly because previous studies showed that both the 3–5-day and the 6–9-day waves can easily be detected with this variable, secondly because relative vorticity constitutes a noisier field, which is more difficult to use.

The different datasets are presented in Sect. 2. Meridional wind component spectral analysis at 700 hPa is presented in Sect. 3, pointing out the two period domains, between 3 and 5 days and between 6 and 9 days. In Sect. 4 the main elements of the 3–5-day and 6–9-day easterly waves kinematics at 700 hPa (preferential tracks, wavelengths, phase speeds) are analyzed for West Africa and tropical Atlantic. For easterly waves of each kind, spatial patterns at 700 hPa are displayed in Sect. 5, for an individual case in summer 1988, for the composite average wind fields, and finally for another individual case observed during the GATE phase I. It is also demonstrated that rainfall and convection organization in the ITCZ, as well as monsoon wind field, are modulated differently by the 3–5-day and the 6–9-day regimes of easterly waves. We finally suggest that the 6–9-day easterly wave regime results from an interaction between the 3–5-day regime of easterly waves and large westward-moving anticyclonic cells related to the Libyan and Azores anticyclones in the Northern Hemisphere, and the St Helena anticyclone in the Southern Hemisphere. These results are discussed in Sect. 6.

2 Data

2.1 NCEP/NCAR reanalyses

The National Centers for Environmental Prediction (NCEP) and the National Center for Atmospheric Research (NCAR) have completed a reanalysis project with a current version of the Medium Range Forecast (MRF) model (Kalnay et al. 1996). This dataset consists of a reanalysis of the global observational network of meteorological variables (wind, temperature, geopotential height, humidity in pressure levels, surface variables, and flux variables like precipitation rates) with a “frozen” state-of-the-art analysis and forecast system at a triangular spectral truncation of T62 to perform data assimilation throughout the period 1958 to present. This enables us to circumvent problems of previous numerical weather prediction analyses due to changes in techniques, models and data assimilation. Data are reported on a $2.5^\circ \times 2.5^\circ$ grid every 6 h (00.00, 06.00, 12.00 and 18.00 UTC), in 17 pressure levels from 1000 hPa to 10 hPa, which are good resolutions for studying synoptic waves. We used data covering the period 1 June–30 September, from 1979 to 1995, with one value per day, by averaging the four daily outputs. As we focus on synoptic easterly waves, we will mainly consider wind fields at 700 hPa. This reanalysis dataset will be considered the “reference” dataset, because it is presently available for the period 1958–1997 and can be used to investigate interannual variability of West African monsoon. In particular it enabled us to examine the wind fields for GATE summer in 1974. The interannual variability of filtered variances during the period 1968–97 will also be presented (see Fig. 4).

2.2 ECMWF reanalyses (ERA)

The European Centre for Medium-Range Weather Forecasts (ECMWF) also recently completed its reanalysis project (ERA), which used a frozen version of their analysis-forecast system, at a triangular spectral truncation of T106 with 31 levels in the vertical, to perform data assimilation, using data from 1979 to 1993 (Gibson et al. 1997). In comparison with NCEP/NCAR reanalyses, there are

also 17 pressure levels from 1000 hPa to 10 hPa but with an additional level at 775 hPa and a missing level at 20 hPa. According to our objectives, daily data have been interpolated on the $2.5^\circ \times 2.5^\circ$ NCEP/NCAR grid. The results have been computed on the 1979–93 period, which is almost similar to the 1979–95 period used with NCEP/NCAR reanalyses. The ERA dataset will be used in comparison to the NCEP/NCAR “reference” dataset, in order to evaluate the quality, the uncertainty of the wind field, and its dynamics produced by the American reanalyses. The climatology established over West Africa by Senouci (1990), with the ECMWF analysis during the period 1980–88, has also been taken into account.

2.3 Monthly GFDL gridded and daily radiosoundings

The upper-air dataset originated from the Geophysical Fluid Dynamics Laboratory (GFDL) Atmospheric Circulation Tape Library (NOAA). It consists of the monthly averages of atmospheric parameters objectively analyzed on a 73×73 global grid (2.5° latitude, 5° longitude) at 11 pressure levels from 1000 hPa to 50 hPa, from May 1958 to December 1989. Data comes from global rawinsonde data (Oort 1978, 1983; Oort and Liu 1993). The data density differs depending on geographical domains. The West African rawinsonde network mainly documents the 4°N – 6°N latitudinal belt, the Sudan-Sahelian zone and some Saharan locations. The West African domain along the 0° meridian is rather well documented and considered highly reliable analyzed area (Oort 1983, p 74). However, the quality of the 1000 hPa and 50 hPa levels is poorer than intermediate levels. To validate the 1979–95 monthly average fields of NCEP/NCAR reanalysis, we have used the climatology established over West Africa with this dataset for the period 1970–88 (Janicot 1993), as well as results published in Fontaine et al. (1995).

To validate the reanalysis outputs, especially regarding daily wind values spectral analysis, we focused on daily radiosoundings of Abidjan (5.25°N ; 3.93°W), Niamey (13.48°N ; 2.17°E) and Tamanrasset (22.78°N ; 5.52°E) at 12.00 UTC, extracted from the ECMWF archive system for the period 1980–95. Unfortunately, these data are not of high quality because of missing values and the occurrence of obviously false measurements. However, after corrections, some comparisons have been performed using these data.

2.4 IRD daily rainfall

Daily rainfall amount at stations located on the West African domain 3°N – 20°N / 18°W – 25°E have been compiled by IRD (Institut de Recherche pour le Developpement; previously ORSTOM), ASECNA (Agence pour la Securite de la Navigation Aerienne en Afrique et a Madagascar) and CIEH (Comite Interafriacain d'Etudes Hydrauliques). These data are available for the period 1979–93, including more than 1300 stations in 1979 and 1980, between 700 and 860 for the period 1981–90, and less than 230 since 1991. We only used this dataset for the period 1979–90. These daily values were interpolated on the NCEP $2.5^\circ \times 2.5^\circ$ grid, by assigning each station's daily value to the nearest grid point and averaging all the values related to each grid point. They were also interpolated in time, related to NCEP daily wind fields since daily rainfall amounts were measured between 06.00 LST of the day and 06.00 LST of the following day. We applied a time-lag of 12 h between the average time of the NCEP daily values (09.00 UTC) and an approximated average time of “daily” precipitation over the West African continent (21.00 LST; Duvel 1989, indicates a maximum of high cloud coverage over land between 18.00 LST and midnight, Sow 1997, points out a maximum of half-hourly precipitation over the Senegal between 17.00 LST and the end of the night, depending on the stations). The greatest density of stations is located between the latitudes 5°N to 15°N on the NCEP grid. Data on latitudes 17.5°N can also be considered since the number of available stations is still high, from 43 stations at 1979 to 32 in 1990.

2.5 OLR/NOAA dataset

Since 1974, launching of polar orbital TIROS-NOAA (National Oceanic and Atmospheric Administration) satellites has enabled us to establish a quasi-complete series of twice-daily measures of outgoing longwave radiation (OLR), at the top-of-the atmosphere and at a resolution of 2.5° latitude/longitude (Grueber and Krueger 1974). In tropical areas, deep convection and rainfall can be estimated through low OLR values. Local measurement times varied during the period 1979–1995 between 02.30 h and 07.30 h in the morning and between 14.30 h and 19.30 h in the afternoon. However, an estimation of the average daily OLR, based on two values separated by 12 h seems rather good if we consider a diurnal cycle for deep convection.

2.6 Comments on reanalyses evaluation

Reanalyses were established with a frozen analysis and forecast system over the whole period considered here. However, variations of kind and quality of instruments providing observations (for instance, changes in rawinsondes or introduction of satellite cloud wind estimates in the 1970s) can lead to large inhomogeneities in some parameters over a long-term period. Moreover, reanalyses do not overcome the problem of data sparsity over areas such as the Sahara and Atlantic. Two kinds of parameters were considered, firstly, those close to the raw observations, such as horizontal winds or sea level pressure, secondly, those largely controlled by the model such as rainfall, vertical velocity or divergence wind field.

We computed with the NCEP/NCAR reanalyses the West African Monsoon Index (WAMI) defined in Fontaine et al. (1995) with GFDL rawinsonde dataset. This index is the difference between the monthly average wind speed at 900 hPa and the zonal wind component at 200 hPa. The correlation coefficient, computed from August values for the period 1968–89, between this index and an equivalent one computed with the NCEP/NCAR wind speed at 200 hPa and 925 hPa is +0.77, and no homogeneity break was found in the NCEP/NCAR index time series.

Correlations were computed for each summer between daily radiosonde 700 hPa meridional wind time series at Tamanrasset, Niamey, Abidjan, and similar NCEP/NCAR values at the nearest grid points. The range of correlations over the 17 summers spread from +0.43 to +0.69 for Tamanrasset, +0.32 to +0.69 for Niamey, +0.44 to +0.72 for Abidjan, with an overall average coefficient of +0.57. Some of these coefficients are low, especially when computed for radiosounding time series with a large number of missing values. Another reason, especially for Niamey's low coefficients, is that the average seasonal cycle in the reanalyses is rarely identical to the radiosounding one.

Rainfall in West Africa, given by the NCEP/NCAR reanalyses, was also compared to observed rainfall indexes (Fontaine et al. 1999). Correlation coefficients between reanalyses precipitation and raingauge-based indexes, computed for the period 1968–1994, are +0.74 for the July–September Guinea coast index and only +0.39 for the Sahel index. The Sahel result is due to a very important decrease of NCEP/NCAR rainfall for this period but, when this artificial trend is removed, interannual variability of residual rainfall is consistent with observed variability. Moreover, this homogeneity break occurs at the end of the 1970s, so it should not have a significant impact in this study which was made for the period 1979–95.

In Kallberg (1997), a homogeneity break in the ERA, resulting in a latitudinal shift of the ITCZ over Central Africa, is shown at the beginning of 1987, seemingly due to the replacement of satellite TOVS cloud cleared radiances data of NOAA-9 by NOAA-10 data, leading to a break in the precipitable water time series (A. Fink, personal communication). This also had consequences in the number of easterly wave tracks over this region (K. Hodges and C. Thorncroft, personal communication). However, it seems that

synoptic activity was not modified over West Africa and the tropical Atlantic. We computed the interannual time series of the filtered variances averaged on West Africa and the tropical Atlantic (see Fig. 4). The NCEP/NCAR and ERA variance time series are highly correlated and no homogeneity break is evident.

3 Spectral analysis

The ITCZ is located at its northernmost position over West Africa in northern summer during the rainy season in the Sahel. From the IRD observation values, the average rainfall pattern during this season consists of a rainbelt of about $6\text{--}7 \text{ mm day}^{-1}$ at 8°N – 10°N (up to more than 14 mm day^{-1} on the Fouta Djalon mountains along the southwest coast of West Africa) with a rapid rainfall decrease northward leading to an average amount of 2 mm day^{-1} at about 15°N . The rainfall field given by NCEP/NCAR reanalyses is qualitatively in agreement with IRD observations (not shown). The rainbelt is located at 7°N – 9°N with a maximum of $7\text{--}8 \text{ mm day}^{-1}$ reaching 12 mm day^{-1} on Fouta Djalon. The northward gradient is very steep too but if the mean rainfall amount is similar in the western Sahel, it decreases too strongly eastward and, as an example, the isohyet 1 mm day^{-1} is located south of Lake Chad whereas a mean value of 2 mm day^{-1} is present in the IRD rainfall field.

The main features of the circulation over West Africa and the tropical Atlantic are present in the NCEP/NCAR reanalyses (monsoon in the lower layers, AEJ at 600 hPa and Tropical Easterly Jet, TEJ, at 200/100 hPa, deep convection in the ITCZ at 5° – 10°N , dry convection over the Saharan heat low at 20°N). The AEJ is located over West Africa in the mid troposphere (Fig. 1a, b). During the rainy season, the core of the jet is moving northward up to 15°N , reaching a maximum mean speed of 12 m s^{-1} and the level of 600 hPa. On the borders of the rainy season, the jet is located at 5°N and has a core speed of 10 m s^{-1} in the 650–700 hPa layer. The main longitudinal variation of the jet is a lowering of the core level westward, from 600 hPa over West Africa to 700 hPa over the tropical Atlantic. A secondary jet axis is present between 700 hPa and 600 hPa at 5°S over Central Africa. It is strongest in August–September (Fig. 1b). This southern jet, limited in longitude, has already been identified with radiosonde data by Burpee (1972) and it also appears in the GFDL radiosonding dataset (Janicot 1993). Comparison of reanalysis values with both observational measures and ECMWF analyses at monthly time scale shows considerable similarity, even concerning vertical velocity (Senouci 1990; Fontaine et al. 1995). Comparisons with ERA (Fig. 1c, d) show that the AEJ in the NCEP/NCAR reanalyses is about 2 m s^{-1} stronger than in the ERA but located at the same latitude, as well as for the easterly maximum along the coast of Central Africa at 5°S .

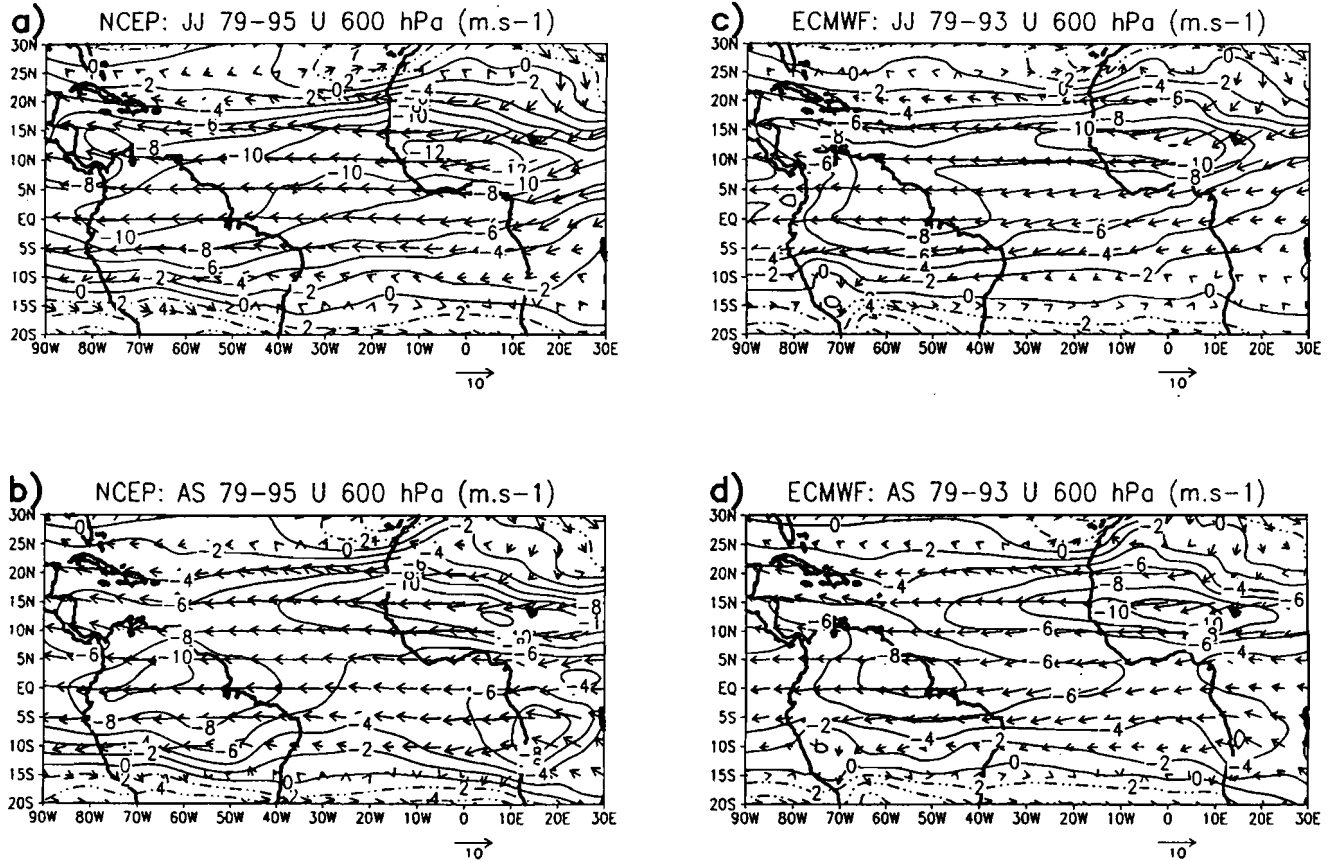


Fig. 1a-d Mean vectors of the NCEP/NCAR wind at 600 hPa in **a** June–July and **b** August–September 1979–1995 and isolines of the zonal wind component. **c, d** Same as **a** and **b** but for ERA for the

period 1979–1993. For vectors only one grid point out of two are displayed. The vector scale is indicated and isolines are expressed in m s^{-1} (dashed lines for westerly component)

When investigating synoptic activity in any part of the world, one of the most useful approaches is to perform spectral analysis. Spectral analysis was done very frequently for the African easterly waves and in most of the papers referenced in the Introduction, a signal was found between 3 and 5 days in the mid troposphere and identified with the “easterly waves”. In another series of papers (de Felice et al. 1990, 1993; Viltard et al. 1997), significant spectral energy was also seen over a second interval of periods between 6 and 9 days, both in radiosonde data and in ECMWF analysis.

Figure 2a, b shows the average latitude/energy spectra computed from individual FFT spectra of NCEP/NCAR 700 hPa meridional wind daily time series from 1 June to 30 September and averaged for the period 1979–1995, over the West African continent (20°W – 10°E) and the tropical Atlantic (60°W – 20°W). Over West Africa, in agreement with previous studies, we find spectral peaks at 3.5 days and 4.5 days in the latitude band 5°S – 20°N , with shorter periods south of 10°N . Between 10°N and 20°N we note a spectral signal between 4 and 5 days and peaks at 5.5, 6.5 and 7.6 days. A larger spectral signal is located north of

20°N for periods between 5 days and 20 days with maxima at about 6 days, 8 days and 10 days. Over the tropical Atlantic, the spectral energy is stronger between 15°N and 30°N for periods between 4 days and 9 days. This confirms the previous studies performed on shorter and different datasets and especially the evidence of spectral signals for the periods 6 to 9 days north of the AEJ (We chose to name the easterly wind core AEJ both over West Africa and tropical Atlantic, Fig. 1 shows that this core is still evident over the ocean at 40°W – 50°W in August–September.)

To test the significance of energy inside these band periods, we applied a procedure similar to that used in Burpee (1972) and Diedhiou et al. (1998). Burpee (1972) considered the percentage of total variance in band-periods as a satisfactory indicator of wave activity. Similar mean FFT power spectra were computed, using $N \times 17$ randomly generated series of 122 elements, where N is the number of grid points used to compute the initial average spectra ($N = 13$ over the longitudes from 20°W to 10°E and $N = 17$ over the longitudes 60°W to 20°W), and 17 is the number of years for the period 1979–95. This process was repeated 1000 times, and for each harmonic the threshold of the upper 1%

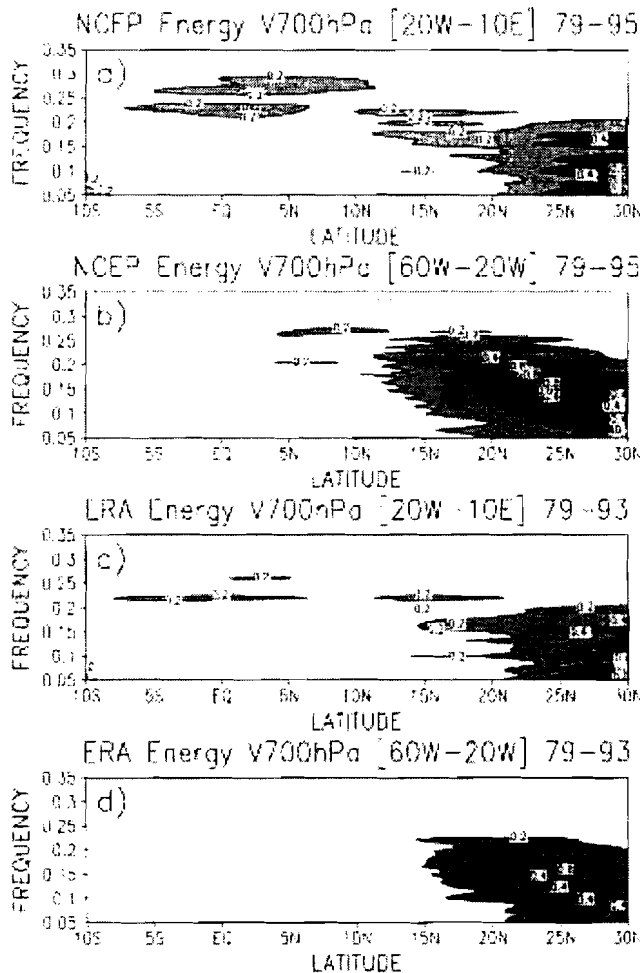


Fig. 2a-d Mean latitude/energy spectrum computed from individual FFT spectra of NCEP/NCAR 700 hPa meridional wind daily time series from 1 June to 30 September, averaged for the period 1979–1995 and **a** for the domain 20°W–10°E and **b** for the domain 60°W–20°W. **c, d** Same as **a** and **b** but for ERA for the period 1979–1993. Latitudes on abscissa are from 10°S to 30°N. Frequencies on ordinate are shown from 0.05 (period 20 days) to 0.35 (period 2.8 days). Energy is in $\text{m}^2 \text{s}^{-2}$

of total variance fraction was selected among these 1000 values. Comparisons with the values of the power spectra show that variance fractions, contained in the three band-periods 3–4 days, 4–5-days and 6–9-days, are significant at least at the 1% statistical level. Figure 2c, d shows similar spectral computations for the ERA. Spectral energy patterns are similar to the NCEP/NCAR ones whereas an overall lower variance, particularly in the 3–5-day periodicities, is evident in ERA spectra.

Spectral analyses were also performed with the NCEP/NCAR vorticity at 700 hPa (not shown). Average spectra computed on 1979–95 are similar to those obtained with the meridional component of the wind. Variance computations based on vorticity were computed for summer 1985 by Reed et al. (1988a, b) with ECMWF analysis wind data. Their variance maxima between 3 and

5 days are located at latitudes 13°N and 20°N over West Africa (see Fig. 4 of Reed et al. 1988b). The spectrum of NCEP/NCAR vorticity for 1985 only, also shows two maxima at these latitudes over West Africa (not shown). We can therefore conclude that the difference of latitude between our average spectra (our Fig. 2) and Reed et al.'s (1988a, b) results (their Fig. 4) is mainly due to the interannual variability of easterly waves.

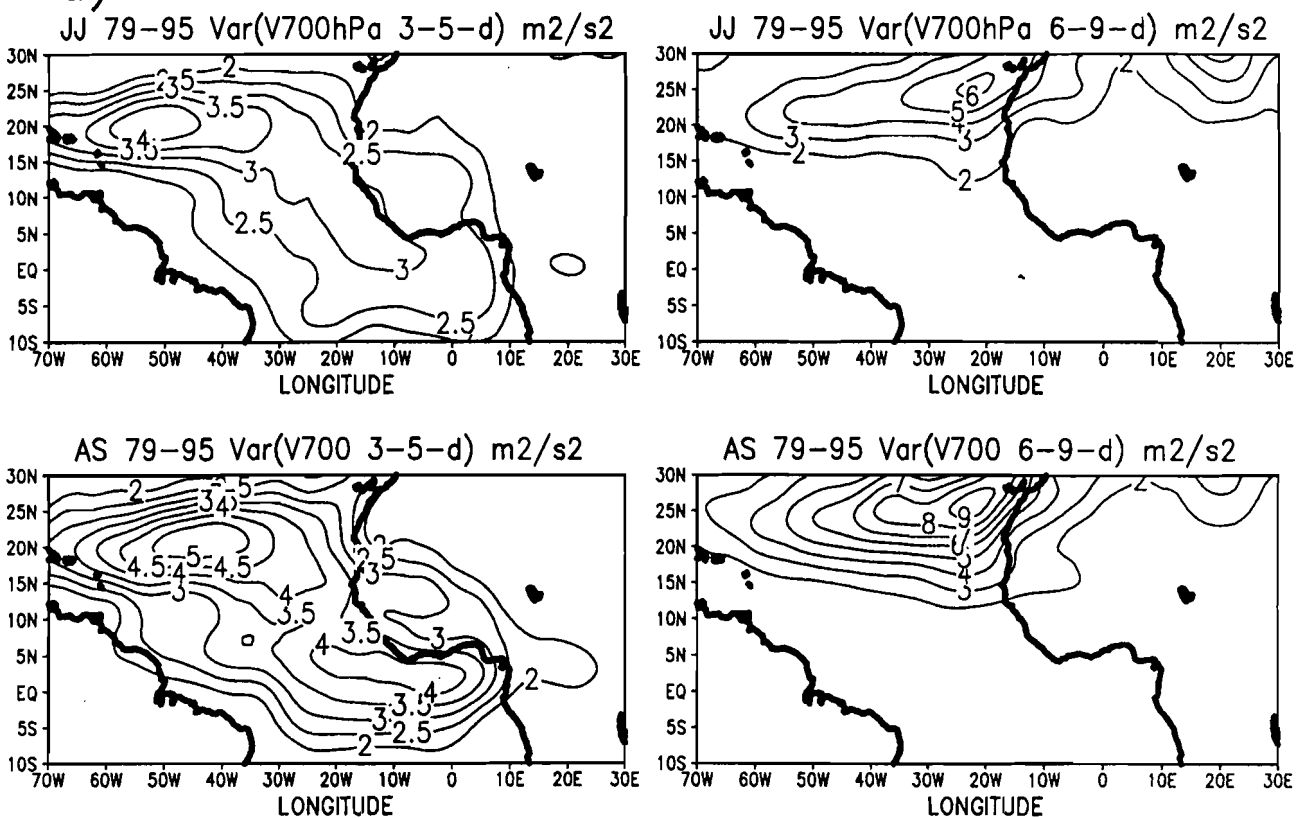
From this spectral analysis and following a classical approach in similar studies, we filtered the wind components at 700 hPa by a bandpass filter, first between 3 and 5 days, and then between 6 and 9 days, by combining highpass and lowpass filters with a very steep cut-off (for the 3–5-day waves for instance, we used a highpass filter with a half-power point at a frequency of $(5.2 \text{ day})^{-1}$ and a lowpass filter with a half-power point at a frequency of $(2.9 \text{ day})^{-1}$). Figure 3a shows the variance of the filtered signal for the meridional component of the NCEP/NCAR wind at 700 hPa averaged for the period 1979–95. For the 3–5-day period filtered signal, the greatest variances are located over West Africa west of 10°E and south of 20°N, over the Gulf of Guinea, and over the tropical Atlantic with high values about 20°N. The signal is clearly enhanced in August–September and two latitudes of variance maximum are differentiated, at 12.5°N over West Africa and at 2.5°N over the Gulf of Guinea. On the southern latitude the signal is extending eastward over Central Africa between the southern edge of the AEJ and the northern edge of the localized maximum of easterly wind at 5°S.

For the 6–9-day period filtered signal, the greatest variances are located further north and east than for the 3–5-day waves, north of 20°N over East and West Africa and north of 15°N over the Atlantic. The signal is stronger over the ocean during the whole summer. It is enhanced over the continent in June–July and over the ocean in August–September. These high variances are located in the area of anticyclonic circulations (see Fig. 1), associated at the surface with the Libyan and Azores anticyclones. Variance decreases strongly southward, being low over West and Central Africa. The variance of filtered zonal wind component was also examined since studies on the 6–9-day wave indicated the large effect of the AEJ (de Felice et al. 1990, 1993; Viltard et al. 1997). The greatest values (not shown) are located at the same latitudes as the meridional component over West Africa but further south over the Atlantic, along 15°N.

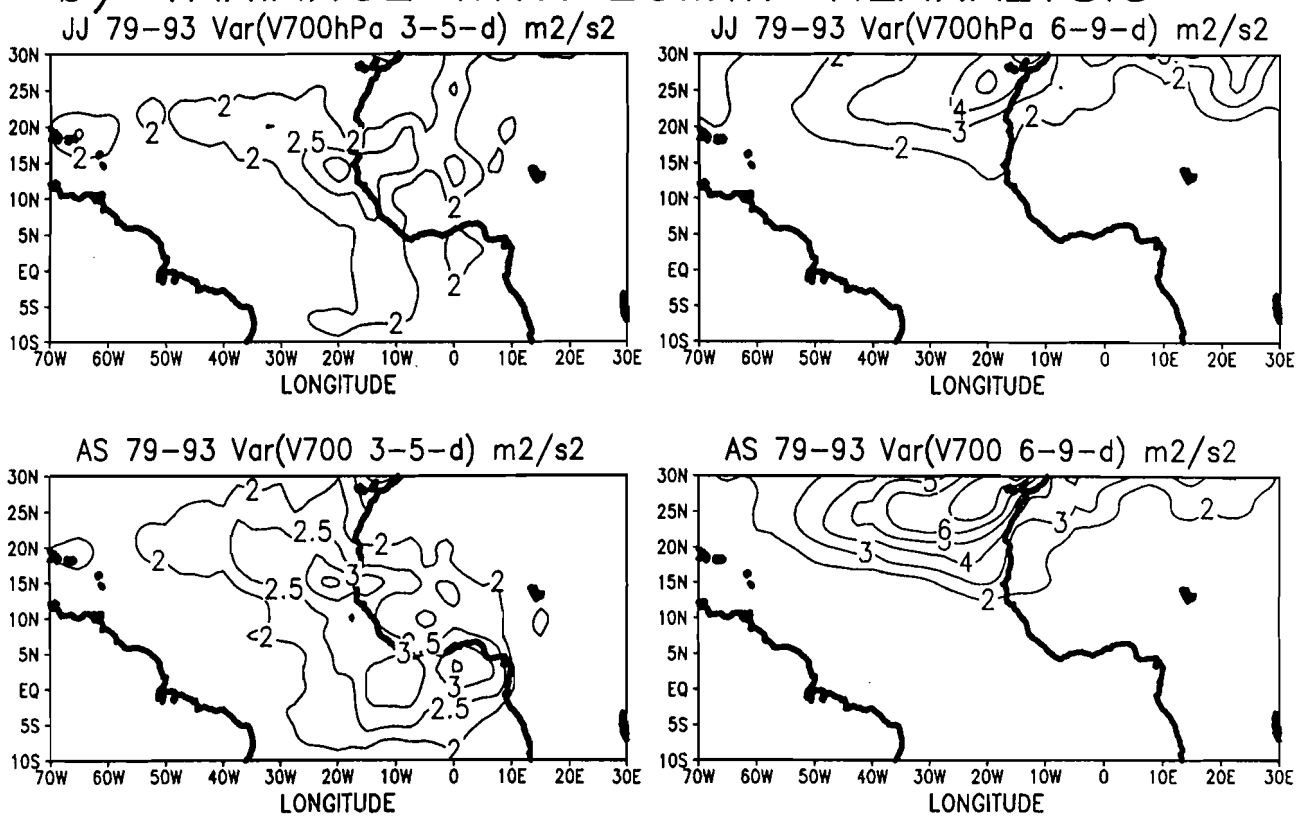
Comparisons were made with daily radiosonde values of meridional wind at 700 hPa. FFT average

Fig. 3 a Mean 1979–1995 variance of the meridional component of the NCEP/NCAR wind at 700 hPa (in $\text{m}^2 \text{s}^{-2}$) in June–July (top) and August–September (bottom), filtered between 3 and 5 days (left) and between 6 and 9 days (right). **b** Same as **a** but for ERA for 1979–1993

a) VARIANCE WITH NCEP REANALYSIS



b) VARIANCE WITH ECMWF REANALYSIS



spectra computed on available complete series are noisier than NCEP/NCAR grid points spectra (not shown). The energy in the 3–5-day band remains high, and it is lower for the 6–9-day band, in agreement with previous results.

Figure 3b shows similar computations for the ERA for the period 1979–93. As shown by Fig. 3, the variance patterns related to the 3–5-day signal display some differences with NCEP/NCAR patterns, in particular over central Atlantic, where the signal is weak. On the other hand a variance maximum is evident at 20°W/15°N along the African Atlantic coast (in agreement with the previous study of Duvel (1990) based on ECMWF analyses). Moreover, the signal is less organized in June–July over the Gulf of Guinea. These patterns are noisier, perhaps resulting from the highest truncation for the ERA (T106 compared to T79). However, the latitudes of variance maxima are similar in the

two reanalysis datasets, 15°N over West Africa, south of the Guinea coast and 20°N over the Atlantic. Finally, the seasonal cycle is similar with an enhancement of synoptic activity in August–September.

The 6–9-day variance patterns are very similar, except that the variances are once again greater in the NCEP/NCAR reanalyses in particular in the western Atlantic. The two maxima associated with the Libyan and the Azores anticyclones are nevertheless evident in the ERA and the same seasonal evolution is displayed with a stronger signal in the Libyan area in June–July and over the ocean in August–September.

Figure 4 displays the interannual variability of the 3–5-day and the 6–9-day filtered variances averaged over West Africa and over the tropical Atlantic, during the period 1968–97 for NCEP/NCAR data and during the period 1979–93 for ERA data. The time series for the two reanalyses are highly correlated at the

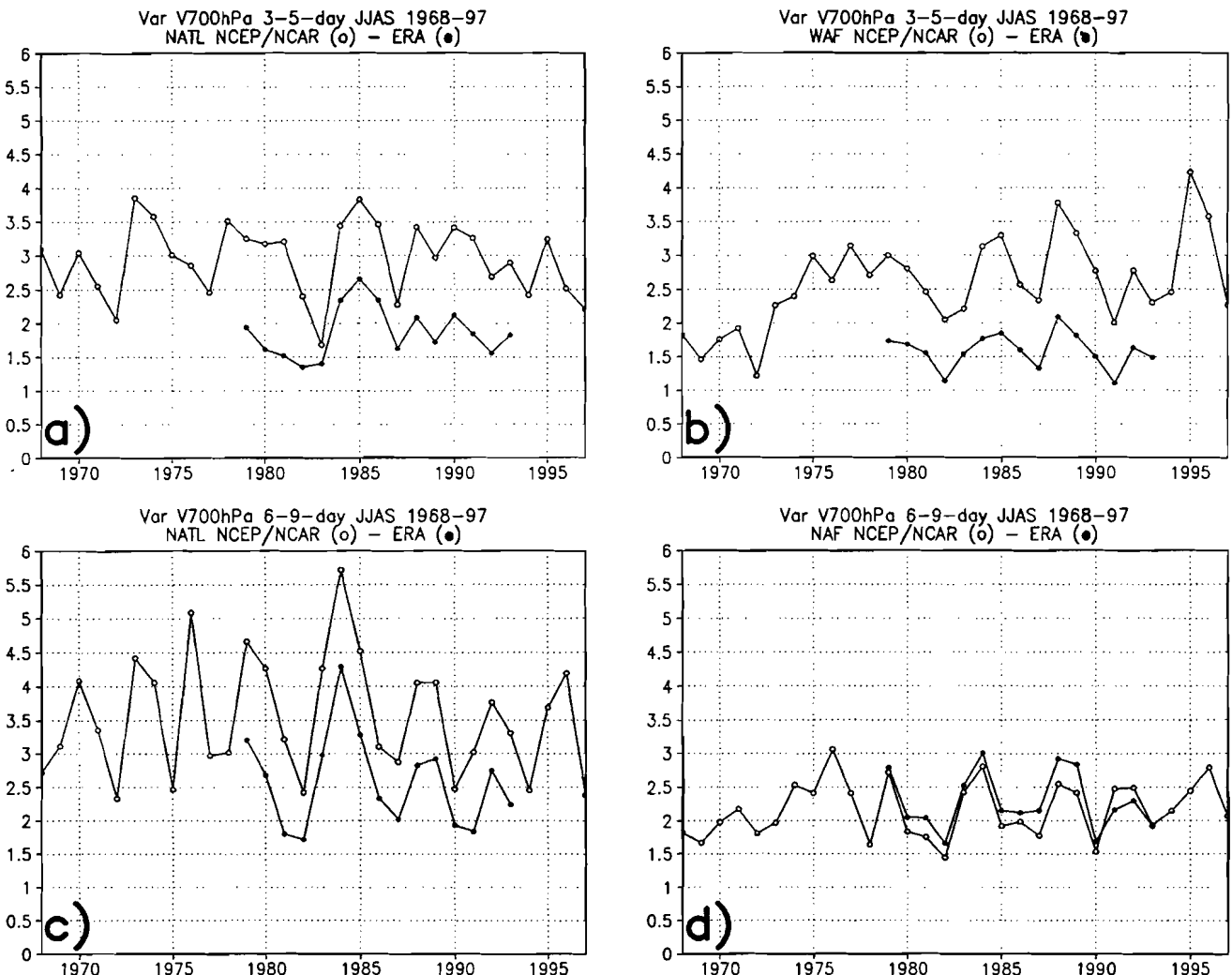


Fig. 4 **a** Time series of mean June–September daily variances ($\text{m}^2 \text{s}^{-2}$) of 3–5-day filtered meridional wind component at 700 hPa averaged over the tropical Atlantic (12.5°N – 30°N / 70°W – 20°W).

b Same as **a** but for West Africa (0° – 20°N / 20°W – 10°E). **c** Same as **a** but for 6–9-day variances. **d** Same as **b** but for 6–9-day variances over North Africa (10°N – 30°N / 20°W – 30°E).

interannual time scale for the common period 1979–93. This can be considered as a good point in the evaluation of the wave activity in the reanalyses. As seen previously, the wave activity is, on the other hand, clearly weaker in ERA. We can also note a positive trend in the NCEP/NCAR 3–5-day variances averaged over West Africa during the period 1968–1997. The reason for such a trend is beyond the scope of this work.

4 Kinematics

In this section, we investigate kinematic characteristics of the 3–5-day and the 6–9-day wind perturbation (preferential tracks, wavelengths, phase speeds) before examining more precisely their patterns in Sect. 5. This

study was based on the filtered meridional component of the wind at 700 hPa and it derived from the method developed by Wallace et al. (1988) on synoptic westerly waves over the Northern Hemisphere. To improve the accuracy of computations, we used a grid of 0.25 degree latitude/longitude by linearly interpolating the 2.5° NCEP/NCAR and ERA data before performing computations. Results are presented for the sequence June–September and averaged on the 1979–95 period for the NCEP/NCAR reanalyses and during the period 1979–93 for ERA (Fig. 5).

4.1 3–5-day waves

To estimate the preferential wave tracks of synoptic waves, we made computations based on one point

a NCEP: KINEMATICS OF 3–5–day WAVES

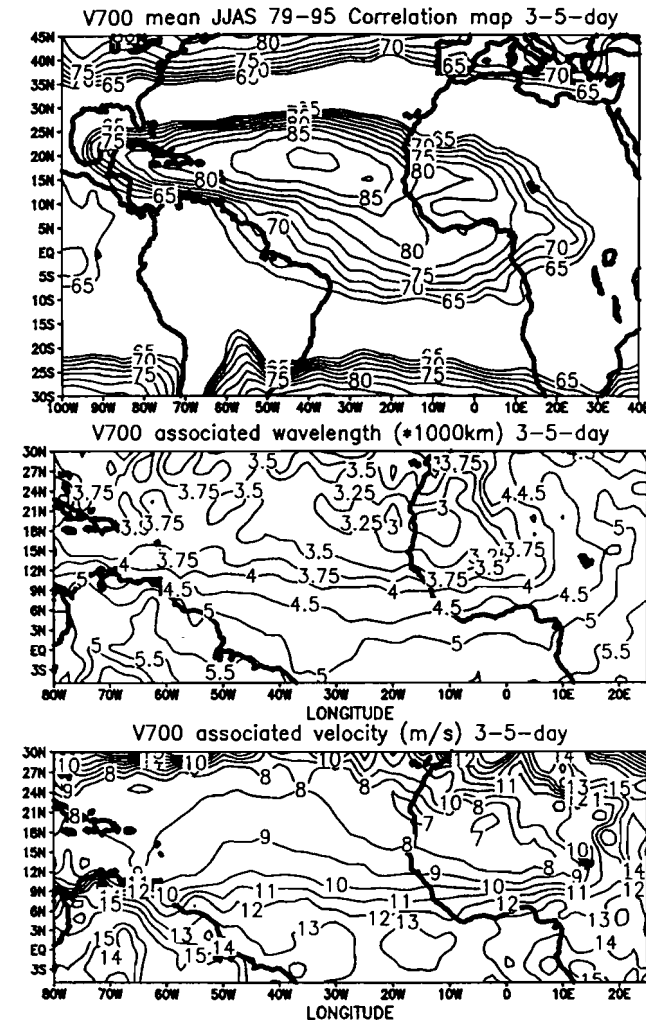


Fig 5 a *Left:* kinematics characteristics computed for the 3–5-day meridional NCEP/NCAR wind components at 700 hPa by the Wallace et al. (1988) method for summers of 1979–1995 (see detail in the text). *Top:* estimated wave tracks; the highest correlation coefficients (expressed in %) display the preferential tracks of the waves.

ECMWF: KINEMATICS OF 3–5–day WAVES

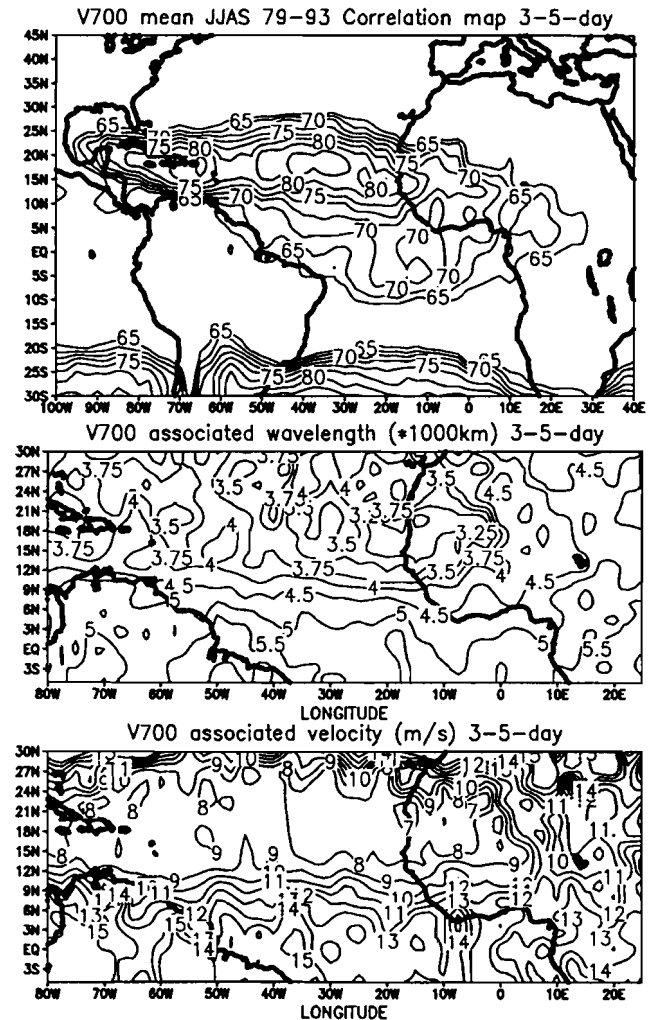
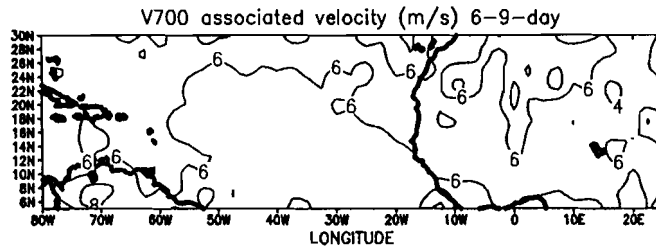
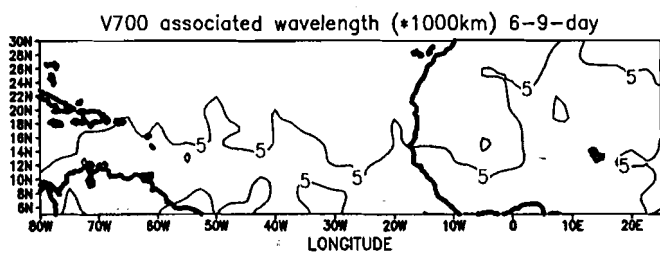
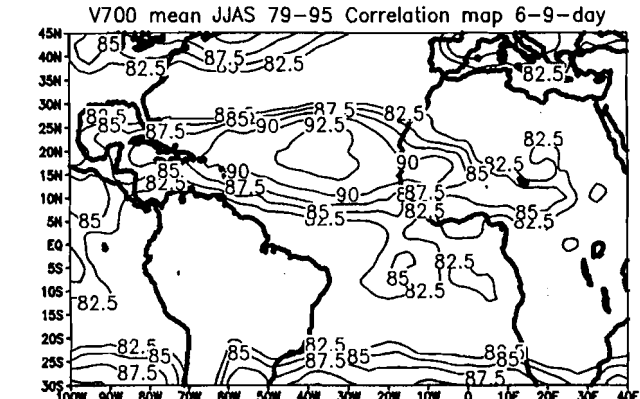


Fig 5 b *Left:* Same as **a** but for ERA for 1979–1993 *Right:* Same as **a** but for 6–9–day meridional wind component; coefficients lower than 82.5% are not displayed on the *top panel*

b NCEP: KINEMATICS OF 6–9-day WAVES



ECMWF: KINEMATICS OF 6–9-day WAVES

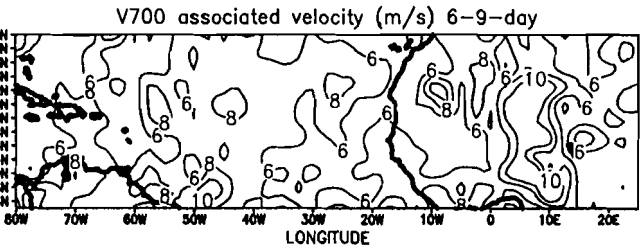
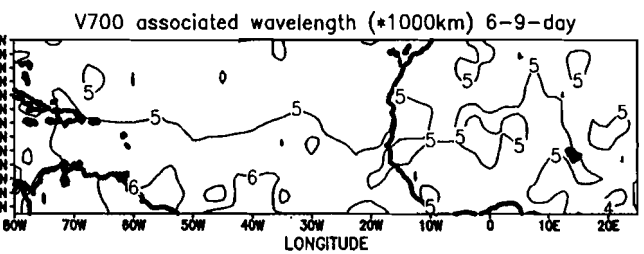
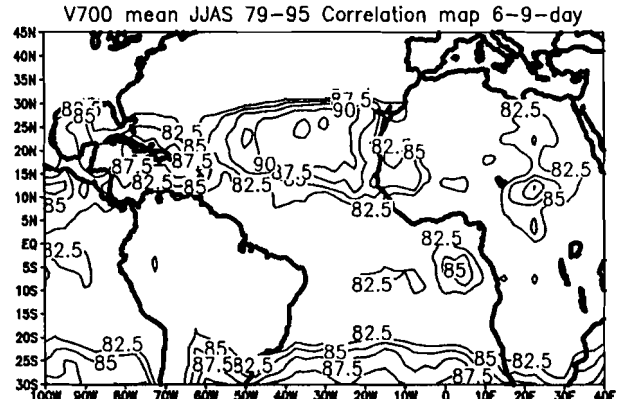


Fig. 5 (Continued)

lag-correlation patterns for each grid point. At each grid point and for each June–September period, the daily time series of the filtered meridional component of the NCEP/NCAR wind at 700 hPa is correlated with the series of the other grid points with a time-lag of +1 day and of -1 day. Then, we localize the nearest grid points eastward and westward of the former grid point where correlation corresponds to a local positive maximum. The average of these two correlation coefficients is assigned to the grid point. This computation is performed for the African/Atlantic domain for each year and the averaged correlation field for the period 1979–95 is displayed (Fig. 5a left). The values of the averaged correlations give an indication of the temporal consistency of the 3–5-day waves and the areas of greatest coefficients are interpreted as preferential tracks of the waves. This is different from highlighting variance maxima. We localize the areas where the waves are the best organized and not necessarily where they are the greatest. Two main

trajectories are indicated over West Africa, west of 10°E, a northern one at 15°N and a southern one at 5°N. These two tracks merge into one over the northern tropical Atlantic along 17.5°N, which ends in the Gulf of Mexico. The greatest correlations are located at 40°W in the Atlantic, where variance is also the highest (see Fig. 3a). In a similar way, the correlations extending further east over Central Africa are consistent with the variance pattern. High correlations are confined to the latitudinal range 10°S–30°N. These are clearly separated from other trajectories in the westerlies north of 35°N and south of 20°S by weaker correlation coefficients. This shows approximately the limited area where the 3–5-day easterly waves are travelling.

An estimation of wavelength and phase speed patterns was made following Wallace et al.'s (1988) method. At each grid point, correlations of the filtered time series between this point and the overall grid points have been computed with no day lag. This grid

point wavelength is deduced from the distance between the locations of the two nearest negative extremes of correlations east and west of the grid point at the same latitude. To find the local wave velocity, we computed the correlation between the filtered grid point time series and the overall grid point time series with +1 and -1 day lags. We computed the distance of the two nearest points east of the former grid point for the -1 day lag and west of the former grid point for the +1 day lag, where positive correlations are the greatest. These two points are interpreted as the location of the easterly wave one day before and one day after. The wave velocity is deduced from this distance. We consider these results only in the areas where the waves are well organized.

For the 3–5-day regime, the most significant feature of the wavelength pattern (Fig. 5a middle) is a high southward gradient. Over West Africa wavelengths are estimated about 3000 km at 17.5°N, and increase to 4500 km over the southern coast at 5°N. This gradient is maintained over the Atlantic whereas wavelengths increase slightly about 3750 km in the gulf of Mexico. The phase speed patterns (Fig. 5a bottom) also show a high southward gradient over West Africa and the Atlantic. The waves phase speed varies from about $8\text{--}9 \text{ m s}^{-1}$ at 15°N to about 12 m s^{-1} at 5°N. The positive correlation observed between wavelength and easterly phase speed is consistent with the barotropic approximation of the vorticity equation (Holton 1979), where the vertical component of absolute vorticity is conserved following the horizontal motion, resulting in an increased westward phase speed with wavelength. The propagation direction is mostly zonal and oriented westward on the domain 30°N–20°S, eastward outside of this domain (confirmed by Hovmoeller diagrams, not shown). If we estimate the resulting period by dividing the wavelength by the phase speed, we find a slight meridional variation over West Africa from a maximum of 5 days at 15°N to a minimum of 4 days at 5°N (not shown). By using FFT, we already noted shorter periods over West Africa, located south of 10°N, between 3 and 4 days (Fig. 2a). This point is detailed in Diedhiou et al. (1998b).

The kinematics patterns obtained from the ERA dataset (Fig. 5a right) are very similar. The main trajectories are located at the same latitudes and, in spite of weaker variances over the Atlantic, the wave consistency is a bit stronger over western Atlantic. The wave organization is weaker over the Gulf of Guinea but the correlation maxima is extending over Central Africa too. Wavelength and phase speed patterns also display a great southward gradient and the values of wavelengths and speeds are very similar. It is difficult to say if the oceanic maxima of correlations correspond to a stronger organization of the waves or if it is due to a free variability in the models, hindered by observations.

4.2 6–9-day waves

Similar computations were made for the 6–9-day waves with filtered meridional wind components at 700 hPa. As for the 3–5-day waves, highest correlation coefficients related to meridional component of the NCEP/NCAR wind (Fig. 5b left) are located in the northern tropical Atlantic between 10°N and 30°N, with maxima at 40°W–30°W between 15°N and 25°N. Only one main track is shown over West Africa along 17.5°N. The same computation performed with the zonal wind component (not shown) indicates the largest correlation coefficients between 10°N and 20°N over the ocean with a unique track over West Africa along 10°N, that is a wave path located southward of the path for the meridional component, at the latitude of the AEJ. Computation of this wave's composite patterns will explain these latitude differences in the next section. We notice an equatorward extension of high correlations in the eastern Atlantic. Whereas 6–9-day wind variances are very low at these latitudes, this signal, regarding variance fraction, is significant for wind components, moisture flux or precipitable water (Cadet and Houston 1984; Cadet and Nnoli 1987; de Felice et al. 1990, 1993).

Computations for the 6–9-day wavelengths and phase speeds, related to the meridional component of the wind, show near constant wavelengths between 4500 and 5000 km in the domain 10°N–30°N, and westward phase speeds (north of 30°N the propagation is eastward) between 6 and 7 m s^{-1} , which is not very different from the 3–5-day wave speeds north of the AEJ. The difference in periodicities between the 6–9-day and the 3–5-day waves can consequently be explained mainly by greater wavelength.

The kinematics patterns computed on the ERA dataset are very similar (Fig. 5b right). The greatest wave consistency is located at the same latitudes but it is somehow lower and less extended in the western Atlantic and in Central Africa. The wavelength pattern is very similar and the phase speeds are a little higher over the Atlantic where the consistency is the greatest.

5 Spatial patterns

In this section, we analyze individual as well as average composite wind fields at 700 hPa, related to the 3–5-day and the 6–9-day spectral signals. To consider the respective wind patterns in the composite fields, we selected reference grid points located over West Africa, along the three latitudes of the main tracks computed in the previous section, at 5°N and 15°N for the 3–5-day signal, and at 17.5°N for the 6–9-day signal. The average variance of the 6–9-day signal over West Africa is weak at 17.5°N (Fig. 3). However, the daily spectral signal, revealed by wavelet transform (see Fig. 6), can

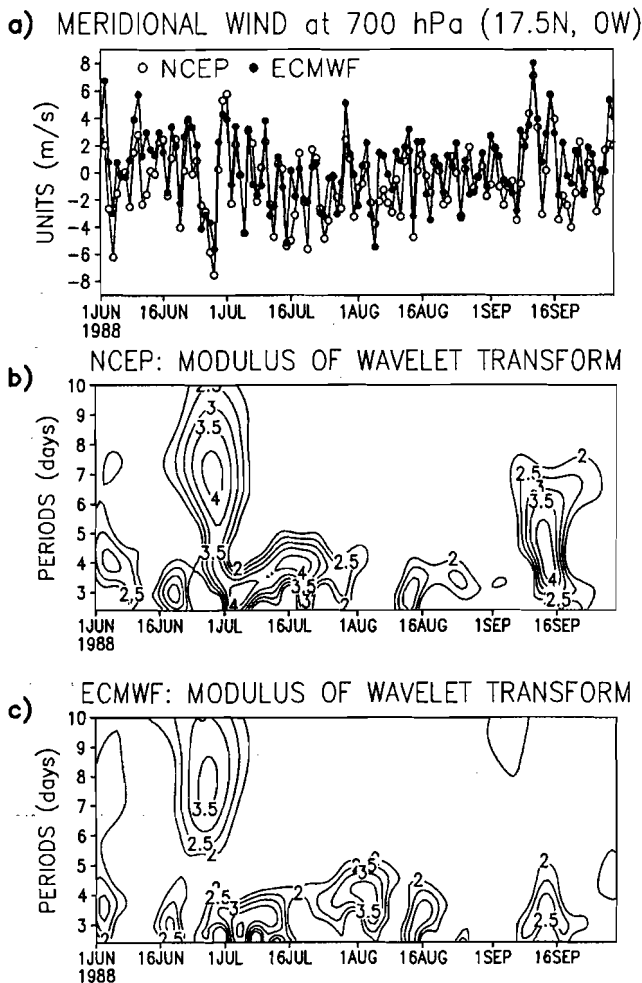


Fig. 6a–c Wavelet analysis of the 122-day time series (June–September 1988) of the meridional wind component at 700 hPa on the grid point 17.5°N/0°W. **a** time series (open circles for NCEP/NCAR, closed circles for ERA). **b** Modulus (ms^{-1}) of the wavelet for NCEP/NCAR. **c** Modulus (ms^{-1}) of the wavelet for ERA. Isopleths below 2 are not displayed

be high during particular time sequences. The composite patterns shown in Fig. 8 also confirm a posteriori that this signal is not so low, and they depict a good spatial organization of the wind field. It finally enables us to show the related rainfall modulation over West Africa.

5.1 An individual case

Figure 6 displays the 700 hPa meridional wind 122-day-series at 17.5°N–0°W for summer 1988, both for the NCEP/NCAR and ECMWF reanalyses and the associated wavelet transforms (see Farge 1992; Torrence and Compo 1998, for a detailed presentation of the method). While classical spectral techniques based on Fourier transform or maximum entropy methods

only supply frequency characteristics, wavelet transforms allows us to detect features both in frequency space and in their temporal localization, i.e. the temporal-frequency characteristics “instantaneous spectrum”. In this study, we used the Morlet wavelet as the mother wavelet, which is convenient for analyzing continuous signals as time series of wind component. The two meridional wind time series are well correlated (correlation is +0.78) and display a large number of synoptic scale fluctuations. The time-frequency diagrams of the wavelet modulus are rather similar for the two reanalyses time series and show high signals both in 3–5-day and in 6–9-day bands. We especially note a similar transition from a 6–9-day regime at the end of June to a 3–5-day regime in the first half of July, which will be studied later. The main difference consists of a stronger 3–5-day signal at the beginning of August in the ERA, and a greater signal in NCEP/NCAR reanalyses in mid-September. High energy values in the 3–5-day band are recurrent during the 122 days whereas 6–9-day signals are more intermittent and occur when the 3–5-day signal is not present. Such a difference in synoptic variability is confirmed when examining other summer time series (not shown) and may explain why the overall 6–9-day variance is weak over West Africa in spite of evidence of 6–9-day synoptic weather systems.

Figure 7a, b shows for the two reanalysis datasets the time sequence of a 3–5-day regime on 10–12 July, 1988, and of a 6–9-day regime on 27–29 June, 1988, at 700 hPa, selected from the wavelet diagram. These wind field patterns are very similar in the two reanalyses. Westward propagation of the two kinds of easterly waves are evident in these panels, as well as their different wavelengths due to contrasted anticyclonic circulations along 25°N. For the 6–9-day regime, two anticyclonic circulations are evident north (at 25°N) and south (at 10°S) of the AEJ over the Atlantic, leading to an acceleration of the zonal wind component of the jet, in accordance with large energy in wavelet transform of zonal wind component (not shown). This symmetric pattern named “duct” by the synopticians in Africa (Dhoneur 1974) is far from evident in the 3–5-day regime where the modulation of the meridional wind component in the jet is large, extending north and south of the jet, and where the ridge is less extended. This 6–9-day pattern shows a larger wavelength than for the classical 3–5-day regime. These patterns are consistent with the results of the kinematics computations presented in the previous section.

5.2 Composite wind fields

In the preceding sections, we have (1) pointed out the main frequency bands related to the meridional component of the wind at 700 hPa, (2) identified the main latitudes of the wave tracks (5°N and 15°N for the

3–5-day period over West Africa, 17.5°N for the 3–5-day period over the Atlantic, and 17.5°N for the 6–9-day period both over West Africa and the Atlantic), and (3) presented a particular example of both 3–5-day and 6–9-day wind field pattern. To confirm these results we computed the composite patterns of these two regimes at 700 hPa.

We computed composite patterns of the NCEP/NCAR 3–5-day regime related to one reference point at 5°N/0°W and another at 15°N/0°W, and of the NCEP/NCAR 6–9-day regime related to a reference point at 17.5°N/0°W. To this purpose, we filtered the 17 NCEP/NCAR daily June–September 700 hPa meridional wind component time series (from 1979 to 1995) of each reference point with a bandpass filters between 3 and 5 days and between 6 and 9 days. Then, for each of the three filtered signals, we selected the days where the meridional wind at 700 hPa is maximum and greater than $+0.5 \text{ m s}^{-1}$. In the summers 1979–95, 505

and 484 cases have been retained for the 3–5-day waves at 5°N and 15°N respectively, and 245 cases for the 6–9-day waves at 17.5°N. Finally, we averaged the unfiltered wind fields at 700 hPa respectively for all the dates selected for each of the filtered signals. Similar computations were made with the ERA for the period 1979–1993. Respectively 448, 431 and 229 cases have been retained for this 15-year period.

By selecting such a threshold of 0.5 m s^{-1} , we have large number of cases, many more than would be identified from the wavelet spectra, especially for the 6–9-day waves which are rather infrequent according to this analysis. However we think that with such large datasets, stable and recurrent synoptic features will be evident.

Wind fields ($u - u^*$; $v - v^*$) are displayed in Fig. 8. At every grid point, the temporal average of zonal (u^*) and meridional (v^*) components of the wind on the 122

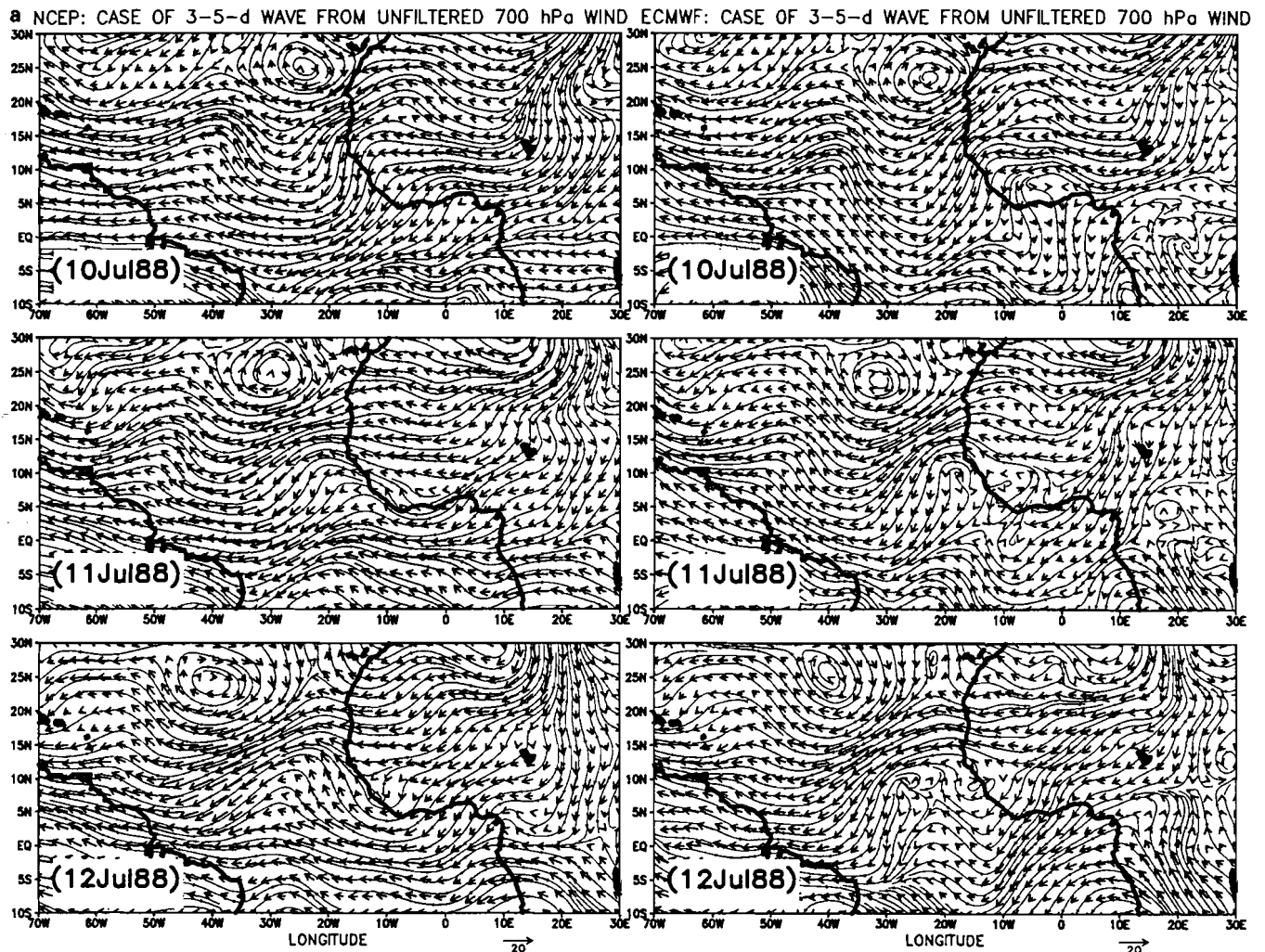


Fig. 7 a Stream lines and vectors of the 700 hPa unfiltered wind field for a sequence of 3–5-day easterly waves regime (10–12 July 1988) for NCEP/NCAR (left) and ERA (right). **b** Same as a but for a sequence of 6–9-day easterly waves regime (27–29 June 1988)

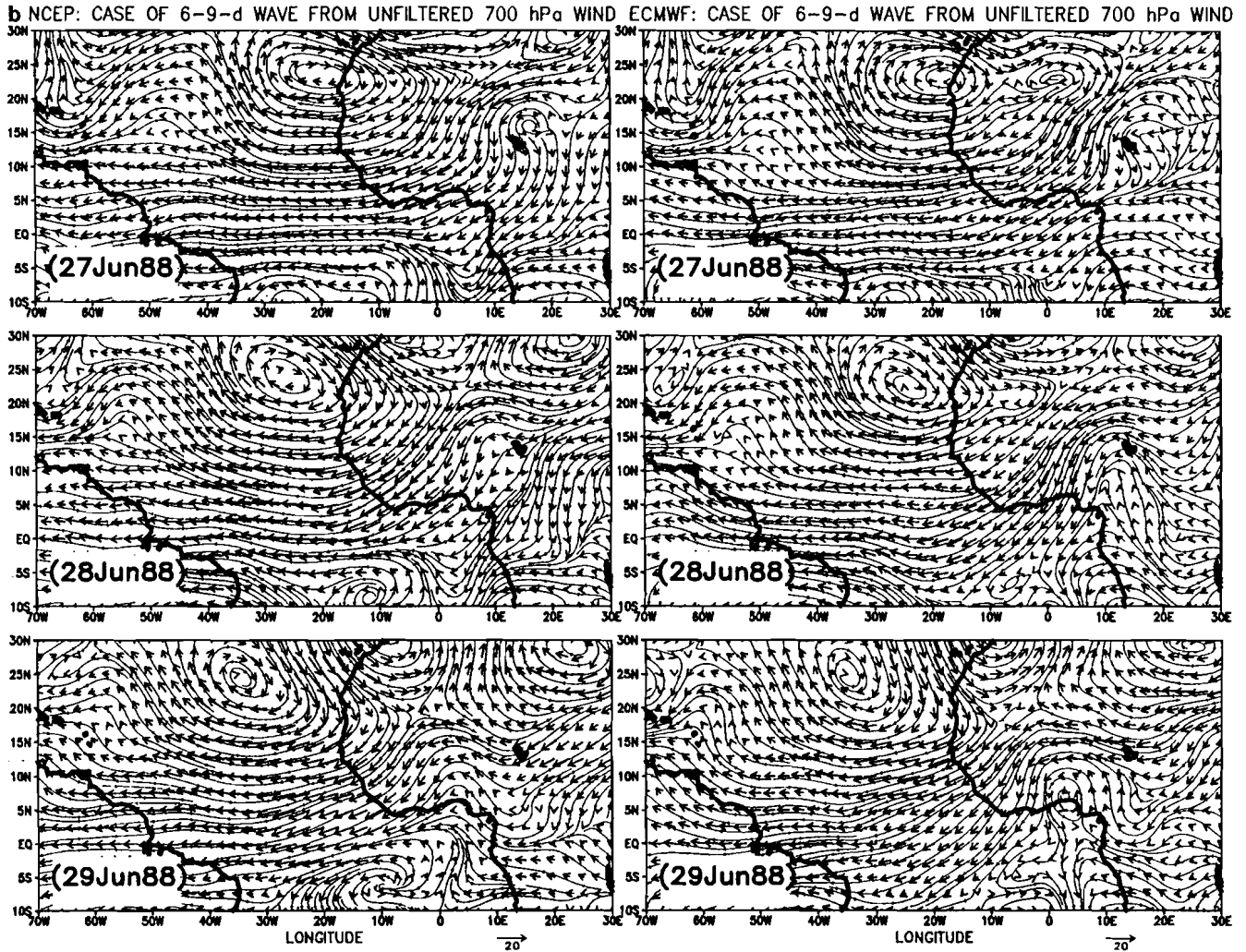


Fig. 7 (Continued)

days of July–September are subtracted from the zonal (u) and meridional (v) wind components. Thus, only the perturbed wind field is displayed (very similar to the filtered signal; not shown). Considering the NCEP/NCAR reanalyses for the 3–5-day signal (Fig. 8 left), we see a marked trough extending meridionally between 30°N and 10°S , with a southeast/northwest tilt north of the AEJ (more marked for the composite wave seen at 15°N) and a southwest/northeast tilt south of the AEJ (more marked for the composite wave seen at 5°N). This is consistent with a zonal momentum transfer from the jet to the wave and with the development of the wave through the barotropic instability of the jet. The composite wave train seen at 15°N includes a second trough at 35°W (10°N – 20°N), implying a wavelength of approximately 2500 km. For the composite wave at 5°N , the average wavelength is greater, about 4000 km. Between the troughs, the ridges are characterized by a moderate anticyclonic circulation.

Over the Atlantic only one wave train is evident between 15°N and 20°N .

Considering the 6–9-day signal shown at 17.5°N / 0°W , the average trajectory is located more to the north and the trough axis extends north of 5°N and is tilted southeast/northwest, still consistent with a zonal momentum transfer from the AEJ to the wave north of the jet. The second trough axis is located at 50°W between 15°N and 30°N , leading to an approximate wavelength of 5500 km. Another difference with the 3–5-day waves is the larger anticyclonic circulation located between the troughs, extending over more than 20° of longitude. Finally, south of the AEJ, the circulation of the 6–9-day regime is reversed, a clockwise circulation being opposed to a counter-clockwise circulation north of the jet, and vice versa, leading to a large modulation of the zonal wind component of the AEJ. The ASECNA forecasters working at Dakar in the 1960s and the 1970s noted the existence of such

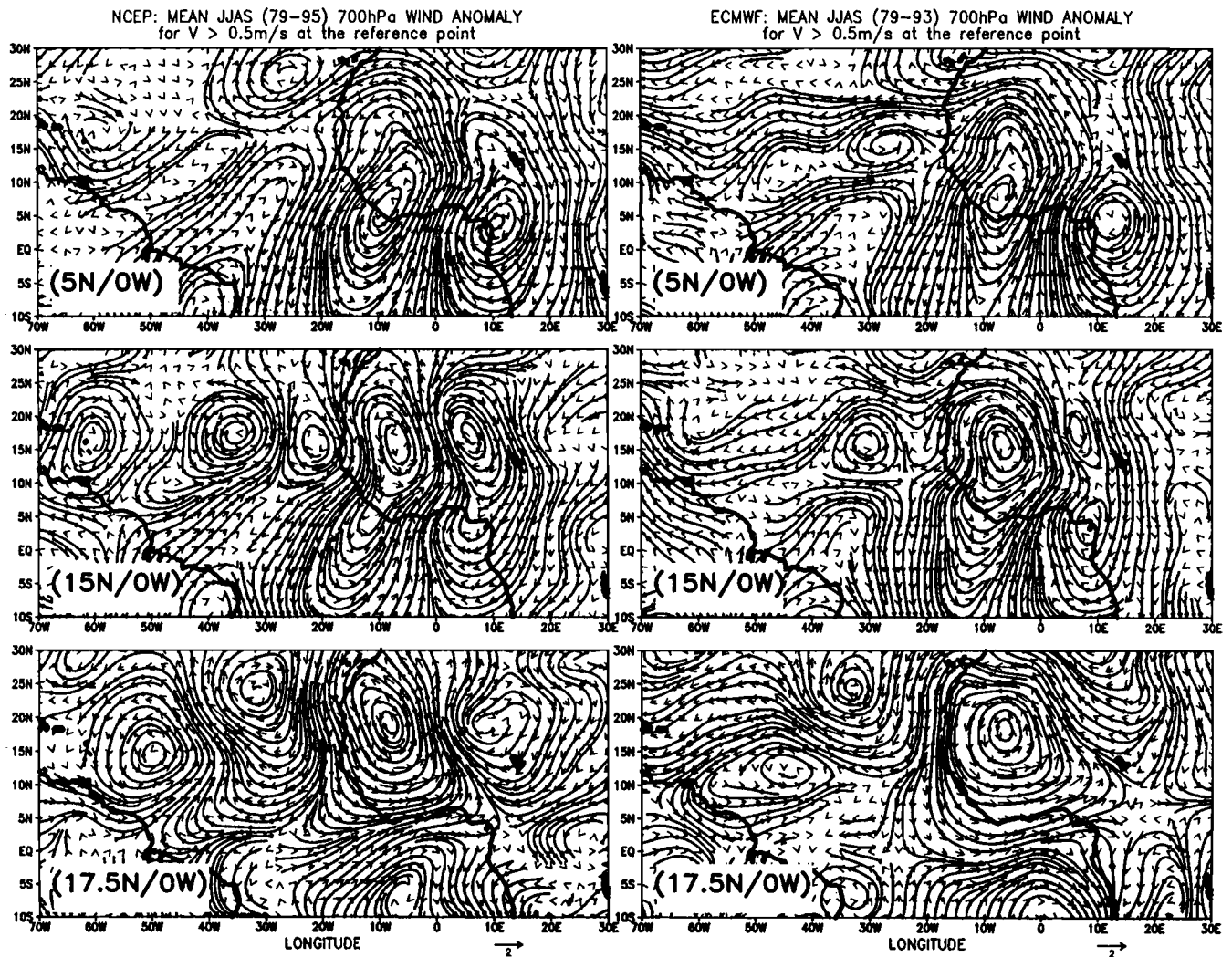


Fig. 8 Stream lines of 700 hPa composite unfiltered wind anomalies related to reference points located at 0° W, and 5° N and 15° N for the 3–5-day regime, 17.5° N for the 6–9-day regime. Composite have been computed by selecting days where the 700 hPa filtered meridional wind at the respective reference point is a maximum and greater than $+0.5 \text{ ms}^{-1}$. At each grid point, the temporal average of

meridional and zonal wind computed for the 122 days of June–September are subtracted from the respective meridional and zonal wind component. *Left:* NCEP/NCAR mean wind field for the period 1979–1995. *Right:* Same as *left* but for ERA for 1979–1993. Scale for the wind (m s^{-1}) is indicated

westward moving tropical anticyclonic cells over West Africa and the tropical Atlantic (see Dhoneur 1974).

Composite wind field patterns computed from ERA (Fig. 8 right) lead to similar conclusions. The patterns are similar to the NCEP/NCAR reanalyses but the spatial organization of the waves is weaker, in particular over the Atlantic, consistently with variance maps (Fig. 3). The southern track of 3–5-day easterly waves is a little further north than in NCEP/NCAR reanalyses (7.5° N instead of 5° N), and the average wavelength of the northern 3–5-day easterly waves is also shorter in ERA.

In the following, we used only NCEP/NCAR reanalyses since they have shown a rather good similarity with ERA.

5.3 Another example of 6–9-day wave during GATE phase I

Figure 9 shows a wavelet transform of the 122-day time series of NCEP/NCAR meridional wind component at 700 hPa in 1974 for the grid point 15° N– 12.5° W. The GATE (Garp Atlantic Tropical Experiment) took place in 1974 when most of the studies and knowledge on the easterly waves were established (see, e.g., Reed et al. 1977; Chen and Ogura 1982). Three phases were defined: phase I (28 June to 27 July), phase II (28 July to 29 August), and phase III (30 August to 19 September).

Figure 9 shows that synoptic activity is mainly characterized in phase I by a 6–9-day regime and in phases II and III by a 3–4-day regime. This diagram confirms

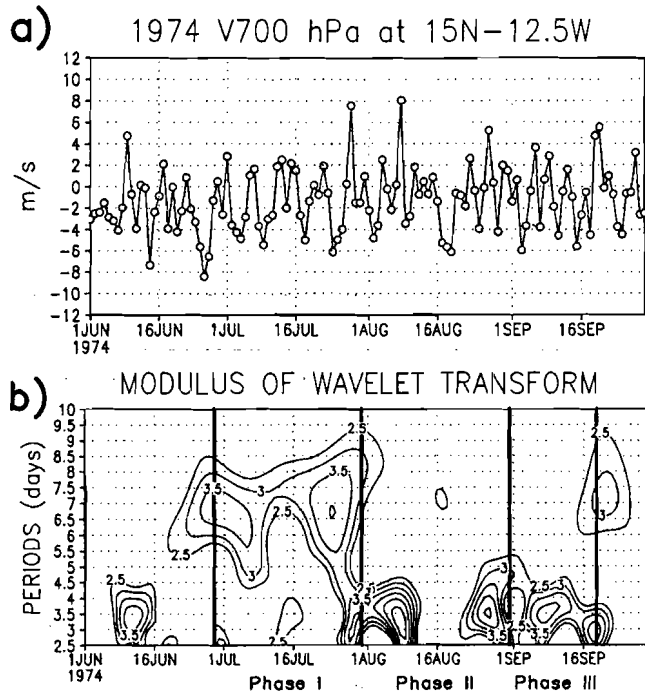


Fig. 9 **a** Time series and **b** modulus (m s^{-1}) of the wavelet transform of the 122-day time series (June–September 1974) for 700 hPa NCEP/NCAR meridional wind component at $15^{\circ}\text{N}/12.5^{\circ}\text{W}$. Isopleths below 2.5 are not displayed. The temporal sequences of the three GATE phases are displayed

the high activity of easterly waves during phase III as noticed by Reed et al. (1977) among others. Most studies have investigated the easterly wave activity during this phase.

Figure 10a displays the 5–12 July sequence of 700 hPa wind field available in the report on the phase field (see GATE Report 17 in the reference list). One of the most interesting points over West Africa during this 8-day sequence is the evidence of a cyclonic center along the Guinea coast during the overall period. The similar time sequence extracted from the NCEP/NCAR reanalyses (Fig. 10b) enables us to display the global circulation pattern in which the southern cyclonic center is embedded and to understand the relationship with the 6–9-day signal seen in the wavelet transform at 15°N . In the reanalysis panels, the cyclonic center is present along the southern coast, especially from 6 to 9 July (giving, from the IRD rainfall dataset, a rainfall peak of 18 mm over the Guinea coast on 8 July, with more than 30 mm at 5°W and more than 20 mm east of 2°E), and then moves westward over the ocean. This center, is in fact, the southern part of a 6–9-day wind field pattern. For instance on 8 July, two easterly wave troughs are located, one at 35°W between 10°N and 30°N , and another at 0°W between 15°N and 20°N . The associated wavelength is about 3500 km. Ahead of these two troughs large anticyclonic

circulations are evident on the western Atlantic and over the northwestern coast of Africa, consistent with the composite 6–9-day wave pattern. The cyclonic circulation over the southern coast of West Africa is located south of the North African anticyclonic circulation, these two circulation centers being on each side of the AEJ whose zonal wind component is enhanced over West Africa (If readers compare this 6–9-day wave pattern with the composite one of Fig. 8, they must consider, first that Fig. 8 shows the wind field anomaly, second that the wave phases are opposed in these two figures, a counter-clockwise circulation, (or clockwise), being located south of the AEJ on Fig. 10b, (or Fig. 8.) The cyclonic center was present over the Guinea coast since 6 July when the northern anticyclonic circulation developed over the western part of northern Africa and persisted until 9 July, when the anticyclonic circulation moved westward over the ocean. Then the two circulation systems moved westward approximately together, the anticyclone over the northern tropical Atlantic, the cyclonic cell along 5°N towards South America, consistent with a westward propagation of an easterly zonal wind maximum (not shown). Another striking point is that on 11 and 12 July there is a large increase of the AEJ over the ocean consistent with a duct pattern similar to those shown in Fig. 7b.

5.4 Associated convection

The difference in the wind field patterns between 3–5-day and 6–9-day weather systems may have implications in rainfall and convection organization. Figure 11 shows the time sequences (day –1, day 0, day +1) of the two 3–5-day and the 6–9-day composites of 700 hPa anomaly wind vectors with the associated rainfall anomalies of IRD dataset. The reference points at 7.5°E , and 5°N , 15°N and 17.5°N respectively clearly show the westward propagation of the rainfall patterns over the limited area of West Africa. Rainfall anomaly at each grid point is indicated by the difference between the average composite daily rainfall and the average daily rainfall for June–September. The anomalies are computed for each year and then averaged over the 1979–90 period.

The highest rainfall anomalies are located on the ITCZ between 5°N and 15°N . There is a close link between the wave and the rainfall pattern of the two wave regimes. The westward propagation speed of the wind field and of the rainfall patterns looks similar. In the 3–5-day regime for both the northern and the southern trajectories, positive rainfall anomalies are located in the trough and ahead of the trough. At $t = 0$, their meridional extension is large, covering the whole West African domain, and consistent with a similar meridional extension of the trough. The related rainfall anomaly pattern is different for the 6–9-day regime. Positive rainfall anomalies are located in the areas

where the zonal component modulation of the AEJ is high, mostly in the cyclonic circulation. However, we can also observe an extension of these positive anomalies eastward in the anticyclonic circulation behind the trough, where we observe a convergence in the zonal wind components. Something else differs: south of 10°N , rainfall anomalies are negative, in a negative vorticity circulation. The greatest rainfall modulation by the two wave regimes is about $+/-1\text{ mm day}^{-1}$, which represents for an average daily rainfall amount of about 6 mm day^{-1} in the ITCZ (and a lower amount in the Sahel), an approximate variation of 30% at least, indicating that these two regimes modulate a significant part of the rainfall amount over West Africa (Viltard et al. 1998 pointed out such a significant rainfall modulation by the 6–9-day signal in 1989).

Figure 12 shows similar composite anomaly fields for NCEP/NCAR rainfall related to the 3–5-day regime at 5°N and at 15°N , and to the 6–9-day regime at 17.5°N , but for 0°W longitude. Rainfall anomaly patterns of the reanalyses are very similar to the observed rainfall anomaly fields over West Africa both in location, sign and amplitude (Fig. 11). Positive rainfall anomalies, especially, extend behind the trough in the 6–9-day regime and are closely linked to the wind field. It means that NCEP model realistically simulates rainfall anomalies induced by synoptic scale weather systems over West Africa. The NCEP/NCAR rainfall, also available over the ocean, helps show the specific spatial organization of rainfall linked to the two regimes: a more zonally extended band of rainfall anomalies for the 6–9-day regime, a more meridional one in the 3–5-day

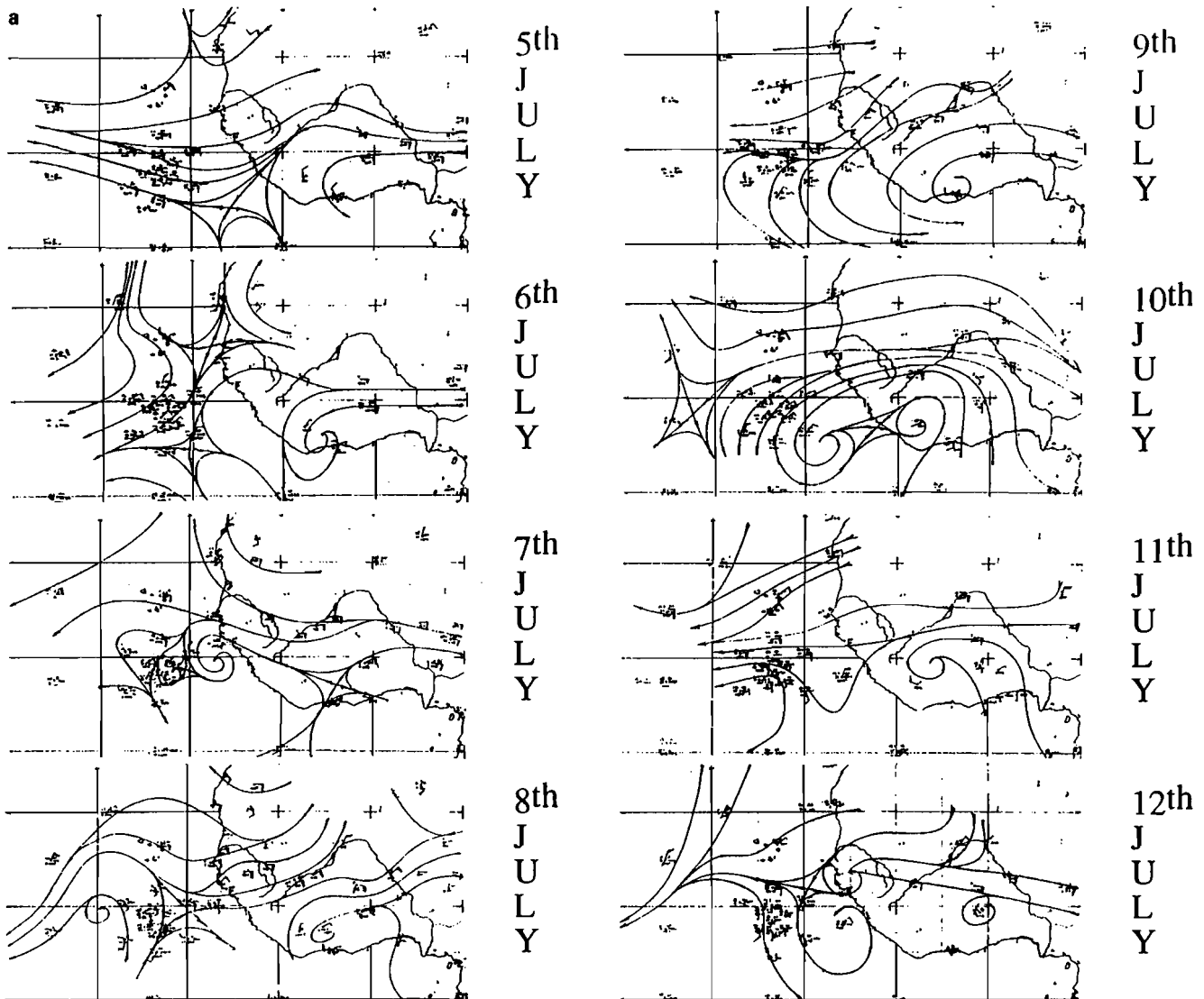


Fig. 10 a A time sequence of the unfiltered 700 hPa wind field during GATE (5–12 July 1974) from the GATE report 17 (see reference list). b Same as a but for the NCEP/NCAR reanalyses

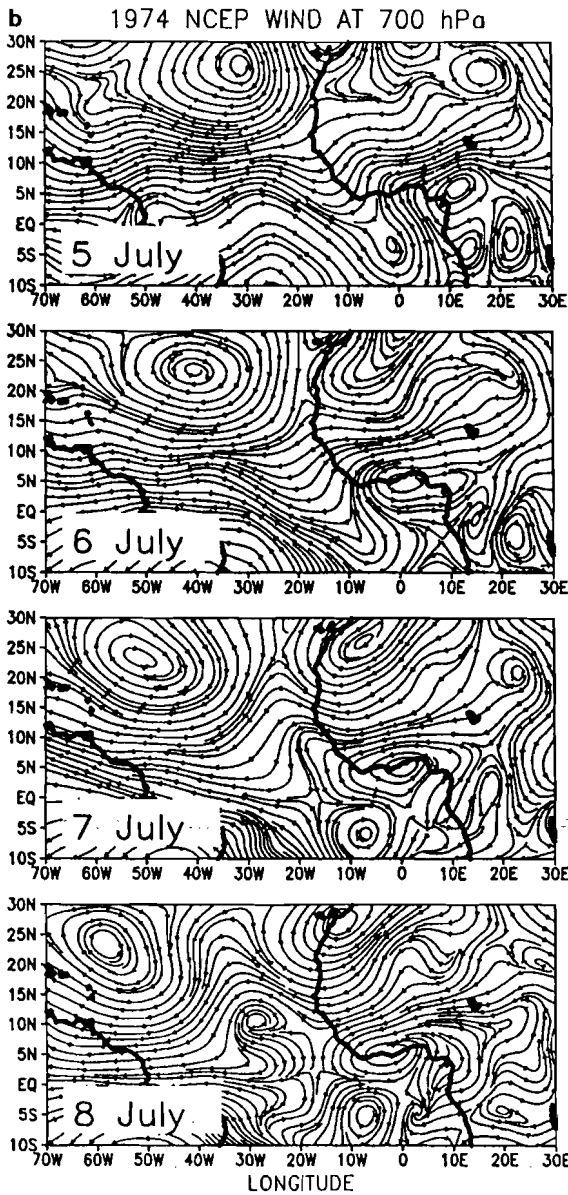


Fig. 10 (Continued)

regime. Concerning this last regime, the different phase speeds of the wave north and south of the AEJ (from 8 m s^{-1} northward to 12 m s^{-1} southward) leads to a more northeast-southwest tilted band of precipitation south of the AEJ, when the 3–5-day wave travels across the Atlantic. Consistency between observed/modelled rainfall and out-going longwave radiation (OLR) departures is very good (not shown), with modulations up to 10 W m^{-2} . OLR is organized differently, related to 3–5-day and 6–9-day regimes, with more zonally extended convective band in the ITCZ for the 6–9-day regime in the trough and behind it, and with more meridionally oriented convective areas in the trough and ahead of it in the 3–5-day regime.

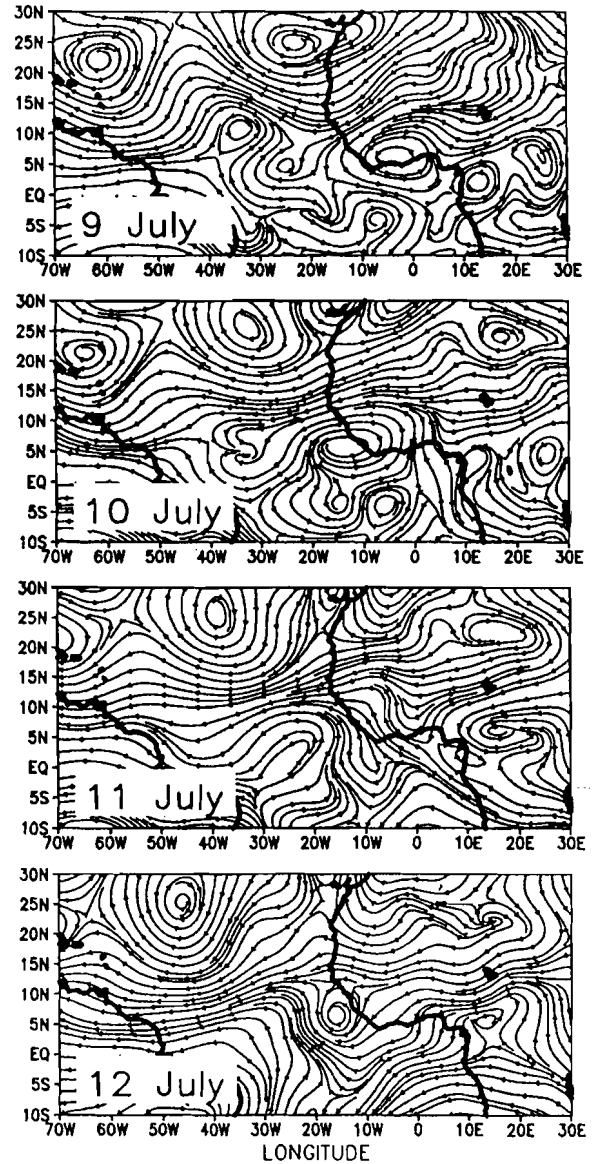
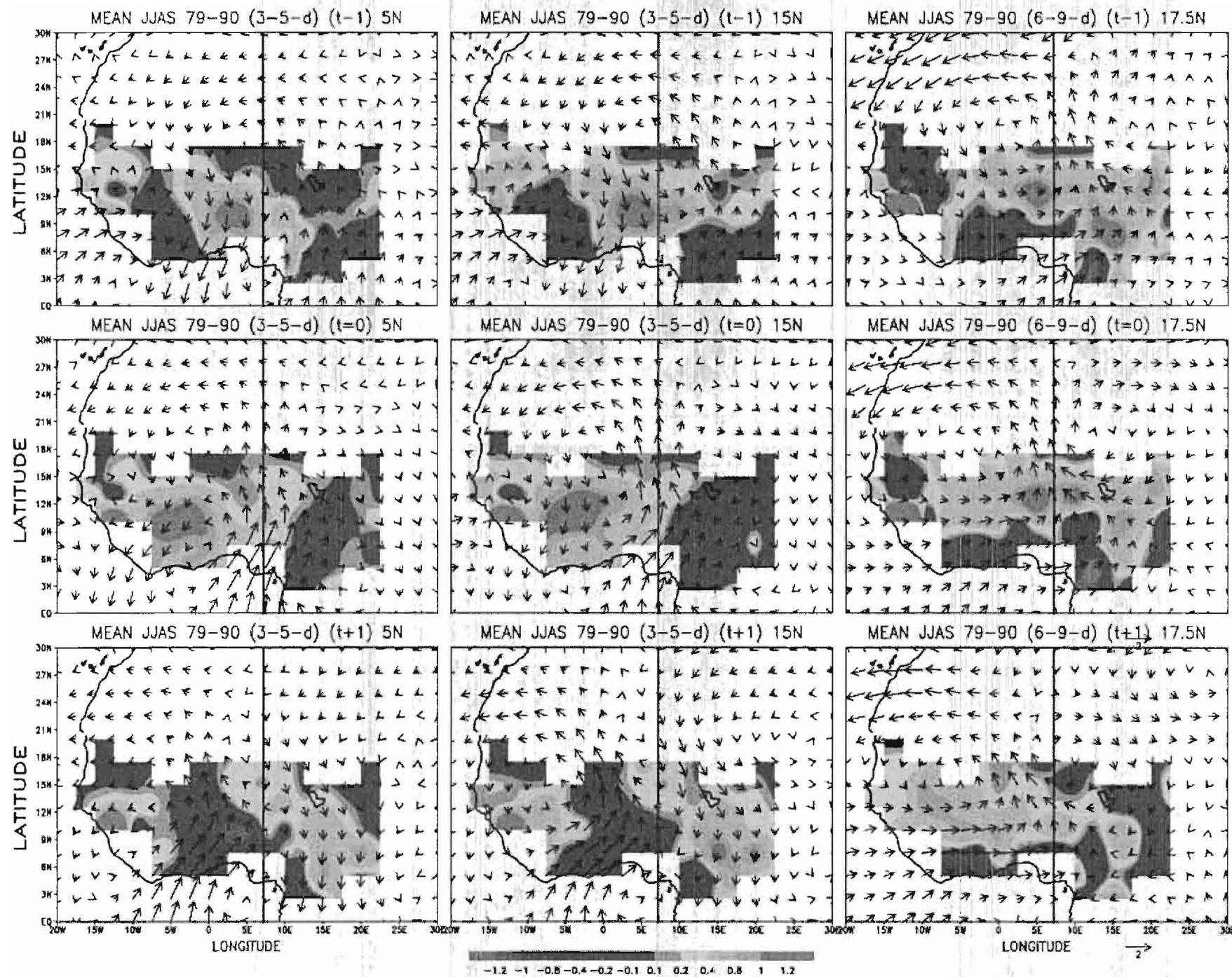


Fig. 11 The 700 hPa composite wind anomalies for the 3–5-day regime at 5°N (left) and 17.5°N (right), and associated rainfall anomalies. Composites have been computed for 1979–1990 by selecting daily 700 hPa wind field where respective 3–5-day or 6–9-day filtered meridional wind at the reference latitude and 7.5°E is a maximum and greater than $+0.5 \text{ m s}^{-1}$; at each grid point, the temporal average of meridional and zonal wind computed for the 122 days of June–September are subtracted from the respective meridional and zonal wind component. IRD rainfall anomaly (mm day^{-1}) at each grid point is the difference between the mean composite daily rainfall and the mean daily rainfall on June–September. Composite fields are shown for the time sequence day-1/day 0/day + 1. Wind scale (m s^{-1}) and color scale are indicated



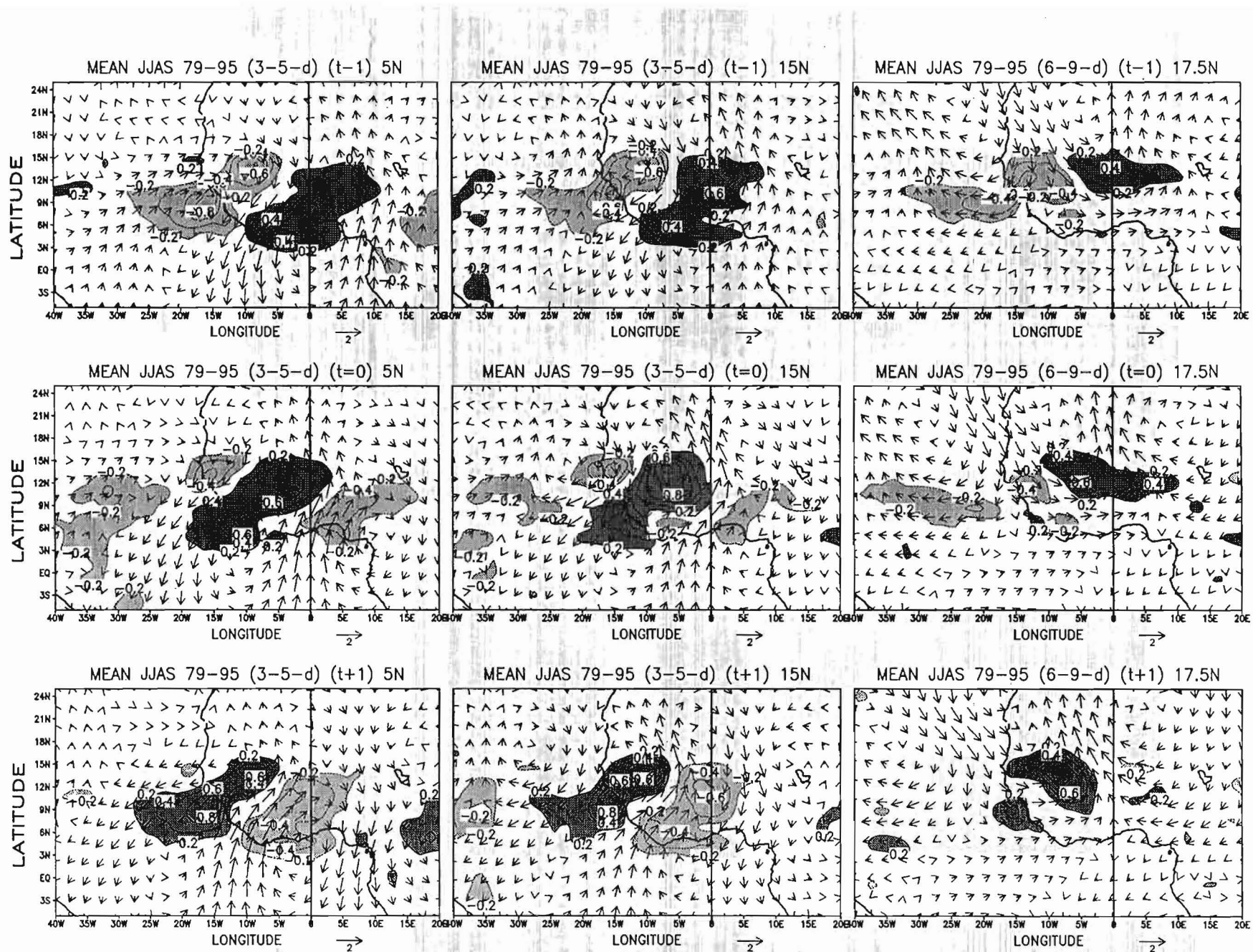


Fig. 12 Same as Fig. 11 but for NCEP/NCAR rainfall. Composite anomalies are computed for 1979–1995 related to reference points located along 0°W at 5°N , 15°N and 17.5°N . Dark (light) gray areas for positive (negative) rainfall anomalies (mm day^{-1}) are indicated.

Since moisture advection and rainfall over West Africa largely depend on monsoon flux variability, we computed the modulation of the 925 hPa wind and relative humidity by the 700 hPa easterly waves (Fig. 13). For the two 700 hPa regimes, the resulting 925 hPa wind field is tightly modulated. A cyclonic circulation north of 15°N moves westward at a speed similar to the speed of the 700 hPa wind field and induces a northward advection of moisture east of the vortex. In the 3–5-day regime, the meridional component of the 925 hPa wind is strongly modulated, leading to a large cyclonic circulation at day 0 over West Africa and a strong southerly flux at day +1. Positive rainfall departures shown in Fig. 11 are located in the 925 hPa trough and are not associated with positive relative humidity anomalies. Ahead of this system, a marked ridge is associated with negative rainfall anomalies (see Fig. 11). The 6–9-day regime modulates mainly the zonal component of the 925 hPa wind at 15°N. The modulation of the meridional component is limited north of 15°N and the cyclonic center at 20°N is zonally elongated. In this regime, the positive rainfall anomalies shown in Fig. 11 are tightly associated with zonally extended positive and relative humidity anomalies both in southerly and westerly winds.

Rainfall anomaly patterns are thus different for the two regimes over West Africa. In the 3–5-day regime, we see a large meridional extension of the different patterns with a close combination between the wave trough, the monsoon trough and the convection. The fact that the trough is meridionally extended in the area of the ITCZ could be helpful for the development of meridionally oriented convective systems by forcing upward motions over a wide band of latitudes. In the 6–9-day regime, the rainfall pattern has a zonally extended structure with a limited meridional extension and looks like the bands of convection which have been found in these regions, especially over the Atlantic (Sadler and Oda 1978). In this synoptic regime, only the southern part of the wave is located in the area of the ITCZ and the modulation of the wind is extended in longitude due to the larger wavelength. This could explain the occurrence of zonally elongated rainfall maxima, not as closely related to the trough position as for the 3–5-day regime, but mostly related to the modulation of the zonal component of the AEJ (especially to the convergence in the zonal wind components) and to the southerly wind anomalies behind the trough.

5.5 The 6–9-day easterly wave regime

We will now analyze an example of transition from a 6–9-day easterly wave regime to a 3–5-day regime and another example of transition from a 3–5-day easterly wave to a 6–9-day regime. These sequences were identified by using the wavelet transforms of 700 hPa meridional wind time series at different grid points of the

NCEP/NCAR reanalyses. The objective is to understand better the set up and dissipation of the 6–9-day regime, as well as its dynamics. The corresponding ERA wind fields have also been examined but they are not shown here. They are very similar to the NCEP/NCAR fields in spite of some localized differences.

5.5.1 Transition from a 6–9-day to a 3–5-day regime

The time sequence of 2–9 August 1979 was chosen. The unfiltered NCEP/NCAR wind fields at 700 hPa are presented in Fig. 14, where **H**, **h**, **A** and **a** depict anticyclonic cells and numbers 1 to 5 the different troughs.

On August 2, the synoptic pattern is the following. A 6–9-day wave pattern is displayed by the system **1-h-3** with an average wavelength of 4000 km, moving westward over the Atlantic during the whole sequence. Trough 3 is in phase with the quasi-stationary trough **2** on 4 and 5 August when travelling from the continent to the ocean, then it continues westward. A high geopotential cell **A** is located over North Africa and remains in this area during most of the sequence. Ahead of trough **1**, another anticyclonic cell, **H**, is observed during the whole sequence and moves northward, then eastward along 40°N, embedded in the mid-latitude westerlies. Behind trough **3**, a small anticyclonic circulation is followed by trough **4**. This system has a small wavelength of about 2000 km and corresponds to a 3–5-day wave-like regime.

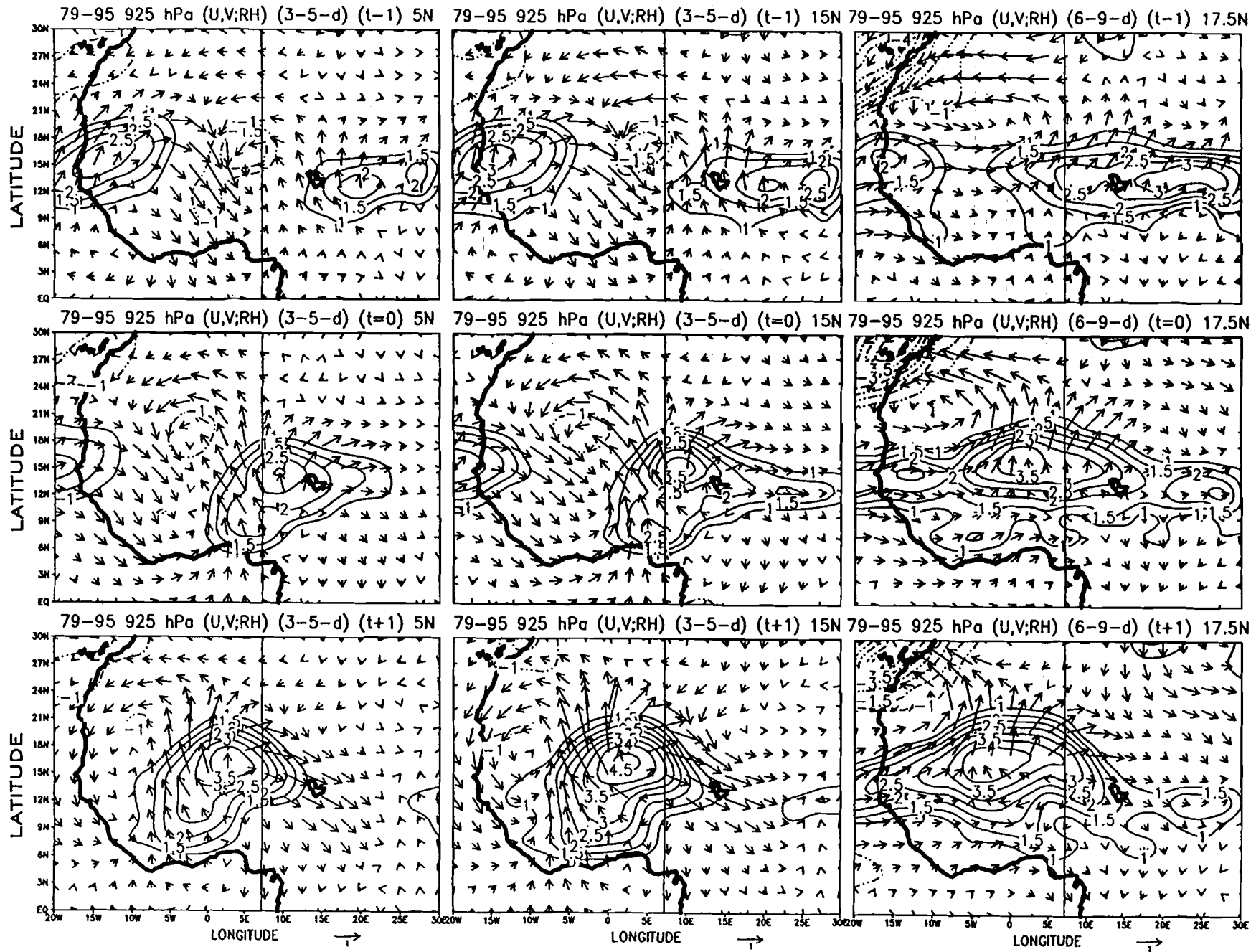
The 8 August, 1979, is the key-date for the establishing of a 3–5-day regime. High geopotential cells **A** and **a** are too weak to prevent the cut-off of cell **a** and the merging of troughs **2** and **4**. Then the 3–5-day wave system **3-a-4** is formed and travels over the Atlantic. On 8 and 9 August, a new trough, **5**, grows at a small distance from trough **4**, about 2000 km depicting the maintenance of the 3–5-day regime.

This example shows evidence of interactions between more or less developed anticyclonic cells over North Africa linked to the quasi-stationary Libyan anticyclone, and troughs associated firstly with the 3–5-day easterly wave regime north of the AEJ, secondly with the quasi-stationary trough located along the western coast of North Africa.

5.5.2 Transition from a 3–5-day to a 6–9-day regime

The time sequence of 21–26 June 1988 was chosen. We have previously shown the sequence of 27–29 June (Fig. 7b) which was identified as a 6–9-day regime. We examine here the setting up of this regime.

The stream lines of unfiltered NCEP/NCAR wind fields at 700 hPa are presented in Fig. 15. The two main anticyclonic circulations are **h** and **h'**. Other small anticyclonic cells, **a** and **a'**, are also identified. The axes of the different troughs are depicted and a number from 1 to 7 is associated with each trough.



On June 21, the synoptic pattern is the following. A 3–5-day easterly wave regime is depicted with three troughs (numbers 1, 3, 4), located on the poleward side of the jet, separated by about 2500 km. Another trough (number 2), is stationary and located along the western coast of North Africa, with a large meridional extension. This trough seems in phase with trough 3. Two anticyclonic circulations are also shown, one h over the Atlantic which is associated with the high geopotential heights of the Azores, and the second h' over North Africa, associated with the Libyan high geopotential heights center. A westward extension of h' , named a , is associated to the ridge between troughs 3 and 4.

On June 22, trough 1 travels westward, troughs 3 and 4 and high h also move, but more slowly. Ridge a , embedded in the wave 3-a-4, moves westward and a cut-off between a and h' can be expected in the following days with the merging of troughs 2 and 4. A new trough 5 appears over North Africa, linked to the low geopotential heights center located along the Moroccan coast. This pattern is similar to the one observed previously on 7 August during the transition towards a 3–5-day regime (Fig. 14).

As 8 August is the key-date for the setting up of a 3–5-day wave regime, 23 June is the key-date for the transition towards a 6–9-day regime. The cut-off between highs a and h' does not occur, as opposed to the case of 8 August. Instead, h' grows, as well as its westward extension, leading to the disappearance of trough 4 and the northward retreat of trough 2 (the advection of low potential vorticity from the ridge of h' can explain this evolution; not shown). Trough 1 moves westward, high h grows too, preventing further westward propagation of trough 3 which remains stationary. The 3–5-day pattern with short wavelengths has disappeared. Trough 5 is maintained over North Africa.

On June 24, the transition towards the 6–9-day regime which is going on, is depicted by the system h -3- h' which travels westward with a great increase of the highs h and h' . Trough 2 turns towards the west, due to a northward advection of low potential vorticity south of it (not shown). Similarly, behind h' , the semi-permanent trough 6 is extending southwestward. Trough 5

moves eastward and a new trough, 7, appears on the poleward side of the AEJ, leading to a short wavelength (about 2000 km) with trough 3.

On June 25, the westward propagation of the system h -3- h' is continuing. The wavelength between h and h' is about 5000 km and consistent with the 6–9-day wave pattern. The interesting points are an apparent eastward displacement of trough 7, increasing the wavelength with trough 3, and the southward move of trough 5, leading to the next cut-off in the high geopotential heights h' and to the appearance behind h' of a new anticyclonic cell a' . In fact, when the ERA wind field is examined, it seems that the eastward propagation of trough 7, also seen on 26 June in the NCEP/NCAR field, might correspond to a new trough growing eastward, maybe due to the AEJ instability. This can also be the result of a misrepresentation of wind field perturbation in the reanalyses over this area, trough 7 being artificial.

On June 26, the wavelength between troughs 7 and 3 increases to about 5000 km. h' becomes an isolated cell moving westward in the 6–9-day wave pattern h -3- h' -7. The three troughs 5, 6' (which is a cut-off of the former trough 6) and 7 converge towards the same area, and merge into a unique trough on 27 June (see Fig. 7b). Behind them, a new cell, a' , grows during the next phase of the 6–9-day wave regime occurring over the following days (Fig. 7b). The cut-off of h is also observed in the ERA wind field, in association with the merging of troughs 5 and 6', trough 7 not being represented.

This time sequence shows how large anticyclonic cells over North Africa can interact with the troughs of a 3–5-day wave regime (which develop because of the instability in the AEJ) to set up a 6–9-day regime. Consistently with the growing anticyclonic cell h' , the key points of this interaction are the failure of a cut-off of anticyclonic cell a ahead of h' and of the merging between troughs 2 and 4 on 22 June, the disappearance of trough 4, the westward propagation of trough 3 and, finally, the merging of troughs 5, 6' and possibly 7 behind h' . These interactions are not limited to subtropical highs and 3–5-day easterly waves north of the jet. As for the transition to a 3–5-day regime, we also have to consider the quasi-stationary trough 2, located along the western coast of North Africa, and its possible merging with troughs linked to the instability of the AEJ.

Fig. 13 The 925 hPa composite wind anomalies associated with the 3–5-day regime at 5°N and 15°N and with the 6–9-day regime at 17.5°N. Composites have been computed for 1979–1995 by selecting daily 700 hPa wind field where respective 3–5-day or 6–9-day filtered meridional wind at the reference latitude and 7.5°E is a maximum and greater than $+0.5 \text{ m s}^{-1}$. Anomalies at each grid point are the difference between the mean composite daily wind and the mean daily wind on June–September. Composite fields are shown for the time sequence day-1/day 0/day +1. Associated relative humidity anomalies at 925 hPa are displayed by isolines in %. Scale for the wind (m s^{-1}) is indicated

6 Discussion and conclusion

We have investigated the synoptic activity of weather systems at 700 hPa over West Africa and the tropical Atlantic. This study was performed for the first time both on ERA and NCEP/NCAR reanalyses and over a long-term period (17 y for NCEP/NCAR, 15 y for

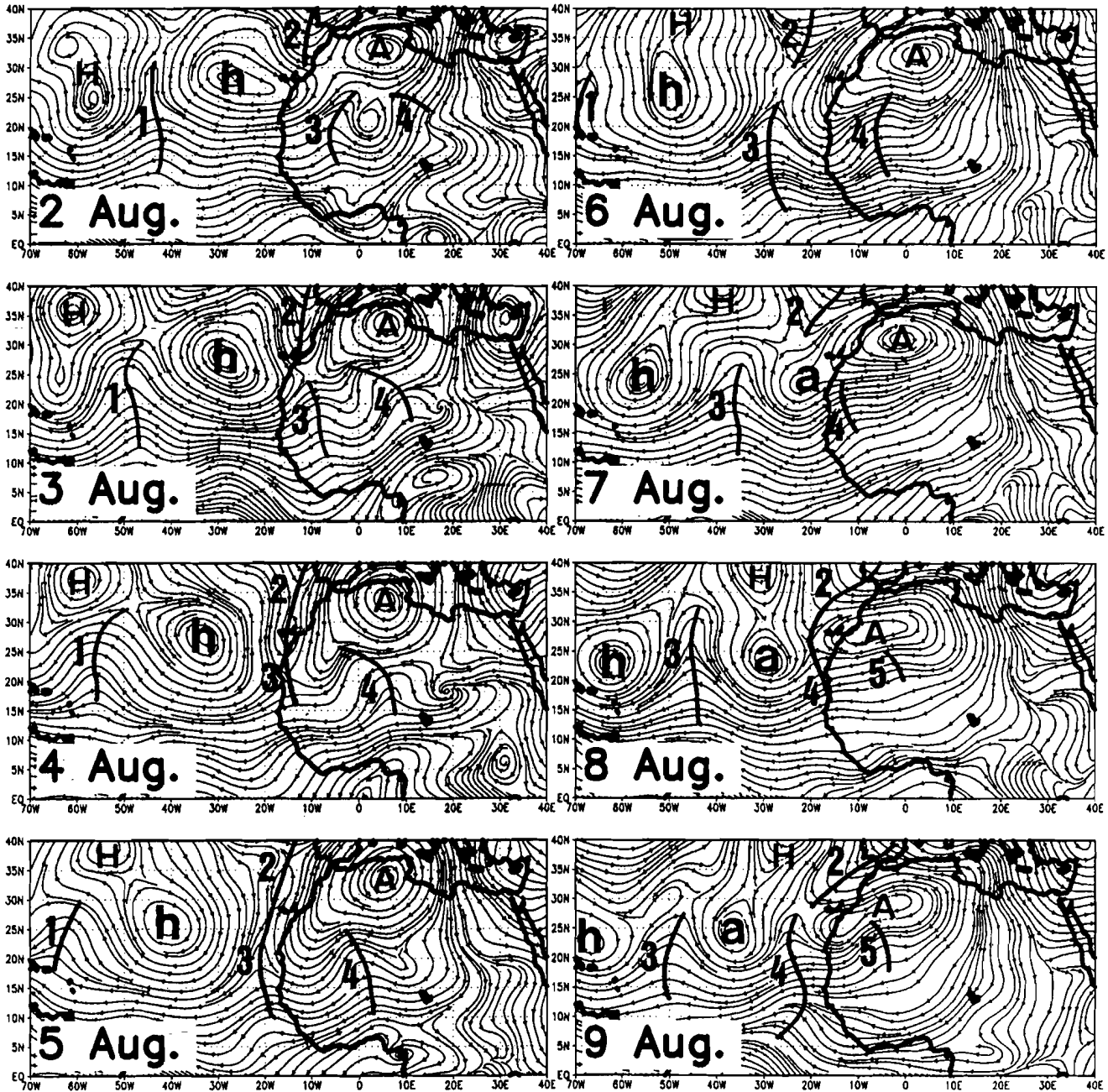


Fig. 14 Stream lines of the NCEP/NCAR 700 hPa unfiltered wind field for the sequence 2–9 August, 1979. Bold H, h, A and a show the

location of anticyclonic cells. Bold numbers 1 to 5 show the locations of the different troughs on these maps (see text)

ERA). It enabled us to analyze the kinematic characteristics of well-known “easterly waves” with a periodicity between 3 and 5 days, and demonstrate the existence of another, more intermittent, regime of easterly waves showing a periodicity approximately between 6 and 9 days. All the results presented here are highly self-consistent. The use of an a priori period band criterion enabled us to separate these two regimes and to prove that each of them constitutes a statistical and meteorological regime of synoptic easterly waves.

Particular points can be discussed about the 3–5-day easterly waves. The evidence of two cyclonic centers north and south of the AEJ has been already identified by Carlson (1969) and Burpee (1974). Automatic classification (Janicot 1992) was performed, based on filtered NCEP/NCAR 700 hPa meridional wind components along 0°W between 5°N and 17.5°N to evaluate the different possible instantaneous patterns of 3–5-day easterly waves. Results (Diedhiou 1998) depict three main categories of 3–5-day wave patterns, one with

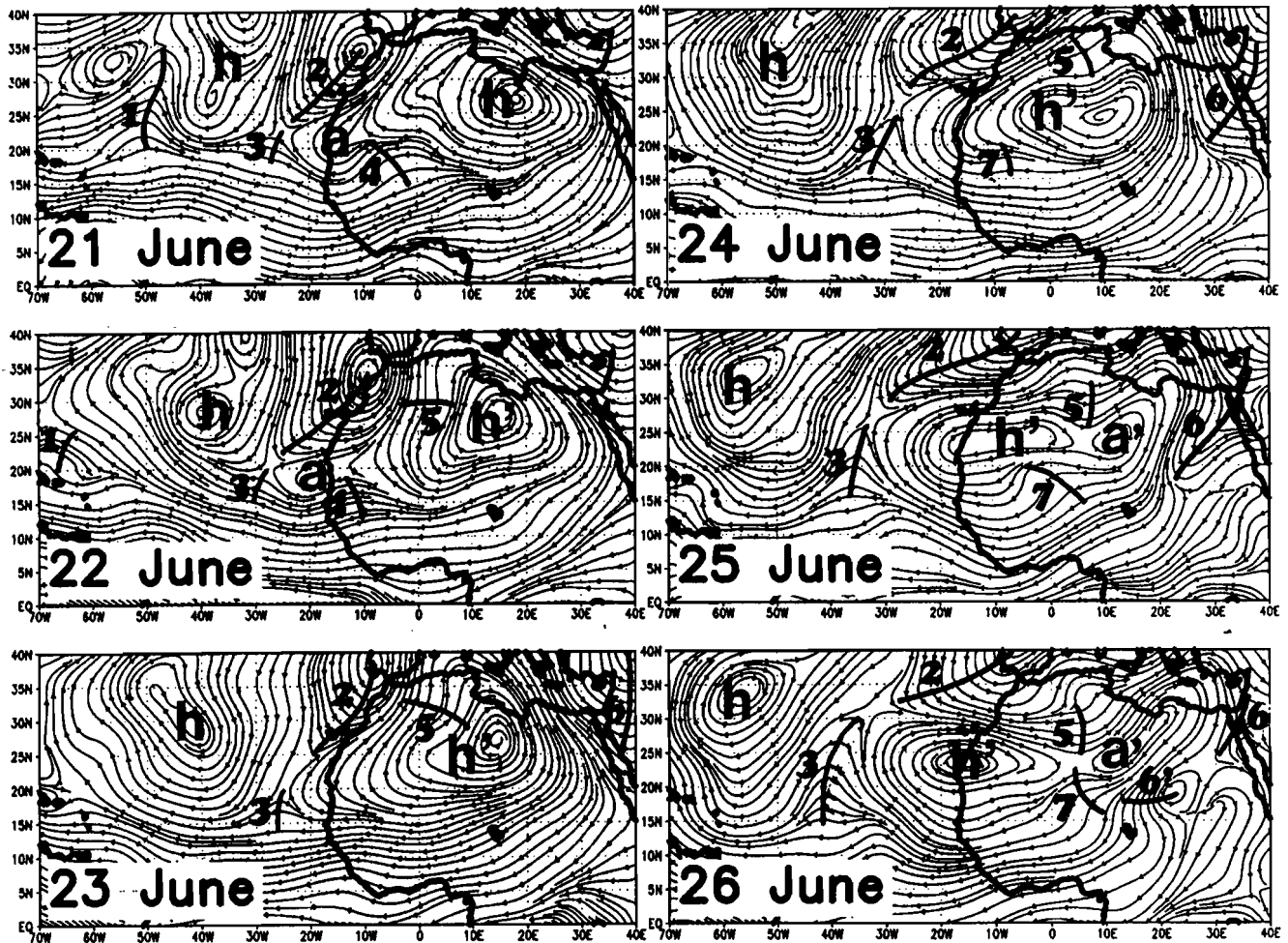


Fig. 15 Stream lines of the NCEP/NCAR 700 hPa unfiltered wind field for the sequence 21–26 June 1988. Bold h and h' show the location of the two anticyclonic cells, a and a' show ridges associated

to h . Bold numbers 1 to 7 show the locations of the different troughs pointed out on these maps

activity centers both north and south of the AEJ, another one with high activity centers mainly on the northern side of the jet, and a final one with high activity centers mainly on the southern side of the jet. Out of 2074 cases, by considering 122 days during June–September for each of the 17 y, 662 (32%) concern the first pattern, 564 (27%) the second one and 848 (41%) the third one. Thus there is an approximate equal distribution of 3–5-day easterly waves extending (1) both north and south of the AEJ, (2) located mainly north of the jet, and (3) and mainly south of the jet.

Another feature shown in ERA and NCEP/NCAR reanalyses is the steep southward gradient of wavelength and phase speed of the 3–5-day easterly waves over West Africa. The reason for such large wavelengths (up to 5000 km) south of the AEJ has not been elucidated. Rennick (1981) showed that an increased horizontal shear of the AEJ is associated with a shorter wavelength of the most unstable wave. Figure 1 points out, at 600 hPa, a weaker horizontal shear of the

zonal NCEP/NCAR wind along the southern track at 5°N, when compared to the northern track at 15°N, consistent with greater wavelengths observed south of the jet. However, the difference in the AEJ northern and southern edges wind shear in ERA is not as marked as in the NCEP/NCAR wind field. Moreover the average wind shear computed on a two-month sequence is not representative of daily wind fields.

The evidence of another regime of easterly waves, in the 6–9-day band period, is the most important result of this study, whereas further investigation remains necessary to better understand the dynamics of such a regime. It is also important to note that whereas the 6–9-day spectral signal is high only north of 15°N over West Africa, the associated synoptic pattern can modulate significantly rainfall and convection southward as far as the Guinea coast. Easterly wave patterns associated with the 6–9-day regime have rarely been analyzed in previous studies and, when this pattern was shown in a few papers, it was interpreted as a classical

3–5-day easterly waves. Some examples can be found in Karyampudi and Carlson (1988) dealing with the Saharan air layer and dust transport, or in Ross (1991) computing the energy budget of such an easterly wave. We have also shown that, for instance during GATE phase I, if the 3–5-day regime was weak, a strong 6–9-day regime occurred during most of this phase. Then any “inactive” time sequence, when few easterly waves are observed on synoptic charts, may be an active 6–9-day regime, inside of which a strong anticyclonic cell is moving westward over West Africa north of the AEJ, and where easterly waves are statistically half as frequent as during a 3–5-day regime.

Another difference pointed out is the large modulation of the jet zonal wind component and the symmetric pattern related to this jet in the 6–9-day wave pattern. While the 3–5-day waves have troughs growing both on the poleward and the equatorward sides of the AEJ, in the 6–9-day wave pattern, a trough north of the jet occurs with an anticyclonic circulation south of it, and vice versa. In GATE phase I, the 6–9-day phase was associated with a cyclonic circulation south of the AEJ over several days, providing precipitation along the Guinea coast. Similar cases have been found, for example during the COPT81 (Convection Profonde Tropicale) in May–June 1981 over Ivory coast, when such a 6–9-day regime occurred at the same time as a sequence of five squall lines in eight days (Roux 1987). It is important to note that an individual cyclonic circulation travelling over the Guinea coast and providing significant precipitations can be embedded in a larger synoptic pattern which was not identified until now. It is also suggested that a large anticyclonic circulation, increasing the meridional wind shear in the AEJ core, can force a strong cyclonic circulation south of the jet, on its cyclonic shear side.

These differences between the two easterly wave patterns thus lead to resulting differences in the modulation of rainfall and convection in the ITCZ, as well as of the monsoon winds. The 3–5-day regime is associated with meridionally extended positive rainfall anomalies in the trough and ahead of it, consistent with the meridional extension of the wave. The 6–9-day regime is linked to a meridional dipole pattern of zonally extended rainfall anomalies over West Africa, with opposite anomaly signs over the Sahel/Sudan band and the Guinea coast. In this regime the convection is mostly increased in the trough and behind it, in association with large modulation of the AEJ zonal wind component, and with a southerly advection of moist air. Behind the trough, the AEJ velocity is greater in the anticyclonic circulation, leading to a similar vertical wind shear increase between the lower and middle levels. This could be a favorable condition for the development of squall lines, and might explain the location of deep convection behind the trough. The large wavelength in this wave pattern could also lead to the development of several mesoscale convective com-

plexes in the same sector of the wave, located at about the same latitude and different longitudes.

The fact that similar results have been found with the NCEP/NCAR modelled rainfall and IRD rainfall in the synoptic composites is a good point in the evaluation of the convective scheme of this model, but it also indicates that this rainfall modulation is mostly induced by the wave patterns since the NCEP/NCAR model does not represent explicitly the mesoscale convective complexes such as squall lines which produce a large part of the precipitation over West Africa. The comparison between NCEP/NCAR reanalyses and ERA showed significant differences in the 3–5-day variances over the Atlantic. In situ wind measurements would be necessary to evaluate the quality of the two reanalysis datasets.

Based on individual case studies, we pointed out that the 6–9-day regime over West Africa can be interpreted as an interaction between strong anticyclonic cells developing over the Saharan heat low and troughs growing on the poleward side of the AEJ in the 3–5-day easterly wave regime. The interaction between the troughs growing on the poleward side of the jet and the quasi-stationary trough along the western coast of North Africa were considered too. Figure 16b shows a Hovmöller time-longitude diagram of the unfiltered zonal wind component at 700 hPa along the latitude 12.5°N from 15 May to 15 July 1988. It depicts westward propagations of easterly wind maxima between East Africa and East Asia. This longitude domain coincides with the occurrence of subtropical high geopotential heights at 700 hPa (Fig. 16a) which help maintain an easterly wind component in the equatorial band at such pressure level. The development of large anticyclonic circulations over the Libyan area could lead to an enhancement of the zonal wind component of the AEJ, the anticyclonic cell and the associated zonal wind maximum area then propagating westward.

More speculatively, we also suggest association of this westward propagation with a possible longitudinal easterly wave, modulating the zonal wind component of the AEJ over West Africa and westward (illustrated in Fig. 16c). A pulse in the northeasterly winds of an anticyclonic cell like the Libyan anticyclone might generate such a resonant wave. Other subtropical anticyclonic cells located westward might also help maintain these zonal wind modulations. The 6–9-day wave analyzed could partly be sustained by such a longitudinal wave. The comparison of the time-longitude diagram for the raw values (Fig. 16b) and the filtered one in the 6–9-day periods shows a good consistency over West Africa and the tropical Atlantic (for instance, the selected example of Fig. 7b is included in the diagram). We could actually, therefore, understand why the troughs in a 6–9-day wave regime, which are located on the poleward side of the AEJ, do not extend on the equatorward side: Fig. 16c shows that the westerly component of the longitudinal wave south of trough

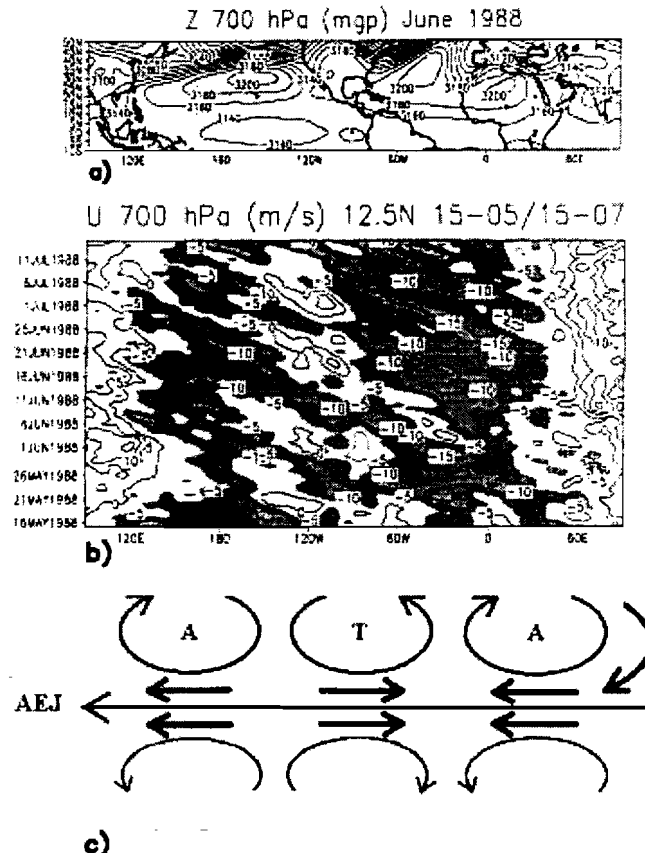


Fig. 16 **a** Mean 700 hPa geopotential heights (mgp) in June 1988. **b** Time-longitude sequence of daily 700 hPa zonal wind component ($m s^{-1}$) at $12.5^{\circ}N$ from 15 May to 15 July 1988; negative values, greater than $5 m s^{-1}$ in absolute value, are shaded. **c** Schematic panel of a 6–9-day wave (A : anticyclone, T : trough), the AEJ, and in bold arrows a wind perturbation on the right side of an anticyclonic circulation, initiating a longitudinal modulation of the zonal wind component in the jet core

"T" is in phase with the cyclonic circulation in this trough, but is in opposite phase of a possible similar cyclonic circulation south of the AEJ. This hypothesis however needs further investigation.

Finally, it seems important to investigate the dynamics of the 6–9-day easterly wave regime through modeling experiments. For instance, we could test the impact of a low potential vorticity source located on the southern edge of the Libyan anticyclone on the modulation of the AEJ wind speed and of the resulting activity of the 3–5-day easterly waves which grow through the combined barotropic-baroclinic instability of the jet. We could also test the hypothesis that the 6–9-day regime could be a secondary normal mode of instability of the AEJ, more intermittent than the 3–5-day mode. The fact that the wavelength of this mode is of the same order as the jet length should nevertheless preclude any instability.

This work will be also carried on by investigating the energetics associated with these two regimes as well as the differences in composite patterns computed over

the continent and over the ocean (Diedhiou et al. 1999). The availability of NCEP/NCAR reanalyses for the period 1958–1997 could also enable us to analyze the interannual variability of the easterly waves and other synoptic weather systems in relation to interannual variations of rainfall over West Africa.

Acknowledgements The authors are indebted to the Climate Diagnostics Center (NOAA, Boulder, CO) for providing the NCEP/NCAR reanalysis database and, to Abraham H. Oort for providing the GFDL Atmospheric Circulation Tape Library 1958–1989. Thanks are also due to Jean Louis Monge for his efficiency in managing the CLIMSERV data base at LMD, Jean Philippe Duvel for accessibility to OLR/NOAA data, Laurent Li for providing the ECMWF reanalyses interpolated on the NCEP/NCAR grid and Cathy Boonne, manager of the IPSL data base, for the extraction of daily radiosonde dataset at ECMWF. Thanks are also given to Jean Luc Melice (IRD) who provided us with the wavelet software, to Marie Farge for discussion on wavelet transform, and to Brian Doty for the availability of the graphics software GrADS. Finally the authors are grateful to the two reviewers for their valuable comments, in particular for the thought concerning the 6–9-day easterly waves. A. Diedhiou has been partly supported by IRD and partly supported by the European Contract WAMP (West African Monsoon Project) ENV4-CT97-0500.

References

- Albignat JP, Reed RJ (1980) The origin of African wave disturbances during phase III of GATE. *Mon Weather Rev* 108:1827–1839
- Burpee RW (1972) The origin and structure of easterly waves in the lower troposphere in North Africa. *J Atmos Sci* 29:77–90
- Burpee RW (1974) Characteristics of North African easterly waves during the summers of 1968 and 1969. *J Atmos Sci* 31:1556–1570
- Burpee RW (1975) Some features of synoptic-scale waves based on a compositing analysis of GATE data. *Mon Weather Rev* 103:921–925
- Cadet DL, Houston SH (1984) Precipitable water over West Africa and the Eastern/Central Atlantic ocean during summer 1979. *J Meteorol Soc Jpn* 62:761–774
- Cadet DL, Nnoli NO (1987) Water vapour transport over West Africa and the Atlantic ocean during summer 1979. *Q J R Meteorol Soc* 113:581–602
- Carlson TN (1969a) Synoptic stories of three African disturbances that developed into Atlantic hurricanes. *Mon Weather Rev* 97:256–276
- Carlson TN (1969b) Some remarks on African disturbances and their progress over the tropical Atlantic. *Mon Weather Rev* 97:716–726
- Chen YL, Ogura Y (1982) Modulation of convective activity by large-scale flow patterns observed during GATE. *J Atmos Sci* 39:1260–1279
- De Felice P, Viltard A, Monkam D, Ouss C (1990) Characteristics of North African 6–9 day waves during summer 1981. *Mon Weather Rev* 118:2624–2633
- De Felice P, Viltard A, Oubuih J (1993) A synoptic-scale wave of 6–9 day period in the Atlantic tropical troposphere during summer 1981. *Mon Weather Rev* 121:1291–1298
- Dhonneur G (1974) Nouvelle approche des realites meteorologiques de l'Afrique Occidentale et centrale, ASECNA. Thesis University of Dakar, Senegal, 385pp and 472pp
- Diedhiou A (1998) Easterly wave regimes over West Africa and the tropical Atlantic. Thesis, University Paris 12, 230pp (in French)
- Diedhiou A, Janicot S, Viltard A, de Felice P (1998a) Evidence of two regimes of easterly waves over West Africa and tropical Atlantic. *Geophys Res Lett* 25:2805–2808

- Diedhiou A, Janicot S, Viltard A, de Felice P, Laurent H (1998b) A fast eastern waves in West Africa troposphere. *Meteorol Atmos Phys* 69:39–47
- Diedhiou A, Janicot S, Viltard A, de Felice P (1999) Composite patterns and energetics of easterly wave disturbances over West Africa and the tropical Atlantic: results from the 1979–1995 NCEP/NCAR reanalyses. Submitted to *Clim Dyn*
- Duvel JP (1989) Convection over tropical Africa and the Atlantic ocean during northern summer. Part I: interannual and diurnal variations. *Mon Weather Rev* 117:2782–2799
- Duvel JP (1990) Convection over tropical Africa and the Atlantic ocean during northern summer. Part II: modulations by easterly waves. *Mon Weather Rev* 118:1855–1868
- Farge M (1992) Wavelets transform and their applications to turbulence. *Ann Rev Fluid Mech* 24:395–457
- Fontaine B, Janicot S, Moron V (1995) Rainfall anomaly patterns and wind field signals over the West Africa in August (1958–1989). *J Clim* 8:1503–1510
- Fontaine B, Janicot S, Roucou P (1999) Observed and modelled surface variability in the tropical Atlantic region and its rainfall impact. *Clim Dyn* (in press)
- GATE report 17 (1975) Report on the field phase of the GARP Atlantic tropical experiment; meteorological atlas, prepared by ISMG. WMO, 179pp
- Gibson JK, Kalberg P, Uppala S, Hernandez A, Nomura A, Serrano E (1997) ERA description. ECMWF Re-Analysis Project. Rep Ser 1, ECMWF, Reading, UK, 72pp
- Grueber A, Krueger AF (1974) The status of the NOAA outgoing longwave radiation data set. *Bull Am Meteorol Soc* 65:958–962
- Holton JR (1979) An introduction to dynamic meteorology. Int. Geophys. Series, 23, 2nd Edn, Academic Press, 391pp
- Janicot S (1992) Spatiotemporal variability of West African rainfall. *J Clim* 5:489–511
- Janicot S (1993) Variability of dynamical fields over Africa (1970–1988); Atlas for validation of general circulation models. Tech Note LMD 187, 131pp
- Kallberg P (1997) Aspects of the re-analysed climate. Project Rep Ser 2, ECMWF, Reading, UK
- Kalnay E, Kanamitsu M, Kistler R, Collins W, Deaven D, Gandin L, Iredell M, Saha S, White G, Woolen J, Zhu Y, Chelliah M, Ebisuzaki W, Higgins W, Janowiak J, Mo KC, Ropelewski C, Wang J, Leetma A, Reynolds R, Jenne R, Joseph D (1996) The NCEP/NCAR 40-year reanalysis project. *Bull Am Meteorol Soc* 77:437–471
- Karyampudi VM, Carlson TN (1988) Analysis and numerical simulations of the Saharan air layer and its effect on easterly wave disturbances. *J Atmos Sci* 45:3102–3136
- Kwon HJ (1989) A reexamination of the genesis of African waves. *J Atmos Sci* 46:3621–3631
- Lamb PJ (1983) West African water vapor variations between recent contrasting Subsaharan rainy seasons. *Tellus A* 35:198–212
- Mass C (1979) A linear primitive equation model of African wave disturbances. *J Atmos Sci* 36:2075–2092
- Norquist DC, Recker EE, Reed RJ (1977) The energetics of African wave disturbances as observed during phase III of GATE. *Mon Weather Rev* 105:334–342
- Oort AH (1978) Adequacy of the rawinsonde network for the global circulation studies tested through numerical model output. *Mon Weather Rev* 106:174–195
- Oort AH (1983) Global atmospheric circulation statistics: 1958–73. NOAA Prof Pap 14:179pp
- Oort AH, Liu H (1993) Upper-air temperature trends over the globe, 1958–1989. *J Clim* 6:292–307
- Paradis D, Lafore JP, Redelsperger JL (1995) African easterly waves and convection. Part I: linear simulations. *J Atmos Sci* 52:1657–1679
- Pytharoulis I, Thorncroft CD (1999) On the existence of warm core African easterly waves. *Mon Weather Rev*, in press
- Reed RJ, Norquist DC, Recker EE (1977) The structure and properties of African wave disturbances as observed during phase III of GATE. *Mon Weather Rev* 105:317–333
- Reed RJ, Hollingsworth A, Heckley WA, Delsol F (1988a) An evaluation of the performance of the ECMWF operational system in analysing and forecasting easterly wave disturbances over West Africa and the tropical Atlantic. *Mon Weather Rev* 116:824–865
- Reed RJ, Klinder E, Hollingsworth A (1988b) The structure and characteristics of African easterly wave disturbances determined from ECMWF operational analysis/forecast system. *Meteorol Atmos Phys* 38:22–33
- Rennick MA (1976) The generation of African waves. *J Atmos Sci* 33:1955–1969
- Rennick MA (1981) Some sensitivity experiments with an African wave model. *J Atmos Sci* 38:106–113
- Ross RS (1991) Energetics of African wave disturbances derived from the FSU global spectral model. *Meteorol Atmos Phys* 45:139–158
- Roux F (1987) The squall lines of COPT81: environment, precipitations, kinematics and thermodynamics. Thesis University of Paris 7, 368pp (in French)
- Sadler JC, Oda LK (1978) The synoptic (A) scale circulations during the third phase of GATE 20 August–23 September 1974. Department of Meteorology, University of Hawaii, UHMET 78-02, 41pp
- Senouci M (1990) Atlas of Africa north of the equator in boreal summer with ECMWF analyses (1980–1988). Int Note LMD 238pp
- Simmons AJ (1977) A note of the instability of the African Easterly Jet. *J Atmos Sci* 34:1670–1674
- Sow CS (1997) Diurnal rainfall variations in Senegal. *Secheresse* 8:157–162
- Thompson RM, Payne SW, Recker EE, Reed RJ (1979) Structure and properties of synoptic-scale wave disturbances in the inter-tropical convergence zone of the eastern Atlantic. *J Atmos Sci* 36:53–72
- Thorncroft CD (1995) An idealized study of African easterly waves. Part III: more realistic basic states. *Q J R Meteorol Soc* 121:1589–1614
- Thorncroft CD, Hoskins BJ (1994a) An idealized study of African easterly waves. Part I: a linear view. *Q J R Meteorol Soc* 120:953–982
- Thorncroft CD, Hoskins BJ (1994b) An idealized study of African easterly waves. Part II: a nonlinear view. *Q J R Meteorol Soc* 120:983–1015
- Torrence C, Compo GP (1998) A practical guide to wavelet analysis. *Bull Am Meteorol Soc* 79:61–78
- Viltard A, de Felice P, Oubuih J (1997) Comparison of the African and the 6–9 day wave-like disturbance patterns over West Africa and the tropical Atlantic during summer 1985. *Meteorol Atmos Phys* 62:91–99
- Viltard A, Oubuih J, de Felice D, Laurent H (1998) Rainfall and 6–9-day wave-like disturbance in West Africa during summer 1989. *Meteorol Atmos Phys* 66:229–234
- Walker J, Rowntree PR (1977) The effect of soil moisture and rainfall in a tropical model. *Q J R Meteorol Soc* 103:29–46
- Wallace JM, Lim GH, Blackmon ML (1988) Relationship between cyclone tracks, anticyclone tracks and baroclinic waveguides. *J Atmos Sci* 45:439–462

Multi-scale description of a Sahelian synoptic weather system representative of the West African monsoon

By J.-L. REDELSPERGER^{1*}, A. DIONGUE¹, A. DIEDHIOU², J.-P. CERON³, M. DIOP³, J.-F. GUEREMY³ and J.-P. LAFORE¹

¹CNRM/GAME, CNRS and Météo-France, France

²LTHE, CNRS and IRD, France

³ENM, Météo-France, France

(Received 20 December 2000; revised 9 August 2001)

SUMMARY

A reference case of a Sahelian weather system observed during the Hydrological Atmospheric Pilot Experiment, HAPEX-SAHEL, in August 1992, is described from a seasonal viewpoint as well as from synoptic and convective system viewpoints. It is shown that the case-study is representative of the climatology at all these scales and presents many interacting scales and physical processes. At intraseasonal scale, the monsoon onset is characterized by an abrupt shift of precipitation together with a latitudinal migration of the African easterly jet (AEJ) and convection. At the month and day scales, the convective activity occurs in an apparent zonal break of the tropical easterly jet. The month of August 1992 exhibits intense synoptic activity. The vorticity field is characterized by northerly (dry) and southerly (wet) components located at 850 hPa on each side of the AEJ. Their intraseasonal modulation on a period of 20 to 40 days leads to active and break phases of the synoptic activity. Around 21 August, the 700 hPa vorticity field features the propagation of a typical easterly wave with a westward propagation of a cyclonic circulation followed by an anticyclonic circulation. Convective activity occurs mainly ahead of the 700 hPa vorticity maximum with the formation of a squall line on Air mountains propagating south-westward at 15 m s^{-1} . The convective system propagates about twice as fast as the vortex core, in contrast with the convection in the European Centre for Medium-Range Weather Forecasts re-analysis which stays in phase with the vorticity. The squall line corresponds to the largest contributor to the systems passing in August 1992 over the HAPEX-SAHEL region; its environmental conditions and its effects on the atmosphere including the surface parameters are presented.

KEYWORDS: HAPEX Scale interactions Squall line Easterly waves

1. INTRODUCTION

The West African region and in particular the Sahelian zone exhibits extremely marked rainfall variability on both interannual and decadal time-scales. In a marginal climate as in the Sahel, such variability can result in severe drought and may impact on desertification processes. Thus the understanding and the forecasting of this variability is required for seasonal prediction of rainfall. This variability can be viewed as a modulation of the seasonal cycle which is mainly characterized by the West African Monsoon (hereafter WAM). Moreover recent observational studies (Le Barbé and Lebel 1997; Le Barbé *et al.* 2002) have indicated that dry years in this region are characterized by a lower frequency of intense convective events, but with their average magnitude remaining unchanged. In that respect, investigating the link between the large-scale circulation features and convection may produce some clues about rainfall variability in the region.

As for all monsoons, the WAM presents many interacting scales and physical processes (Fig. 1). Key features of the WAM are precipitating weather systems of which the most important are the synoptic-scale easterly waves (e.g. Reed *et al.* 1977) and the mesoscale convective systems such as squall lines (e.g. LeMone 1983). Both are relatively well understood and have been the object of numerous studies, but they have generally been studied independently. Hence, our knowledge of the scales of interactions between them is still very limited. It is based on observations and numerical

* Corresponding author: CNRM/GAME, 42 Av Coriolis, 31057 Toulouse Cedex, France.

e-mail: jean-luc.redelsperger@meteo.fr

© Royal Meteorological Society, 2002.

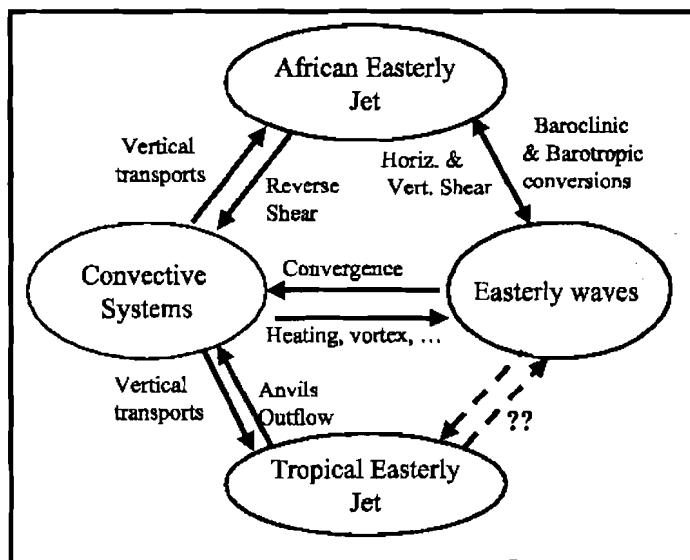


Figure 1. Interactions between main atmospheric features observed over West Africa.

studies and, to a lesser extent on theoretical works. Two main field experiments, GATE* and COPT81, have advanced our understanding of African waves and squall lines, respectively.

The African easterly wave (AEW) has been the object of many modelling and observational studies for over a half-century. This wave has been shown to be associated with much of the rain over West Africa, as well as with tropical cyclones originating there and crossing the Atlantic Ocean. Burpee (1972, 1974) estimated the wavelength to be 4000 km by spectral analysis and 3000 km by composite techniques. It is observed between June and September west of 30°E, propagating at 8 m s^{-1} . He showed that this could be explained by a combination of baroclinic and barotropic instabilities associated with the African easterly jet (AEJ). The GATE experiment (Betts 1974) allowed a more detailed account. Reed *et al.* (1977), applying a composite technique to the waves of the GATE Phase III, showed differences between observations over the ocean and over land. This and many other studies have shed light on the structure and origin of the AEW as well as on its modulation of convection (e.g. Chen and Ogura 1982; Duvel 1990). However, the dependence of the AEW structures on various environmental parameters (e.g. the tropical easterly jet (TEJ) and AEJ) as well as the scales of their interaction with convection, remain poorly understood.

Mesoscale convective systems are generally large (up to 1000 km across) with lifetimes from 12 hours to a few days, and correspond in general to squall lines (e.g. Desbois *et al.* 1988). Squall lines are responsible for the majority of the rainfall in the African Sahel. They often produce large rainfall and propagate fast (up to 15 m s^{-1}). They consist of organized convective lines generally associated with a trailing stratiform region. Observations show the existence of preferred regions of convective activity within the AEW. It is also recognized that convection strongly modifies the atmosphere at large scales. This problem of scale interaction is difficult to treat in its entirety because of the range of scales spanned. Squall lines are known to be efficient in transporting

* Global Atmospheric Research Program Atlantic Tropical Experiment.

heat, moisture and momentum (e.g. Lafore *et al.* 1988), mainly due to their high degree of organization and fast propagation. Being able to predict WAM convective systems would thus be useful both for the prediction of local rainfall and for large-scale weather prediction.

Coarse resolution General Circulation Models (GCMs), used to make seasonal and climate predictions, generally have a poor representation of the synoptic weather systems which produce precipitation. One of the main reasons for this is that GCMs are not able to explicitly represent mesoscale weather systems. Therefore, it is unclear whether we can have confidence in a GCM prediction of rainfall if it cannot represent the weather systems which are observed to provide this rainfall. It has long been recognized that global climate models used to predict climate change have problems predicting changes on regional scales. It is likely that regional scales are badly reproduced in GCMs due to a combination of poor resolution and poor representation of physical processes (mainly parametrization of moist convection and land-surface processes). A recent intercomparison of simulations in the framework of a European project (WAMP 1999) shows that GCMs predict the onset of the WAM too early in the season (see also Lebel *et al.* 2000).

All these considerations lead us to recognize that the understanding of African weather systems and their representation in GCMs require an integrated approach which considers a whole range of phenomena and their interactions at different scales. To address this issue, it is strongly desirable to have a multi-scale description of a reference case of a weather system representative of the WAM. The goal of the present paper is to describe such a case diagnosed from seasonal and interannual viewpoints (section 2), as well as from synoptic (section 3) and convective system (section 4) viewpoints. This case will also serve as a reference case for a multi-scale numerical study thanks to the use of a hierarchy of models (from cloud-resolving models to climate models). We have chosen to focus on the case of a squall line which occurred between 21 and 22 August 1992 over the Sahel and was observed during HAPEX-SAHEL (the Hydrological Atmospheric Pilot Experiment conducted in Niger (Goutorbe *et al.* 1994)).

2. INTERANNUAL AND INTRASEASONAL SCALES

Rainfall is one of the most characteristic parameters used to describe the interannual variability of climate over West Africa (e.g. Nicholson 1989; Hulme 1992). For example, the latitudinal evolution of the rainfall band is well correlated with the displacement of the intertropical convergence zone (ITCZ). To place the year 1992 in an interannual context, two different rainfall datasets are used: the climatology of Hulme (1992) available at the monthly scale, and the daily rainfall data compiled by IRD (Institut de Recherche pour le Développement, formerly ORSTOM), ASEENA (Agence pour la Sécurité de la Navigation Aérienne en Afrique et à Madagascar) and CIEH (Comité Inter-africain d'Études Hydrauliques).

Time-latitude evolution of monthly rainfall over West Africa (mean over 10°W–10°E) as extracted from the Hulme database is plotted for the year 1992 in Fig. 2(a). The pattern depicts two aspects of the rainfall season over this area. The first one corresponds to the beginning of the main rainfall season (end of April to end of June over West Africa). This period can be considered as a monsoon pre-onset during which only regions over the Guinea coast experienced rainfall. The second aspect is related to the middle and the end of the main rainy season when the monsoon is well established. The regions concerned are located between 9 and 16°N. The rainfall season in the monthly mean climatology (1979–93) of Hulme (Fig. 2(b)) shows similar behaviour though slight

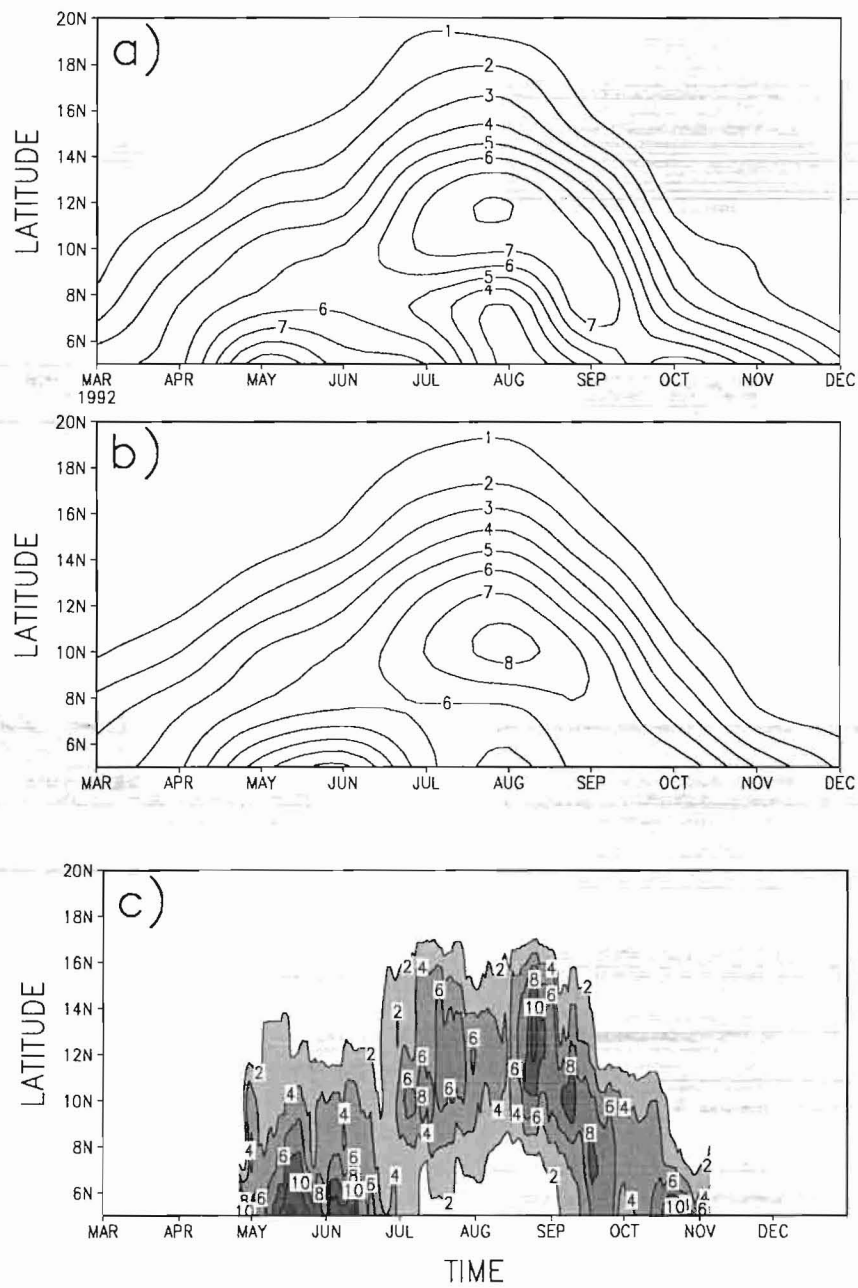


Figure 2. Time-latitude diagram of rainfall (mm day^{-1}) averaged over 10°W to 10°E from the Hulme (1992) monthly climatology: (a) for the wet season of 1992 and (b) for the average over 1979–93. Also (c) from the IRD (see text) daily database for the wet season of 1992. A 10-day running-mean filter has been applied to the IRD data. The contour interval is 1 mm day^{-1} in (a) and (b), and 2 mm day^{-1} in (c) where values greater than 2 mm day^{-1} are shaded.

differences can be seen. In particular, the second rainfall season over the coast in August is more marked in 1992.

The second dataset corresponds to the daily rainfall amount for stations located in West Africa on the domain $3\text{--}20^\circ\text{N}$, $18^\circ\text{W}\text{--}25^\circ\text{E}$. This dataset covers the period 1979–93. For the present purpose, the rainfall amount is zonally averaged between 10°W and 10°E . The features found in the Hulme monthly dataset are also reproduced in this high-resolution dataset (Fig. 2(c)) even if, in general, the signal is stronger. This dataset highlights the high-frequency variability of rainfall over these regions. In these Sahelian areas rainfall is mainly explained by mesoscale convective systems like squall lines (Le Barbé and Lebel 1997); thus each rainfall peak during the August and September period generally corresponds to a mesoscale convective system. This high-frequency aspect minimizes the monthly-scale differences, discussed above, between the year 1992 and the 1979–93 climatology. Such a fine-scale dataset clearly shows an abrupt shift of precipitation from $5\text{--}10^\circ\text{N}$ to the $10\text{--}15^\circ\text{N}$ band. In this respect 1992 appears as a normal year with a latitudinal shift on 20 June, close to 24 June which is the mean date determined from an analysis of the years 1968–92 (Sultan and Janicot 2000).

Two dynamical features are also known to be important in characterizing the mean climate over West Africa (e.g. Burpee 1972; Reed *et al.* 1977; Thorncroft and Hoskins 1994): the AEJ centred around 600–700 hPa, and the TEJ found at about 200 hPa. Figure 3(a) shows the AEJ (700 hPa) and TEJ (200 hPa) mean cores in August 1992 from the European Centre for Medium-Range Weather Forecasts (ECMWF) re-analysis dataset (ERA) together with the mean outgoing long-wave radiation (OLR) characterizing the convective activity. The National Oceanic and Atmospheric Administration (NOAA) OLR pattern highlights the location of the ITCZ by presenting two areas of convective maxima: one over central Africa and another along the West African coast. Its mean latitudinal position, east of 10°E , is around 10°N . The associated OLR anomaly from the August mean derived from the years 1979–93 (Fig. 3(b)) shows an increase in the convective activity over central Africa and the central Sahel, in a latitudinal band between 5 and 17.5°N , with a maximum covering the Niamey area (around 2.5°E). In 1992 the AEJ core is located around 15°N along the northern edge of the area of maximum convection, whereas the TEJ is at the southern part of the convective zone over the Guinea Coast (Fig. 3(a)). The TEJ structure over Africa is more complex and stronger in August (17 m s^{-1}) than the AEJ (10 m s^{-1}). The main TEJ core is located east of 25°E and corresponds to the upper branch of the Walker circulation initiated by summer convective activity over India. The TEJ exit occurs at about 25°E and 10°N and corresponds to the first maximum of convection previously noticed over central Africa. A second TEJ core is observed along the southern flank of the second maximum of convection located over the West African coast. Two processes could explain this second TEJ core: (i) the injection of mass by the convective activity occurring to the east; and (ii) the geostrophic response to the latent-heat release over the Guinea zone. In other words, the main convective activity occurs in an apparent zonal break of the TEJ. The main ascent resulting from this convective activity is thus located between the upper-level relative outflow (25°E) and the inflow (15°W) at its east and west sides, respectively. This relationship between convection and upper-level jets presents similarities with that observed at midlatitudes (Uccellini and Kocin 1987; Cammas *et al.* 1999; Mallet *et al.* 2000), and needs to be studied thoroughly for tropical regions.

The intraseasonal variability of these features can be seen from the time variation of the OLR, AEJ and TEJ as a function of the latitude at longitude 2.5°E near Niamey in Fig. 3(c)). Successive south–north and north–south migrations of convection maxima are observed around the end of June and the beginning of September, respectively.

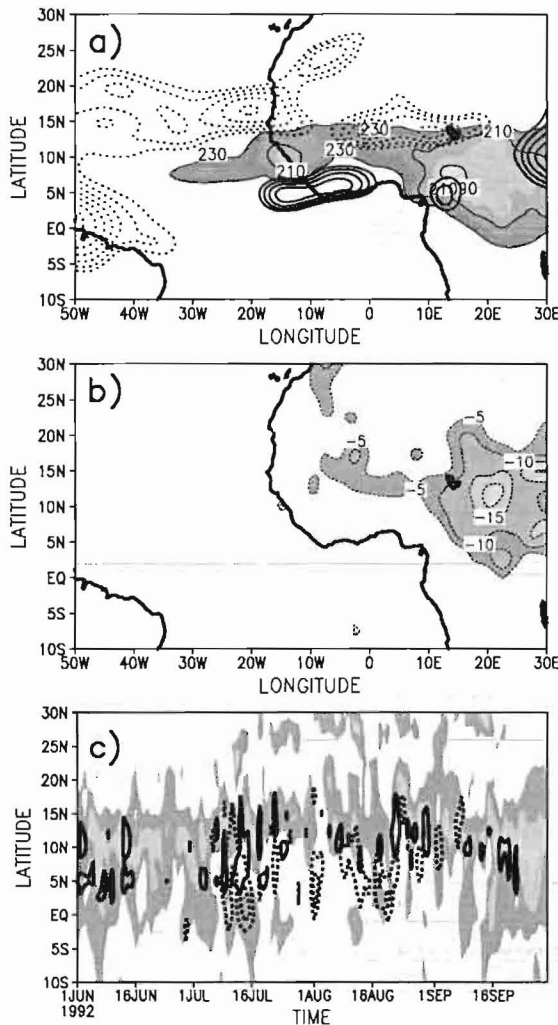


Figure 3. Convective activity and mean winds: (a) for August 1992, NOAA outgoing long-wave radiative flux (OLR; $<250 \text{ W m}^{-2}$ shaded), African easterly jet (AEJ) at 700 hPa (dotted lines for values $\leq -6 \text{ m s}^{-1}$) and tropical easterly jet (TEJ) at 200 hPa (solid lines for values $\leq -14 \text{ m s}^{-1}$); (b) OLR anomaly in August 1992 from the August average of 1979–93; (c) latitudinal evolution over the wet season of 1992 at 2.5°E of OLR (solid lines correspond to 200 W m^{-2}), AEJ at 700 hPa ($\leq -6 \text{ m s}^{-1}$ shaded) and the TEJ at 200 hPa (dotted lines for values $\leq -14 \text{ m s}^{-1}$). The AEJ and TEJ are taken from the ECMWF re-analysis.

During the intervening period, the AEJ follows this latitudinal migration. At the beginning and the end of the rainy season, the AEJ core is located north of the convective maxima and its magnitude is greater than that of the TEJ. The TEJ is reinforced during the middle of the rainy season (July–August) when it is located on the southern boundary of convection.

To further characterize the intraseasonal variations during 1992, we chose to use the 850 hPa vorticity field, which is thought to be representative of the activities of AEWs (e.g. Reed *et al.* 1977). As the AEW period is known to be 3–5 days, the variance of the 850 hPa vorticity field has been computed on a 2.5–6 day window (Fig. 4). It was computed from the ERA over the 1992 monsoon season (May to

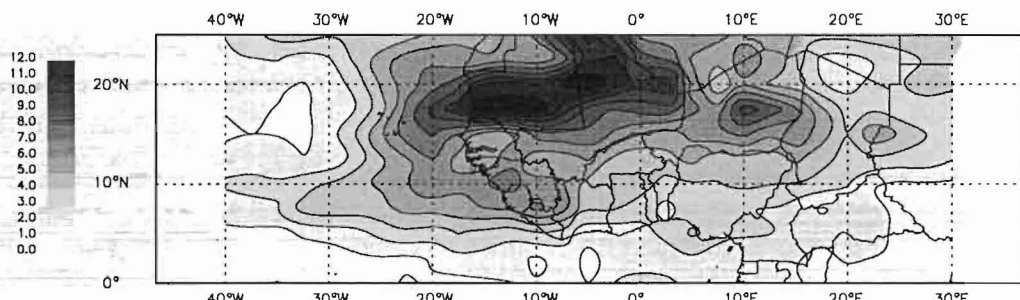


Figure 4. Horizontal cross-sections of vorticity variance at 850 hPa (2.5–6 day window) from ECMWF re-analyses for May–October 1992 (contour interval is 10^{-11} s^{-2}).

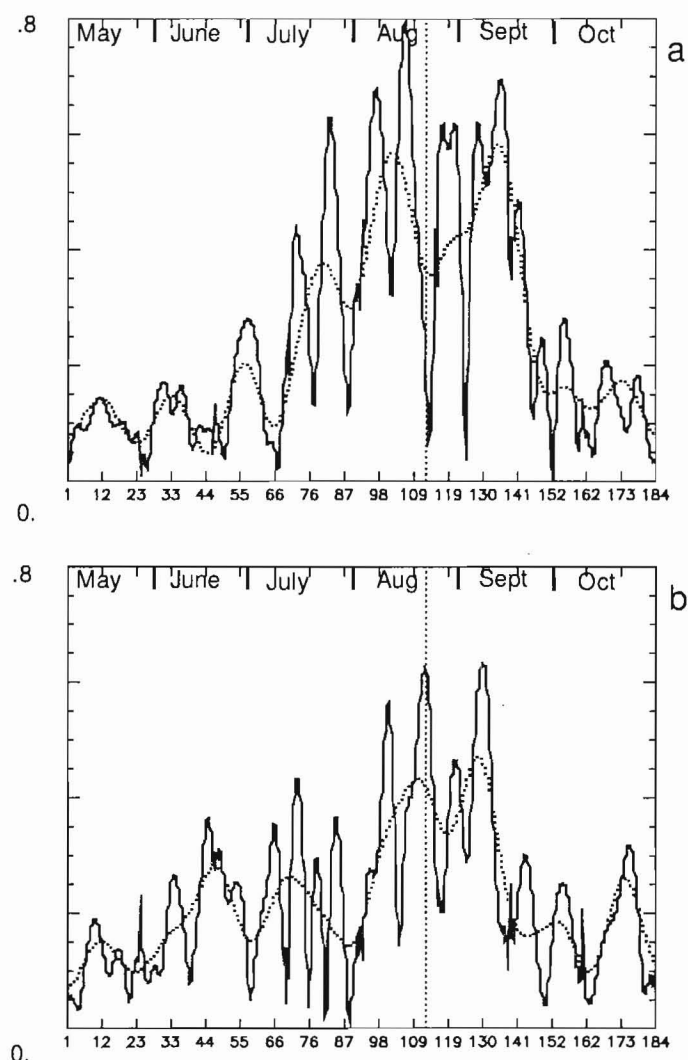


Figure 5. Evolution of time modulus (10^{-4} s^{-1}) from 1 May to 31 October 1992 for the two first rotated complex orthogonal function analysis modes of 2.5–6-day filtered vorticity at 850 hPa: (a) first mode (northerly component), and (b) second mode (southerly component). Dotted lines represent the signal after 20-day low-pass filtering. Dotted vertical line corresponds to 21 August.

October). This field exhibits, for 1992, a typical pattern which has already been found for other years (e.g. Reed *et al.* 1988; Ceron and Gueremy 1999; Diedhiou *et al.* 1999). The decomposition of this 2.5–6 day bandpass filtered 850 hPa vorticity field using a rotated complex orthogonal function analysis (RCEOFA) enables it to be partitioned into two components, both longitudinally elongated (not shown) as described in Ceron and Gueremy (1999): a northern part located around 18°N with a maximum around 10°W, and a southern part located around 8°N with a maximum around 20°W. It has been called the ‘dual track’ pattern by Ceron and Gueremy (1999). The vorticity activity is thus characterized by northerly (dry) and southerly (wet) components (NC and SC, respectively) located at 850 hPa on each side of the AEJ, with the NC having the largest amplitude. Figure 5 depicts the time evolution of the time modulus of these first two complex modes, the first being associated with the NC and the second with the SC. These time moduli correspond to the amplitude of the envelope of the 2.5–6-day bandpass filtered 850 hPa vorticity, giving direct information on the modulation of the synoptic activity by longer-period processes. It clearly shows a sharper seasonal modulation for the NC compared to the SC, with a start of the synoptic activity at the beginning of June for the SC and later in the month for the NC. The AEW activity peaks in August for both components and decays at the end of September. In addition to this seasonal modulation, intraseasonal modulation can be seen on the 20-day low-pass filtered signal. This intraseasonal modulation exhibits a period of around 20–40 days with active and break phases of the synoptic activity. The timing of these break phases can be determined by considering the days for which the two modulus time series have minima (i.e. around 7 June, 7 and 28 July, 1 and 27 September). However, this result needs to be confirmed using another method, as the two complex principal component time series are by mathematical construction uncorrelated over the considered period (May to October). Keeping this in mind, one can see that the SC (NC) tends to have a large (small) amplitude before the convective system presently studied (i.e. 21 August), while it is the opposite after this event. These features need to be explored more thoroughly, and illustrate the complex interactions between vorticity fields and convection. More insight will be given on this issue in the next section.

3. SYNOPTIC SCALE

Following the previous interannual and intraseasonal view, the synoptic-scale dynamics (taken from the ERA at 00, 06, 12 and 18 UTC) and the convective activity are analysed for a 10-day period centred on the date of the considered convective event (21 August). The OLR is used as a proxy for the convection and is extracted from the CLAUS (Cloud Archive User Service) dataset. The NCEP/NCAR* re-analysis dataset has also been used to assess some results from the ERA. Figures 6(a) to (f) present longitude–time diagrams of several fields for this period. The 700 hPa vorticity field (averaged between 5 and 20°N) clearly exhibits a westward propagation of maxima (cyclonic circulation) followed by minima (anticyclonic circulation). This illustrates the propagating AEW interacting with the studied convective event. Starting on 16 August at around 28°E, the vorticity maximum propagates with a regular phase speed (around 4 m s^{-1}) until the end of 21 August, when it is located at around 10°E. After the convective development, the phase speed increases twofold (8.7 m s^{-1}), with the vorticity maximum being located at around 21°W at the end of the considered period. Corroborating the RCEOFA analysis, the regime of the AEW changes after the convective event

* National Centers for Environmental Prediction/National Center for Atmospheric Research.

occurrence, which follows an increase in the AEW amplitude (Figs. 4(b) and 6(a)). Similar time evolutions in the location and propagation of vorticity maxima are also observed on the NCEP re-analyses (not shown). These changes in phase speed and amplitude need, nevertheless, to be studied carefully when using direct observations.

On the observed OLR latitude-time diagram (Fig. 6(b)), local maxima of convective activity are observed ahead of the 700 hPa vorticity maximum. The convective event presently studied is well-defined, being quite isolated in time (21–22 August) and having one of the smallest absolute values (less than 210 W m^{-2}). Its apparent propagation speed is 15 m s^{-1} , whereas the convective element existing on preceding days propagates at 8.7 m s^{-1} . In both cases the convective system moves about twice as fast as the vortex core. The OLR extracted from the ERA (Fig. 6(c)) also shows maxima of convective activity along the same axis. Nevertheless, the analysed OLR is located behind the observed one and in phase with the vorticity. These differences between observations and analysis represent a major issue from the modelling perspective, as the location and the speed of the diabatic heating relative to those of the vortex are fundamental in terms of dynamics (e.g. Cho and Jenkins 1987). This is relevant to the difficult problem of convection parametrization in GCMs, a key point for forecast and climate modelling (e.g. Moncrieff *et al.* 1997). An examination of ECMWF operational forecast data (D. Gregory and C. Thorncroft, personal communication) shows spurious behaviour in this case. The vorticity anomaly develops extremely rapidly, producing a convective system that is too intense.

The 925 hPa meridional moisture flux (averaged between 5 and 20°N) latitude-time diagram (Fig. 6(d)) depicts the monsoon flow. An increase in its magnitude is clearly observed on 21 August and is in phase with the increase in the 700 hPa vorticity magnitude. Globally the moist monsoon flux propagates westward in phase with the motion of vorticity and convection. Illustrated by the zonal wind at 200 and 700 hPa, respectively (Figs 6(e) and (f)), the behaviour of the TEJ and AEJ agree with the previous analysis at seasonal scale (Fig. 3). Convection thus occurs at the exit of the main TEJ (Fig. 6(e)). Maxima of convection and the TEJ propagate westward at the same speed. At the present stage of our understanding, the cause and effect relationships are, nevertheless, unknown. Another striking feature is the position of synoptic (Fig. 6(a)) and convective (Fig. 6(b)) activities occurring between two AEJ maxima (Fig. 6(f)). In other words, the AEJ appears to weaken in the region of wave and convective activity. It is necessary to be careful in interpreting these results as few observed data are available. The weakening of the AEJ could, thus, be due mainly to the explicitly resolved barotropic and baroclinic instabilities leading to the AEW development. The representation of the momentum transport induced by the convective system is more questionable in the model analysis as it depends on the subgrid-scale parametrization.

It has been demonstrated (Charney and Stern 1962) that the criterion for a flow to be unstable is that either the potential vorticity (PV^*) gradient on isentropic surfaces must change sign in the fluid interior, or the PV gradient in the fluid interior must have an opposite sign to that of the surface temperature gradient. Time sequences (21–24 August 1992) of PV and AEJ cores at 700 hPa from the ERA (Fig. 7) are consistent with the Charney–Stern theorem. The AEJ core is located in the area of negative meridional gradient of PV and the associated instability is found only south of this jet. This location is consistent with the previous RCEOFA analysis (Fig. 5). The PV field shows a westward propagation of the trough representing the disturbance in the wind

* In this paper PV is measured in PVU where $1 \text{ PVU} = 10^{-6} \text{ K m}^2 \text{ kg}^{-1} \text{s}^{-1}$.

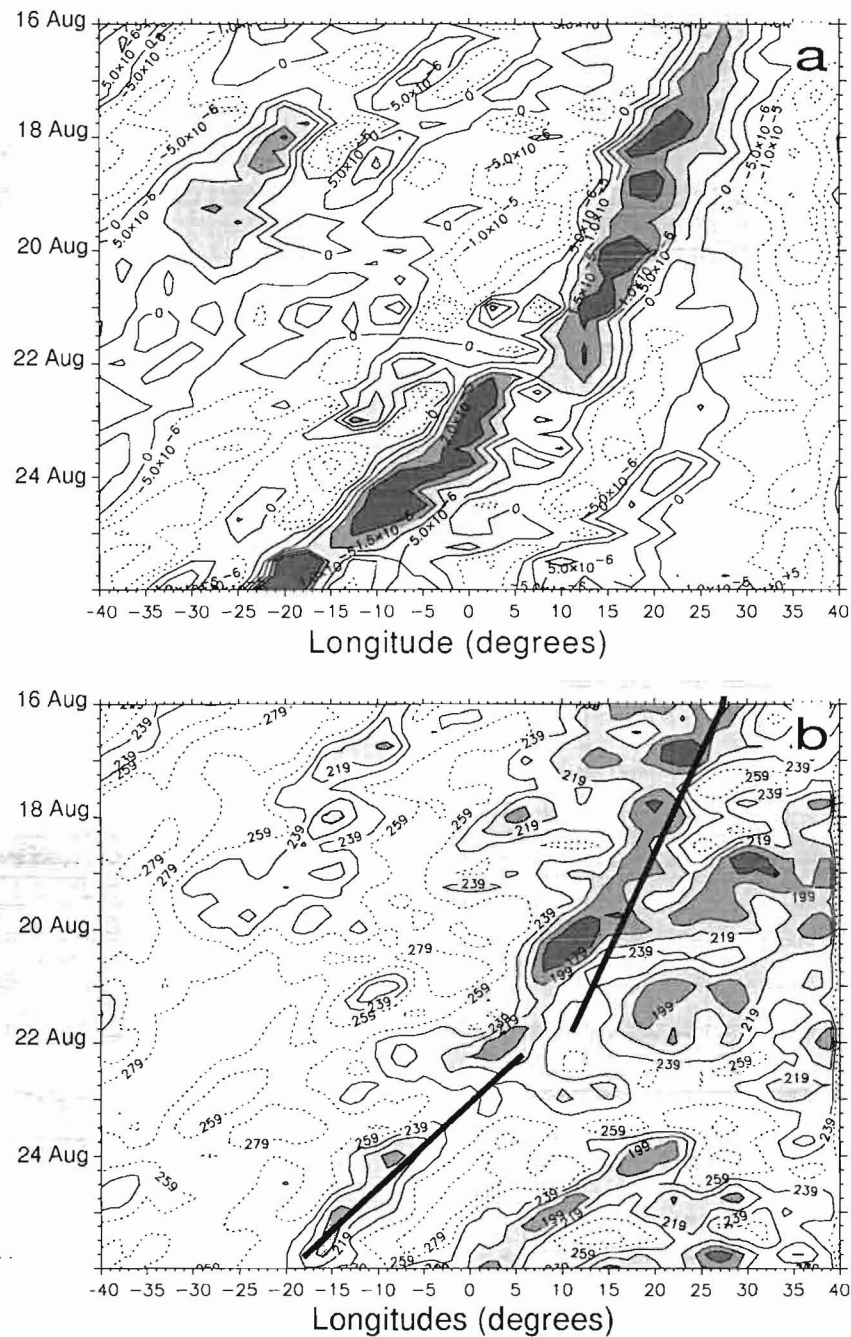


Figure 6. Time-longitude diagrams for 16–26 August 1992 from ECMWF re-analyses (ERA; except (b)): (a) vorticity at 700 hPa (contour interval $5 \times 10^{-6} \text{ s}^{-1}$), (b) observed outgoing long-wave radiation (OLR; contour interval 20 W m^{-2}), (c) ERA OLR (contour interval 20 W m^{-2}), (d) monsoon flux at 925 hPa (contour interval $25 \text{ m s}^{-1} \text{ g kg}^{-1}$), (e) zonal wind at 200 hPa (contour interval 3 m s^{-1}) and (f) zonal wind at 700 hPa (contour interval 3 m s^{-1}). Fields on (a) to (d) are averaged between 5 and 15°N . For consistency with Fig. 2(a), zonal winds at 200 and 700 hPa are averaged between 2.5 and 10°N , and 10 and 20°N , respectively. Dotted and solid lines on (e) and (f) correspond to positive and negative values, respectively. Heavy solid lines on (b) to (f) represent the main axis of the 700 hPa vorticity maximum as deduced from (a).

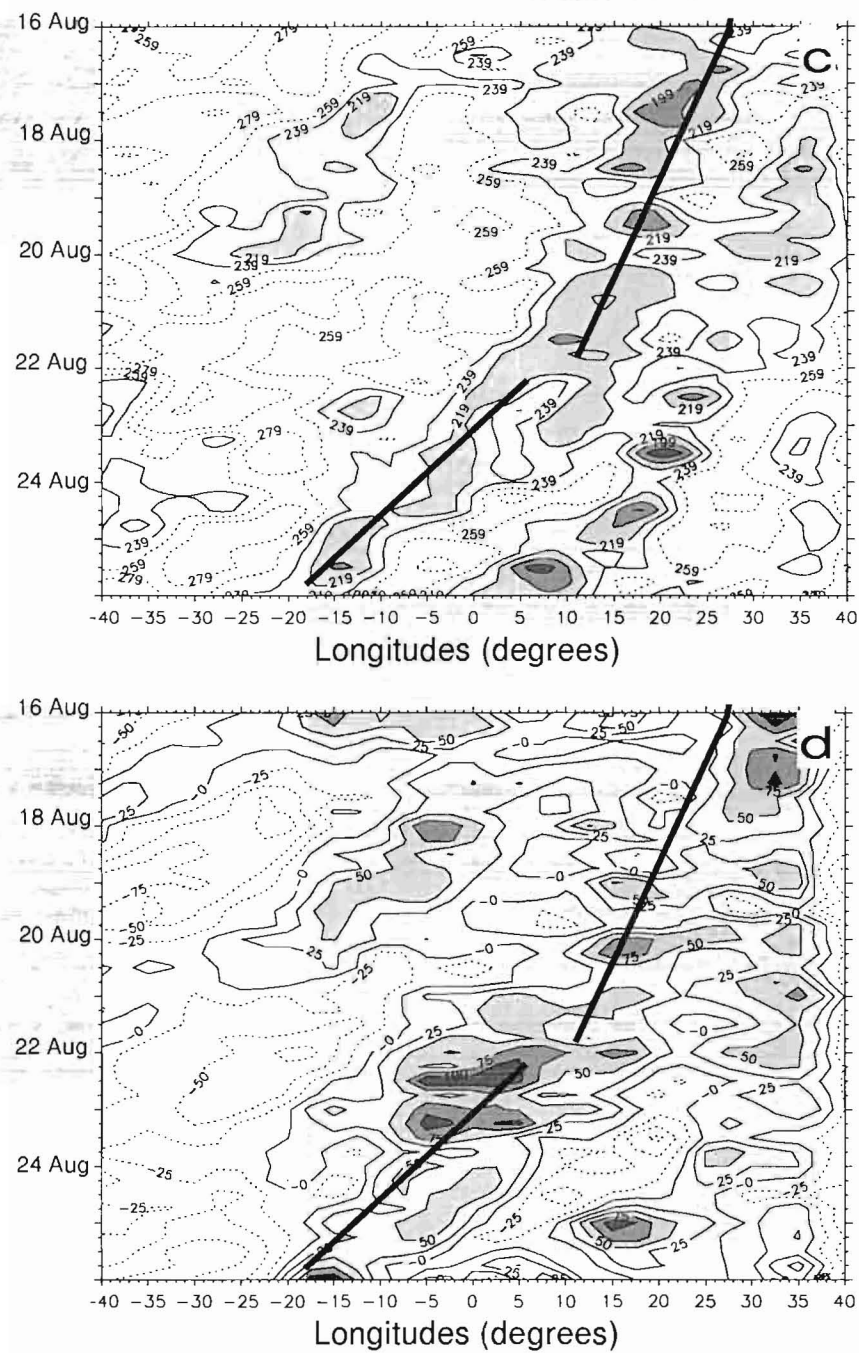


Figure 6. Continued.

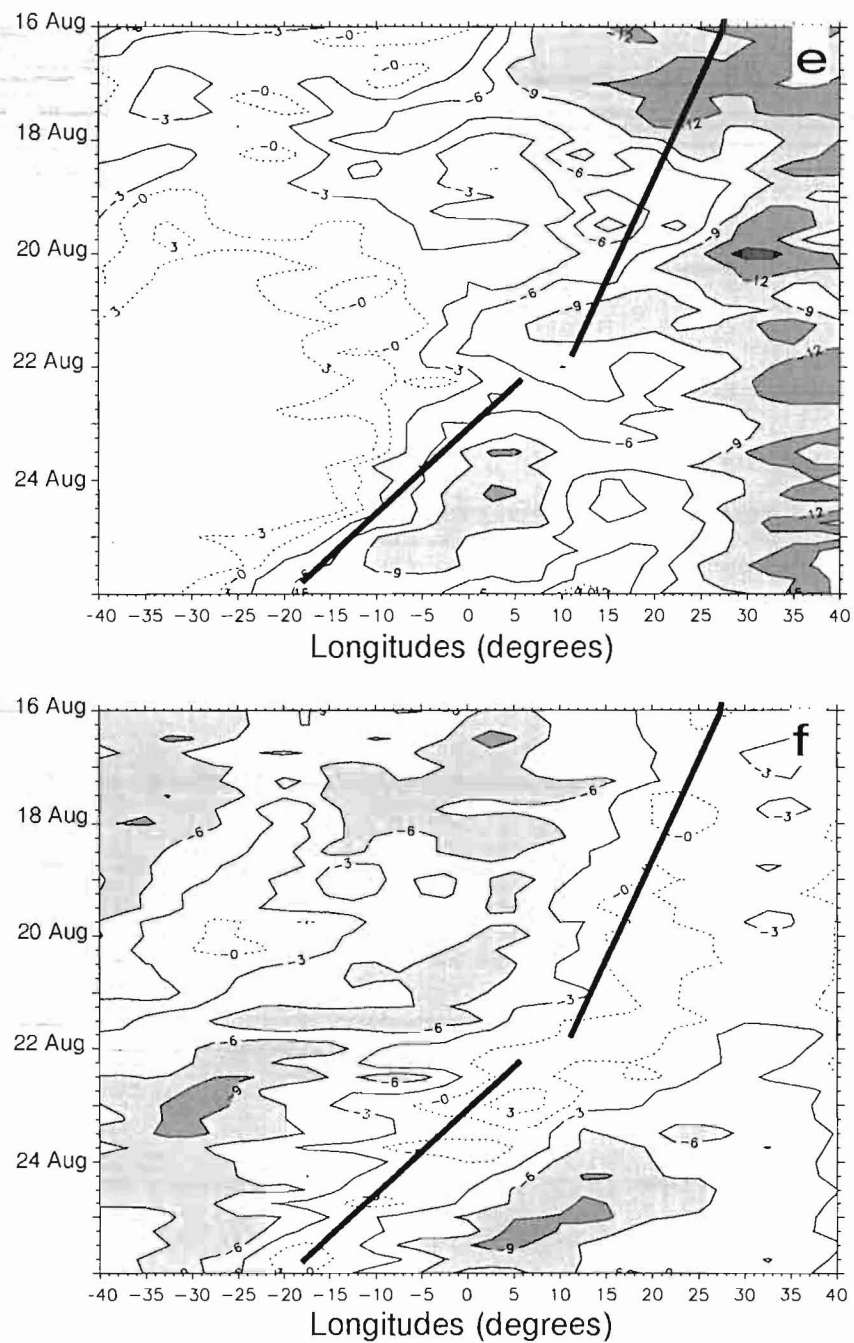


Figure 6. Continued.

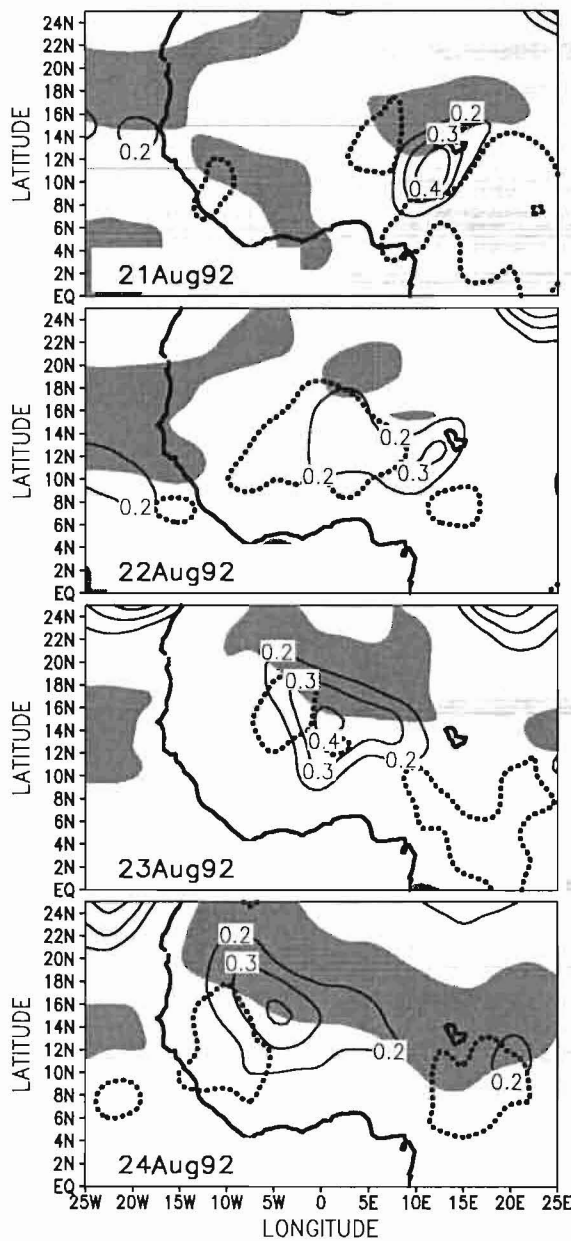


Figure 7. Horizontal cross-sections of potential vorticity (PV) at 700 hPa from the ECMWF re-analysis (isolines in PVU) at 00 UTC from 21 to 24 August 1992. The African easterly jet core (shaded regions for winds larger than 7 m s^{-1}) and outgoing long-wave radiation (heavy black isoline representing the 200 W m^{-2} contour) are superposed.

field. As previously viewed on the time-latitude diagram (Fig. 6(a)), the propagation of the trough accelerates after 21 August. As on 23 August this trough is located around 0°W and another trough (Fig. 6(a)) is found around $20\text{--}25^\circ\text{E}$; the wavelength of this disturbance can be estimated to be 2500–3000 km. The AEJ core located north of this instability area moves westward at the same velocity as the trough. Convection (OLR minima) is located ahead of the trough and has its maximum on 22 August. From the

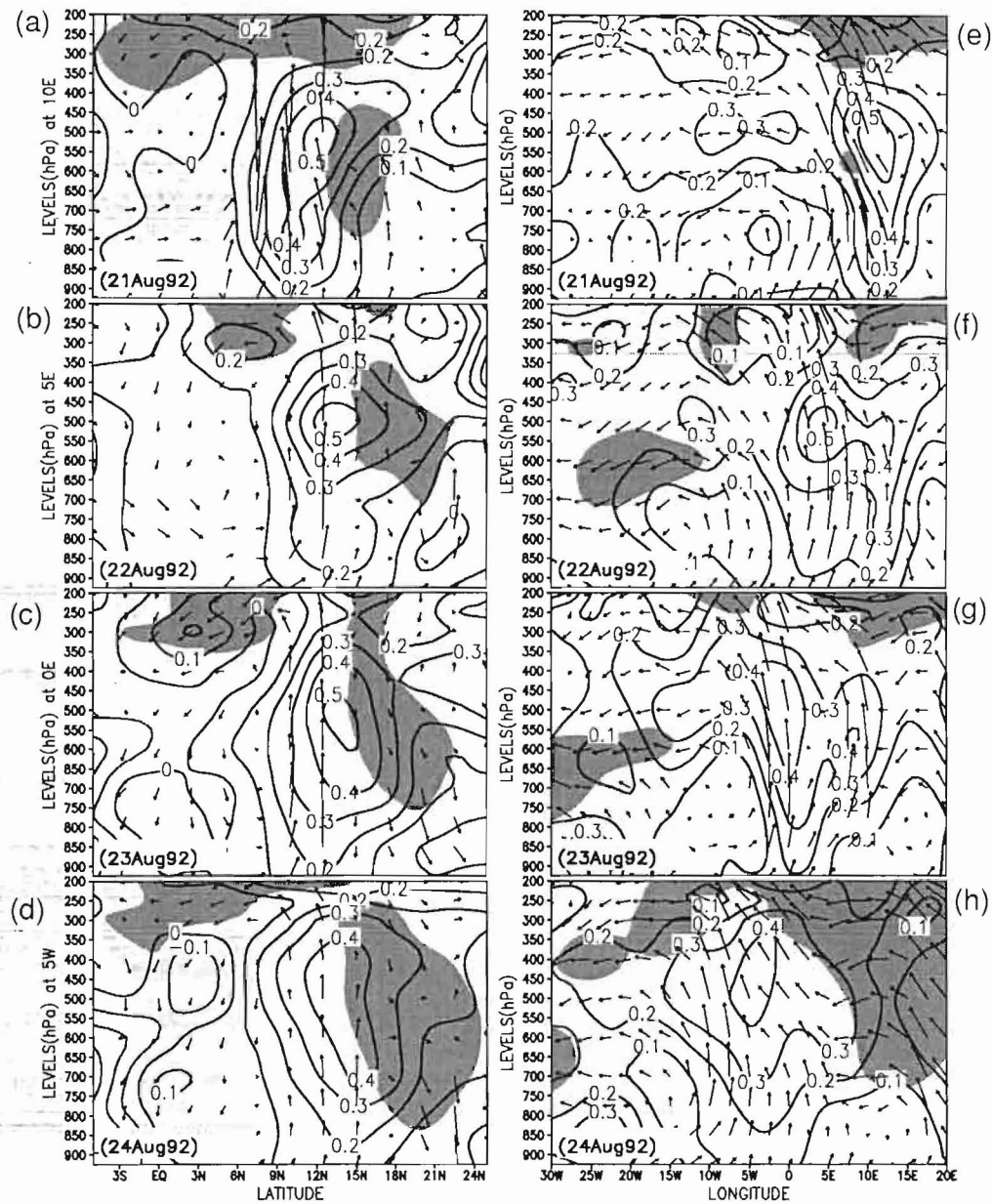


Figure 8. Vertical cross-section from the ECMWF re-analysis of airflow (arrows), potential vorticity (PV; isolines in PVU) and zonal wind maxima (shaded regions for winds below -10 m s^{-1}) at 00 UTC from 21 to 24 August 1992. Meridional plans along the PV core axis at: (a) 10°E on 21 August, (b) 5°E on 22 August, (c) 0° on 23 August, and (d) 5°W on 24 August, respectively. (e), (f), (g) and (h) show zonal plans at 12.5°N on 21, 22, 23 and 24 August, respectively.

description of these interactions between the disturbances in the wind field, the AEJ and the convection, it can be concluded that the present case-study corresponds to a 3–5-day easterly wave (Reed *et al.* 1977; Chen and Ogura 1982; Duvel 1990).

To go further with this synoptic-scale description, time sequences (21–24 August 1992) of vertical cross-sections of PV, zonal wind core and flow are now analysed

along the zonal and meridional directions (Fig. 8). The various fields exhibit very coherent structures throughout the time of interest. More noteworthy, the fields of the NCEP re-analysis exhibit similar structure and time evolution, which increases the confidence in the present analysis. The axis of the PV core (as determined from Fig. 7) is located around 15°N up to 300 hPa (Figs. 8(a) to (d)). The mid-level zonal winds have systematic maxima on the north side of this PV core, whereas the upper-level winds (TEJ) have maxima on the south side. If upward motion is found in the trough, the flow in the south is generally weak and mainly downward. From 21 to 22 August, the flow in the north is characterized by upward motion at low levels over the heat low. The trough is located in the northern sector of the wind disturbance as found in idealized numerical studies (e.g. Thorncroft and Hoskins 1994; Paradis *et al.* 1995). In the zonal plan view at 12.5°N (Fig. 8(e)) the area of maximum PV is located at 15°E on 21 August 1992, and extends from the surface to 300 hPa with a core around 500 hPa. Upward motions are found in and west of the trough, whereas the AEJ is generally weak in the trough region. This pattern moves westward and the core at 500 hPa reaches its maximum on 22 August (Fig. 8(f)). Ahead of this trough two areas of low PV are found, with minima around 300 and 800 hPa. The associated winds in the lower layers are weak in magnitude (22–23 August). The eastward orientation of the wind behind the trough (mainly visible in Fig. 8(h) for 24 August) and the associated vertical PV contour may contribute to the westward propagation of the disturbance (Thorncroft 1995; Thorncroft and Flocas 1997).

Examination of cross-sections (not shown) of the meridional and vertical components of the wind and the temperature over West Africa reveals two distinct areas of convection. The first area corresponds to the deep moist convection inside the ITCZ between 9 and 12°N ; the second one is located further north at 22°N , extending upwards to 600 hPa and characterizing the dry convection in the Saharan heat low, also corresponding to the confluence area of the monsoon flow with the dry north-easterly Harmattan wind. Outside of these convective areas motions are subsiding and the whole pattern describes the regional structure of a Hadley circulation (e.g. Thorncroft and Haile 1995). The meridional cross-sections of temperature (not shown) clearly depict the heat-low over West Africa from the surface to 700 hPa north of 15°N . This meridional northward temperature gradient is replaced above by a weaker southward gradient. This pattern is consistent with the existence of the AEJ with a core located at 600 hPa at the level of the gradient reversal. This jet is maintained by a direct circulation with warm rising air in the heat-low and cool air subsiding southward, leading to an easterly acceleration due to the conservation of angular momentum (Thorncroft and Blackburn 1999).

Focussing in time and space on the convective event studied in this paper, Fig. 9 shows four consecutive plots (at intervals of 6 hours, starting on 21 August at 12 UTC) of the wind and vorticity at 700 hPa (from the ERA) superimposed on the Meteosat brightness infrared (IR) temperature field. On 21 August at 12 UTC, the main feature of the cyclonic circulation is the positive maximum of vorticity centred at 11°N and 11°E . This cyclonic circulation is followed from the east by an anticyclonic circulation, the two centres being characteristic of the southern mode (referred to as SC in section 2) of an AEW as deduced from the RCEOFA. To the north of this vortex lies the AEJ with a wind speed of around 10 m s^{-1} . North of the AEJ and west of this main vortex, a secondary cyclonic circulation with a weaker amplitude is observed, and this characterizes the northern mode (NC) described in section 2. This secondary vortex corresponds to a dry air mass, as shown by the $6.3 \mu\text{m}$ water-vapour channel of Meteosat (not shown). This dry air intrusion originates from higher latitudes and could correspond to a stratospheric intrusion in the troposphere.

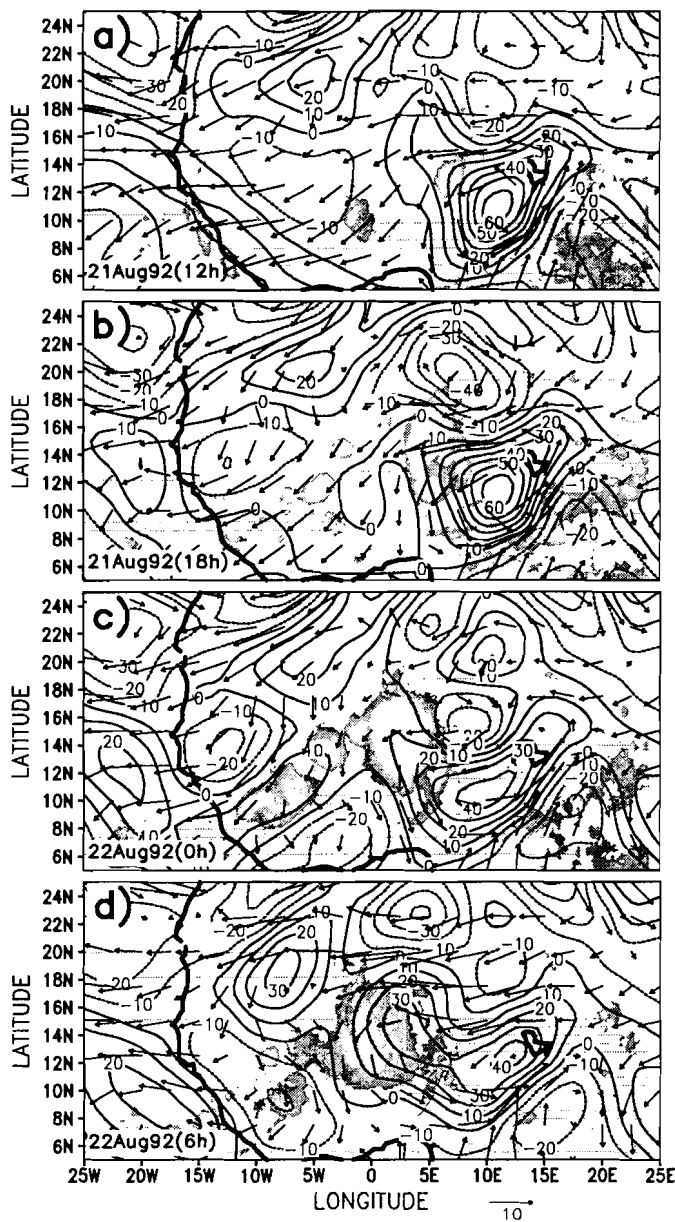


Figure 9. Horizontal cross-sections of wind and vorticity (PVU; isolines scaled by 10^{-6} s^{-1}) at 700 hPa for: (a) 21 August 1992 at 12 UTC, (b) 21 August 1992 at 18 UTC, (c) 22 August 1992 at 00 UTC, and (d) 22 August 1992 at 06 UTC. Infrared Meteosat temperatures are superposed (shaded $< 250 \text{ K}$).

Local convective maxima are observed in the north-west of the main vorticity maximum. At 18 UTC, the convective system has considerably broadened; its meridional and longitudinal extensions exceed 7 and 5° , respectively. At the same time an increase in the intensity of both vortices (NC and SC) is observed. We should be cautious with the interpretation of these vorticity features since the dataset is model dependent. Nevertheless, there is a westward propagation of both the AEW and the convective

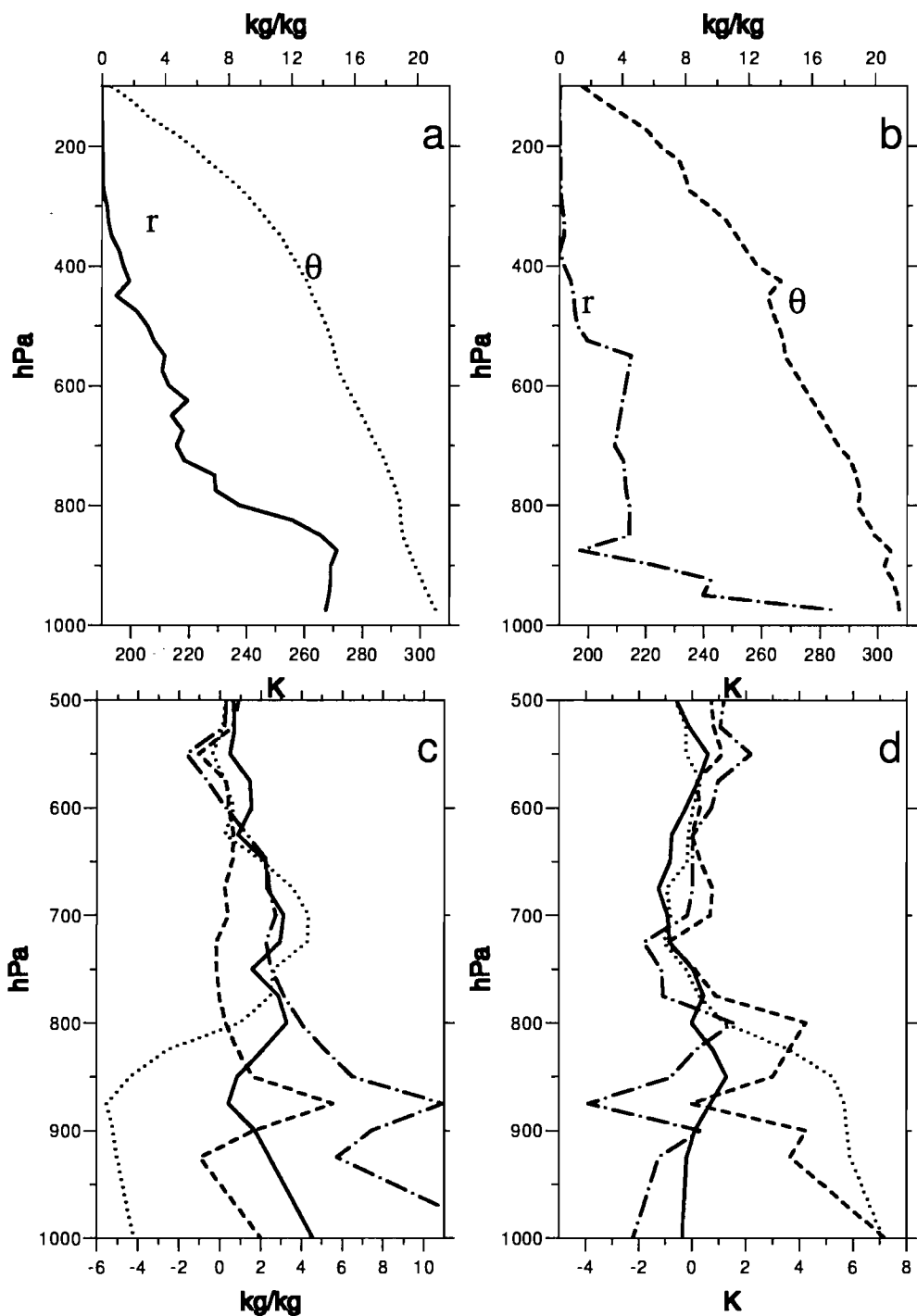


Figure 10. Comparisons of humidity mixing ratio (r) and potential temperature (θ) from observed soundings with ECMWF operational analysis (OPA) and the ECMWF re-analysis (ERA). Observed soundings: (a) for Niamey site (13.30°N , 2.22°E) at 17 UTC 21 August 1992 (HAPEX soundings), and (b) for Gao site (16.72°N , 3°W) at 12 UTC 21 August 1992. Differences OPA minus observations, and ERA minus observations for: (c) water-vapour mixing ratio, and (d) potential temperature; with solid lines for ERA at Niamey, dotted lines for OPA at Niamey, dashed-dotted lines for ERA at Gao, and dashed lines for OPA at Gao.

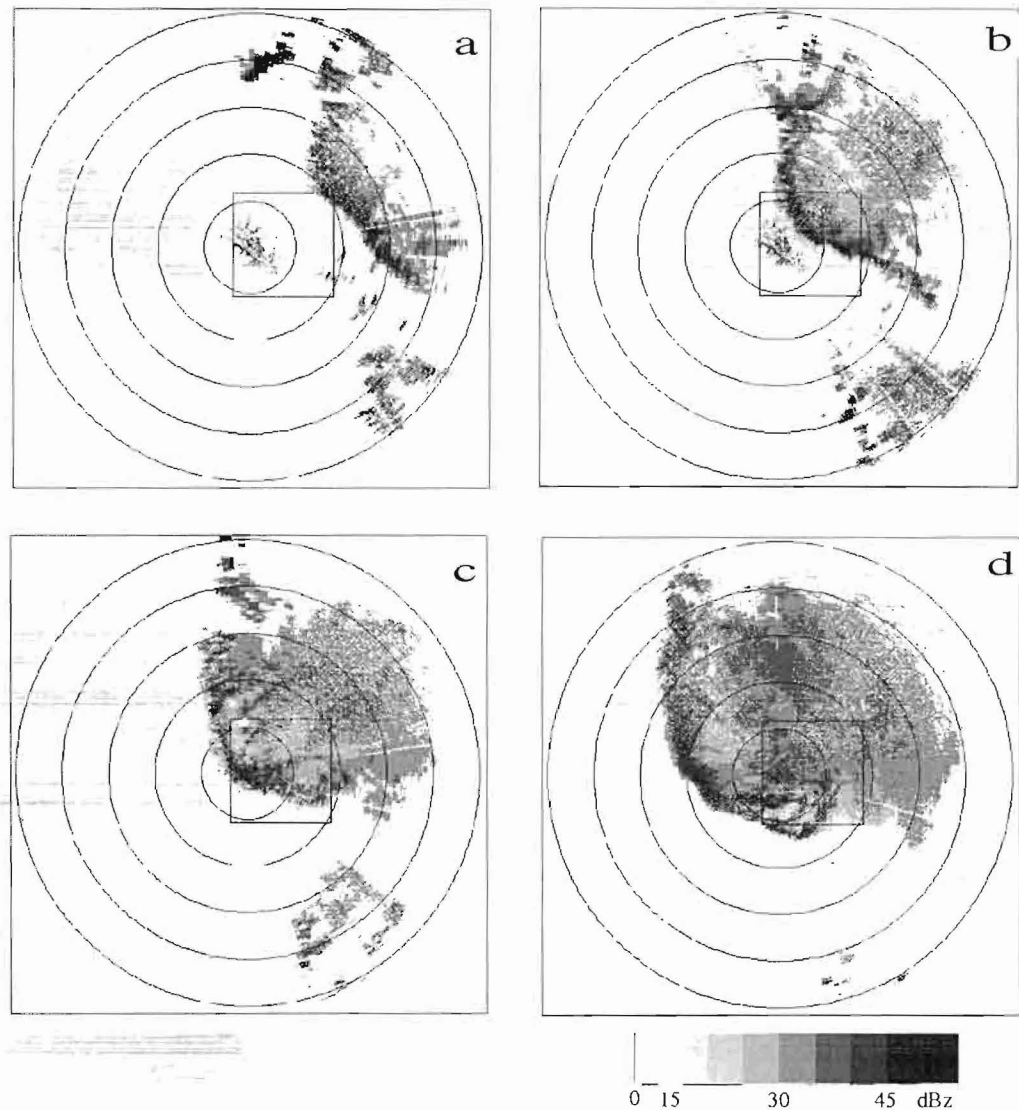


Figure 11. Radar PPIs on 21 August 1992 at: (a) 2030 UTC, (b) 2130 UTC, (c) 2230 UTC, and (d) 2400 UTC over a 250 km square. The square represents the HAPEX-SAHEL network (see Fig. 12).

system, the phase speed of the former being about a quarter of the phase speed of the latter. On 22 August at 00 UTC, the convective system is still in its mature stage and the intensity of the AEW weakens. The main cyclonic part of the NC (20°N , 7°W) tends to extend southward and intensify. This evolution is confirmed at 06 UTC (Fig. 9(d)), as the NC is overcoming the SC which is still decaying, with the convective system as a whole starting to decay. From Meteosat images, the convective system seems to decay around 03 UTC on 22 August. Along with the evolution of the vorticity and brightness temperature fields, it is worthy of notice that the AEJ is always located behind the convective system and that it is shifting a little northward. This pattern is consistent with analyses of previous diagnoses (Figs. 5 and 6).

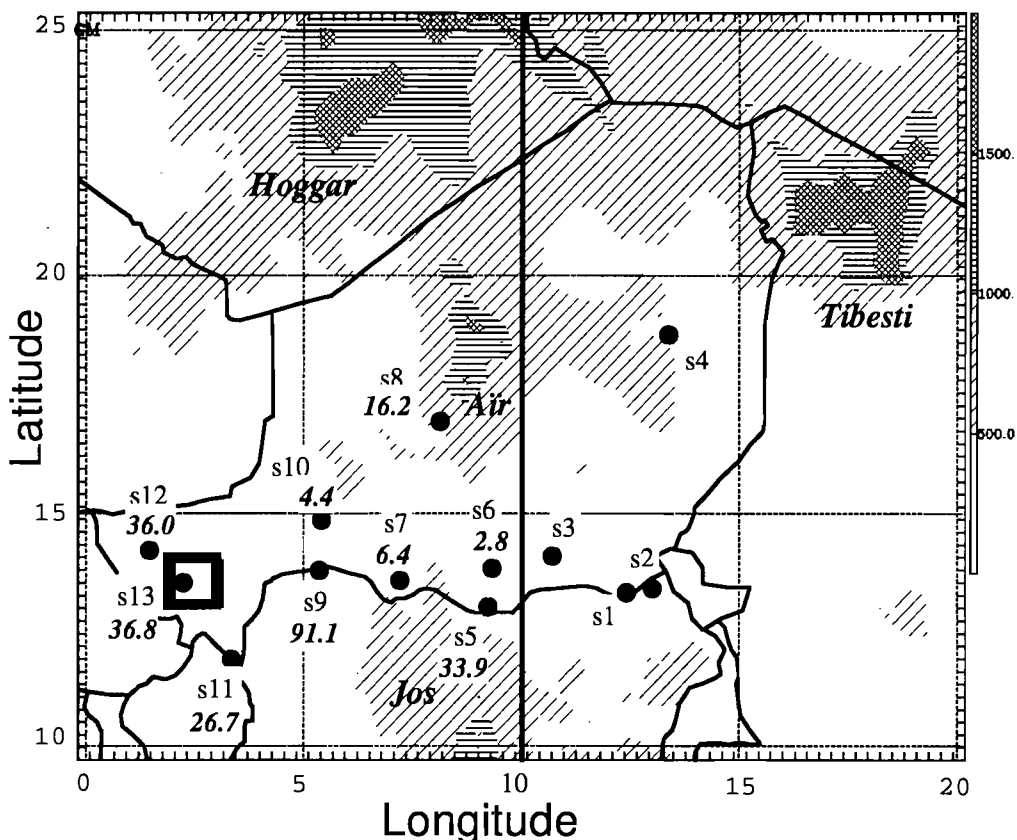


Figure 12. Map showing the location of ground stations over Niger and 24 h accumulated precipitation (mm), with orography superposed. (Below 500 m is white; 500–1000 m slanting lines; 1000–1500 m horizontal lines; above 1500 m crossed lines.) The location of the HAPEX-SAHEL field experiment is indicated by a square ('S' numbers correspond to the observation network; S13 refers to the operational ground station located at Niamey airport).

The ECMWF operational analysis and the ERA have been compared and evaluated against observations from synoptic ground stations, HAPEX-SAHEL soundings and other soundings over West Africa available on the ECMWF database of observations. Large-scale features like the monsoon flux, the AEW and the associated AEJ are represented by both analyses, but the monsoon flux penetrates farther over the continent in the ERA than in operational analysis. The main differences between the two analyses concern the vertical structure of lower levels including the boundary layer. Illustrating these differences, Fig. 10 shows two radio-soundings representing two contrasting regions, namely around 13 and 17°N. The fields in the boundary layer as given by the operational analysis are much too dry and too warm over the Sahel. The improvements in the soil water representation and initialization introduced after 1992 (Viterbo and Beljaars 1995; Mahfouf and Viterbo 1998) seem to be the main reason for the better overall structure of the boundary layer in the ERA. The profile of temperature and the surface humidity are thus clearly improved. Nevertheless, the ERA overestimates the humidity in the full troposphere in both regions but especially in the Sahelian region.

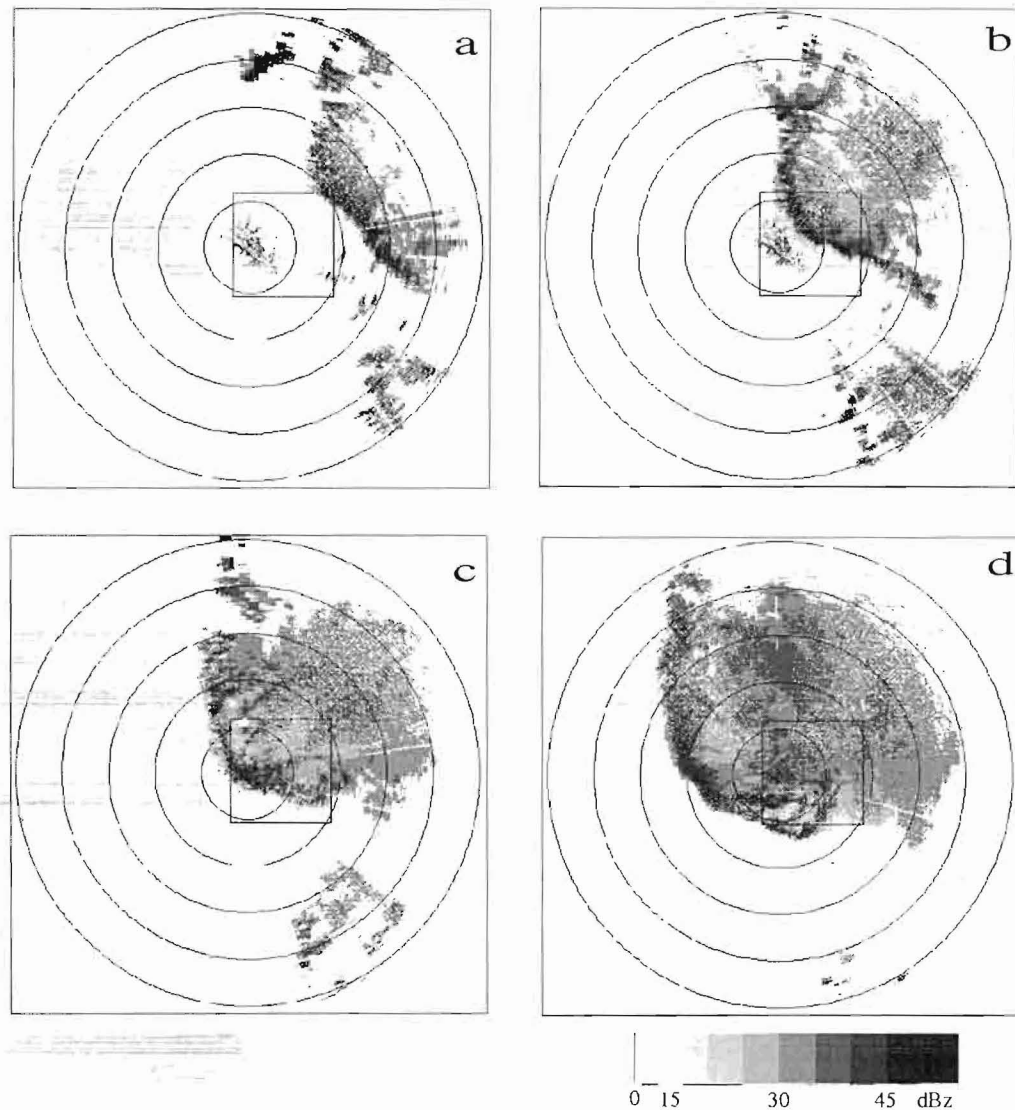


Figure 11. Radar PPIs on 21 August 1992 at: (a) 2030 UTC, (b) 2130 UTC, (c) 2230 UTC, and (d) 2400 UTC over a 250 km square. The square represents the HAPEX-SAHEL network (see Fig. 12).

system, the phase speed of the former being about a quarter of the phase speed of the latter. On 22 August at 00 UTC, the convective system is still in its mature stage and the intensity of the AEW weakens. The main cyclonic part of the NC (20°N , 7°W) tends to extend southward and intensify. This evolution is confirmed at 06 UTC (Fig. 9(d)), as the NC is overcoming the SC which is still decaying, with the convective system as a whole starting to decay. From Meteosat images, the convective system seems to decay around 03 UTC on 22 August. Along with the evolution of the vorticity and brightness temperature fields, it is worthy of notice that the AEJ is always located behind the convective system and that it is shifting a little northward. This pattern is consistent with analyses of previous diagnoses (Figs. 5 and 6).

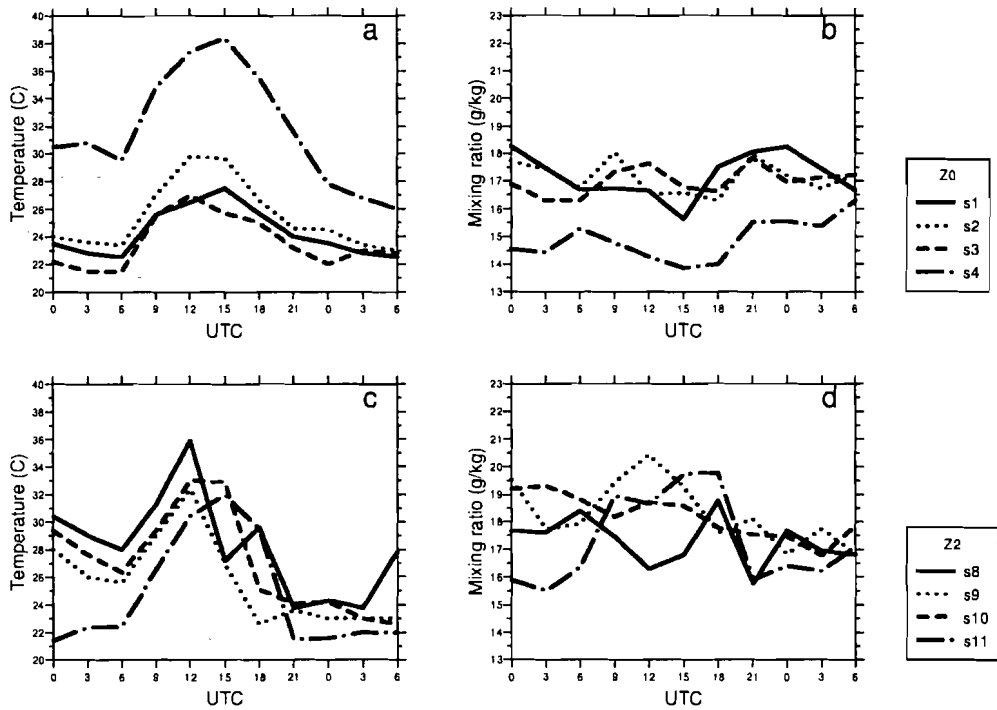


Figure 13. Time series at $z = 2$ m from ground stations over Niger of: (a) temperature for undisturbed regions (stations s1, s2, s3 and s4); (b) as (a) but for humidity mixing ratio; (c) temperature for disturbed regions (stations s8, s9, s10 and s11); (d) as (c) but for mixing ratio. See Fig. 12 for location of stations.

4. CONVECTIVE-SYSTEM SCALE

(a) Life cycle

The convective activity associated with the AEW described in the previous section is in fact originally composed of two elements. The first event, of weak intensity, is triggered in the early morning (06 UTC, i.e. 0700 hours local time) just to the north of Jos Plateau (10° E, 13° N); it develops westward and produces a mean amount of 14 mm of rain per station. The second event is generated near midday (11 UTC) over the Air mountains area (9° E, north of 16° N; Fig. 9). Convective cells propagate down the slopes of the mountains and are quickly structured into a squall line moving southwestward with strong intensity. The lifetime of the whole system is about 24 hours with a speed of propagation of 15 m s^{-1} . Several studies have pointed out that squall lines often form over these two mountain regions (e.g. Rowell and Milford 1993; Laing and Fritsch 2000). Detailed structure of the leading convective region can be seen from the 250 km range radar plan position indicator (PPI) scans conducted in the HAPEX-SAHEL area (Fig. 11). The largest reflectivity values are not continuous but are localized within 10 km size convective cells in the along-line direction, as described in numerous papers based on radar observations of such systems (e.g. Houze 1977; Chalon *et al.* 1988). Behind the leading edge, a trailing stratiform region with less precipitation is identified on the 2230 UTC radar scan. Comparison of brightness temperatures from the IR channel of Meteosat and the 85.5 GHz microwave channel of the Special Sensor Microwave/Imager available at 17 UTC (not shown) supports this description of the convective system, and allows us to identify a forward anvil in front of the convective

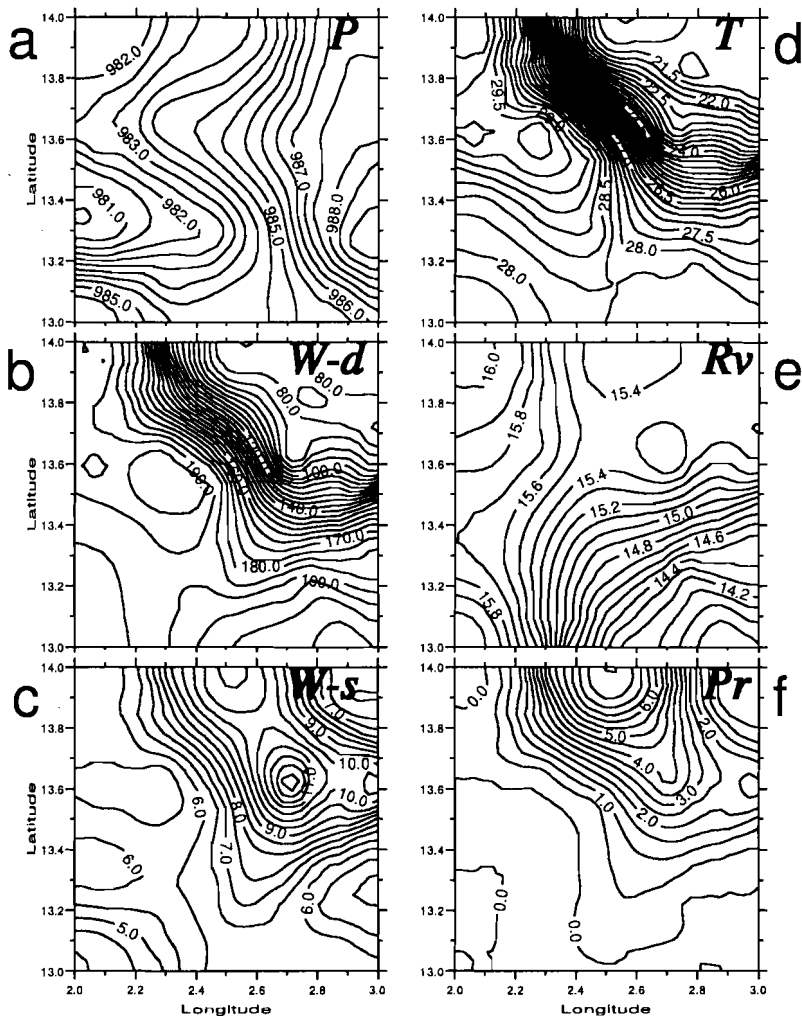


Figure 14. Horizontal fields of: (a) pressure (interval 0.5 hPa), (b) wind direction (interval 5 degrees), (c) wind speed (interval 0.5 m s⁻¹), (d) temperature (interval 0.25 degC), (e) humidity mixing ratio (interval 1 g kg⁻¹), and (f) precipitation (interval 1 mm) accumulated over 10-minute intervals, as observed by HAPEX-SAHEL ground stations at 2130 UTC 21 August 1992.

band. These forward clouds are due to the TEJ present at around 200 hPa. This is a common feature of squall lines observed over West Africa (e.g. Chong *et al.* 1987; Chalon *et al.* 1988).

(b) Surface

To complete the description of the squall line, it is important to determine its effect on the atmospheric parameters. In addition to the data from the network implemented for the HAPEX-SAHEL experiment, surface measurements from 13 ground stations over the Niger were also obtained. The precipitation accumulated over the 24 h corresponding to the lifetime of the squall line is given on Fig. 12. The squall line passed over stations S8, S10, S11, S12 and S13 (see numbering of the stations on Fig. 12) and gave rainfall

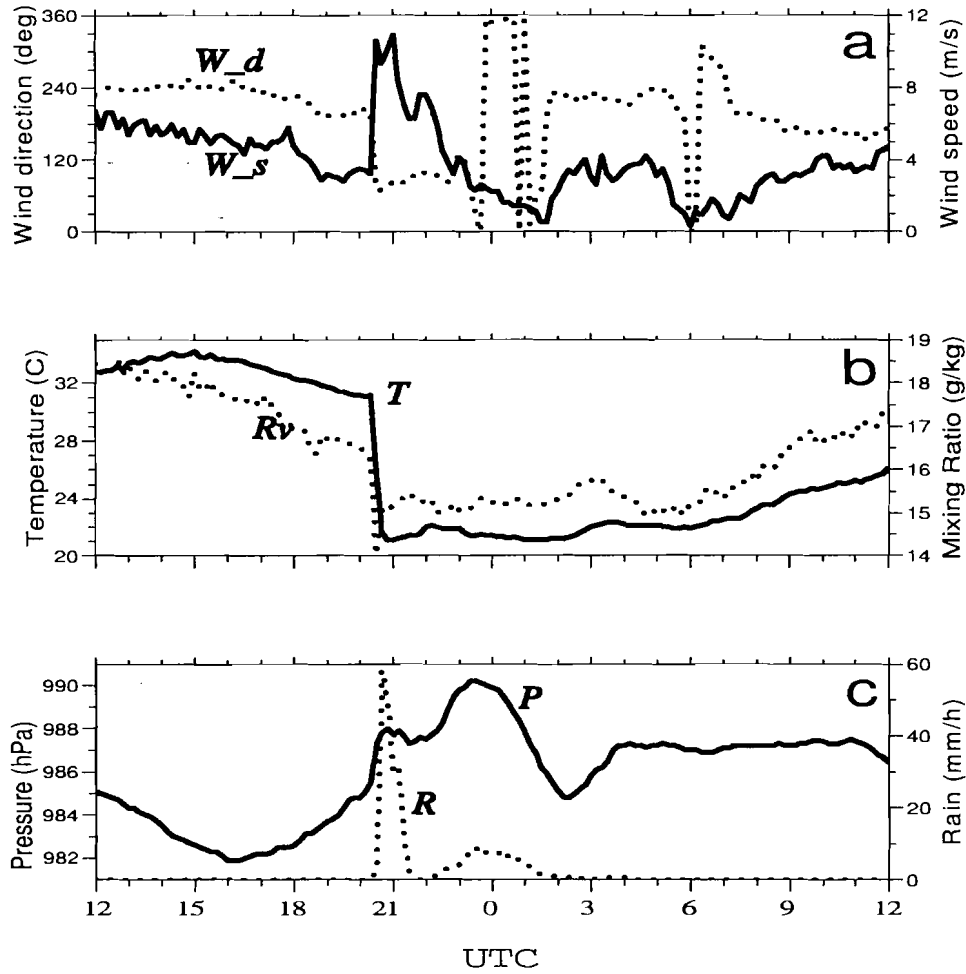


Figure 15. Time series from 21 August 12 UTC to 22 August 12 UTC for a HAPEX-SAHEL ground station at 2.8°E, 13.86°N: (a) wind speed and direction, (b) temperature and humidity mixing ratio, and (c) pressure and precipitation. Precipitation totals were measured over 10-minute intervals.

ranging from 4.4 (S10) to 36.8 mm (S13). Station S9 shows a larger value (91.1 mm) corresponding to the effect of the two convective systems as described above. To show the effect of the squall line at the surface, Fig. 13 compares the time evolution of temperature and moisture fields for disturbed and undisturbed regions. In undisturbed regions (Figs. 13(a) and (b)), the diurnal cycle of temperature is large and increases northward from 6 degC at 13°N to 12 degC at 18°N. The north-south gradient of temperature (≈ 6 K/1000 km) and moisture (≈ -1.5 g g $^{-1}$ /1000 km) can be roughly estimated in comparing station S4 (around 19°N) with stations S1, S2 and S3 (located between 13 and 14°N). The stations in the disturbed region (Figs. 13(c) and (d)) show high values of temperature and moisture (up to 36 K and 20×10^{-3} g g $^{-1}$ before the passage of the squall line). Strong modifications of the diurnal cycle due to the passage of the squall line are observed at these stations. Sharp temperature and moisture drops are observed of up to 10 K and 4×10^{-3} g g $^{-1}$, and their timing is coherent with the

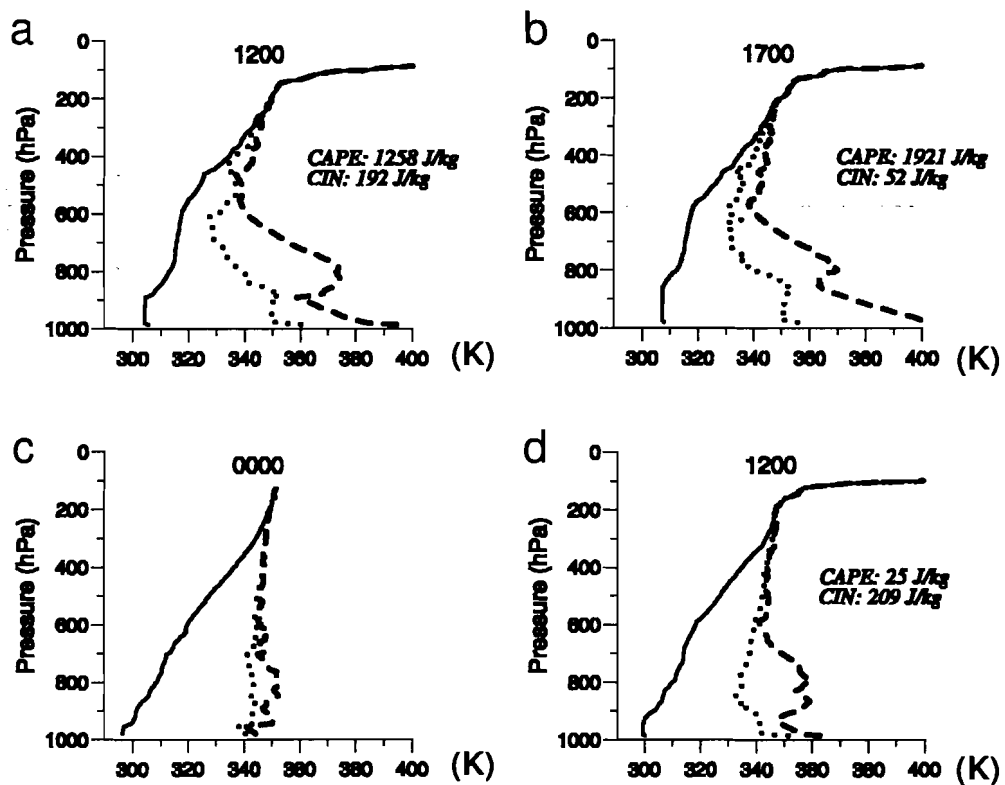


Figure 16. Vertical profiles of potential temperature, θ (continuous line), equivalent potential temperature, θ_e (dotted line), and saturation equivalent potential temperature, θ_{es} (dashed line) at Niamey: before the squall line passage on 21 August 1992 at (a) 12 UTC, and (b) 17 UTC; (c) in the stratiform region of the squall line on 22 August 1992 at 00 UTC, and (d) behind the squall line on 22 August at 12 UTC. CAPE and CIN values (see text) are indicated for a parcel following the pseudo-adiabat starting at the first level.

southward propagation of the squall line. Again ground stations located to the north (e.g. S8) show warmer and drier air than those further south.

(c) Observations over the HAPEX-SAHEL area

As seen in Fig. 11(b), the squall line at 2130 UTC occupies the upper-right quarter of the main experimental box (degree square). For this reason, the surface parameters measured by the network of 12 ground stations have been interpolated to this time (Fig. 14). Before the arrival of the squall line, the air is characterized by the warm and moist south-westerly monsoon flow. An intriguing feature is the relatively dry air located in the south-eastern part of the domain. Looking at the same field for an earlier time, this dry air seems to be progressively advected from the south, whereas no similar signature exists in other fields. The passage of the squall line leads to the sequence of: pressure rise (5 hPa), wind shift and surge, temperature drop (8 K), weak humidity drop, and rainfall (maximum of 125 mm h^{-1}). The present convective system is the largest contributor of all the systems passing in August 1992 over the HAPEX region, accounting for 20% of the total rainfall (Taupin *et al.* 1993). The time evolution of the surface parameters as shown for one station (Fig. 15) emphasizes the surface signature induced by the gust front associated with the leading convective edge. This is also observed for other African squall lines (Chong *et al.* 1987; Chalon *et al.* 1988; Redelsperger and Lafore 1988).

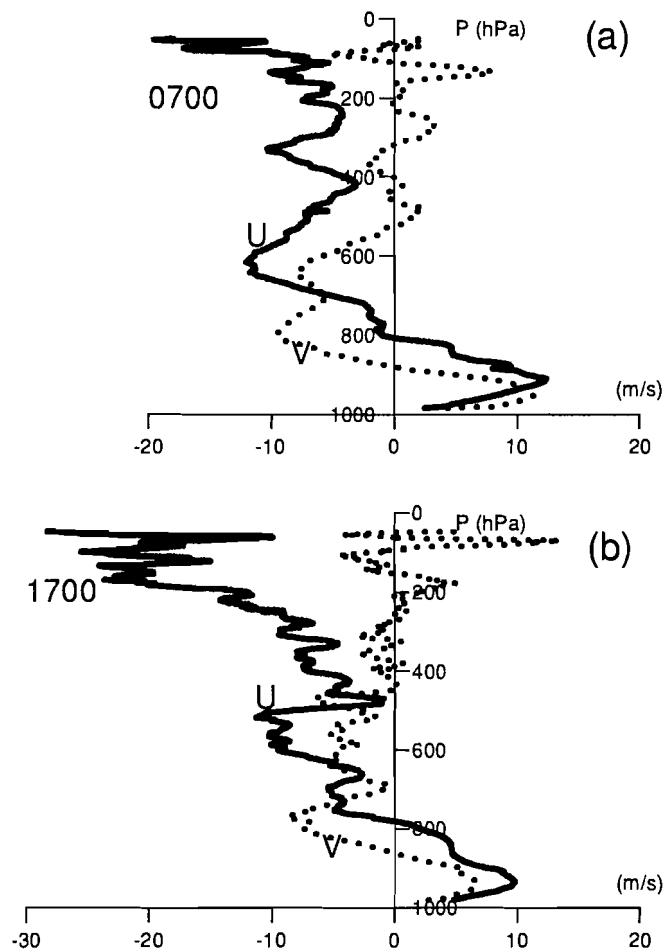


Figure 17. Profiles of zonal (continuous line) and meridional (dotted line) wind components at Niamey on 21 August 1992 at (a) 07 UTC, and (b) 17 UTC.

Four soundings in terms of potential temperature θ , equivalent potential temperature θ_e , and saturation equivalent potential temperature θ_{es} are presented in Fig. 16. The soundings before the passage of the convective system (Figs. 16(a) and (b)) show strong conditional instability with a CAPE (convective available potential energy) of 1258 and 1921 J kg^{-1} at 12 and 17 UTC, respectively (assuming pseudo-adiabatic motion). Large values of CIN (convective inhibition) of 192 and 52 J kg^{-1} were also observed at 12 and 17 UTC, respectively. The CIN results from strong subsidence of the 600–900 hPa layer maintaining a strong inversion. With a CIN of about 50 J kg^{-1} , vertical motions of about 10 m s^{-1} are necessary to trigger convection. Thus, even with large-scale convergence, isolated deep convection is not able to develop locally. In contrast, the density current associated with the squall line provides sufficient lifting energy to overcome the CIN barrier. The inversion existing before the passage of the squall line, thus contributes to the increase of the moist static energy stored in the boundary layer. It is noteworthy that the CIN barrier is quickly rebuilt after the passage of the squall line (Fig. 16(d)) due to the existence of large-scale mid-tropospheric subsidence. Ahead of the squall line, high values of static humidity energy (θ_e) at low levels correspond to the monsoon flow,

whereas at mid-levels the air is relatively cold and dry leading to a minimum of θ_e . This dry layer is characteristic of the pre-environmental atmosphere of squall lines (Barnes and Sieckman 1984). It also corresponds to the altitude of the AEJ and has fundamental importance in terms of convective downdraughts (Zipser 1977; Redelsperger and Lafore 1988). These downdraughts themselves feed the current density of the squall line. Confirming this fact, the minimum of the θ_e profile corresponds roughly to the value observed by the ground station just after the passage of the leading convective edge (Fig. 15). By 00 UTC on 22 Aug 92 (Fig. 16(c)), the rear part of the stratiform region being still over the site (Fig. 9(c)), the atmosphere has been cooled below 700 hPa and warmed and moistened above. Above 600 hPa the air is saturated, indicating the presence of the trailing stratiform anvil. Below, the profiles are consistent with the presence of unsaturated mesoscale downward motion as observed in the stratiform region of squall lines (e.g. Zipser 1977). After the passage of the squall line the atmosphere is strongly stabilized (Fig. 16(d)). The diamond shape between the θ_e and θ_{es} curves is characteristic of subsiding air.

Figure 17 shows that the wind profile also shows typical pre-environmental characteristics of African squall lines (e.g. Bolton 1984): a south-westerly monsoon flow at low levels, the AEJ around 600 hPa, and the TEJ around 100–200 hPa. The only positive values of the westerly component correspond to the monsoon flow. As the observed squall line propagation is 15 m s^{-1} westward, the air is always inflowing to the system except in the TEJ region.

5. CONCLUSION

A key aspect of the WAM is the precipitating weather systems associated with synoptic-scale easterly waves. Both phenomena are relatively well understood when studied separately, whereas the knowledge of their interactions is still very limited. The understanding of African weather systems and their representation in GCMs requires an integrated approach, which involves considering a whole range of phenomena at different scales and their interactions. As a first step this paper has described a reference case of a Sahelian weather system from a seasonal and interannual viewpoint, as well as from a synoptic and convective system viewpoint.

The year 1992 is representative of the 1979–93 climatology. At intraseasonal scale, the monsoon onset is characterized by an abrupt shift of precipitation from the $5\text{--}10^\circ\text{N}$ band to $10\text{--}15^\circ\text{N}$ around 20 June. During this period, the AEJ maximum at around 700 hPa is located along the northern flank of the area of maximum convection and follows the latitudinal migration of rainfall. The convective activity occurs in an apparent zonal break of the TEJ. The resulting main ascent is thus located between the upper-level relative outflow and inflow on its east and west sides, respectively. This relationship between convection and the upper-level jets occurs on monthly as well as daily time-scales. These similarities with midlatitude cases need to be studied thoroughly for tropical regions. For the present case-study, the AEJ appears to weaken in the region of the wave and convection, but these results are taken from a model analysis with only few available observational data. The behaviour of the AEJ should be the main result of explicitly resolved barotropic and baroclinic instabilities leading to AEW development and the momentum transport induced by the convective system as parametrized in the model. Field data and numerical experiments are necessary to investigate this issue.

The month of August 1992 is a very active period in terms of synoptic activity. The vorticity fields are characterized by northerly (dry) and southerly (wet) components located at 850 hPa on each side of the AEJ. The activity peaks in August for both

components and decays at the end of September. Their intraseasonal modulation over periods of 20 to 40 days lead to active and break phases of synoptic activity. The dates of these break phases can be determined by considering the days for which the two components present a minimum. This result, with possible forecast implications, needs to be confirmed using complementary approaches.

The SC (NC) tends to have a large (small) amplitude before the major convective event occurring on 21 August, while the reverse applies after this event. Both the water-vapour channel of Meteosat and the ERA show that the northerly vortex corresponds to a dry-air intrusion and seems to originate from higher latitudes. All these features need to be explored more thoroughly with other case-studies, and illustrate the interactions between the synoptic and convective scales.

Around 21 August, the 700 hPa vorticity field featured the propagation of a typical easterly wave, with the westward propagation of cyclonic circulation followed by an anticyclonic circulation. Consistent with the Charney-Stern (1962) theorem, the AEJ core is located in the area of negative meridional gradient of PV with the associated instability found only south of this jet. The PV field shows westward propagation of the trough located in the northern sector of the wind disturbance as found in idealized numerical studies.

Convective activity occurred mainly ahead of the 700 hPa vorticity maximum. A typical squall line formed on 21 August over the Ajr mountains and propagated south-westward at 15 m s^{-1} , whereas previous convective elements existing for several days propagated at 8.7 m s^{-1} . At the beginning of the period, the vorticity maximum propagated with a phase speed of 4 m s^{-1} , whereas after the squall line development the phase speed doubled (8.7 m s^{-1}). In both periods the convective system moved about twice as fast as the vortex core. The OLR extracted from the ERA was located behind the observed one and remained in phase with the vorticity field. These differences between observations and analysis can represent a major issue from the modelling perspective. Indeed, the differences in location and speed between the diabatic heating and the vortex have crucial consequences in term of dynamics. This relates to the difficult problem of convection parametrization in GCMs, a key point for forecast and climate modelling.

The squall line was the largest contributor to the systems passing over the HAPEX region during August 1992. It was composed of a convective part with intensely precipitating 10 km-size cells in the along-line direction, and a trailing stratiform section. The passage of the squall line led to a sequence of pressure rise, wind shift and surge, temperature drop, weak moisture drop and rainfall. Strong conditional instability, but also strong CIN, existed before the passage of the convective system. Thus, even with the presence of large-scale convergence, isolated deep convection is not able to develop locally. In contrast, the density current associated with the squall line provides sufficient lifting energy to overcome the CIN barrier. This barrier is quickly rebuilt after the squall line passage due to the existence of large-scale mid-tropospheric subsidence, whereas the free troposphere is strongly stabilized. The wind profile exhibits typical environmental characteristics preceding African squall lines: a south-westerly monsoon flow at low levels feeding the system, the AEJ and the TEJ. The air is always flowing into the system except in the TEJ layer.

The present paper has shown that, as for all monsoon systems, the WAM involves many interacting scales and physical processes as summarized in Fig. 1. This case-study of a weather system representative of the WAM, serves, hopefully, as a first reference case for a multi-scale numerical approach thanks to the use of a hierarchy of models (from cloud-resolving to climate models). It is important to note that the interactions

between the convective and synoptic scales occurring in this region are rather well-defined and believed to typify the interactions occurring in the tropics. Improvements in our understanding, and of their representation in GCMs should be beneficial to all tropical atmospheric research.

ACKNOWLEDGEMENTS

This research was in part supported by the EC Environment and Climate Research Programme (contract ENV4-CT97-0500). We would like to express our gratitude to Chris Thorncroft who led the West African Monsoon Project (WAMP). We are indebted to Steve Wright and Thierry Lebel for their comments on an earlier version of paper. We wish also to thank Jean-Paul Goutorbe and Pierre Bessemoulin who provided us the surface data from the HAPEX-SAHEL experiment and the operational ground stations over Niger, respectively.

REFERENCES

- | | | |
|--|------|--|
| Barnes, G. M. and Sieckman, K. | 1984 | The environment of fast- and slow-moving tropical mesoscale convective cloud lines. <i>Mon. Weather Rev.</i> , 112 , 1782–1794 |
| Betts, A. K. | 1974 | The scientific basis and objectives of the US convection subprogram for GATE. <i>Bull. Am. Meteorol. Soc.</i> , 55 , 304–313 |
| Bolton, D. | 1984 | Generation and propagation of African squall lines. <i>Q. J. R. Meteorol. Soc.</i> , 110 , 695–721 |
| Burpee, R. W. | 1972 | The origin and structure of easterly waves in the lower troposphere of North Africa. <i>J. Atmos. Sci.</i> , 29 , 77–90 |
| | 1974 | Characteristics of north African easterly waves during the summers of 1968 and 1969. <i>J. Atmos. Sci.</i> , 31 , 1556–1570 |
| Cammas, J. P., Pouponneau, B., Desroziers, G., Santurette, P., Joly, A., Arbogast, P., Mallet, I., Caniaux, G. and Mascart, P. | 1999 | FASTEX IOP17 cyclone: Introductory synoptic study with field data. <i>Q. J. R. Meteorol. Soc.</i> , 125 , 3393–3414 |
| Ceron, J. P. and Gueremy, J. F. | 1999 | Validation of the space-time variability of African easterly waves simulated by the CNRM GCM. <i>J. Climate</i> , 12 , 2831–2855 |
| Chalon, J. P., Jaubert, G., Roux, F. and Lafore, J. P. | 1988 | The west African squall line observed on 23 June during COPT81: Mesoscale structure and transports. <i>J. Atmos. Sci.</i> , 45 , 2744–2763 |
| Charney, J. G. and Stern, M. E. | 1962 | On the stability of internal baroclinic jets in a rotating atmosphere. <i>J. Atmos. Sci.</i> , 19 , 159–172 |
| Chen, Y.-L. and Ogura, Y. | 1982 | Modulation of convective activity by large scale flow patterns observed in GATE. <i>J. Atmos. Sci.</i> , 39 , 1260–1279 |
| Cho, H. R. and Jenkins, M. A. | 1987 | The thermal structure of tropical easterly waves. <i>J. Atmos. Sci.</i> , 44 , 2531–2539 |
| Chong, M., Amayenc, P., Scialom, G. and Testud, J. | 1987 | A tropical squall line observed during the COPT81 experiment in West Africa. Part I: Kinematic structure inferred from dual-doppler radar data. <i>Mon. Weather Rev.</i> , 115 , 670–694 |
| Desbois, M., Kayiranga, T., Gnamien, B., Guessous, S. and Picon, L. | 1988 | Characterization of some elements of the Sahelian climate and their interannual variations for July 1983, 1984 and 1985 from the analysis of METEOSAT ISCCP data. <i>J. Climate</i> , 1 , 867–904 |
| Diedhiou, A., Janicot, S., Viltard, A., de Felice, P. and Laurent, H. | 1999 | Easterly wave regimes and associated convection over West Africa and the tropical Atlantic: Results from NCEP/NCAR and ECMWF reanalyses. <i>Clim. Dyn.</i> , 15 , 795–822 |
| Duvel, J. P. | 1990 | Convection over tropical Africa and the Atlantic Ocean during northern summer. Part II: Modulation by easterly waves. <i>Mon. Weather Rev.</i> , 118 , 1855–1868 |

- Goutorbe, J. P., Lebel, T., Tinga, A., Bessemoulin, P., Brouwer, J., Dolman, H., Engman, T., Gash, J. H. C., Hoepffner, M., Kabat, P., Kerr, Y. H., Monteny, B., Prince, S., Said, F., Sellers, P. and Wallace, J.
- Houze, R. A. 1977 Structure and dynamics of a tropical squall line system observed during GATE. *Mon. Weather Rev.*, **105**, 1540–1567
- Hulme, M. 1992 Rainfall changes in Africa: 1931–1960 to 1961–1990. *Int. J. Climatol.*, **12**, 685–699
- Lafore, J.-P., Redelsperger, J.-L. and Jaubert, G. 1988 Comparison between a three-dimensional simulation and Doppler radar data of a tropical squall line: transport of mass, momentum, heat and moisture. *J. Atmos. Sci.*, **45**, 3483–3500
- Laing, A. G. and Fritsch, J. M. 2000 The large-scale environments of the global populations of meso-scale convective complexes. *Mon. Weather Rev.*, **128**, 2756–2776
- Le Barbé, L. and Lebel, T. 1997 Rainfall climatology of the HAPEX-Sahel region during the years 1950–1990. *J. Hydrol.*, **188–189**, 1–4, 43–73
- Le Barbé, L., Lebel, T. and Tapsoa, D. 2002 Rainfall variability in West Africa: A hydrological perspective. *J. Climate*, in press
- Lebel, T., Delclaux, F., Le Barbé, L. and Polcher, J. 2000 From GCM scales to hydrological scales: Rainfall variability in West Africa. *Stochastic Environ. Res. and Risk Assessment*, **14**, 275–295
- LeMone, M. A. 1983 Momentum flux by a line of cumulo-nimbus. *J. Atmos. Sci.*, **40**, 1815–1834
- Mahfouf, J. F. and Viterbo, P. 1998 'Land surface assimilation'. Pp. 319–347 in Proceedings of the ECMWF seminar on data assimilation, September 1996. Available from ECMWF Shinfield Park, Reading, UK
- Mallet, I., Cammas, J. P., Mascart, P. and Bechtold, P. 2000 Effects of cloud diabatic heating on the early development of the FASTEX IOP17 cyclone. *Q. J. R. Meteorol. Soc.*, **125**, 3439–3467
- Moncrieff, M. W., Gregory, D., Krueger, S. K., Redelsperger, J.-L. and Tao, W. K. 1997 GEWEX Cloud System Study (GCSS) Working Group 4: Precipitating convective cloud systems. *Bull. Am. Meteorol. Soc.*, **78**, 831–845
- Nicholson, S. E. 1989 African drought: Characteristics, causal theories and global teleconnections. *Am. Geophys. Union, Geophys. Monogr.* **52**, 7, 79–100
- Paradis, D., Lafore, J. P., Redelsperger, J. L. and Balaji, V. 1995 African easterly waves and convection. Part I: Linear simulations. *J. Atmos. Sci.*, **52**, 1657–1679
- Redelsperger, J.-L. and Lafore, J.-P. 1988 A three-dimensional simulation of a tropical squall line: Convective organization and thermodynamic vertical transport. *J. Atmos. Sci.*, **45**, 1334–1356
- Reed, R. J., Norquist, D. C. and Recker, E. E. 1977 The structure and properties of African wave disturbances as observed during phase III of GATE. *Mon. Weather Rev.*, **105**, 317–333
- Reed, R. J., Hollingsworth, A., Heckley, W. A. and Delsol, F. 1988 An evaluation of the performance of the ECMWF operational system in analysing and forecasting easterly wave disturbances over Africa and the tropical Atlantic. *Mon. Weather Rev.*, **116**, 824–860
- Rowell, D. P. and Milford, J. R. 1993 On the generation of African squall lines. *J. Climate*, **16**, 1181–1193
- Sultan, B. and Janicot, S. 2000 Abrupt shift of the ITCZ over West Africa and intra-seasonal variability. *Geophys. Res. Lett.*, **27**, 3353–3356
- Taupin, J. D., Lebel, T., Cazenave, F., Greard, M., Kong, J., Lecocq, J., Adamson, M., d'Amato, N. and Ben Mohamed, A. 1993 'EPSAT-NIGER, Campagne 1992'. IRD and DMN Report. Available from T. Lebel, LTÉ, Grenoble, France
- Thornicroft, C. D. 1995 An idealized study of African easterly waves. III: More realistic basic states. *Q. J. R. Meteorol. Soc.*, **121**, 1589–1614
- Thornicroft, C. D. and Blackburn, M. 1999 Maintenance of the African easterly jet. *Q. J. R. Meteorol. Soc.*, **125**, 763–786

- Thorncroft, C. D. and Flocas, H. A. 1997 A case study of Saharan cyclogenesis. *Mon. Weather Rev.*, **125**, 1147–1165
- Thorncroft, C. D. and Haile, M. 1995 The mean dynamic and thermodynamic fields for July 1989 over the tropical north Africa and their relationship to convective storm activity. *Mon. Weather Rev.*, **123**, 3016–3031
- Thorncroft, C. D. and Hoskins, B. J. 1994 An idealized study of African easterly waves. II: A nonlinear view. *Q. J. R. Meteorol. Soc.*, **120**, 983–1015
- Uccellini, L. W. and Kocin, P. J. 1987 The interaction of jet streak circulation during heavy snow events along the east coast of the United States. *Weather and Forecasting*, **2**, 289–308
- Viterbo, P. and Beljaars, A. C. M. 1995 A new land surface parameterisation scheme in the ECMWF model and its validation. *J. Climate*, **8**, 2716–2748
- WAMP 1999 'West African Monsoon Project: Second annual report'. Available from C. Thorncroft, University of Reading, Reading, UK
- Zipser, E. I. 1977 Mesoscale and convective scale downdrafts as distinct components of squall line structure. *Mon. Weather Rev.*, **105**, 1568–1589

Relationship between easterly waves and mesoscale convective systems over the Sahel

Vincent Mathon

MSE, IRD, BP 5045, 34032 Montpellier Cedex, France

Arona Diedhiou

LTHE, IRD, BP 53, 38041 Grenoble Cedex 9, France

Henri Laurent

CTA-IAE-ACA, 12228-904 - São José dos Campos/SP, Brazil

Received 12 November 2001; revised 23 January 2002; accepted 28 January 2002; published XX Month 2002.

[1] Relationship between Sahelian mesoscale convective systems and easterly waves is studied at various time and space scales during 5 rainy seasons (1st July–15th September 1990–1994). This study focuses on a sub-population of MCSs called organised convective systems (OCS) which account for most of the rainfall. Wave activity periods are detected by spectral analyses on the 700 hPa meridional wind component, information on the convective systems is derived from an automatic tracking algorithm and rainfall data of the EPSAT-Niger experiment. We observe a modulation of OCS cloud cover at synoptic-scale during easterly wave activity, with an increase of the cloud cover in and ahead of the trough but OCS rainfall efficiency is maximum behind of the wave trough. At seasonal scale, OCS number and cloud cover distributions are not significantly affected by easterly wave occurrences, which means that the latter are not directly associated to the interannual variability of rainfall. INDEX TERMS: 3314 Meteorology and Atmospheric Dynamics: Convective processes; 3364 Meteorology and Atmospheric Dynamics: Synoptic-scale meteorology; 3374 Meteorology and Atmospheric Dynamics: Tropical meteorology

1. Introduction

[2] Easterly waves are an important component of the West African climate as they modulate rainfall and convection [e.g. Burpee, 1972; Reed *et al.*, 1977; Duvel, 1990; Diedhiou *et al.*, 1998; Diedhiou *et al.*, 1999]. Typically they have a period of 3–5 days and propagate westward with a phase velocity of about 7–8 degrees longitude per day. Although easterly waves are known to modulate rainfall and convection, the relationships between easterly waves and MCSs are not well documented. This paper aims to analyse the relationship between MCS and easterly waves from the seasonal scale to the mesoscale. Three datasets have been used. The NCEP/NCAR dataset [Kalnay *et al.*, 1996] consists of a reanalysis of the global observational network of meteorological variables (wind, temperature, geopotential height, humidity) with a single version of the forecast model of the NCEP (National Center for Environmental Prediction). In this study we use the 700 hPa wind reported on a 2.5° × 2.5° grid every 6 hours (00:00, 06:00, 12:00 and 18:00 UTC) on the periods 1 June–30 September from 1990 to 1994. The second dataset consists of information on MCS life-cycles obtained from an automatic tracking algorithm applied on METEOSAT full resolution images (ie. time resolution of 30

minutes and spatial resolution of about 5 km, see Mathon and Laurent [2001] for a detailed description and evaluation of the method). MCSs are here defined as cloud clusters with a size larger than 5000 km² at the brightness temperature threshold 233 K. The tracking technique yields MCS size, speed, location and vertical development during the life-cycle. The third dataset is rainfall data from the EPSAT-Niger experiment [Lebel *et al.*, 1992]. The experiment started in 1990 with a hundred recording raingauges covering a 160 * 110 km² area hereafter referred to as the E-N study area. In 1994, the network was reduced to 30 gauges. Lebel and Amani [1999] have shown that such a network is able to estimate precisely the average rainfall over the E-N study area at the event scale and beyond. In the following we will make use of homogeneous 5' rainfall series recorded by the 30 gauges network between 1990 and 1994. These 5' rainfall data are accumulated in order to produce event rainfall at each gauge, according to the criteria given in section 1-c. In order to have an homogeneous dataset combining these three different sources of information, the period of study has been limited to the 1st July to the 15th September over 5 years (1990–1994).

2. Methodology

2.1. Easterly Waves Detection

[3] Easterly waves are detected using wavelet analysis on the meridional wind component at 700 hPa. This level is in the range of those commonly used to study synoptic-scale easterly waves. The wavelet analysis is performed for the NCEP grid point closest to the EPSAT-Niger area (2.5E–12.5N), see Diedhiou *et al.* [1999] for more details on the methodology. Periods characterised by a maximum of the wavelet modulus in the 3–10 day band periods are retained. In a second step we verify that an easterly wave disturbance at synoptic-scale does exist. In such a case, we use the 3–10-day filtered wind field at 700 hPa to determine in which wave sector the EPSAT-Niger area and the convective systems are located. This methodology may not allow us to detect every easterly wave but it makes us confident that the selected dates correspond to actual easterly wave disturbances at synoptic scale.

2.2. MCS Classification

[4] In this paper we use a classification that attempts to depict objectively MCSs that account for most of rainfall over the central Sahel. The so-called Organized Convective Systems (OCSs) are defined at 233 K but they must contain at least one cluster at 213 K with a size larger than 5000 km², a lifetime greater than 3 hours and a mean speed greater than 10 m.s⁻¹ [Mathon, 2001]. Over the Sahel, OCSs are associated with approximately 80% of the cloud cover at threshold 233 K while accounting for only 12% of the total MCS number. Figure 1 shows that the OCS contribution in

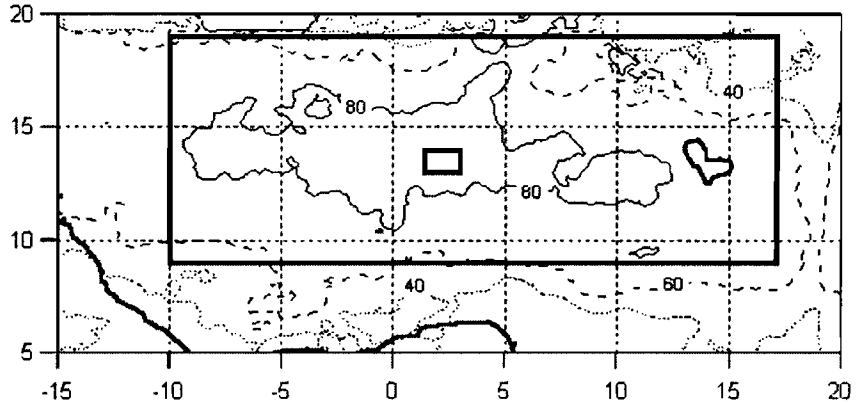


Figure 1. OCS contribution (%) to the total MCS cloud coverage (233 K). The central Sahel and the EPSAT-Niger area are outlined. 80%, 60% and 40% isolines are drawn in full, dashed and dotted lines respectively.

term of cloud cover at threshold 233 K is generally larger than 80% in the 12°N–16°N belt and larger than 60% almost everywhere in the central Sahel. Over the EN-area, OCSs contribute to 93% of the total rainfall [Mathon, 2001].

2.3. OCS Rainfall Characterisation

[5] In order to study OCS rainfall characteristics we use a concept of rainfall event derived from the one of *Amani et al.* [1996]. The most efficient E-N rain events can be defined as follow:

at least 80% of the gauges must record a rain depth equal or greater than 1 mm during the event;
there should not be a rainfall interruption of more than 30 minutes over the whole network. If all 30 gauges do not report any rain during a continuous 30-minute period then this is the end of the rain event.

[6] The major rain events as defined above explain approximately 75% of the total rainfall recorded over the EN-area [*D'Amato and Lebel*, 1998].

[7] To study rainfall characteristics of the satellite observed OCSs we have to deal with window-effects which are unavoidable when comparing a window-limited ($16,000 \text{ km}^2$) measurement of a convective cloud which may only partly cover the instrumented area. Our approach to reduce this effect consists of selecting OCSs according to their overlapping surface with the instrumented area. We have tested several overlapping surface thresholds at different temperature thresholds (253 K, 233 K and 213 K) so as to explain most of the major rain events defined above while eliminating most of the other cases. The best compromise was found with OCSs covering more than 80% of the EN-area at threshold 233 K. These criteria allow us to select 45% of the OCSs that correspond to 78% of the total rainfall over the EN-area. Hereafter, only OCSs which satisfy the 80% overlapping criterion are considered for rainfall characterisation.

3. OCSs and Easterly Waves Relationships

3.1. Relationships at Synoptic Scale

[8] Figure 2a shows the distribution of the OCS cloud cover according to the wave sector over the central Sahel. As expected, OCSs are more frequently located at and ahead of the trough. However, when considering separately the southern (9°N – 14°N) and the northern (14°N – 19°N , Figure 2b) part of the central Sahel, one observes a radical change of the easterly wave modulation. As shown by *Duvel* [1990], OCSs are less frequently located in the northern flux sector compared to the other sectors. He suspected that humidity advection by easterly waves could play a significant

role over the northern part of the Sahel where the humidity transport by the monsoon flux is less important than that observed to the south.

[9] Figure 2c documents the relationships between easterly waves and OCSs at the genesis and the termination of their life-cycle. Note that initiations and separations (resp. dissipations and mergings) exhibit similar behaviours (not shown). Genesis occur preferentially at and ahead of the trough whereas terminations are more frequently observed ahead of the trough. Keeping in mind that we consider only four sectors, results of Figure 2c are consistent with those of *Payne and McGarry* [1977]. However, the amplitude of the modulation is significantly weaker in our study. This may be due to differences in the definition of the genesis or the termination of a life-cycle. Note also that their study is limited to the phase III of GATE and includes the adjacent Atlantic ocean.

3.2. Relationships at Seasonal Scale

[10] The previous section confirmed that easterly waves modulate OCS cloud cover. One might ask whether or not easterly wave occurrences modify the global OCS statistics over the whole Sahel and at the scale of the rainy season. Table 1 shows the OCS number and cloud cover during periods of wave activity and inactivity. A simple scaling by proportion of the duration of wave activity and inactivity indicates that easterly waves do not have any significant impact on parameters at such time and space scale. As OCSs provide most of the rainfall over the Sahel, this suggests that easterly waves are not

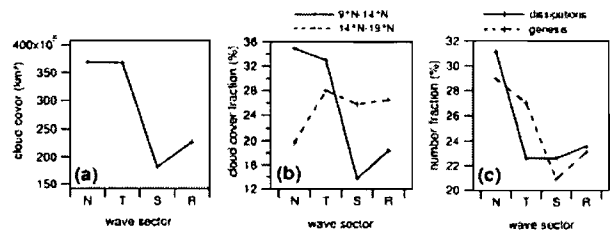


Figure 2. a) OCS cloud cover distribution (km^2 , 233 K) versus wave sector (Northerly flux, Trough, Southerly flux and Ridge). b) Easterly waves modulation of OCS cloud cover (%) over the southern and the northern part of the central Sahel. c) Frequency (%) distribution of the location of OCSs versus wave sector at their genesis and their dissipation. A total of 411 OCSs was observed over the central Sahel during the 5 summers studied.

Table 1. OCS Number and Cloud Cover (233K , km^2) Over the Central Sahel During Five Summers (1st July–15th September) for Periods of Wave Activity and Inactivity are Considered Separately

	OCS number	OCA cloud cover (10^9 km^2)
	Wave activity	Wave inactivity
Observed	411	729
Scaled	742	729
	1.15	1.94
	2.06	1.94

Also indicated are the number and the cloud cover after scaling by proportion of the accumulated duration of wave activity and wave inactivity.

the main factor in the interannual variability of rainfall for this region.

[11] Figure 3 shows the distributions of the OCS number and cloud cover versus lifetime after scaling by proportion of the duration of easterly waves activity and inactivity. There are no significant differences between the distributions. Thus, long-lived OCS occurrences are not specially favoured by the presence of easterly waves.

3.3. Relationships at Mesoscale

[12] The results shown in Figure 4 are obtained using the methodology explained previously. Thus, window-effects are limited and we can then expect to relate rainfall variability to physical processes. It can be reminded that only the most energetic waves and the most rain producing OCSs are considered here.

[13] Figure 4a shows the accumulated rain yield and cloud cover associated with OCSs during periods of wave activity. Over the EN-area, both the cloud cover and the rain yield are modulated by easterly waves with a preferential location at the trough. The modulation of rainfall is primarily correlated to the modulation of cloud occurrences. However, more detailed investigations indicate that easterly waves also modulate OCS rainfall efficiency. Indeed, as shown in Figure 4b, the mean rain yield per OCS over the EN-area is larger behind the trough, in the southerly flux sector than in the other sectors. Also shown in Figure 4b is the ratio between the accumulated cloud cover over the EN-area and the accumulated rainfall. Again, OCS occurrences are associated with more rainfall when they are located in the southerly flux sector. This suggests that easterly waves may affect results obtained using satellite-derived rainfall estimation methods such as the GPI [Arkin, 1979]. Humidity advection by easterly waves, which appears to be a significant process (Figure 2b), might also affect OCS rainfall efficiency. However results in

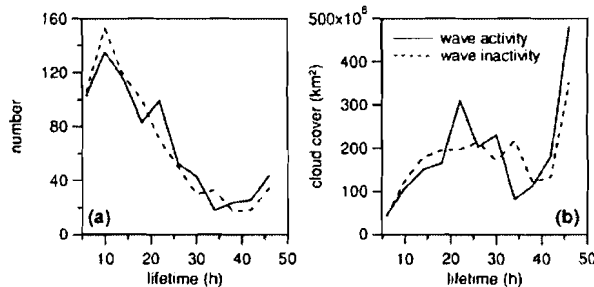


Figure 3. a) OCS number and b) cloud cover (233K , km^2) versus lifetime during periods of wave activity and inactivity. The distributions have been scaled by proportion of the accumulated duration of wave activity and inactivity and only OCSs which have crossed the central Sahel have been considered.

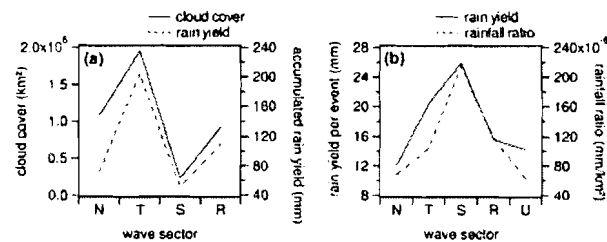


Figure 4. Characteristics of the OCS cloud cover and rainfall versus wave sectors (N, T, S, R). a) OCS 233 K cloud cover (km^2) and rain yield (mm) over the E-N area cumulated during the periods of wave activity observed during 5 years. b) OCS averaged rain yield (mm) and mean ratio between OCS rainfall and cloud cover (mm/km^2). Results obtained during wave inactivity are referred to the U sector.

Figure 4b have to be moderated. Cases satisfying criteria defined in section 1-c during easterly wave activity are relatively rare (only 25 cases over 5 summers).

4. Conclusion

[14] This paper documents the relationship between African easterly waves and OCSs over the central Sahel at different space and time scales. OCSs are very rain-efficient systems which provide 93% of rainfall over the EN-area and 80% of the 233 K cloud cover over the central Sahel [Mathon, 2001].

[15] At synoptic scale, results obtained by previous studies are confirmed. OCSs are located preferentially at and ahead of the trough in the southern part of the Sahel and at and behind the trough in the north. However, we have shown that OCS initiations and dissipations are only slightly modulated by easterly waves compared to the Payne and McGarry [1977] study. We suspect that it is primarily due to differences in the definition of the genesis or the termination of a life-cycle or to the fact that their study is limited to phase III of GATE and includes the adjacent Atlantic ocean.

[16] The study at larger scales (over the whole Sahel and for the core of the Sahelian rainy season), shows that easterly wave occurrences during the season do not significantly modify the OCS number or the OCS cloud cover distributions. These results suggest that easterly waves are not the main factor in the interannual variability of rainfall over the region. However, at the scale of the EN-area, we have found that OCS rain efficiency is maximum in the southerly flux sector. Despite the small number of cases available for this study, it can be argued that humidity advection by the southerly flux favours rainfall production.

[17] **Acknowledgments.** The authors are very thankful to Climate Diagnostics Center (NOAA, BOULDER, CO) for providing the reanalyses dataset, to Jean Louis Monge for his efficiency in managing the CLIM-SERV data base at LMD and to Thierry Lebel for discussion on the observed rainfall data over Niamey.

References

- Amani, A., T. Lebel, J. Rousselle, and J. D. Taupin, Typology of rainfall fields to improve rainfall estimation in the Sahel by the area threshold method, *Water Resour. Res.*, 32, 2473–2487, 1996.
- Burpee, R. W., The origin and structure of easterly waves in the lower troposphere of north Africa, *J. Atmos. Sci.*, 29, 77–90, 1972.
- D'Amato, N., and T. Lebel, On the characteristics of the rainfall events in the Sahel with a view to the analysis of climatic variability, *Int. J. Climatol.*, 18, 955–974, 1998.
- Diedhiou, A., S. Janicot, A. Viltard, P. de Felice, and H. Laurent, Easterly waves regimes and associated convection over West Africa and the tro-

- pical Atlantic: Results from the NCEP/NCAR and ECMWF reanalyses, *Clim. Dynamics*, 15, 795–822, 1999.
- Diedhiou, A., S. Janicot, A. Viltard, and P. de Felice, Evidence of two regimes of easterly waves over West Africa and the tropical Atlantic, *Geophys. Res. Lett.*, 25, 2805–2808, 1998.
- Duvel, J. P., Convection over tropical Africa and the Atlantic ocean during northern summer. Part II: Modulation by easterly waves, *Mon. Wea. Rev.*, 118, 1855–1868, 1990.
- Kalnay, E., M. Kanamitsu, R. Kistler, and W. Collins, et al., The NCEP/NCAR 40-years reanalysis project, *Bull. Amer. Meteor. Soc.*, 77, 437–471, 1996.
- Lebel, T., and A. Amani, Rainfall estimation in the Sahel: what is the ground truth?, *J. Appl. Meteor.*, 38, 555–568, 1999.
- Lebel, T., H. Sauvageot, M. Hoepffner, M. Desbois, B. Guillot, and P. Hubert, Rainfall estimation in the Sahel: The EPSAT-Niger experiment, *Hydrol. Sci. J.*, 37, 201–215, 1992.
- Mathon, V., Etude climatologique des systèmes convectifs de méso-échelle en Afrique de l'ouest., PhD thesis, Paris VII, 250 pp., 2001.
- Mathon, V., and H. Laurent, Life cycle of the Sahelian mesoscale convective cloud systems, *Quart. J. Roy. Meteor. Soc.*, 127, 377–406, 2001.
- Payne, S., and M. M. McGarry, The relationships of satellite inferred convective activity to easterly waves over West Africa and the adjacent ocean during phase III of GATE, *Mon. Wea. Rev.*, 105, 413–420, 1977.
- Reed, R. J., D. C. Norquist, and E. E. Recker, The structure and properties of African wave disturbances as observed during Phase III of GATE, *Mon. Wea. Rev.*, 105, 317–333, 1977.

Arona Diedhiou, LTHE, IRD, BP 53, 38041 Grenoble Cedex 9, France.
(diedhiou@lmg.inpg.fr)

Henri Laurent, CTA-IAE-ACA, 12228-904 - São José dos Campos/SP, Brazil.

Vincent Mathon, MSE, IRD, BP 5045, 34032 Montpellier Cedex, France.

The West African Monsoon Dynamics. Part I: Documentation of Intraseasonal Variability

BENJAMIN SULTAN AND SERGE JANICOT

LMD/IPSL, CNRS, Ecole Polytechnique, Palaiseau, France

ARONA DIEDHIOU

Laboratoire d'Etudes des Transferts en Hydrologie et Environnement, IRD, Grenoble, France

(Manuscript received 20 May 2002, in final form 9 January 2003)

ABSTRACT

Intraseasonal variability in the West African monsoon is documented by using daily gridded datasets of rainfall and convection, and reanalyzed atmospheric fields, over the period 1968–90. Rainfall and convection over West Africa are significantly modulated at two intraseasonal timescales, 10–25 and 25–60 day, leading to variations of more than 30% of the seasonal signal. A composite analysis based on the dates of the maximum (minimum) of a regional rainfall index in wet (dry) sequences shows that these sequences last, on average, 9 days and belong to a main quasiperiodic signal of about 15 days. A secondary periodicity of 38 days is present but leads to a weaker modulation. During a wet (dry) sequence, convection in the ITCZ is enhanced (weakened) and its northern boundary moves to the north (south), while the speed of the African easterly jet decreases (increases), the speed of the tropical easterly jet increases (decreases), and the monsoon flow becomes stronger (weaker), all these features being similar to the ones associated with interannual variability characterizing wet and dry years.

This modulation of convection at intraseasonal timescales is not limited to West Africa but corresponds to a westward-propagating signal from eastern Africa to the western tropical Atlantic. An enhanced monsoon phase is associated with stronger cyclonic activity in the low levels over the Sahel associated with stronger moisture advection over West Africa. Five days before the full development of the wet phase, a stronger cyclonic circulation at 20°E induces enhanced southerly winds along 25°E where convection enhances, while another westward-propagating cyclonic circulation is located at 0°. This atmospheric pattern is linked to the enhancement of the subsiding branch of the northern Hadley cell at 35°N, northerly advection of drier air over West Africa, and to increased dry convection in the heat low at 20°N. It propagates westward, leading to a zonally extended area of enhanced monsoon winds over West Africa consistent with the occurrence of the wet phase.

1. Introduction

Rainfall variability over West Africa has usually been analyzed either through mesoscale convective systems (MCS; Laing and Fritsch 1993, 1997; Hodges and Thorncroft 1997; Mathon and Laurent 2001), synoptic-scale easterly waves (Reed et al. 1977; Duvel 1990; Diedhiou et al. 1999), interannual timescale variability, and/or the decadal timescale of the long-term drought over the Sahel (Lamb 1978a,b; Folland et al. 1986; Rowell et al. 1995; Ward 1998; Rowell 2001; Janicot et al. 2001). Very few studies have investigated the West African monsoon through the intraseasonal timescale. Kilibadis and Weickmann (1997) have shown some connections at the 6–30-day timescale between convection

in the region 5°–15°N, 10°–20°E and moisture advection over West Africa during northern summer. More recently, Janicot and Sultan (2001) showed preliminary results of the evidence of specific intraseasonal variability in convective activity and low-level atmospheric circulation during the summer monsoon in West Africa. Grodsky and Carton (2001) showed that intraseasonal modulation of convection can also occur during northern spring in the ITCZ over the tropical Atlantic and they suggested a mechanism based on land–sea interactions.

A more detailed documentation of intraseasonal variability in the West African monsoon during northern summer is presented here. The data are described in section 2 and the summer of 1968 is shown in section 3 as an example of intraseasonal timescale rainfall fluctuations. In section 4 we describe the composite intraseasonal sequences of Sahel rainfall and we detail the associated atmospheric circulation patterns in section 5. Conclusions are given in section 6.

Corresponding author address: Dr. Serge Janicot, Laboratoire de Météorologie Dynamique, Ecole Polytechnique, 91128 Palaiseau Cedex, France.
E-mail: janicot@lmd.polytechnique.fr

2. Datasets

Independent datasets have been used to investigate the intraseasonal timescale variability of convection in the West African monsoon. Two of them describe rainfall and convection variability, two others are the European and U.S. reanalyses. They document the period 1968–90 and the subperiod 1979–90, which belong to a dry long-term sequence of the rainfall regime over West Africa compared to the long-term mean (Hastenrath 1995). We will show that all the results obtained with these different datasets coming from independent sources (rain gauge amounts, satellite measurements, atmospheric variables from radiosoundings, pibals, etc.), are very consistent.

a. The NCEP–NCAR reanalyses

The National Centers for Environmental Prediction–National Center for Atmospheric Research (NCEP–NCAR) have completed a reanalysis project with a current version of the Medium-Range Forecast (MRF) model (Kalnay et al. 1996). This dataset consists of a reanalysis of the global observational network of meteorological variables (wind, temperature, geopotential height, humidity on pressure levels, surface variables, and flux variables like precipitation rate) with a “frozen” state-of-the-art analysis and forecast system at a triangular spectral truncation of T62 to perform data assimilation throughout the period 1948 to the present. This makes it possible to circumvent problems of previous numerical weather prediction analyses due to changes in techniques, models, and data assimilation. Data are reported on a $2.5^\circ \times 2.5^\circ$ grid every 6 h (0000, 0600, 1200, and 1800 UTC), on 17 pressure levels from 1000 to 10 hPa, which are good resolutions for studying synoptic weather systems. We used data covering the period 1 June–30 September, from 1968 to 1990, with one value per day by averaging the four outputs of each day.

b. The IRD daily rainfall

Daily rainfall amount at stations located on the West African domain $3^\circ\text{--}20^\circ\text{N}$, $18^\circ\text{W}\text{--}25^\circ\text{E}$ have been compiled by the Institut de Recherche pour le Developpement (IRD), the Agence pour la Securite de la Navigation Aeriennne en Afrique et a Madagascar (ASECNA), and the Comite Inter-africain d'Etudes Hydrauliques (CIEH). These data are available for the period 1968–90, including more than 1300 stations from 1968 to 1980, and between 700 and 860 for the period 1981–90. These daily values were interpolated on the NCEP $2.5^\circ \times 2.5^\circ$ grid, by assigning each station daily value to the nearest grid point and averaging all the values related to each grid point. They were also interpolated in time, related to NCEP daily wind fields since daily rainfall amounts were measured between 0600 of the

day and 0600 local solar time (LST) of the following day. We applied a time lag of 12 h between the average time of the NCEP daily values (0900 UTC) and an approximated average time of “daily” precipitation over the West African continent (2100 LST; Duvel 1989), which indicates a maximum of high cloud coverage over land between 1800 and 0000 LST [Sow (1997) points out a maximum of half-hourly precipitation over the Senegal between 1700 LST and the end of the night, depending on the stations.] The greatest density of stations is located between the latitudes $5^\circ\text{--}15^\circ\text{N}$. Data on latitudes 17.5°N can also be taken into account since 30–45 stations are available.

c. The NOAA/OLR dataset

Since 1974, launching polar orbital National Oceanic and Atmospheric Administration (NOAA) Television Infrared Observation Satellite (TIROS) satellites has made it possible to establish a quasi-complete series of twice-daily measures of outgoing longwave radiation (OLR), at the top of the atmosphere and at a resolution of 2.5° latitude-longitude (Gruber and Krueger 1984). The interpolated OLR dataset (Liebmann and Smith 1996) provided by the Climate Diagnostics Center has been used here. In tropical areas, deep convection and rainfall can be estimated through low OLR values. Local hours of the measures varied during the period 1979–90 between 0230 and 0730 in the morning and between 1430 and 1930 in the afternoon. Since the deep convection over West Africa has a strong diurnal cycle, the sample of daily OLR based on two values separated by 12 h is enough to get a daily average. Moreover this dataset has been already widely used for tropical studies.

d. The ECMWF Reanalyses (ERA-15)

The European Centre for Medium-Range Weather Forecasts (ECMWF) completed a first reanalysis project (ERA-15), which used a frozen version of their analysis-forecast system, at a triangular spectral truncation of T106 with 31 levels in the vertical, to perform data assimilation using data from 1979 to 1993 (Gibson et al. 1997). Compared to NCEP–NCAR reanalyses, there are 17 pressure levels from 1000 to 10 hPa, with an additional level at 775 and no level at 20 hPa. According to our objectives, daily data have been interpolated on the $2.5^\circ \times 2.5^\circ$ NCEP–NCAR grid. The ERA-15 dataset has been used in comparison with the NCEP–NCAR dataset in order to evaluate the uncertainty of the wind fields produced by both reanalyses. Previous studies using these two reanalysis datasets already demonstrated their consistency over West Africa for describing both interannual and synoptic timescale variability, if we consider the period after 1968 (Diedhiou et al. 1999; Poccard et al. 2000; Janicot et al. 2001). The comparisons done here related to intraseasonal timescale variability also showed high consistency between these two data-

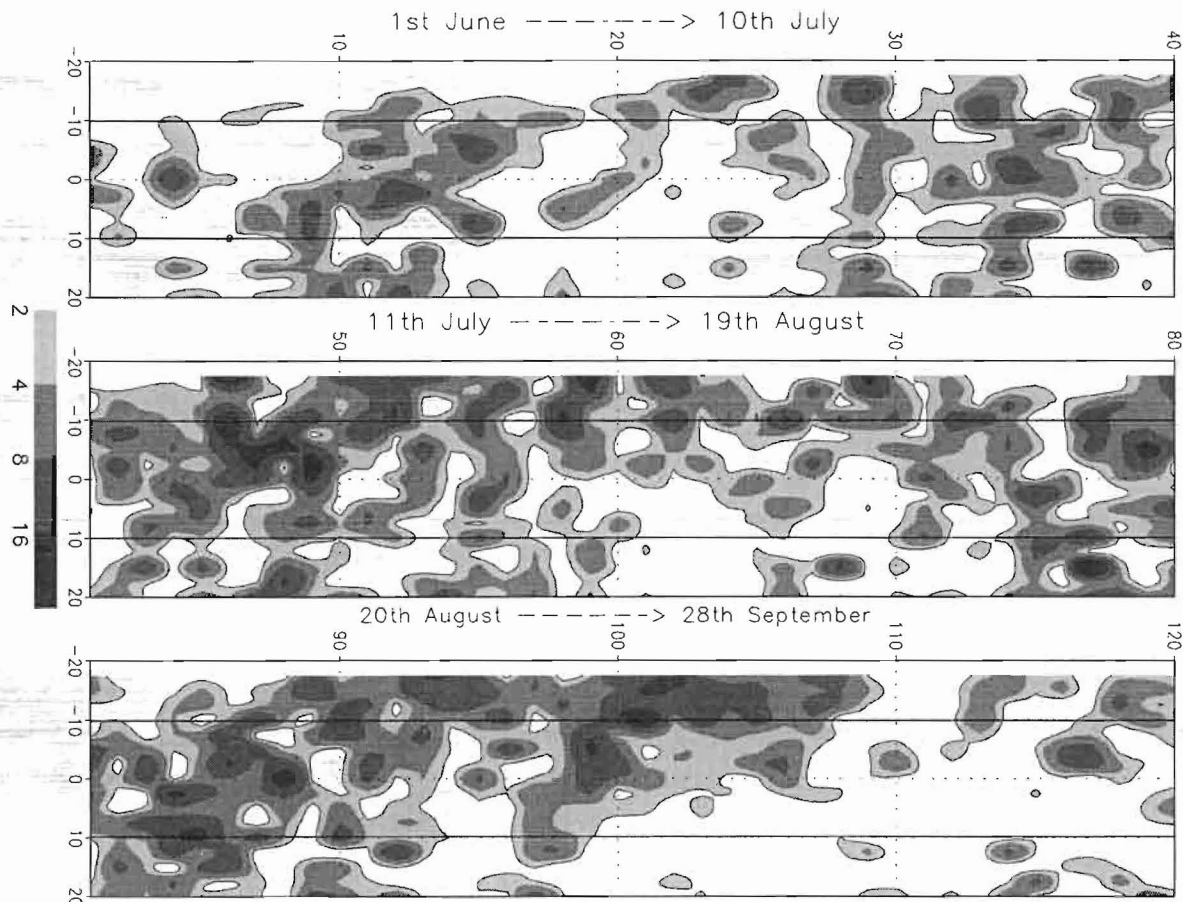


FIG. 1. Lon-time diagram of IRD daily rainfall (mm) averaged on the grid meshes at 12.5° and 15°N over West Africa for the summer of 1968 (1 Jun–28 Sep; i.e., 120 days). Vertical lines delineate longitudes 10°W and 10°E .

sets, so only results obtained from the NCEP–NCAR reanalysis, which covers the longest period 1968–90, will be shown in this paper.

3. Intraseasonal rainfall variability over West Africa in 1968

During the northern summer over West Africa, the ITCZ is centered along 10°N and extends in latitude over more than 10° (see, e.g., Sultan and Janicot 2000). The ITCZ consists of westward-traveling MCSs whose mean trajectories lie between 10° and 15°N (Mathon and Laurent 2001). Figure 1 shows a longitude–time diagram from 20°W to 20°E , of IRD daily rainfall averaged over the grid meshes at 12.5° and 15°N for the summer of 1968. Similar results have been obtained with computations performed at 10°N , the latitude of the mean rainfall maximum in the ITCZ (not shown). Different phases of high or low convective activity are clearly observed. During this year, the monsoon developed rapidly over West Africa from 27 June corresponding to the summer monsoon onset associated to an

abrupt shift of the ITCZ (see Sultan and Janicot 2000; Sultan et al. 2003, for more details about the definition of the monsoon onset). This is characterized in Fig. 1 by the occurrence at the end of June of a band of higher rainfall simultaneously at all longitudes. Besides this monsoon onset sequence, main active monsoon phases can be detected, one before the onset, between 10 and 15 June, and several ones after the onset, one around mid-July (day 45), another one in the second half of August (centered on day 85), and a third around day 100 (8 September). Contrary to this, a less active convection sequence occurred, just before the monsoon onset in the second half of June (this decrease of convection is a recurrent character of the preonset stage; see Sultan and Janicot 2000; Le Barbé et al. 2002; Sultan et al. 2003), then around 1 August (day 60), and also around 20 September (day 110).

Figure 2a shows the time series from 1 June to 30 September 1968 of daily rainfall averaged over the grid meshes 12.5° and 15°N , from 10°W to 10°E (white bars). The black area behind the daily rainfall values represents the daily values of the seasonal rainfall cycle,

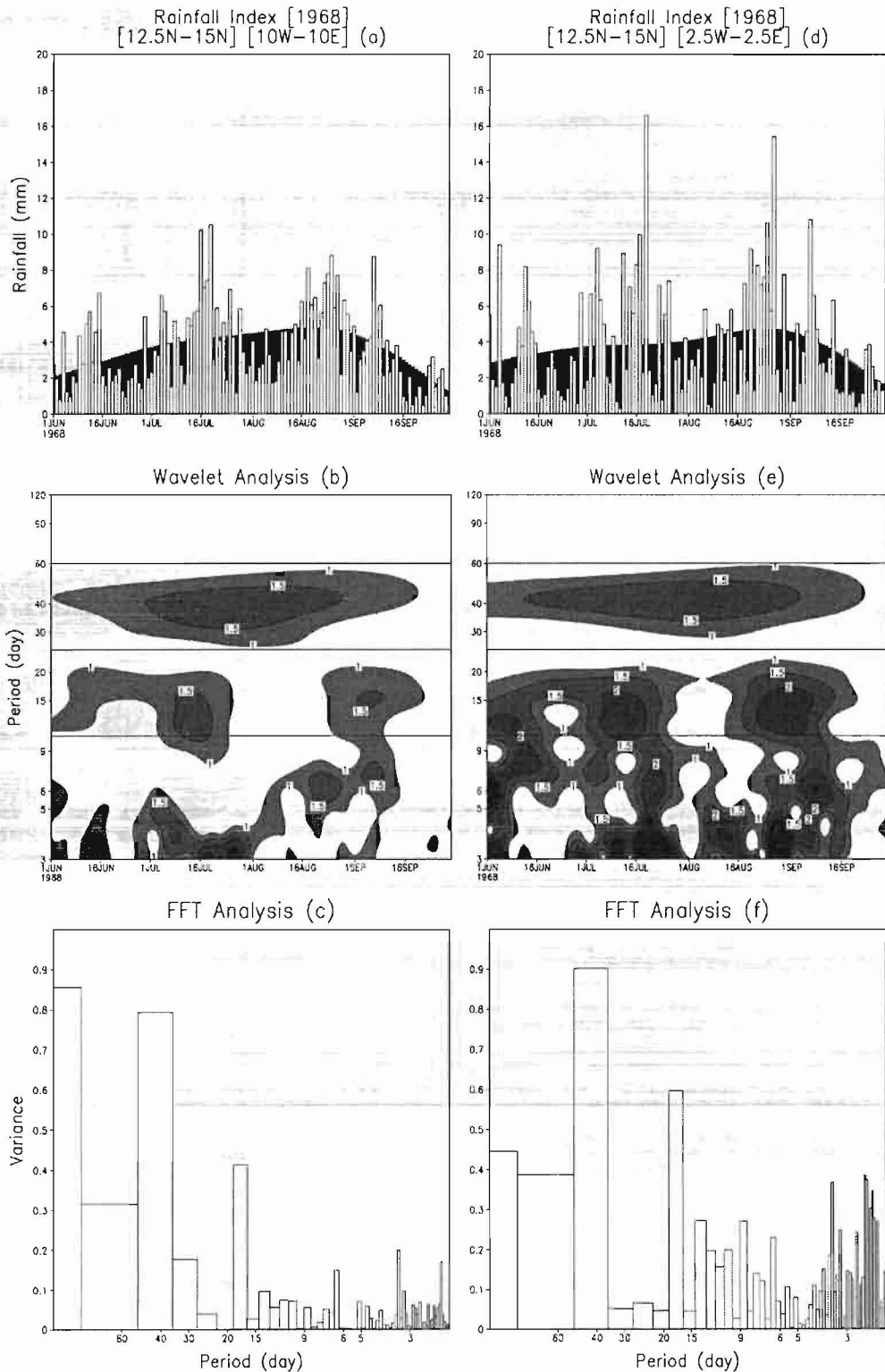


FIG. 2. (a) Daily rainfall time series from 1 Jun to 30 Sep 1968 averaged over the grid points from 12.5° to 15° N and from 10° W to 10° E (bars). Values are expressed in mm. The black area behind the daily rainfall values represents

computed as the seasonal-filtered signal where only rainfall fluctuations greater than 60 days are retained by using a nonrecursive filter (Scavuzzo et al. 1998). These computations (in Fig. 2 as well as in Fig. 3) have been done of the time series from 1 March to 30 November to avoid edge effects. The domain 10°W – 10°E , also delineated in Fig. 1, is located in the heart of West Africa and in Fig. 2a it captures the different rainfall sequences described in Fig. 1. The rainfall seasonal cycle over this area is very clear with weaker rainfall at the beginning and at the end of the time series, and with the greatest values in August when the ITCZ is located at its northernmost latitude. Sequences longer than 10 days of persistent high or low rainfall amounts can also be noticed along the course of the monsoon season, consistent with Fig. 1. The wavelet diagram of the rainfall time series (Fig. 2b) highlights this intraseasonal timescale variability as intermittent signals with more variance into two-period intervals, the first between 10 and 25 days and the second between 25 and 60 days. The signal in the 25–60-day band is related to the three low rainfall sequences occurring, first before the monsoon onset in the second half of June, second at the beginning of August, third in mid-September; and to the two high rainfall sequences, in mid-July and in the second half of August. The signal in the 10–25-day band represents shorter time fluctuations occurring at different stages of the monsoon season. The Fast Fourier Transform (FFT) spectrum computed over the whole June–September period is shown in Fig. 2c. Intraseasonal variability appears clearly in the band of 40 days and in the band between 15 and 20 days. The range of the variance in these spectral bands is of the same order as the range for the seasonal signal. Figures 2d–f show similar diagrams but for a rainfall time series averaged over a more local domain 12.5° – 15°N , 2.5°W – 2.5°E . In this case, short time variability is enhanced, due to the local scale influence of MCS and of synoptic-scale easterly waves. However, even at this smaller spatial scale, rainfall variability due to intraseasonal-scale fluctuations is still maintained at a high level of variance (Fig. 2e). The FFT spectrum (Fig. 2f) shows a weaker variance for the seasonal cycle, enhanced variance at the two intraseasonal-scale bands, and a higher signal for periodicities lower than 5 days. Significance tests have been applied on the FFT spectra by following the procedure similar to the one used in Burpee (1972) and Diedhiou et al. (1998). One thousand series of 122 elements have been randomly generated and FFT has been performed on each series. For each harmonic, the thresh-

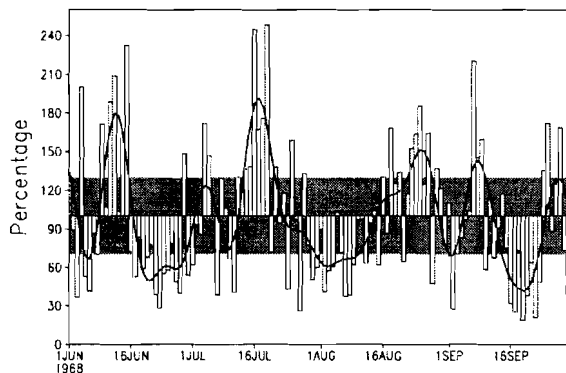


FIG. 3. Daily rainfall time series from 1 Jun to 30 Sep 1968, averaged over the domain 12.5° – 15°N , 10°W – 10°E . Bars represent the ratio of the unfiltered rainfall to the seasonal-filtered rainfall signal where only periodicities greater than 60 days are retained. The black curve represents the similar ratio but is filtered to remove periodicities lower than 10 days. These values are expressed in percentages of the seasonal timescale signal. The gray area is bounded by the levels of 130% and 70%.

old of the upper 5% of total variance fraction has been selected among the 1000 values. It represents between 4% and 5% of the variance for each harmonic. For the two FFT spectra of Fig. 2, the seasonal peak, the 40 peak and the 15–20 peak are all significant peaks. They are equal to 18.0%, 16.7%, 8.7%, respectively, for the spectrum of the regional rainfall index (Fig. 2c), and 4.8%, 9.6%, 6.4%, respectively, for the spectrum of the local rainfall index (Fig. 2f).

To better characterize the intraseasonal timescale rainfall fluctuations and to clearly separate them from interannual variability, we used the following procedure. First we define a seasonal cycle specific to each year by computing the low-filtered rainfall time series where only periodicities greater than 60 days are retained. Figures 2a and 2d show such seasonal cycles (the black curve) determined for 1968. Then for each day of this year we compute the ratio of the daily rainfall to the seasonal cycle. We then obtain a daily rainfall anomaly related to the seasonal cycle of this year. It enables the removal of the effect of interannual variability that would have been present if we computed a mean seasonal cycle by averaging each daily value over the period 1968–90 for instance. Figure 3 shows the corresponding time series for 1968, averaged over the domain 12.5° – 15°N , 10°W – 10°E (bars). The black curve represents the similar ratio but filtered to remove periodicities lower than 10 days (due to easterly waves and

←

the daily values of the seasonal rainfall cycle computed as the seasonal-filtered signal where rainfall fluctuations lower than 60 days are removed. (b) Modulus of the wavelet analysis of the daily rainfall time series presented in (a). Only periods lower than 120 days are presented. Horizontal lines delineate periods of 10, 25, and 60 days. Values greater than 1 are shaded. (c) FFT spectrum of the daily rainfall time series presented in (a). (d) Same as (a) but for the daily rainfall time series averaged from 12.5° to 15°N and from 2.5°W to 2.5°E . (e) Same as (b) but for the daily rainfall time series presented in (d). (f) Same as (c) but for the daily rainfall time series presented in (d).

MCS activity) and to focus on intraseasonal variability. These values are expressed in percentages of the seasonal timescale signal. For instance, a value of 120% for one day on the black curve means that the rainfall modulation due to the 10–60-day variability represents a positive fluctuation of 20% of the rainfall modulation due to the seasonal cycle for this day. The different intraseasonal rainfall sequences, already shown in the previous figures, are highlighted in Fig. 3. Some of them last more than 10 days with a maximum departure level greater in absolute value than 30% of the rainfall amount due to the seasonal cycle. This represents high modulations of the rainfall regime over West Africa during northern summer and contributes significantly to the total rainfall amount of the monsoon season. It also suggests that there must be a persistent effect in temporal rainfall fluctuations at timescales higher than those due to the synoptic easterly waves or to the MCS.

From this analysis performed on the summer 1968, it appears that intraseasonal timescale variability, characterizing rainfall fluctuations in the 10–60-day range, can be a significant timescale in the West African monsoon dynamics, not only when considering rainfall averaged on a regional area but also at a local scale. This topic is now explored on the period 1968–90 and with other atmospheric variables, by performing composite analyses based on the regional rainfall index computed on the domain 12.5° – 15° N, 10° W– 10° E for the summers of the period 1968–90.

4. Composite intraseasonal sequences of the regional rainfall index

The black curve in Fig. 3 represents the ratio of the 10–60-day filtered rainfall to the seasonal cycle value for each day of the summer of 1968 expressed in percentages of the seasonal timescale signal. For instance, a value of 120% for one day on the black curve means that the rainfall modulation due to the 10–60-day variability represents a positive fluctuation of 20% of the rainfall modulation due to the seasonal cycle for this day. Figure 4 shows the histogram of these ratios gathering all 122 days of the 23 summer time series from 1968 to 1990 (bars). Black full line shows the same computation but for the 10–25-day filtered signal instead of the 10–60-day signal, and the dashed-dotted line is for the 25–60-day filtered signal. We chose a separation at 25 days because the wavelet diagrams are similar to the ones in Fig. 2b but, for the other years, indicate that such a separation of the spectral interval of 10–60 days is reasonable since there is always a minimum of variance around this periodicity (not shown). In Fig. 4, the distributions for the 10–60- (bars), 10–25- (full line), and 25–60-day (dashed-dotted line) values are rather symmetric with maxima centered on 100% of the seasonal cycle (that is a null contribution of the intraseasonal-scale rainfall fluctuations). However these distributions extend away from this centered value

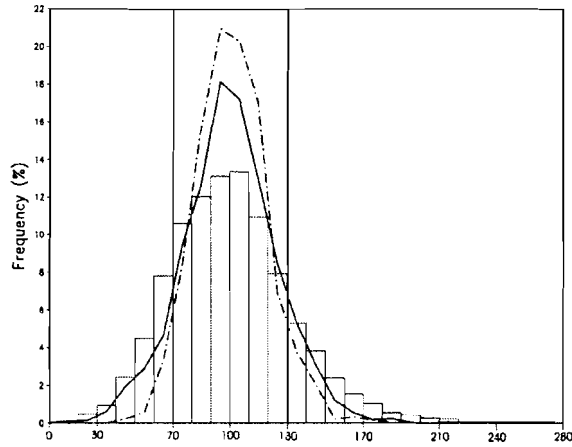


FIG. 4. Histogram of the ratio of the daily regional rainfall index (after filtering periodicities lower than 10 days) to the seasonal-filtered daily rainfall signal (where only periodicities greater than 60 days are retained). This histogram gathers all the days of the 23 summer time series from 1968 to 1990 (bars). The black full line shows the same computation for the ratio of the 10–25-day filtered signal to the seasonal-filtered signal, and the dashed-dotted line shows the ratio of the 25–60-day filtered signal to the seasonal-filtered signal. Vertical lines represent the levels 70% and 130%.

and we get a high amount of intraseasonal-scale daily rainfall fluctuation occurrences greater than 30% in absolute value: 15.8% greater than 130% and 16.3% lower than 70%. These occurrences of extreme values are the most frequent for the 10–60-day filtered signal, then for the 10–25-day filtered signal, and finally for the 25–60-day filtered signal, but the differences are small. This result means that the existence of an intraseasonal timescale modulation of daily rainfall like the one observed during the summer monsoon in 1968 is valid for the whole period 1968–90.

To better characterize these intraseasonal timescale modulations of daily rainfall over West Africa, composite analyses have been performed on all 23 summers. For each summer, we retained the dates (called t_0) where the regional rainfall ratio, similar to the one represented by the full line in Fig. 3, is maximum (minimum) and greater (lower) than 130% (70%) to define wet (dry) sequences. These rainfall modulations represent the contribution of the 10–60-day variability to the seasonal cycle. As said before, a value of 120% means that the rainfall modulation due to the 10–60-day variability represents a positive fluctuation of 20% of the rainfall modulation due to the seasonal cycle. We computed the corresponding mean composite time sequences, from t_0 – 10 days to t_0 + 10 days, by averaging all the wet sequences and all the dry sequences, using t_0 as the time reference (bars in Fig. 5a). Over the period 1968–90 we got an average of 3.9 wet and 4.5 dry sequences per season during June–September, with the highest occurrences in June (30%) and the lowest ones in August (18%). The mean modulation of the regional rainfall amount is quite high, up to 160% for wet sequences and

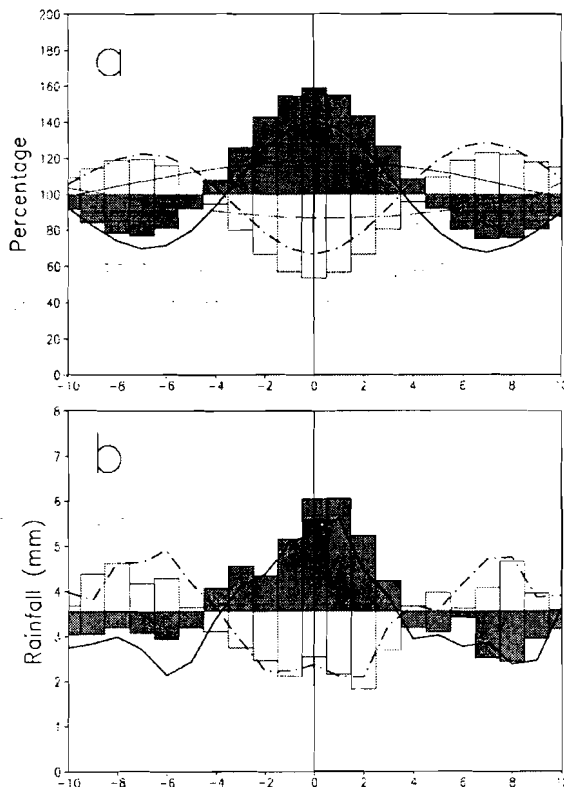


FIG. 5. (a) Time series of wet (black bars) and dry (white bars) mean composite time sequences of rainfall modulation averaged over the domain 12.5° – 15° N, 10° W– 10° E. These values represent the ratio of the daily rainfall, where periodicities lower than 10 days are removed, to the seasonal-filtered rainfall signal where only periodicities greater than 60 days are retained. They are expressed in percentages of the seasonal timescale signal. The wet (dry) composites have been computed by selecting days over the periods Jun–Sep 1968–90 where the regional rainfall ratio is a max (min) and is greater than 130% (lower than 70%) of the seasonal timescale signal. All these wet (dry) sequences have been averaged by considering as the reference data t_0 the days of max (min) percentage and by computing the averages of the percentages from $t_0 - 10$ days to $t_0 + 10$ days. The full (dashed-dotted) curve shows the composite wet (dry) sequence determined from the same t_0 reference dates but by averaging values from the 10–25-day filtered signal. The thin full (dashed) curve shows the composite wet (dry) sequence determined from the dates t_0 reference dates but by averaging values from the 25–60-day filtered signal. (b) (bars) Same as (a) but for the composite sequences computed with the same t_0 reference dates by using the regional rainfall values without dividing by the seasonal-filtered signal. The full and dashed-dotted curves represent sequences similar to the ones displayed with bars but from the t_0 reference dates determined from the 10–25-day filtered regional rainfall signal.

down to 60% for dry sequences. These sequences are preceded and followed by weaker rainfall anomalies of the opposite sign. Whereas the signal results from the rainfall variability between 10 and 60 days, the mean wet and dry sequences last 9 days and belong to a quasi-periodic fluctuation whose corresponding period is quite short, about 15 days. Similar computations done from the same t_0 reference dates but with the 10–25-day fil-

tered signal (full and dashed-dotted curves in Fig. 5a) confirm this conclusion by showing quite similar time sequences with only small differences: the 10–25-day mean composite sequences have a similar periodicity and consist of more symmetric fluctuations with weaker rainfall anomalies around t_0 and higher anomalies of opposite signs ($t_0 - 7$ and $t_0 + 7$). These differences are due to the influence of the 25–60-day variability. Computations done with this signal led to a composite periodicity at about 38 days with rather weak rainfall fluctuations (see thin full and dashed curves in Fig. 5a). So the whole 10–60-day signal is dominated by the 10–25-day signal. Figure 5b shows, displayed with bars, similar composite sequences computed with the same t_0 reference dates but using the regional rainfall values without dividing by the seasonal-filtered signal. We see that at t_0 the difference of the mean rainfall amount between the mean wet and dry phases is very high, from 2 to 6 mm day^{-1} , confirming the significance of an intraseasonal timescale variability in the monsoon dynamics over West Africa. The full and dashed-dotted curves represent sequences similar to the ones displayed with bars but from the t_0 reference dates determined from the 10–25-day filtered regional rainfall signal. It provides highly similar sequences, confirming the dominance of the 10–25-day variability on intraseasonal timescale rainfall fluctuations.

Similar computations have been performed on OLR values averaged on the same domain 12.5° – 15° N, 10° W– 10° E over the period 1979–90. Due to the scale value of this variable (values between 210 and 240 W m^{-2} in the ITCZ), the threshold levels selected are 95% and 105% of the seasonal-filtered signal. The results obtained are quite consistent with those from the rainfall values, with high variations between wet and dry sequences, up to 40 W m^{-2} , from 220 from the wet sequence at t_0 to 260 W m^{-2} for the dry sequence at t_0 (not shown).

We have confirmed in this section that rainfall variability at intraseasonal timescale is a significant feature of the West African monsoon, and that it is mainly defined by fluctuations between 10 and 60 days, with a dominant periodicity range between 10 and 25 days. So, in the following, we focus on the intraseasonal timescale fluctuations between 10 and 25 days, and look at the connections between this rainfall regime and atmospheric circulation.

5. Composite intraseasonal sequences of enhanced/weakened monsoon phases

a. Mean convection and wind fields at t_0

Unfiltered mean convection and wind fields have been computed for the composite 1968–90 summer wet and dry sequences at t_0 , the different t_0 times for the wet (dry) sequences being selected when the 10–25-day filtered regional rainfall index is maximum (min-

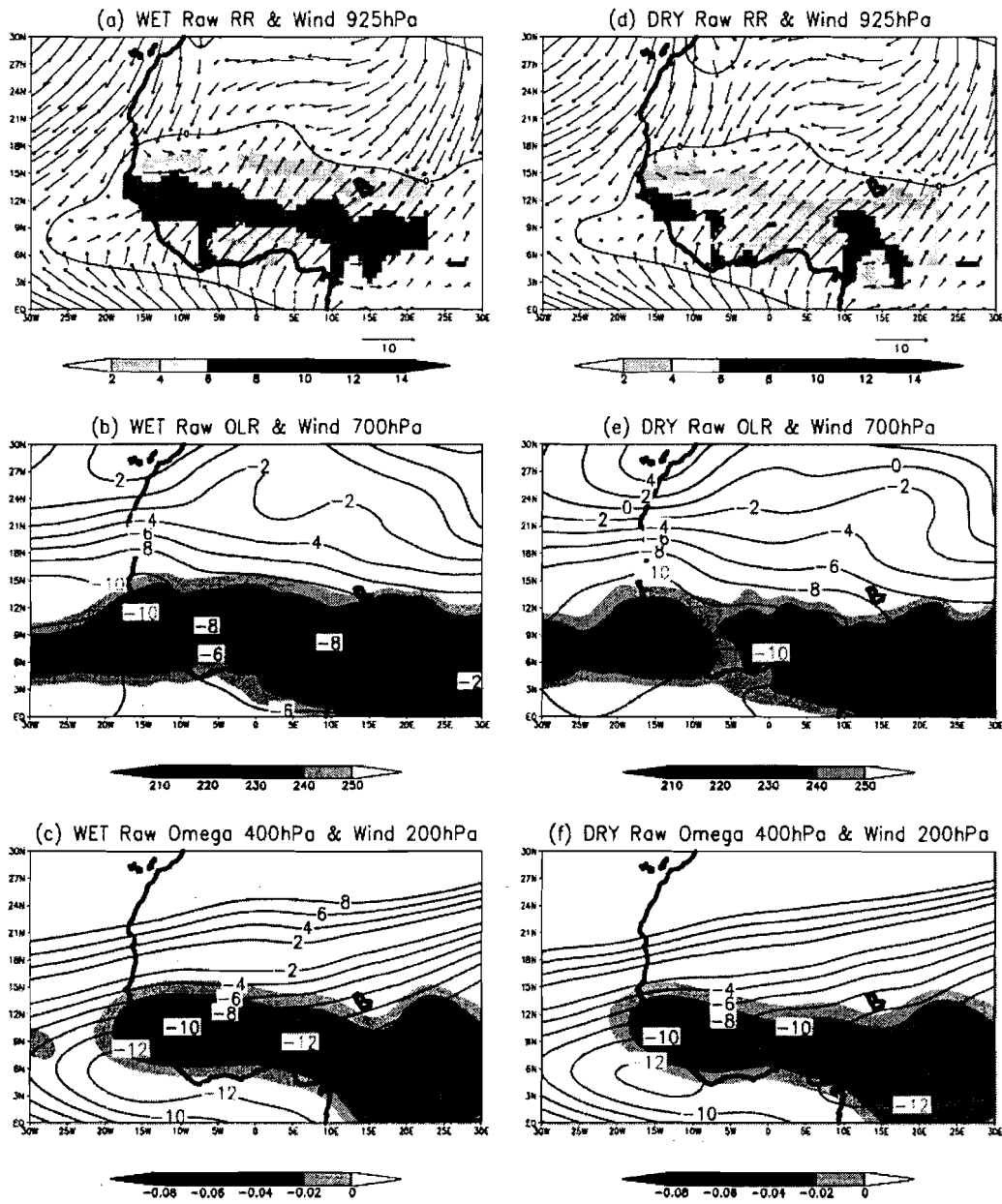


FIG. 6. (a) Unfiltered mean rainfall and 925-hPa wind fields for the composite 1968–90 summer wet sequence at t_0 . Rainfall is displayed in colors and expressed in mm day^{-1} . The wind is expressed in vectors and its scale (m s^{-1}) is displayed below. The black line represents the zero isoline of the zonal wind component to delineate the domain of the monsoon wind. (b) Same as (a) but for the OLR values (colors, in W m^{-2}) and the wind speed at 700 hPa (isolines in m s^{-1}). (c) Same as (a) but for the NCEP–NCAR vertical velocity at 400 hPa (colors, Pa s^{-1}) and the wind speed at 200 hPa (isolines in m s^{-1}). (d) Same as (a) but for the composite dry sequence at t_0 . (e) Same as (b) but for the composite dry sequence at t_0 . (f) Same as (c) but for the composite dry sequence at t_0 . Wet (dry) sequences are selected when the 10–25-day filtered regional rainfall index is max (min) and greater (lower) than 30% of the seasonal-filtered rainfall signal.

imum) and greater (lower) than 30% of the seasonal-filtered rainfall signal. Figure 6a shows the corresponding rainfall and 925-hPa wind fields for the wet sequence at t_0 . The black line represents the zero isoline of the zonal wind component to delineate the domain

of the monsoon winds. Figure 6d shows the similar fields for the dry sequence. The impact of the 10–25-day intraseasonal variability on the ITCZ rainfall field appears in these two figures as very high through the differences in the rainfall amounts and their spatial

extent, which confirms the previous results. We observe very clearly that during a dry phase, rainfall over West Africa is lower than during a wet phase, convection is strongly decreased in the heart of the ITCZ, and the northern boundary of the rainfall area is displaced by several degrees to the south. The amplitude of the rainfall difference is very high related to its mean as seen in Fig. 5b. Moreover, the rainfall modulation between a wet phase and a dry one concerns the whole of West Africa, both in latitude and in longitude, meaning that these intraseasonal timescale variations belong to an extended spatial pattern. During a dry phase, the northern boundary between the dry northeasterly winds and the moist southwesterly winds, delineated by the zero isoline of the zonal wind component, is weakly modified except a southward displacement at the longitude of Lake Chad (15°E). We also observe that the area of the southwesterly winds over the tropical Atlantic off the western coast of West Africa is less extended, meaning a weaker moisture advection over West Africa.

Figures 6b and 6e show similar fields for OLR and the wind speed at 700 hPa. OLR values are consistent with rainfall values, highlighting the deep convection decrease in the ITCZ during a dry phase. The wind fields characterize the location of the African easterly jet (AEJ) in the midlevels of the troposphere, and show an increase of the speed of this jet during a dry phase by about 2 m s^{-1} . At higher levels (Figs. 6c and 6f), the NCEP–NCAR upward velocities at 400 hPa are also weaker in the ITCZ during a dry phase, and the wind speed at 200 hPa, describing the tropical easterly jet (TEJ), is also weaker by about 1 m s^{-1} . It is worth noticing that the differences in the dynamical features of the West African monsoon between wet and dry phases at the intraseasonal timescale are similar to the ones observed at the interannual timescale (Newell and Kidson 1984; Fontaine and Janicot 1992). We suggest that similar connections between convection and the atmospheric circulation over West Africa must operate at both these timescales.

b. Time sequence of convection and low-level wind fields

Figure 7 shows the composite “wet–dry” time sequence of the unfiltered rainfall and 925-hPa wind fields from $t_0 - 7$ days to $t_0 + 7$ days by a step of 2 days. As for Fig. 6, wet (dry) sequences are selected when the 10–25-day filtered regional rainfall index is maximum (minimum) and greater (lower) than 30% of the seasonal-filtered rainfall signal. The rainfall values displayed in the figure are the ratio of the wet–dry–unfiltered rainfall to the seasonal-filtered rainfall signal. They are expressed in percentages of the seasonal time-

scale signal.¹ The corresponding composite 925-hPa wind field is computed as the unfiltered wind difference between the wet and the dry sequences. All the unfiltered fields presented in Fig. 7 and in the following figures are very similar to the filtered ones computed from the 10–25- or the 10–60-day filtered values. As the rainfall fields have a limited geographical extension, due to the limited available dataset, Fig. 8 shows the same sequence but on a larger domain by using OLR values. In this figure, the wind fields, displayed by streamlines, have been computed using a 3-day moving average to get a bit smoother fields for a better clarity; OLR values are the unfiltered wet–dry differences, not expressed in percentages as it is done for rainfall. Rainfall fields in Fig. 7 (computed from the period 1968–90) and OLR fields in Fig. 8 (computed from the available period 1979–90) show very similar anomalies, and both are very consistent with the wind anomaly fields (computed from the period 1968–90 in both Figs. 7 and 8). It is worth while to repeat that all these datasets come from independent measurements. The vector fields in Fig. 7 provide the amplitude of the wind anomalies and the streamlines in Fig. 8 help to better see the patterns of the wind fields.

Patterns in Figs. 7 and 8 characterize the modulations due to a typical intraseasonal wet phase occurring over West Africa. Reverse patterns must be considered for a typical dry phase. The total wind fields are the superposition of these modulations on the mean wind field presented in Figs. 6a and 6d. At this stage of the study, we do not provide any mechanism to explain the onset and the development of such a typical intraseasonal wet phase. Doing so would require us to focus on individual cases. Here by the composite approach based on large datasets we only document how convection and atmospheric circulation patterns are modulated during this composite time sequence. At the end of this part, we add some comments about how this can be interpreted.

At $t_0 - 7$, rainfall deficit over West Africa is at the highest stage, preceding the following setup of the intraseasonal wet sequence; at this time the regional rainfall index for the wet sequence has its lowest value before the convective maximum (Fig. 5). This dry stage is consistent with an extended enhanced advection of dry air from a northerly low-level atmospheric circulation. This circulation is first associated with the enhancement of the anticyclonic circulation centered at 20°N , 25°W , second with the enhancement of the cyclonic center located above Lake Chad (15°N , 15°E)

¹ We first compute the mean wet rainfall anomaly expressed in percentages of the seasonal timescale signal, averaged for all the wet retained cases. For instance, a value of 120% means that the rainfall modulation due to the wet cases represents a mean positive fluctuation of +20% of the rainfall modulation due to the seasonal cycle. We do the same for the dry cases, say for instance 70%, that is a modulation of -30%. We compute the wet minus dry difference, that is $(+20) - (-30) = +50\%$ and we express this value as 150% in Fig. 7.

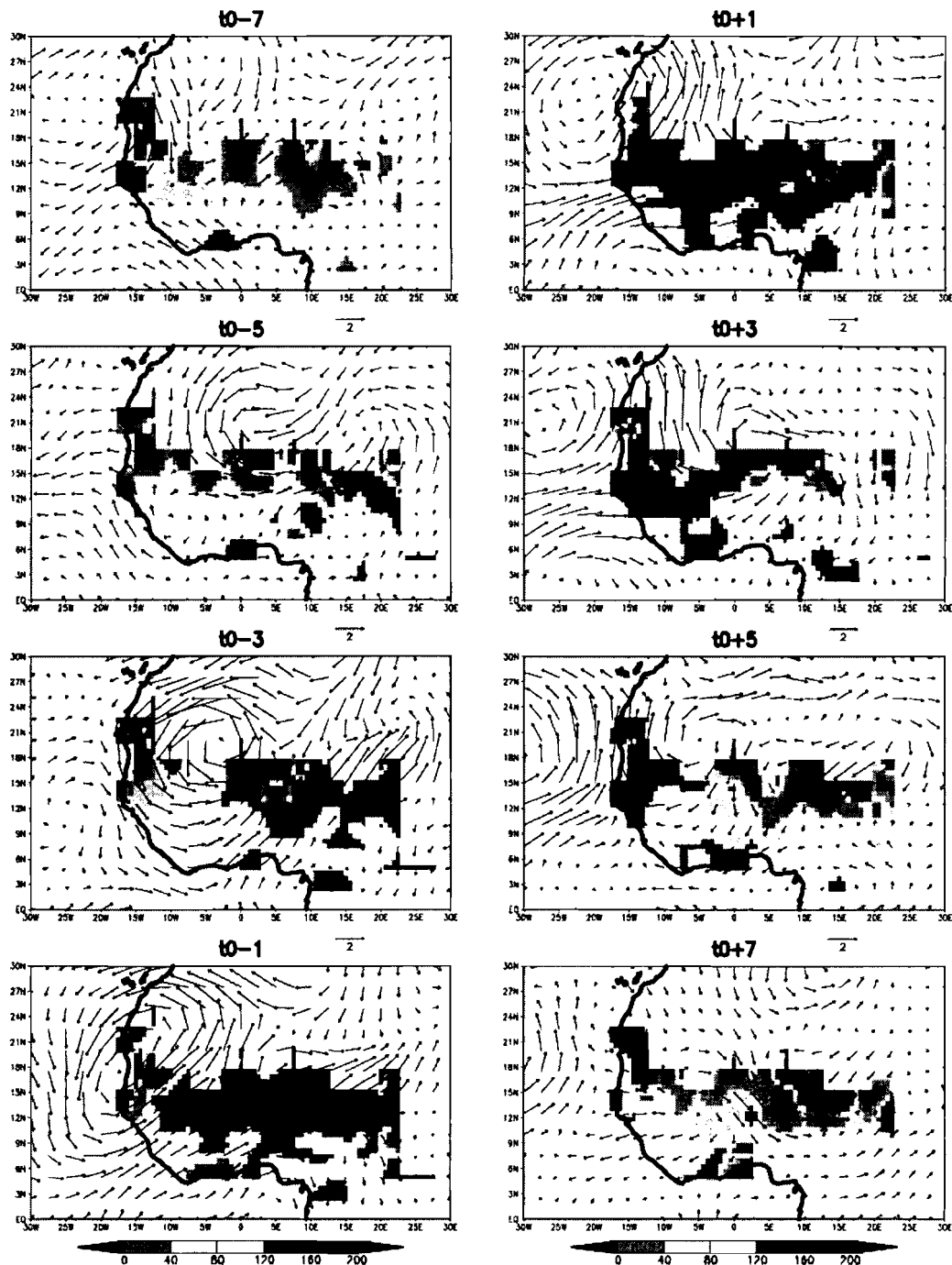


FIG. 7. The composite 1968–90 wet–dry time sequence of the unfiltered rainfall field (colors) and the 925-hPa wind field (vector) from $t_0 - 7$ days to $t_0 + 7$ days by a step of 2 days. Wet (dry) sequences are selected when the 10–25-day filtered regional rainfall index is max (min) and greater than 30% of the seasonal-filtered rainfall signal. The rainfall values displayed in the figure are the ratio of the daily unfiltered rainfall to the seasonal-filtered rainfall signal. They are expressed in percentages of the seasonal timescale signal and displayed for values lower than 80% and greater than 120%. The corresponding composite 925-hPa wind field is computed as the unfiltered wind difference between the wet and the dry sequences. The scale (m s^{-1}) is displayed below.

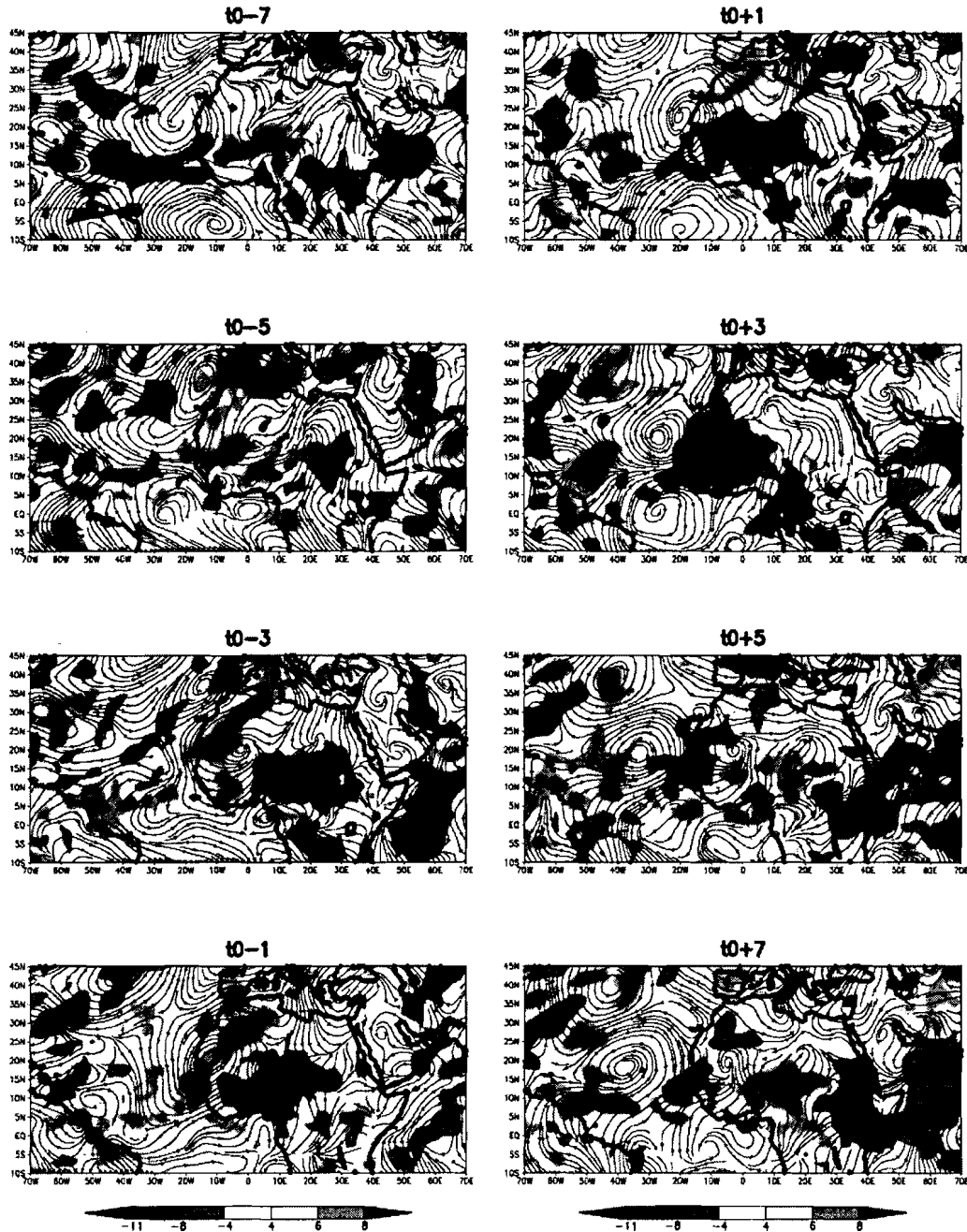


FIG. 8. Same as Fig. 7 but for OLR values instead of rainfall values, and displayed on a wider domain. In this figure, the 925-hPa wind fields are displayed by streamlines and have been computed using a 3-day moving average to get a bit smoother field for better clarity. The composite OLR sequence has been computed from the available period 1979–90 and the composite wind sequence from the period 1968–90. OLR values (W m^{-2}) are the unfiltered value differences between wet and dry sequences, and not expressed in percentages as it is done for rainfall on Fig. 7.

with a northeast–southwest axis of the associated trough. The area of decrease convection over West Africa is surrounded westward and eastward by enhanced convective areas that represent the preceding (westward)

and the coming (eastward) intraseasonal wet phases (Fig. 8).

At $t_0 - 5$, positive rainfall anomalies associated with the coming wet phase appear in the northeastern part of

the domain. Figure 8 shows that this enhanced convective area first developed over central Africa in an increased southerly wind field linked to the enhanced trough located along 20°E over the Sahara. At this time, two abnormal cyclonic centers are present, the first one at 20°N, 0°, already seen above Lake Chad at $t_0 - 7$, which has moved westward, the second one being stationary at 20°N, 15°E. These two cyclonic centers are associated with an increased westerly wind field over most of West Africa.

At $t_0 - 3$, the enhanced convective area is now well developed east of 0° in the enhanced southwesterly wind field associated with the two cyclonic centers, the first one continuing westward and now centered at 20°N, 5°W, whereas the second one is still stationary at 20°N, 20°E. These two centers, separated by about 25° longitude, lead to a zonally extended area of enhanced moist southwesterly winds over West Africa, consistent with the buildup of a similarly extended area of enhanced convection in the ITCZ.

At $t_0 - 1$, the first cyclonic center is now located along the western coast of West Africa and the enhanced convective area extends westward in the increased southerly winds located east of this center, covering most of West Africa. The second cyclonic center remains between 20° and 30°E, and is linked, with the first center, to the enhanced southwesterly wind field over all of West Africa. In the southwesterly wind field between the two cyclonic centers, an abnormal anticyclonic ridge appears northwest of Lake Chad. This indicates the following cutoff of the large cyclonic circulation over West Africa, due to the fact that the first cyclonic center continues on westward whereas the second one is still maintained around 20°E. We notice at this stage that the positive anomalies of rainfall and convection cover the whole area where the ITCZ is located during northern summer, with the highest values located on the northern boundary of the ITCZ, that is, the latitudes of the Sahel area where we find most of the MCS trajectories. This is consistent with the rainfall and OLR patterns of Fig. 6 where we observe both the enhanced convection in the ITCZ and the northward extension of its northern boundary during a wet phase.

At $t_0 + 1$, all of West Africa is under the influence of the wet intraseasonal phase despite the fact that the ridge has now developed into a closed anticyclonic circulation at 15°N, 5°W. This may be due to the convergence between abnormal southwesterly winds still associated with the first cyclonic center now located at 20°W and abnormal easterly winds along 10°N associated with the anticyclonic center. A second abnormal anticyclonic circulation is now formed above Lake Chad (it was slightly formed at $t_0 - 1$) and is linked to an abnormal northerly wind field over central Africa, that is, weakened southerly winds. This wind field has merged with the enhanced northerly wind field located above the Sahara previously associated with the second quasi-stationary cyclonic center, which leads then to a

large abnormal northerly wind field evident from 45°N to 10°S along 20°E. These dry northerly winds also mark very clearly the eastern boundary of the enhanced convection area of the wet phase. It is worth noting at this stage the evidence of another abnormal cyclonic circulation centered at 40°N, associated with the increased northerly winds at 20°E and north of 20°N since $t_0 - 3$. The role of atmospheric interactions from midlatitudes in the initiation of these intraseasonal timescale sequences over West Africa should be considered, but it is out of the scope of this paper.

At $t_0 + 3$, the enhanced convective area is now located westward of 0° in the remaining enhanced southerly winds located between the cyclonic center at 30°W and the anticyclonic center at 0°. The enhanced convective area may have been also maintained since $t_0 - 1$ by a stronger westerly moisture advection located over the tropical Atlantic off the western coast of West Africa. Behind the anticyclonic center, enhanced northerly winds develop and are associated with the extension of the dry phase following the wet phase. Negative values for rainfall and positive values for OLR appear east of Lake Chad, in concomitance with the increased northerly winds previously present at 20°N and now associated with a new anticyclonic ridge north of 20°N and between 10° and 30°E.

At $t_0 + 5$, the positive rainfall and negative OLR anomalies associated with the wet phase are now limited along the western coast of West Africa while the cyclonic center goes on propagating westward over the tropical Atlantic. We note a northward extension of these anomalies along the coast up to North Africa, already present in the preceding days, in the latitudinally extended area of abnormal southerly winds. The weakened convective area is now widely developed east of 0° in the abnormal northerly winds now covering most of West Africa and are both associated with the westward-moving anticyclonic center and the development of the anticyclonic ridge at 20°E. East of this decreased convective area, a new enhanced convective area is developing above eastern-central Africa in increased southerly winds, which will become the next intraseasonal wet phase.

Finally, at $t_0 + 7$, the weakened convective area goes on propagating westward. This stage corresponds to the time where the regional rainfall index for the wet sequence has its lowest value after the convective maximum (Fig. 5). This area is surrounded westward and eastward by enhanced convective areas that first represent (westward), the preceding wet phase associated with the cyclonic center still moving westward over the tropical Atlantic, and second (eastward), the next developing wet phase.

In this description, we have not attempted to introduce any cause and effect relationship. Instead, at this stage we introduce the concept of the "suprasynoptic" scale developed for the medium-range forecast (Persson 1984; Atger 2000). The idea is that the range of predictability

depends on the spatial scale of the phenomena that we want to predict. So to achieve reliable medium-range forecasts beyond 3 days, we must give up the synoptic scale and consider a larger scale, the suprasynoptic scale where the synoptic details are smoothed or filtered. Such suprasynoptic patterns appear to be similar to the classic synoptic fields except that they belong to a larger spatial scale and that they develop and propagate more slowly. This can be associated with the concept of weather types that induce specific characteristics and distributions of the classic synoptic weather systems. This is what we observe over West Africa (Fig. 8) where the wind field patterns are similar to the synoptic-scale easterly waves but with a greater wavelength (about 6000 km for the suprasynoptic scale instead of 3000 km for the synoptic scale) and a slower westward propagation (4° lon day $^{-1}$ instead of 8° day $^{-1}$), finally giving a period of about 15 days for the suprasynoptic scale instead of 4 days for the synoptic scale. We do not provide any mechanism for the occurrence of such weather types but we show their existence and indicate that they represent a modulation of the synoptic-scale activity at a larger scale. This corresponds to the dominant periodicities that we highlighted at the 10–25-day range, and not necessarily to the longer timescale, 25–60-day, which may be more specific to the intraseasonal timescale such as for the Madden-Julian Oscillation (MJO) for instance (Matthews 2002).

We can consider more precisely the modulation of the synoptic-scale easterly wave activity by the intraseasonal variability. Easterly wave activity over the Sahel can be characterized by the 700-hPa meridional wind component at 15°N , 0° (Diedhiou et al. 1999). Figure 9 displays the mean 1968–90 intraseasonal wet–dry composite of the wavelet modulus of the NCEP–NCAR 700-hPa meridional wind component at 15°N , 0° , from $t_0 - 15$ to $t_0 + 15$. Wavelet analyses have been completed separately for each wet and dry time sequence. Then, the individual “wet” wavelet spectra have been averaged, as well as the individual “dry” wavelet spectra, and we finally computed the difference of the two mean spectra. Figure 9a shows an enhancement of the easterly wave fluctuations for the periodicities 2.5–8 days from $t_0 - 2$ and $t_0 + 4$ during a typical intraseasonal wet sequence. It represents about 20% of the mean signal associated to these waves. When integrating the values of this diagram over the periods 2.5–10 days, we can observe a mean periodicity of 14 days for the amplitude of the wavelet signal, with a maximum at $t_0 + 1$ and two minima at $t_0 - 6$ and $t_0 + 8$ (Fig. 9b). Such variability in the easterly wave activity over the Sahel has recently been pointed out for the individual year 1992 (Redelsperger et al. 2002). We show here that it is valid for a high number of years and that it is embedded in a specific mode of intraseasonal variability that we designed as suprasynoptic.

As it was noticed previously, the distribution of the wet and the dry phases is not strictly uniform along the

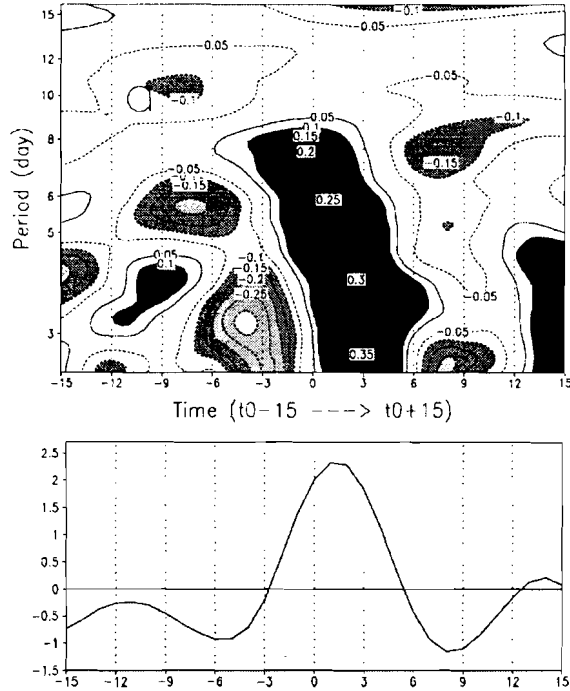


FIG. 9. Mean 1968–90 intraseasonal wet–dry composite of the wavelet modulus of the NCEP–NCAR 700-hPa meridional wind component (m s^{-1}) at 0° , 15°N , from t_0 minus 15 days to t_0 plus 15 days. (a) Only periods lower than 15 days are presented. Values greater than 0.1 are shaded. (b) The modulus time series generated by scale averaging over the 2.5–10-day period band is expressed in standardized anomalies.

northern summer. Their occurrences are the highest in June (30%) and the lowest in August (18%). An automatic classification (Janicot 1992) of the 10–25-day 925-hPa wind field patterns at t_0 has been performed for separately the wet and the dry phases into three classes. The three classes are seasonally distributed, one class gathering most of the phases of June, another class the phases for July–August, and a last one for September. Then, when recomputing the difference wet–dry fields at t_0 for the “June” class, the “July–August” class and for the “September” class, we get three wind field patterns close to the composite one of Fig. 7, but with a strong and well-organized July–August field, a rather well-organized September field, and a weaker organized June field (not shown). So the intraseasonal phase distribution is a bit biased toward June, but the composite summer wind fields are more representative of the July–August and the September phases, that is, in the heart of the West African summer monsoon.

Figure 10 displays the longitude–time diagram of the wet–dry sequence of unfiltered OLR along the latitude band 12.5° – 15°N , from $t_0 - 25$ to $t_0 + 25$, and from 40°E to 70°W . This diagram highlights the westward propagation of longitudinally extended areas of enhanced and weakened convection already seen over

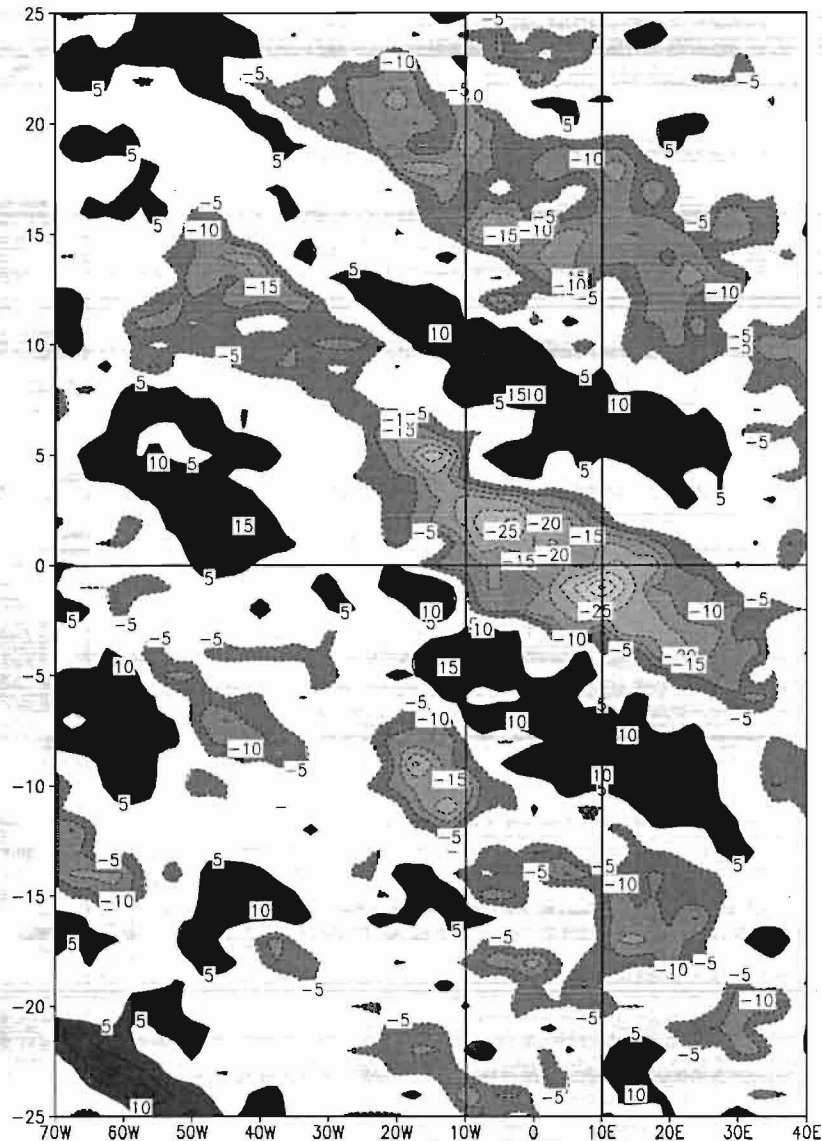


FIG. 10. Lon-time diagram of the composite 1979–90 wet-dry sequence of the unfiltered OLR values along the latitude band 12.5° – 15° N, from $t_0 - 25$ days to $t_0 + 25$ days. The computation method is the same as for Fig. 8. Vertical lines delineate the area 10° W– 10° E.

West Africa but that, in fact, extend from eastern Africa to the western tropical Atlantic. The signal associated to the wet-dry phase over West Africa at t_0 disappears along 50° W because the OLR anomalies move northward at $t_0 + 15$, where they are still evident on the three following days (not shown). The signal is logically the greatest over West Africa around t_0 since it has been selected through the regional rainfall index on this area, and the highest values go up to more than 30 W m^{-2} in absolute value. We also observe that the typical wet sequence centered on t_0 is embedded in a sequence of several intraseasonal phases, two of them before it and

two of them after it. As these phases were computed from unfiltered values, this figure highlights the significant modulation of convection over West Africa at an intraseasonal timescale centered around 15 days, as seen in Fig. 5.

c. Vertical structure of the intraseasonal signal

Figure 11 shows latitude-pressure cross sections along the band 10° W– 10° E of the meridional circulations associated with the intraseasonal signal. For simplicity, we use here the “Hadley” nomenclature whereas

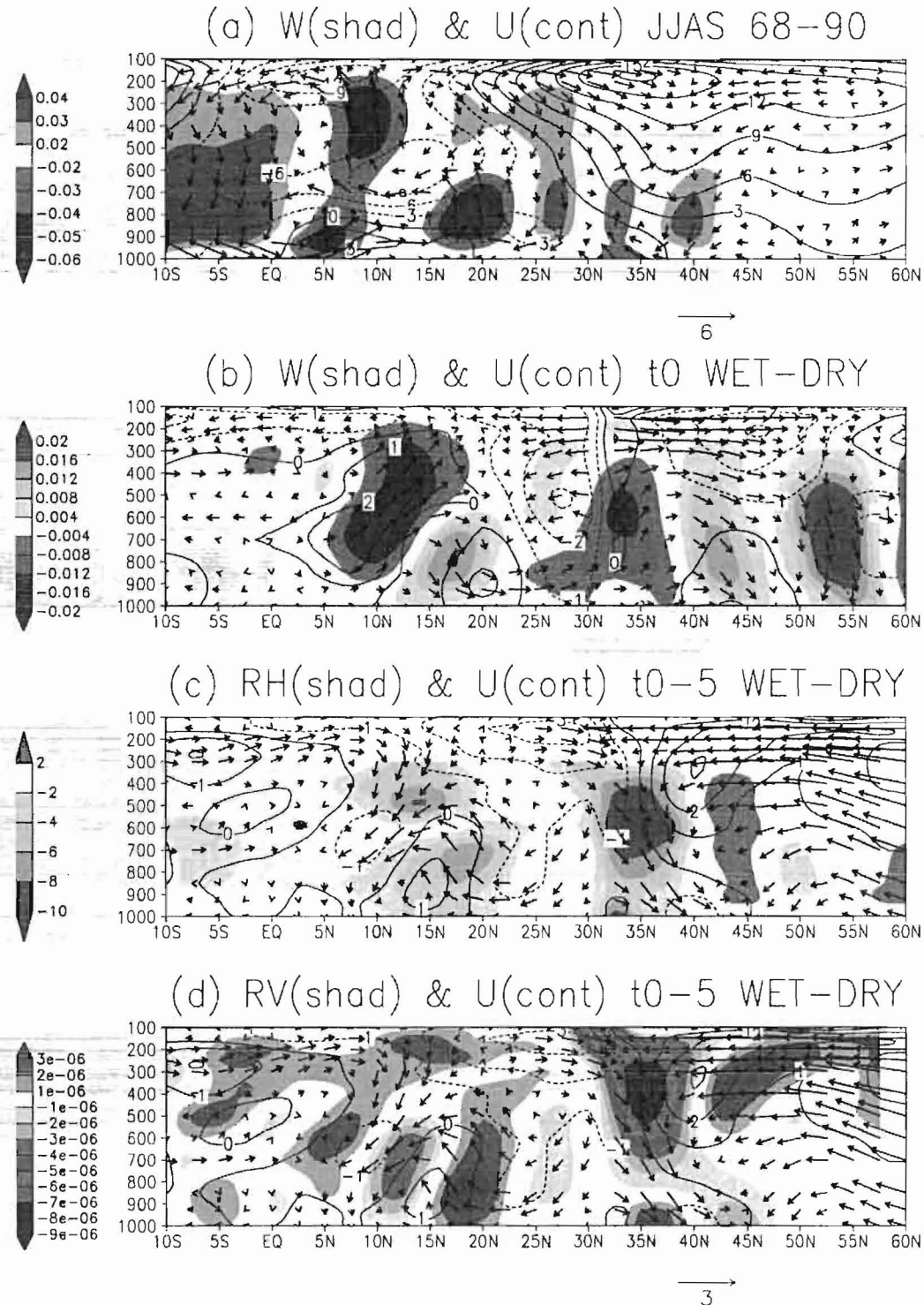


FIG. 11. (a) Lat-pressure cross section of the (10°W – 10°E) averaged meridional circulation computed on Jun–Sep 1968–90. Vectors display the (v, w) circulation, colors the amplitude of the vertical velocity (negative upward), and isolines the zonal wind (m s^{-1}). (b) Same as (a) but for the unfiltered mean meridional-vertical wind field of the composite 1968–90 summer wet-dry sequence at t_0 . The vertical velocity is displayed in colors and expressed in Pa s^{-1} . The zonal wind component is displayed in isolines (m s^{-1}). (c) Same as (b) but at $t_0 - 5$ with colors representing relative humidity (%). (d) Same as (c) but with colors representing relative vorticity (s^{-1}).

the 10°W – 10°E band is too small a longitude band to use it. Figure 11a presents the mean meridional circulation (vectors, with colors areas for vertical velocity) computed on June–September 1968–90, as well as the zonal wind component (isolines). The main features of the circulation over these regions are evident: two Hadley-type circulations with the specific structure over West Africa of upward velocities in the whole troposphere at the location of the ITCZ at 10°N , and subsiding velocities south of the equator and between 25° and 40°N ; upward velocities limited to the lower troposphere associated to the dry convection in the heat low at 20°N ; the westerly winds of the monsoon layer between the equator and 20°N ; the two easterly jets, the AEJ in the midlevels between 10° and 15°N and the TEJ in the upper troposphere at 5°N ; the subtropical westerly jet in the upper troposphere at 35°N .

Figure 11b shows the unfiltered mean meridional circulation of the composite 1968–90 summer wet–dry sequence at t_0 . The vertical velocity differences are displayed in colors and the zonal wind anomalies in isolines. We see again that the specific wet phase is characterized by a stronger deep convection in the ITCZ that extends to the north, as well as a decreased dry convection in the heat low. This leads to an enhanced southern Hadley-type circulation and a weakened northern Hadley-type circulation. In consistency with the pattern of the anomalous meridional circulation, we observe positive zonal wind anomalies over West Africa depicting the enhancement of the monsoon winds in the low levels and the decrease of the AEJ in the midlevels, as well as negative anomalies in the upper levels leading to an enhancement of the TEJ and a weakening of the subtropical westerly jet. The associated relative vorticity anomaly pattern (not shown) indicates that the circulation pattern seen at 925 hPa (Fig. 7) is in fact present in the part of the troposphere under the 500-hPa level with a rather barotropic structure.

Figures 11c and 11d show similar patterns of meridional circulation but for $t_0 - 5$. At this time (see Fig. 8), the zone of enhanced convection that will be present over West Africa at t_0 is located east of Lake Chad, embedded in an enhanced southerly low-level flow linked to the cyclonic center at 20°N , 20°E . The other cyclonic center is located at 20°N , 0° . These centers are associated over West Africa with two axes of enhanced northerly dry flow, one coming from the Mediterranean Sea along 15°E , another one located between the western coast of West Africa and the Greenwich meridian. This dry wind field is associated with a weakened convection over West Africa and a dry rainfall sequence preceding the occurrence of the wet sequence coming from the east. Figure 11c depicts the modulation of the mean meridional circulations on 10°W – 10°E as well as the relative humidity anomalies. This circulation pattern is opposite to the one related to t_0 (Fig. 11a). At $t_0 - 5$, the subsidence in the northern Hadley-type circulation between 30° and 40°N is enhanced, linked to an ab-

normal wind convergence above 300 hPa, and the subsiding air is drier than normal. This air diverges at the lower levels and a part of it is directed toward the south as it has just been described (Fig. 8). Then it can mix into the heat low where dry convection increases. The zonal wind field at these levels, as well as the relative vorticity field (Fig. 11d), shows that the cyclonic vorticity increases in the heat low that extends on the vertical. This increase of the heat low activity and of the associated meridional overturning may induce a stronger intrusion of drier air into the ascending air column of the ITCZ and a weakening of deep convection and of the southern Hadley-type circulation. This abnormal mean wind field pattern may induce interactions between the midlatitudes and the ITCZ, in particular by favoring southerly advection of dry air from the northern midlatitudes as it is shown for instance in Roca et al. (2002). However this hypothesis needs a specific examination of ensembles of air parcel trajectories, which is out of the scope of this study.

6. Conclusions

Rainfall variability over West Africa has usually been analyzed either through the MCS scale, the synoptic scale, or the interannual and decadal scales. Very few studies have investigated the West African monsoon through the intraseasonal timescale. A documentation of such variability has been produced by using daily gridded datasets of rainfall, convection, and reanalyzed atmospheric fields over the period 1968–90. Rainfall and convection over West Africa are significantly modulated at two intraseasonal timescales, 10–25 and 25–60 days, leading to variations of more than 30% of the seasonal signal. A composite analysis based on the dates of maximum (minimum) of a regional rainfall index in wet (dry) sequences shows that these sequences last in average 9 days and belong to a main quasi-periodic signal of about 15 days. A secondary periodicity of 38 days is present but leads to a weaker modulation. During a wet (dry) sequence, convection in the ITCZ is enhanced (weakened) and its northern boundary moves to the north (south), while the speed of the African easterly jet decreases (increases), the speed of the tropical easterly jet increases (decreases), and the monsoon flow becomes stronger (weaker), all these features being similar to the ones associated with interannual variability characterizing wet and dry years.

This modulation of convection at intraseasonal timescales is not limited to West Africa, but corresponds to a westward-propagating signal from the eastern Africa to the western tropical Atlantic. The enhanced (weakened) phases of the West African monsoon are associated with a stronger cyclonic (anticyclonic) activity over the Sahel, linked to stronger (weaker) moisture advection over West Africa. Five days before the full development of the wet phase, a stronger cyclonic circulation at 20°E induces enhanced southerly winds along 25°E

where convection enhances, while another westward-propagating cyclonic circulation is located at 0° . This atmospheric pattern is linked to the enhancement of the subsiding branch of the northern Hadley cell at 35°N , of the northerly advection of drier air over West Africa, and to increased dry convection in the heat low at 20°N . It propagates westward leading to a zonally extended area of enhanced monsoon winds over West Africa consistent with the occurrence of the wet phase.

We have proposed to apply the concept of the suprasynoptic scale developed for the medium-range forecast. To achieve reliable medium-range forecasts beyond 3 days, the synoptic scale must be given up and a larger scale, the suprasynoptic scale must be considered where the synoptic details are smoothed or filtered. Such suprasynoptic patterns appear to be similar to the classic synoptic fields except that they belong to a larger spatial scale and that they develop and propagate more slowly. This can be associated with the concept of weather types that induce specific characteristics and distributions of the classic synoptic weather systems like easterly waves or of the MCS life cycle. We showed the existence of such weather types over West Africa and indicated that they represent a modulation at a larger scale of the synoptic-scale activity of easterly waves. This corresponds to the dominant periodicities that we highlighted at the 10–25-day range, and not necessarily to the longer time-scale, 25–60 days, which may be more specific to the intraseasonal timescale such as for MJO for instance.

We did not provide any mechanism for the occurrence of such weather types; it should be the next step. One of the main questions that arose is the role of scale interactions between MCS and synoptic-scale weather systems like easterly waves (Redelsperger et al. 2002). Kiladis and Weickmann (1997), studying the 6–30-days fluctuations of convection over West Africa, suggested that such a signal could be induced by convection. This raises the question of the role that one MCS can play on the following convection. At a local scale, Taylor et al. (1997) suggested that a MCS can induce a moistening of the boundary layer, favorable to the development of a new MCS at the same location, as was observed during the Hydrology–Atmosphere Pilot Experiment in the Sahel (HAPEX-Sahel) field experiment in 1992 (Taylor and Lebel 1998). Could such a local inter-MCS connection work at a larger scale through interactions with the monsoon flow and/or synoptic easterly waves to build the intraseasonal-scale variability observed over West Africa? It is one of the questions that the international project of the African Monsoon Multidisciplinary Analyses (AMMA; information available online at <http://medias.obs-mip.fr/amma>) wishes to address.

Acknowledgments. We are thankful to NOAA–CIRES Climate Diagnostics Center (Boulder, CO) for providing the NCEP–NCAR reanalysis dataset and the interpolated OLR dataset from their Web site (<http://www.cdc.noaa.gov/>). We also thank the two anonymous

reviewers who helped to improve this paper. This research was in part supported by the EC Environment and Climate Research Programme (Contract: EVK2-CT-1999-00022).

REFERENCES

- Atger, F., 2000: The medium-range weather forecast in France (in French). *La Météorologie*, 8th Series, **30**, 61–86.
- Burpee, R. W., 1972: The origin and structure of easterly waves in the lower troposphere in North Africa. *J. Atmos. Sci.*, **29**, 77–90.
- Diedhiou, A., S. Janicot, A. Viltard, and P. de Felice, 1998: Evidence of two regimes of easterly wave over West Africa and the tropical Atlantic. *Geophys. Res. Lett.*, **25**, 2805–2808.
- , —, —, —, and H. Laurent, 1999: Easterly wave regimes and associated convection over West Africa and the tropical Atlantic: Results from NCEP/NCAR and ECMWF reanalyses. *Climate Dyn.*, **15**, 795–822.
- Duvel, J. P., 1989: Convection over tropical Africa and the Atlantic Ocean during northern summer. Part I: Interannual and diurnal variations. *Mon. Wea. Rev.*, **117**, 2782–2799.
- , 1990: Convection over tropical Africa and the Atlantic Ocean during northern summer. Part II: Modulation by easterly waves. *Mon. Wea. Rev.*, **118**, 1855–1868.
- Folland, C. K., T. N. Palmer, and D. E. Parker, 1986: Sahel rainfall and worldwide sea temperature 1901–1985. *Nature*, **320**, 602–607.
- Fontaine, B., and S. Janicot, 1992: Wind field coherence and its variations over West Africa. *J. Climate*, **5**, 512–524.
- Gibson, J. K., P. Kalberg, S. Uppala, A. Hernandez, A. Nomura, and E. Serrano, 1997: ERA description. ECMWF Re-Analysis Project, Rep. Series 1, ECMWF, Reading, United Kingdom, 72 pp.
- Grodsky, S. A., and J. A. Carton, 2001: Coupled land/atmosphere interactions in the West African monsoon. *Geophys. Res. Lett.*, **28**, 1503–1506.
- Gruber, A., and A. F. Krueger, 1984: The status of the NOAA outgoing longwave radiation data set. *Bull. Amer. Meteor. Soc.*, **65**, 958–962.
- Hastenrath, S., 1995: *Climate Dynamics of the Tropics*. Kluwer, 488 pp.
- Hodges, K. I., and C. D. Thorncroft, 1997: Distribution and statistics of African mesoscale convective weather systems based on the ISCCP METEOSAT imagery. *Mon. Wea. Rev.*, **125**, 2821–2837.
- Janicot, S., 1992: Spatiotemporal variability of West African rainfall. Part I: Regionalizations and typings. *J. Climate*, **5**, 489–497.
- , and B. Sultan, 2001: Intra-seasonal modulation of convection in the West African monsoon. *Geophys. Res. Lett.*, **28**, 523–526.
- , S. Trzaska, and I. Poccard, 2001: Summer Sahel-ENSO teleconnection and decadal time scale SST variations. *Climate Dyn.*, **18**, 303–320.
- Kalnay, E., and Coauthors, 1996: The NCEP/NCAR 40-Year Reanalysis Project. *Bull. Amer. Meteor. Soc.*, **77**, 437–471.
- Kiladis, G. N., and K. M. Weickmann, 1997: Horizontal structure and seasonality of large-scale circulations associated with sub-monthly tropical convection. *Mon. Wea. Rev.*, **125**, 1997–2013.
- Laing, A. G., and J. M. Fritsch, 1993: Mesoscale convective complexes in Africa. *Mon. Wea. Rev.*, **121**, 2254–2263.
- , and —, 1997: The global population of mesoscale convective complexes. *Quart. J. Roy. Meteor. Soc.*, **123**, 389–405.
- Lamb, P. J., 1978a: Large scale tropical surface circulation patterns associated with Subsaharan weather anomalies. *Tellus*, **30**, 240–251.
- , 1978b: Case studies of tropical Atlantic surface circulation patterns during recent sub-Saharan weather anomalies: 1967 and 1968. *Mon. Wea. Rev.*, **106**, 482–491.
- Le Barbé, L., T. Lebel, and D. Tapsoba, 2002: Rainfall variability in West Africa during the years 1950–90. *J. Climate*, **15**, 187–202.
- Liebmann, B., and C. A. Smith, 1996: Description of a complete

- (interpolated) outgoing longwave radiation dataset. *Bull. Amer. Meteor. Soc.*, **77**, 1275–1277.
- Mathon, V., and H. Laurent, 2001: Life cycle of Sahelian mesoscale convective cloud systems. *Quart. J. Roy. Meteor. Soc.*, **127**, 377–406.
- Matthews, A. J., 2002: Intraseasonal variability over West Africa. Preprints, *25th Conf. on Hurricanes and Tropical Meteorology*, San Diego, CA, Amer. Meteor. Soc., 652–653.
- Newell, R. E., and J. E. Kidson, 1984: African mean wind changes between Sahelian wet and dry periods. *J. Climatol.*, **4**, 27–33.
- Persson, A., 1984: The use of spectrally filtered products in medium-range weather forecasting. ECMWF Tech. Memo. 90, Reading, United Kingdom, 47 pp.
- Poccard, I., S. Janicot, and P. Camberlin, 2000: Comparison of rainfall structures between NCEP/NCAR reanalysis and observed data over tropical Africa. *Climate Dyn.*, **16**, 897–915.
- Redelsperger, J. L., A. Djongue, A. Diedhiou, J. P. Ceron, M. Diop, J. F. Gueremy, and J. P. Lafore, 2002: Multi-scale description of a Sahelian synoptic weather system representative of the West African monsoon. *Quart. J. Roy. Meteor. Soc.*, **128**, 1229–1257.
- Reed, R. J., D. C. Norquist, and E. E. Recker, 1977: The structure and properties of African wave disturbances as observed during Phase III of GATE. *Mon. Wea. Rev.*, **105**, 317–333.
- Roca, R., C. Piriou, J. P. Lafore, and J. L. Redelsperger, 2002: Extratropical dry air intrusions in the West African monsoon region. Preprints, *25th Conf. on Hurricanes and Tropical Meteorology*, San Diego, CA, Amer. Meteor. Soc., 277–278.
- Rowell, D. P., 2001: Teleconnections between the tropical Pacific and the Sahel. *Quart. J. Roy. Meteor. Soc.*, **127**, 1683–1706.
- , C. K. Folland, K. Maskell, and M. N. Ward, 1995: Variability of summer rainfall over Tropical North Africa (1906–1992): Observations and modelling. *Quart. J. Roy. Meteor. Soc.*, **121**, 669–704.
- Scavuzzo, C. M., M. A. Lamfri, H. Teitelbaum, and F. Lott, 1998: A study of the low-frequency inertio-gravity waves observed during the Pyrenees Experiment. *J. Geophys. Res.*, **103** (D2), 1747–1758.
- Sow, C. S., 1997: Diurnal rainfall variations in Senegal. *Secheresse*, **8**, 157–162.
- Sultan, B., and S. Janicot, 2000: Abrupt shift of the ITCZ over West Africa and intra-seasonal variability. *Geophys. Res. Lett.*, **27**, 3353–3356.
- , —, and A. Diedhiou, 2003: West African monsoon dynamics. Part II: The “pre-onset” and the “onset” of the summer monsoon. *J. Climate*, **16**, 3407–3427.
- Taylor, C. M., and T. Lebel, 1998: Observational evidence of persistent convective-scale rainfall patterns. *Mon. Wea. Rev.*, **126**, 1597–1607.
- , F. Saïd, and T. Lebel, 1997: Interactions between the land surface and mesoscale rainfall variability during HAPEX-Sahel. *Mon. Wea. Rev.*, **125**, 2211–2227.
- Ward, M. N., 1998: Diagnosis and short-lead time prediction of summer rainfall in tropical North Africa at interannual and multi-decadal timescales. *J. Climate*, **11**, 3167–3191.

Seasonal cycle and interannual variability of the Sahelian rainfall at hydrological scales

Thierry Lebel, Arona Diedhiou, and Henri Laurent

Laboratoire d'étude des Transferts en Hydrologie et Environnement (UMR 5564), IRD, Grenoble, France

Received 10 December 2001; revised 16 December 2002; accepted 11 March 2003; published 29 April 2003.

[1] Sahelian rainfall is characterized both by a strong interannual variability and by periods of long-lasting droughts, such as the years 1970–1997. The controlling factors of this variability have been the subject of a significant amount of research, but most of this research is carried out using low-resolution averages, typically, monthly to seasonal in time and over $5^\circ \times 5^\circ$ grid boxes (or larger) in space. This paper is an attempt at characterizing the Sahelian rainfall regime at finer scales, with the objective of establishing links between the seasonal cycle and the interannual variability. To that end, high space-time resolution data sets are analyzed. One is composed of around three hundred daily rain gauges covering a $1,700,000 \text{ km}^2$ area for the period 1951–1990. The second is a set of full resolution Meteosat images covering the years 1989–1999, allowing for a systematic tracking of the mesoscale convective systems (MCSs). The third data set was produced from an experimental network of recording rain gauges covering $16,000 \text{ km}^2$ in the region of Niamey, Niger, during the years 1990–2000. The analysis of the regional daily rainfall data set tends to revisit the common vision of the seasonal cycle of the Sahelian rainfall. It is shown that the average regime is in fact composed of two subregimes. One is an oceanic regime characterized by a progressive increase of the moist air flow from the ocean into the continent, associated with the seasonal migration of the ITCZ from its southern position in the boreal winter to its northern position in the boreal summer. The second regime is a continental regime in which rain is mostly produced by large convective systems embedded in the easterly circulation. This continental regime sets in abruptly during the second half of June, and 90% of the Sahelian rainfall is then produced by a small number (12% of the total number) of large and organized mesoscale convective systems. The mean event rainfall associated with these systems is larger than the mean event rainfall observed in the oceanic regime. The average proportion of the Sahelian rainfall occurring during the continental regime represents between 75% and 90% of the total annual rainfall. It is thus necessary to study this regime in order to understand the interannual rainfall variability of the region better. It is shown, for instance, that the main factor of interannual variability is the variability of the number of the large convective systems from year to year. It is also shown, using NCEP/NCAR reanalysis, that the easterly waves, which are a major synoptic feature of the region, are not systematically associated with rain-efficient convective systems and that further studies are needed to understand the differences between wet and dry waves.

INDEX TERMS: 3309 Meteorology and Atmospheric Dynamics: Climatology (1620); 3354 Meteorology and Atmospheric Dynamics: Precipitation (1854); 3374 Meteorology and Atmospheric Dynamics: Tropical meteorology; 1812 Hydrology: Drought; *KEYWORDS:* West African Monsoon, Sahel, rainfall, seasonal cycle, convective systems

Citation: Lebel, T., A. Diedhiou, and H. Laurent, Seasonal cycle and interannual variability of the Sahelian rainfall at hydrological scales, *J. Geophys. Res.*, 108(D8), 8389, doi:10.1029/2001JD001580, 2003.

1. Introduction

[2] The variability of rainfall in West Africa has been the subject of several studies in recent years making substantial contributions toward the identification of the numerous factors that may control this variability, whether considering

ocean SSTs [Palmer, 1986; Lamb and Pepple, 1992; Janicot *et al.*, 1996; Fontaine *et al.*, 1998; Ward, 1998; Rowell, 2001], continental surface conditions [Charney *et al.*, 1977; Semazzi and Sun, 1997; Zheng and Eltahir, 1998; Wang and Eltahir, 2000], or atmospheric structures. [Burpee, 1972; Reed *et al.*, 1977; Cook, 1997; Thorncroft and Blackburn, 1999; Diedhiou *et al.*, 1998, 1999]. Obviously, all these factors interact in a complex way and it is possible to imagine that the importance of each controlling factor has

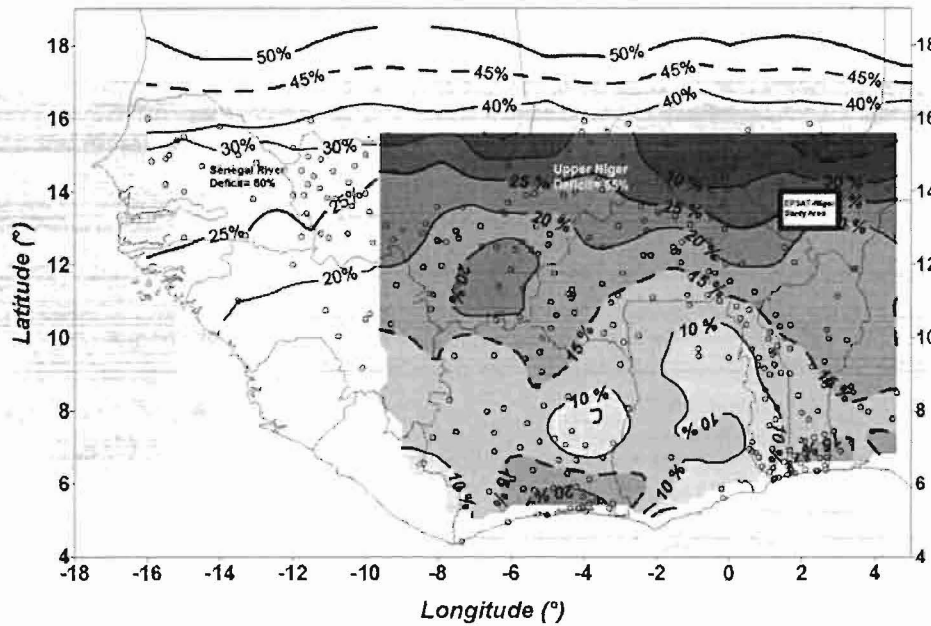


Figure 1. Map of the relative rainfall deficit of the years 1971–1990 compared to the wet years 1951–1970. Over the Sahel the deficit increases from 20% in the south to 50% in the north. The discharge deficit for the same period on the two largest Sahelian catchments (Sénégâl and upper Niger) is indicated. The corresponding average rainfall deficit is about 30% over the Sénégâl basin and 25% over the upper Niger basin. The area with filled contours is the region over which the average seasonal cycle was studied, using the daily reading rain gauges marked by open circles.

varied over the years, as pointed out by *Janicot et al.* [2001] showing significant differences in SST versus Sahelian rainfall correlation fields, depending on the period taken into account for the study. These authors show that the control from the oceans was probably not the same during the period 1954–1973, mostly composed of wet years (dominance of the Atlantic dipole), and during the period 1970–1989, almost exclusively composed of dry years (dominance of the ENSO signal, a warm ENSO event being associated with a lower than normal rainy season over the Sahel). Most surprising is the fact that when carried out over an intermediate period, still another region appears to dominate, that is the Indian Ocean. A number of reasons may be envisaged for explaining such an unstable behavior: modifications in the signal of the oceans themselves (the impact of the ENSO on the Sahelian rainfall becoming stronger, due to a decadal scale evolution of the global SST field); changes in the vegetation over the continent leading to a progressive shift in the meridional gradients of static energy, thus impacting on the signature of the oceans; modifications in the global atmospheric circulation, induced by changes in the global SST field and/or in the atmosphere itself.

[3] A vast majority of the diagnostic studies cited above consider rainfall patterns at large space-timescales, using monthly rain accumulations as their basic input data. To further progress in the understanding of how the various control factors might influence the Sahelian rainfall and impact on the regional water cycle, time has come to consider smaller scales. There are two main reasons for this. First, the Sahelian rainfall is mostly of convective origin. In a preliminary study, *Laurent et al.* [1998] esti-

mated that mesoscale convective systems (MCSs) produced 95% of the annual rainfall in the region of Niamey. They also showed that there was a strong co-fluctuation of the number of MCSs and of the total annual rainfall. It thus seems important to characterize these systems over the region and to study the synoptic structures capable of influencing their occurrence. Understanding how rainfall variability impacts on water resources variability is a second reason for studying the rainfall patterns at finer scales than monthly or seasonal. As shown in Figure 1, the discharge deficit computed in relative terms for the dry period 1970–1989 at the outlet of the large river basins of the region was twice the rainfall deficit. This amplification is linked to the intermittent nature of the rainfall signal forcing the hydrologic systems. The nonlinear response of these systems is strongly dependent on the timing of occurrence of the rain events. A dry spell will not have the same hydrological impact when it happens through a reduction of the average intensity of the rain events or as a reduction of the number of events over a given period, or as a mixture of both.

[4] As many rain events are associated with MCSs, there is a need to characterize the Sahelian rainfall regime at the scale of the convective event, in order to obtain a coherent vision from both the atmospheric and the hydrological points of view. This paper is therefore built around three converging investigations that are presented after a brief description of the data available to us (section 2). First, in section 3, the mean seasonal cycle of rainfall over West Africa is studied from daily rain observations. This tends to identify two regimes in the West African monsoon: an oceanic and a continental regime. This latter regime is associated with the Sahelian rainy season. Section 4 is

devoted to the study of the elements determining the seasonal cycle of this continental regime; these include rain events, convective systems and easterly waves. In section 5, it is shown that the interannual variability of Sahelian rainfall is strongly conditioned by the number of convective systems observed in the continental regime. A final discussion of future work concludes the paper.

2. Data Sets

[5] The study presented here makes use of four data sets. One consists of daily rainfall records obtained from a network of three hundred gauges covering an area of 1,700,000 km² ($14^{\circ} \times 10^{\circ}$) and a period of 40 years (1951–1990). This data set is described by *Le Barbé et al.* [2002] and the area covered is boxed in Figure 1. The second data set is an ensemble of full resolution Meteosat IR images, covering the months of July through September for the years 1989–1999. This data set is described by *Mathon and Laurent* [2001], the area covered being the whole of West Africa. The third data set comes from the high space-time resolution EPSAT-Niger network, covering 16,000 km² in the surroundings of Niamey, Niger (see Figure 1 for the location of the study area and *Lebel et al.* [1995] for a description of the network and the sensors used). This network of tipping bucket rain gauges with digitized recording has now operated for 12 years (1990–2001). There is thus a period of 10 years (1990–1999) jointly covered by the METEOSAT data set and the EPSAT-Niger data set, allowing for a precise quantification of the rainfall produced by each convective system over the EPSAT-Niger study area during the core of the rainy season. Finally, use will be made of the long-term reanalysis datasets of the National Center for Environmental Prediction/the National Center for Atmospheric Research (NCEP/NCAR; period 1979–1995) in order to characterize the atmospheric environment of the Sahelian MCSs.

3. Seasonal Cycle of the West African Monsoon

3.1. Classical Vision

[6] The West African Monsoon (WAM) is characterized by a seasonal cycle controlled by the meridional migrations of the sun and the associated maximum of received solar energy. The maximum of precipitation occurs in the Intertropical Convergence Zone (ITCZ). At its southernmost position, the boreal winter solstice, the ITCZ is located over the Guinea Gulf. It then moves northward, reaching its northernmost position in the boreal summer. At that time of the year the northern edge of the ITCZ (the ITF) may be located as far north as 18°N, even reaching 20°N. Since the maximum of received solar energy in the atmosphere regularly moves from south to north, so does the ITCZ according to the common vision of its dynamics. This in turn implies a progressive and regular onset of rain on the continent. A zone of subsidence trails the southern edge of the ITCZ. There are consequently two periods of rainfall on the coast, separated by a short dry season, when the zone of subsidence is over the continent. This zone rarely moves further than 7°N or 8°N. North of these latitudes the seasonal cycle is a regime of a single rainy season. The length of this rainy season decreases from 8 months or so in

the south to 3 months in the northern Sahel, since the ITCZ reaches this region only in June and retreats in September.

[7] Of course, this is an average climatology, and it has long been known that it is subject to a marked interannual variability. The ITCZ, for instance, may be confined south of 15°N on certain years or it can reach its normal position but retreat much earlier than normally. In both cases rainfall over the Sahel is in strong deficit. However, in this classical vision of monsoon dynamics, the main feature of the rainfall regime is a progressive transition from a regime of two rainy seasons on the coast to a single rainy season in the Sahel.

3.2. Revised Scheme Based on the Analysis of Daily Rainfall

[8] A few recent studies [*Eltahir and Gong*, 1996; *Fontaine et al.*, 1999] have suggested the importance of meridional gradients of moist static energy in controlling the dynamics of the WAM. A converging result of the theoretical study of *Eltahir and Gong* [1996] and of the data analysis presented by *Le Barbé et al.* [2002] is the nonlinear behavior of the rain onset on the West African continent. The two diagrams in Figure 2 are a clear illustration of this. They are derived from the regional daily rainfall data set. Regional daily rainfall maps were first obtained using a 2D kriging algorithm, for a period of 10 months (1 February to 30 November), the interpolation being performed on the $14^{\circ} \times 10^{\circ}$ grid at a $0.5^{\circ} \times 0.5^{\circ}$ resolution. Each map is a representation of the average over the years 1950–1990. These 300 maps considered together provide a 3D (latitude, longitude, day of year) representation of the rainfall regime. The two diagrams of Figure 2 are time-latitude sections in this 3D representation, each for a given longitude. This allows the examination of the time dynamics of the rain intrusion on the continent along two south to north transects. The two maps are similar on a few key points. First, the two well-known maxima of rain are clearly visible at the coast and, north of 10°N, there is a unique zone of rain. This conforms to the well-known basics of the rain climate in this region. There is, however, another common point between these two maps, which is a clear departure from the classical vision of the monsoon dynamics discussed above. Indeed, one can clearly see, looking for instance at the isohyet 5 mm/day, that the Sahelian rainy season is not totally connected to the first rainy season at the coast. Starting mid-June, a sudden reinforcement of the mean daily rainfall occurs between 9°N and 12°N. It then propagates rapidly to the north during the month of June. This jump is more abrupt on the 5°W map than on the 2°E map, but in both cases the idea of a rain front progressing regularly from the coast to the Sahel is challenged. Looking at these two maps, one could define the Sahel as the region where there is a sudden reinforcement of rain happening at the same time over a band covering several degrees in latitude. Before discussing further this issue, a few other important points deserve to be mentioned here, even though they concern the whole regime of West Africa, rather than the Sahel specifically.

[9] First, there is a transition zone, roughly located between 7.5°N and 9.5°N, where the rainfall regime is not characterized by one or two well identifiable rain peaks but rather by a succession of three maxima, each corresponding

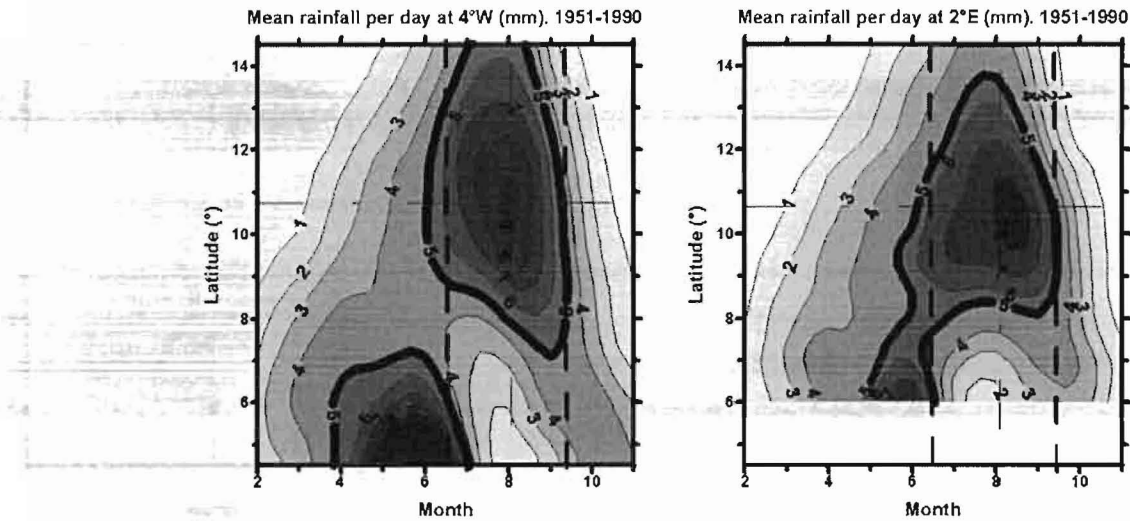


Figure 2. Space-time diagrams of the mean daily rainfall (1951–1990) for two cross sections: (left) 4°W and (right) 2°E . On the x axis, numbers indicate the start of the month (i.e., the representation starts 1 February and ends 31 October).

to one of the three steps in the WAM dynamics. The first maximum corresponds to the progressive intrusion of humidity from the ocean, peaking in May at 7.5°N (Bouaké in Figure 3), and in June at 9.5°N (Kafolo in Figure 3). Then there is a second maximum occurring at the beginning of July, corresponding to a change of regime, the “monsoon jump” (already mentioned by *Sultan and Janicot* [2000] and *Le Barbé et al.* [2002]). Finally, there is a third maximum, observed in September (the exact date depends on the latitude), corresponding to a retreat of the rain zone toward the coast. This is a second point worth noting: while the first rainy season at the coast is clearly disconnected from the sudden reinforcement of rain in the Sahel in June, the second rainy season occurs in continuity with the Sahelian rainy season, as is visible in Figure 2, indicating a regular and progressive retreat of the monsoon. Note however that this retreat is very rapid (less than one month) as compared to the preliminary onset which is spread over a 4-month period (February–June).

[10] Figure 3 provides a closer look at the Sahelian seasonal cycle. Obviously the main feature of this cycle is the single rainy season. However, the existence of a plateau is visible at Houndé (11.5°N) in June, corresponding to a secondary minimum in the hyetograms of the transition zone (Bouaké and Kafolo). This plateau is also visible, albeit less clearly, at Niafunké. During this first phase, the rain zone regularly progresses into the Sahel (note the linearity of the hyetograms and the regular time lag with increasing latitude) but it does not produce significant rain in the northern Sahel. It is only when the second phase abruptly sets in that significant rain is rapidly observed over the whole region. This second phase also has some influence on the transition zone, but in a reduced way. The coast is not affected. As may be seen from Figure 2, the timing of the monsoon jump depends slightly on the longitude considered, which might well be linked to the orientation of the monsoon flow (blowing from southwest) and to the presence of coastal chains like the Fouta-Djalon and the Atakora. Further studies are needed on the local atmos-

spheric circulations interfering with the global monsoon dynamics.

[11] Synthesizing the above findings we propose to distinguish two regimes in the WAM. The first is an oceanic regime, characterized by a regular onset of rain on the continent, clearly reaching 11°N at the end of May but having effects as far north as 14°N to 15°N . The second regime may be qualified as continental, since it starts more or less independently of the oceanic regime and is characterized, as will be seen below, by the predominance of large and intense convective systems originating in the Sahel itself. These two regimes are superimposed together in the transition zone, thus defining the Soudanian climate as an intermediate between a coastal (Guinean) climate, one rainy

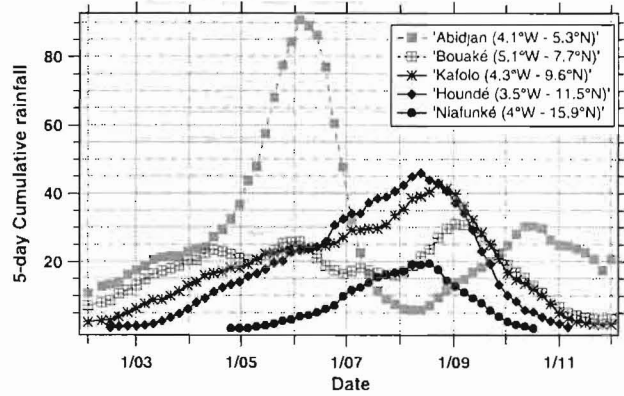


Figure 3. Seasonal cycle along a transect centered at 4°W . Values are 5-day cumulative rainfall averaged over the years 1951–1990. Abidjan has a coastal regime with two well marked rainy seasons. Bouaké has a Soudanian regime with three less pronounced maxima. Houndé and Niafunké are two Sahelian stations with a single rainy season. Kafolo is at the boundary between the Sahelian and the Soudanian regions.

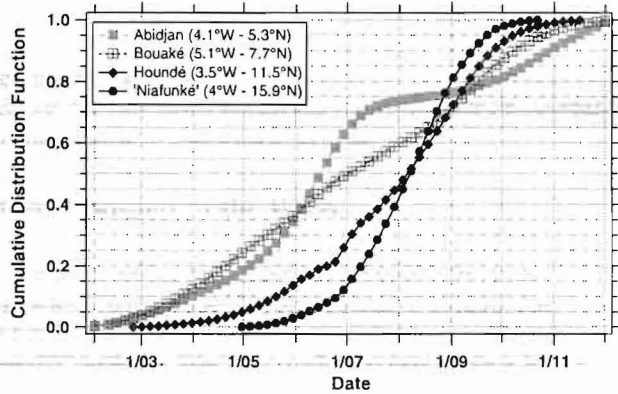


Figure 4. Cumulative distribution function of the total annual rainfall at four stations of Figure 3. For the two Sahelian stations it is seen that the continental regime which starts at the end of June, accounts for 75% (Houndé) and 90% (Niafunké) of the total annual rainfall, respectively.

season associated with the oceanic regime and a second rainy season associated with the continental regime, and the Sahelian climate, mostly dominated by the continental regime.

[12] It has already been stressed by *Le Barbé and Lebel* [1997] that most of the rain deficit of the dry years in the Niamey region, was produced by a deficit of rain during the core of the rainy season rather than by a shorter rainy season. In the light of the above discussion it is implied that it is the continental regime that was mostly affected. Figure 4 shows that the continental regime accounts for between 75% and 90% of the total annual rainfall over the Sahel, depending on the latitude considered. In order to progress in our understanding of the strong interannual variability of the Sahelian rainfall it is therefore necessary to link the seasonal cycle and the interannual variability, focusing on the continental regime. This will be done by

characterizing the rain events that shape this regime and by looking simultaneously at the convective systems that produce these rain events.

4. Rain Events, Convective Systems and Synoptic Weather Systems in the Continental Regime of the WAM

4.1. Rain Events

[13] Time intermittency is a critical aspect of rain. In the tropics, where rain is mostly of convective origin, this intermittency is controlled to the first order by a succession of convective systems. While convective systems lasting for more than 24 hours account for more than 60% of the total cloud cover over the Sahel, as shown by *Mathon and Laurent* [2001], they generally produce rain for only a few hours at a given location, due to their relatively high speed of displacement. These periods of rain are separated by several hours or days of no rainfall. *Le Barbé and Lebel* [1997] have proposed a model that is able to retrieve the statistics of rain event occurrences and of cumulated event rainfall from the statistics of the daily rainfall. The model was validated on several Sahelian data sets and has proven to be an efficient tool for the analysis of the overall climatology of rain events over West Africa [*Le Barbé et al.*, 2001]. An example of this is given in Figure 5, where the time-latitude diagram of the daily rainfall R at 5°W of Figure 2 is decomposed into a map of the mean daily number of events, n , and a map of the mean event rainfall, h .

[14] The space-time dynamics of these two signals may be studied in much the same way as the space-time dynamics of the daily rainfall R , remembering that, at each node of the grid, we have $R = nh$. Note that the h map is blanked for values of n below 0.1, since the deconvolution algorithm does not provide reliable values of h when n is too low.

[15] The two maps display extremely meaningful and coherent patterns. The h map is characterized by a regular

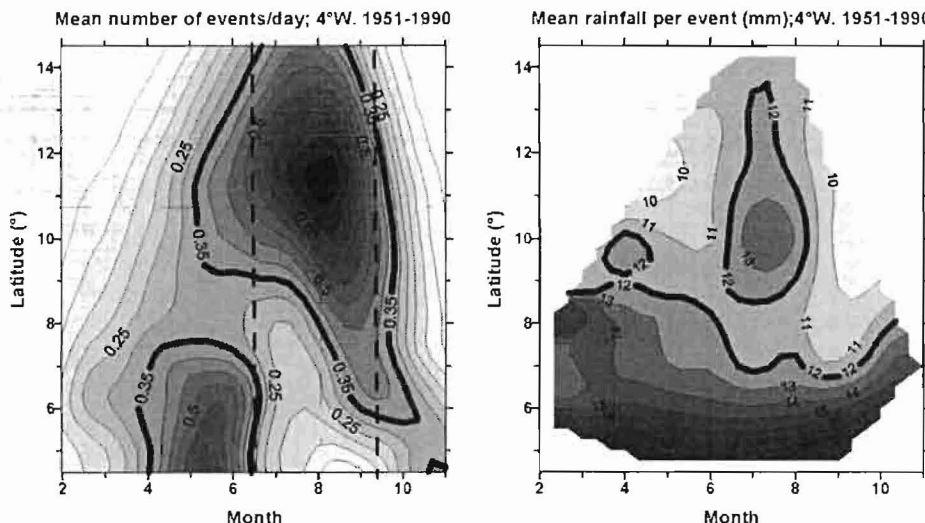


Figure 5. Space-time diagrams of the mean number of rain events per day and of the mean event rainfall (1951–1990) at 4°W. On the x axis, numbers indicate the start of the month (i.e., the representation starts 1 February and ends 31 October).

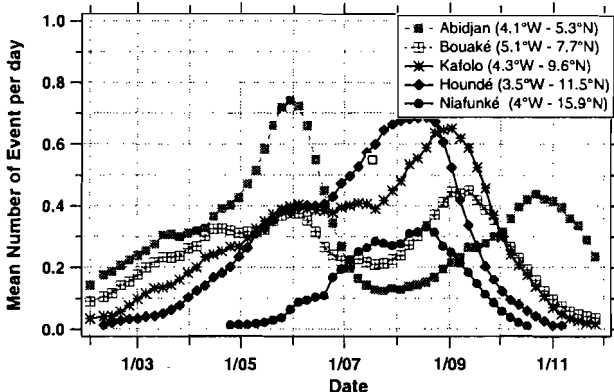


Figure 6. Rain event regime along a transect centered at 4°W .

zonal decrease of h from the coast up to 8.5°N , and by a nucleus of stronger h values in the Sahel between mid-June and August, when the continental regime sets in. The n map looks very similar to the R map of Figure 2. Indeed, the space-time pattern of the R map is almost totally derived from the space-time pattern of the n map. The influence of h is mostly visible in shaping the area of larger R -values over the Sahel. Here again, a more detailed analysis is possible by looking at the curves obtained at a few stations along a south to north transect (Figure 6). Comparing Figures 3 and 6 shows how the transition between the oceanic regime and the continental regime at the end of June affects the rainfall regime in the north of the zone of Soudanian climate (Kafolo) and in the south of the Sahel (Houndé). In Kafolo, there is a decrease in the occurrence of rain events due to a weakening of the oceanic regime. At the same time, the mean rainfall per event increases, due to a larger proportion of more intense rain events corresponding to the beginning of the continental regime. At Houndé there is a similar behavior. At both stations, the result is an increase in rainfall at the beginning of July. Then, a clear difference appears between the two stations. Both the number of events and the 5-day rainfall increase continuously at Houndé, during July until mid-August when it peaks at 0.7 events/day, corresponding to a strong influence of the continental regime. Kafolo, on the other hand, is located at the southern edge of the region of maximum occurrence of large convective systems associated with intense rain events (Figure 7). The number of rain events remains stable around 0.7 events/day for the whole of July.

4.2. Convective Systems

[16] In an earlier work combining ground data from the EPSAT-Niger network and Meteosat data, Laurent *et al.* [1998] found that, over the region of Niamey, most of the intense rain events producing 80% of the annual rainfall were associated with large cloud clusters well identified from IR imagery. A more comprehensive study carried out by Mathon and Laurent [2001] on a 1989–1998 Meteosat data set has later shown that, for the period extending from July to mid-September (corresponding to the continental regime defined above), there is a region of maximum occurrences of mesoscale convective complexes (MCCs), defined following the criteria of Maddox [1980]. This

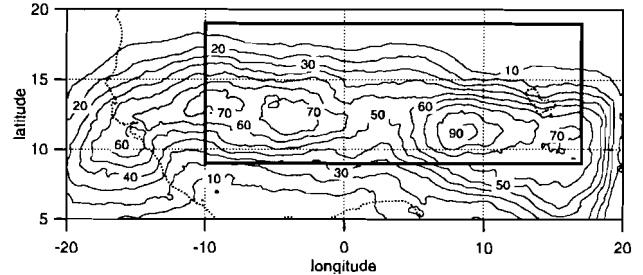


Figure 7. Spatial distribution of mesoscale convective complex (MCC) occurrences over West Africa for the period 1 July to 15 September. Values refer to the total number of MCCs recorded over the years 1989–1999 [after Mathon, 2001].

region is precisely centered on $11\text{--}13^{\circ}\text{N}$, spreading in longitude between 10°W and 15°E (Figure 7). According to Laing *et al.* [1999], these MCCs produce 22% of Sahelian rainfall. This proportion is not sufficiently large to account for the year-to-year variability of Sahelian rainfall. Mathon and Laurent [2001], on the other hand, have shown that long-lived Mesoscale Convective Systems (MCSs) defined at 233 K account for 60% of the Sahelian deep convective coverage at 213 K. In their study, MCSs are defined as cloud clusters larger than 5000 km^2 at the 233 K temperature threshold and long-lived MCS are those lasting for more than 24 hours. During the period of the continental regime, the total number of MCSs recorded over the box shown in Figure 7 is a little less than 20000 for the years 1990–1999. As may be seen from Figure 8, a very small number of this total population accounts for most of the cloud coverage. In fact, 80% of the total cloud coverage at 233 K is produced by the 240 largest systems, that is little more than 12% of the MCSs. The minimum size of these 240 largest MCSs is greater than $50,000 \text{ km}^2$. They include 23 MCCs. In order to quantify the rainfall produced by these large systems, only those which covered at least 80% of the $16,000 \text{ km}^2$ EPSAT-Niger study area were retained. Since the rain gauges of the EPSAT-Niger network record 5-minute rainfalls, it is possible to compute precisely the rain produced by each system during its

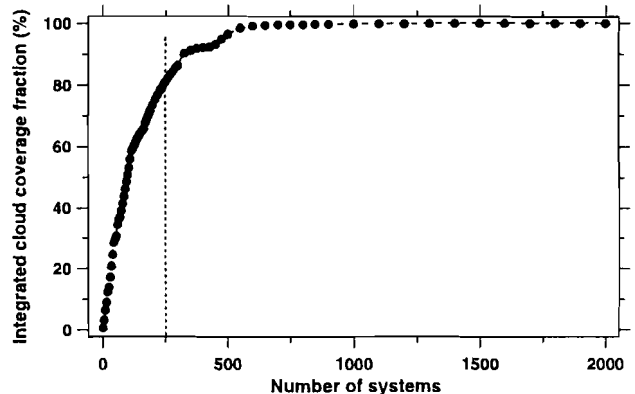


Figure 8. Cumulative distribution function of the cloud cover at 233K computed over JAS for the period 1990–1999.

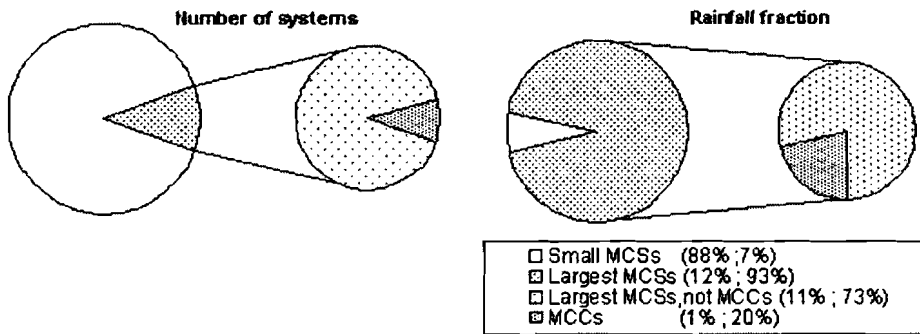


Figure 9. Proportion of the rainfall associated with the continental regime that is produced by the largest convective systems. These systems are producing 93% of the rainfall recorded over the EPSAT-Niger study area ($16,000 \text{ km}^2$), while they represent only 12% of the total number of MCSs observed over the region (statistics computed over the years 1989–1999 for the period 1 July to 15 September).

passage over the study area. The calculation synthesized in Figure 9 gave the following results: (1) the largest 12% of the systems produce 93% of the July–September (JAS) rainfall in this part of the Sahel with an average event rainfall of 14.7 mm and (2) the MCCs (that are all included in the largest 12% of the systems) represent only 1% of the total number of systems, producing 20% of the JAS rainfall. Figure 9 is very close to the statistic of *Laing et al.* [1999], given that the period and area considered for their calculation is significantly different from those of *Mathon and Laurent* [2001]. This also confirms that, even though MCCs are by far the most rain efficient systems, producing on average 19 mm per event, they account for a relatively small share of the JAS rainfall because they are few in number.

[17] Since the subpopulation of MCCs is too small for climatological analysis, it is necessary to select a larger population of MCSs, objectively defined, that account for a more significant share of the JAS rainfall. A detailed analysis of the most efficient systems in our sample revealed that they all include at least one 213 K cluster, imbedded in a larger 233 K cluster and lasting for more than 3 hours. It was further found that by selecting among these systems those moving at a speed greater than 10 ms^{-1} when passing over the ground validation area, we obtained a subpopulation of rain efficient systems very similar to the subpopulation of the largest 12% of the systems selected in Figure 7. It similarly accounts for more than 90% of the JAS rainfall in the region of Niamey. Based on these two criteria, 213 K clusters lasting for more than 3 hours and ground speeds larger than 10 ms^{-1} , it is possible to objectively count the number of rain efficient systems passing over the ground validation area each year. This opens the way for relating this number to the JAS rainfall for a given year, as will be seen in section 5.

4.3. Synoptic Weather Systems

[18] Since the work of *Carlson* [1969], *Burpee* [1972, 1974], and *Reed et al.* [1977], easterly waves have been identified as key synoptic features modulating convection and rainfall over the Sahel. They have a wavelength between 1500 km and 4000 km and a speed of about 8 m/s, giving rise to periods between 2.5 and 5.5 days. These 3–5 day easterly waves occur in the low- and

middle-troposphere and are linked to the African Easterly Jet (AEJ) located in the vicinity of 15°N and 600 hPa, which satisfies the *Charney and Stern* [1962] barotropic and baroclinic instability criterion.

[19] *Duvel* [1990] was the first to investigate the relationship between easterly waves and cloudiness using ECMWF analyses and METEOSAT images. Although carried out on a sample limited to the summer of 1985, this study led to results similar to those obtained by *Burpee* [1974] and *Reed et al.* [1977] using the GATE radio sounding data. Maximum low-level convergence and upward vertical motion, as well as the greatest convective cloud cover and the largest precipitation amounts, are located in the region ahead and slightly south of the wave trough. However at 20°N , the positive rainfall anomalies are located behind the trough between the southerly wind and ridge sectors, indicating the primary influence of the northward horizontal transport of moisture. No vertical tilt is evident south of the AEJ because of the influence of convective heating whereas at 15°N and further north a vertical tilt opposed to the vertical wind shear shows the significant role of dry baroclinic processes in cloud free areas. At these latitudes, deep convection has a primary maximum in the southerly wind sector, fuelled by the horizontal transport of moisture. At and ahead of the trough axis, there is highly suppressed cloud condition consistent with strong shallow dry convection. According to the work of *Thompson et al.* [1979], it seems that latent heat release plays a major role in energizing the waves over land whereas diabatic effects appear to extract wave energy over the ocean.

[20] Recently, *Diedhiou et al.* [1998, 1999] have identified two main periodicities, one lying between 3 and 5 days and the other between 6 and 9 days. The 3–5-day easterly waves are more active in August–September. They have a mean wavelength and a mean phase speed varying from 3000 km and 8 m/s north of the AEJ to 5000 km and 12 m/s south of the jet. Rainfall, convection and the monsoon flux are significantly modulated by these waves, with convection in the ITCZ being enhanced in and ahead of the trough. The 6–9-day waves are mostly observed along one main track, located north of the AEJ along 17.5°N . The mean wavelength is about 5000 km, and the mean phase speed is about 7 m/s. The perturbation of the wind field is then mostly evident at and north of the AEJ latitude. It is similar to the

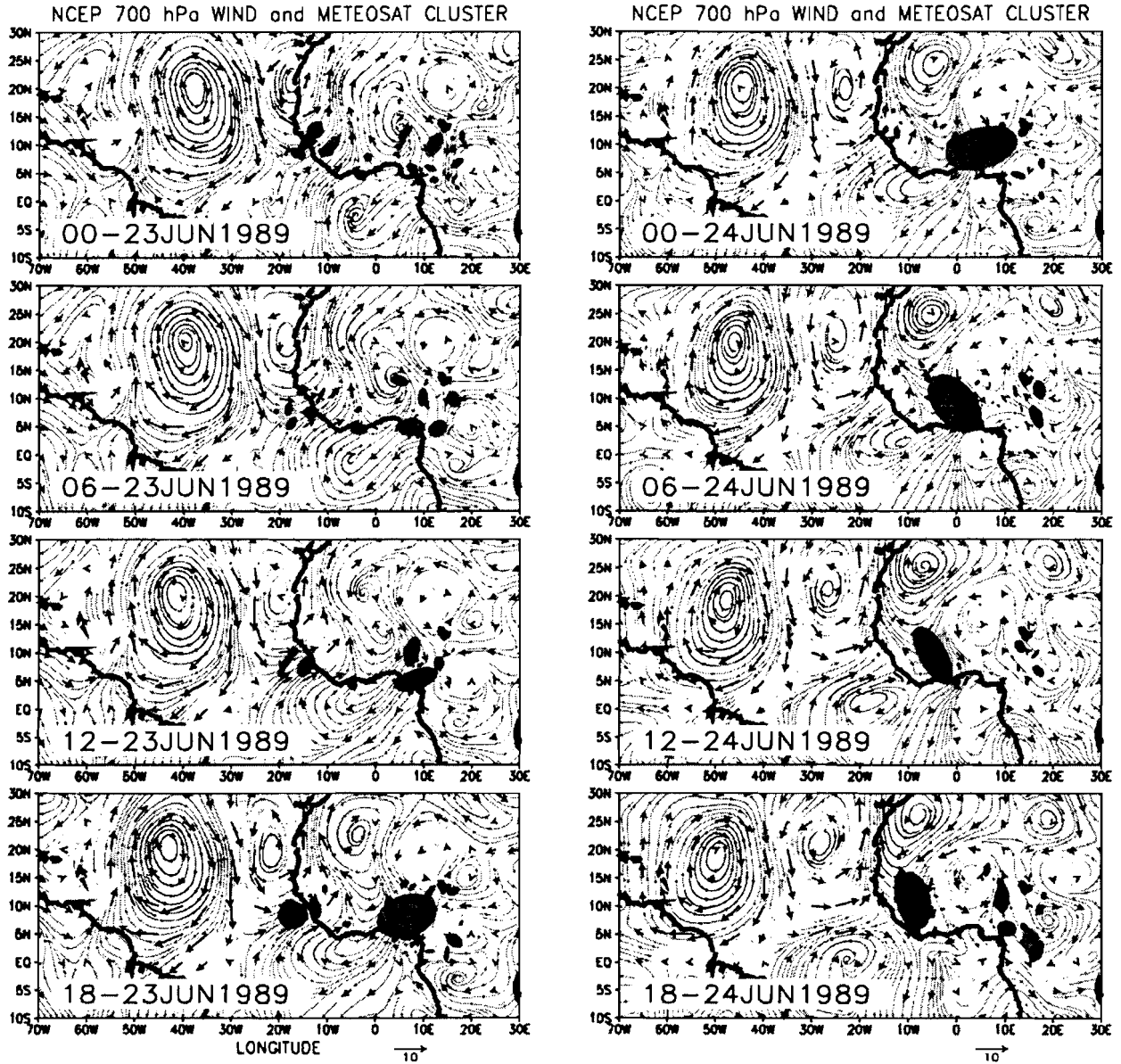


Figure 10. Illustration of an interaction between wave and convection during a time sequence from 0000 UT, 23 June 1989, to 1800 UT, 24 June 1989. The streamlines represent the disturbances in the NCEP/NCAR reanalyses wind field at 700 hPa filtered between 3 and 10 days. The shaded ellipsoids are cloud clusters obtained at 3 METEOSAT temperature threshold: 253°K (light gray/red), 233°K (dark gray/blue) and 213°K (black and violet). See color version of this figure in the HTML.

northern part of the 3–5-day wave, except that the more developed circulation centers, traveling a little further northward, lead to a large modulation of the zonal wind component of the jet. These 6–9-day easterly waves also significantly modulate rainfall and convection but in a different way from 3–5-day waves, resulting in zonal convective bands in the ITCZ, extending mostly in and behind the trough. Over the continent, the 6–9-day waves are more active at the beginning and at the end of the rainy season. Figure 10 is an illustration of how a large MCS evolves in a synoptic atmospheric disturbance from 0000 UT, 23 June 1989, to 1800 UT, 24 June 1989. Over the

Atlantic, a strong anticyclonic cell crosses the ocean reaching the Brazilian coast at the end of the period considered. It is followed by a 6–9-day wave, associated with clusters of small size (small dark-gray ellipsoids), located behind the trough in a southern flux. The 6–9-day wave is itself followed by a 3–5-day wave located over Central Africa at 0000 UT, 23 June. In the initial phase, one can observe an ensemble of small clusters located in and ahead of the trough. They get organized into a large cluster by the end of the day. This cluster starts moving westward with the 3–5-day wave, extending from 8°N to 15°N and approaching the ocean at the end of the next day.

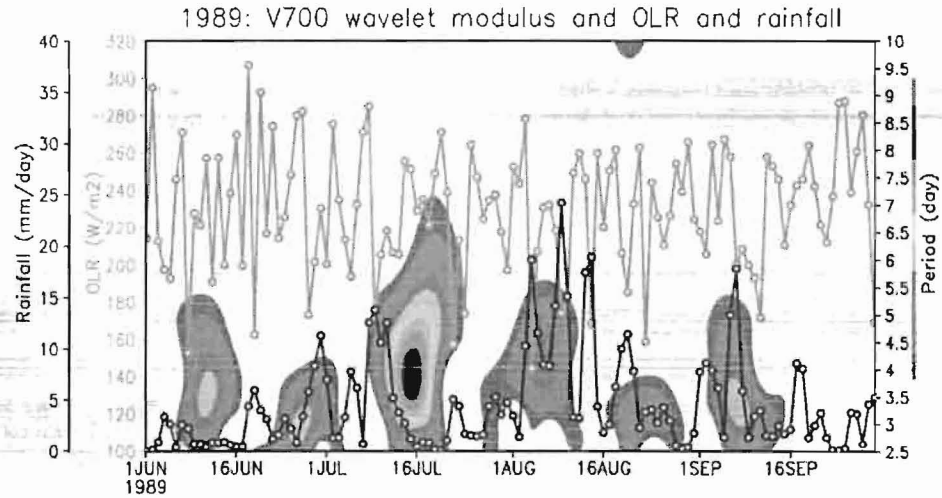


Figure 11. Evolution from June to September 1989 of the different wave regimes (wavelet modulus on the meridional wind at 700 hPa, shaded), the OLR (gray/orange line) and the observed daily rainfall (black dashed line). See color version of this figure in the HTML.

[21] Combining the NCEP/NCAR reanalyses, satellite measurement of the Output Longwave Radiation (OLR) and the observed daily rainfall, it is possible to analyze the seasonal cycle of rainfall and convection in interaction with easterly waves. Figure 11 shows the evolution of the OLR and of the observed rainfall for the Niamey grid point from June to September 1989 superimposed on the wave regime characterized by a Morlet-wavelet analysis of the meridional wind at 700 hPa. Wavelet analysis (shaded) confirms that most of the disturbances over the Sahel have a period lying between 3 and 5 days, the maximum in the 6–9-day band period occurring mainly in the beginning and at the end of the rainy season.

[22] Analyzing the association between waves and rain reveals a rather complete pattern. From 1 to 10 August and around 7 September, waves are associated with cold clouds and high rainfall heights (wet waves). The waves observed during the second week of June and around 21 August are associated with dry events and cold clouds (OLR between 180 and 200 W/m² for the first case and less than 160 W/m² for the second) and almost no observed rainfall at the surface (dry waves). There is also a “warm” wave observed around 16 July, which is not associated with either convection or rain at the surface. Finally, on 14 August, a strong convection (OLR less than 170 W/m²) and a high rainfall (up to 15 mm) are recorded without any wave. As the modulus of the wavelet is positively correlated to the variance of the wave, all this indicates that the variance of the wave, considered only from the fluctuations of the meridional wind, is not a good indicator of the rainfall variability. Convection and rainfall can occur without any easterly waves present and not all easterly waves are associated with rainfall.

5. Interannual Variability

[23] As shown by Figure 12, the interannual variability of Sahelian rainfall is strongly linked to its seasonal cycle. In Figure 12 the difference of the average rainfall between the 20 driest years and the 20 wettest years is represented in the following way. First, the mean annual relative deficit of

the 20 driest years for grid mesh j , (the resolution of the grid being $0.5^\circ \times 0.5^\circ$) is computed as:

$$D_j = (R_{\text{wet}}(j) - R_{\text{dry}}(j)) / R_{\text{wet}}(j),$$

where $R_{\text{wet}}(j)$ is the average annual rainfall of the 20 wettest years and $R_{\text{dry}}(j)$ is the average annual rainfall of the 20 driest years.

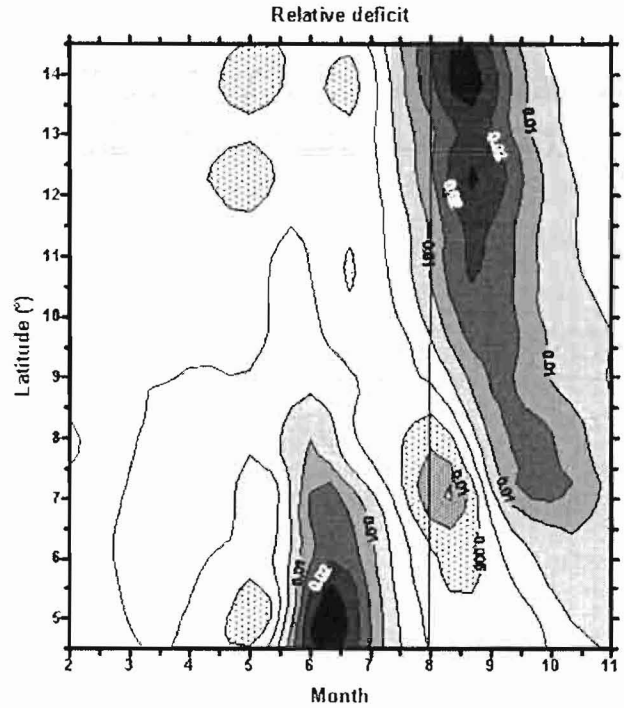


Figure 12. Hovmoeller diagram of the relative rainfall deficit between a composite of the 20 wettest years and a composite of the 20 driest years at 4°W. Shaded areas correspond to lower rainfall in dry years, while dotted areas correspond to higher rainfall in dry years.

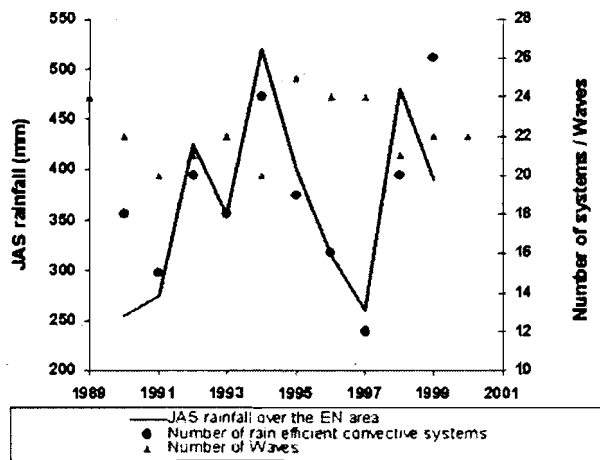


Figure 13. Rainfall recorded over the EPSAT-Niger study area, versus the number of large convective systems and the number of easterly waves.

[24] Then, for each day of the year, i , the relative deficit for grid mesh j , is computed as:

$$D_{i,j} = (R_{\text{wet}}(i,j) - R_{\text{dry}}(i,j))/R_{\text{wet}}(i,j).$$

The variable plotted in Figure 12 is

$$\delta_{i,j} = D_{i,j}/D_j$$

The integral of $\delta_{i,j}$ over the whole year for a given mesh j is equal to 1. If the entire deficit were evenly distributed over a hundred days, the value of $\delta_{i,j}$ would be equal to 0.01. Focusing on the Sahelian latitudes, it appears in this Figure 12 that all the rainfall deficit of the dry years is due to a rainfall deficit concentrated between mid-July and the end of September, that is during the period of the continental regime identified in section 3. Dry years are also characterized by the months of the oceanic regime (April–June) having a slightly larger than normal rainfall in the south (dotted area in Figure 12), although this might not be a statistically significant trend. This is a confirmation of the results of D'Amato and Lebel [1998], stating that dry years in the Sahel are not so much determined by a late start of the rainy season, but rather by a marked deficit during the core of the rainy season. Robock *et al.* [1993], in their work on the creation of regional climate scenarios, also found that the time between rainstorms is greater in dry years during the core of the rainy seasons.

[25] This rainfall deficit during July–September is associated with a lower number of the large rain-efficient convective systems identified in section 4.2, as is clear from Figure 13. By comparison, the mean event rainfall produced by these large systems does not vary significantly from year to year (not shown). Figure 13 also shows that the number of easterly waves recorded for a given year is not significantly correlated to the rainfall of that year. This has two consequences. First, monitoring the convective systems from IR images of geostationary satellites provides a simple tool for drought monitoring over an entire region such as the Sahel. It should be kept in mind however, that strong local

gradients may exist and that ground data are a necessary complement to these satellite data. Secondly, it remains elusive to explain the year to year variation in the number of rain-efficient convective systems by simply looking at the synoptic weather patterns. It is therefore important to better understand at the intraseasonal scale the links between the life cycle of Sahelian convective systems and synoptic weather patterns, in order to improve our comprehension of the interannual variability.

6. Conclusion

[26] Rainfall in the Sahel, and more generally in all semi-arid regions of the world, displays a large degree of variability over a range of timescales. This variability is rarely characterized at relevant scales from an hydrological point of view despite the often dramatic consequences of intraseasonal dry spells and pluri-annual droughts on the water cycle of these regions. Rain events are a key element of the rainfall regime of semi-arid regions. They are associated with convective systems. To understand the hydrological impact of dry spells and droughts, it is therefore necessary to describe the rainfall regime at the scale of these rain events. This study provides such a description for the seasonal cycle and the interannual variability of Sahelian rainfall. Three complementary data sets were used to this end, covering 40 years for the regional daily rain gauge network, and 10 years for a full resolution meteosat data set and a high-resolution recording rain gauge network.

[27] It was initially shown that the seasonal cycle comprises two phases. The first phase corresponds to a progressive onset of rain on the West African continent from the tropical Atlantic. For that reason, this phase is considered to be as an oceanic regime. The second phase involves a sudden jump in the mean daily rainfall and mean daily number of rain events that occur concurrently over the whole Sahelian band. An overwhelming proportion of large convective systems embedded in the easterly circulation characterizes this second phase. Given the contrast between these two phases, the first has been referred to as an “oceanic regime” and the second as a “continental regime”. The continental regime starts at the end of June and represents from 75% (in the south) to 90% (in the north) of the total annual rainfall in the Sahel. A small number of large and rain efficient convective systems account for more than 90% of the rainfall in the continental regime, each of these systems producing in average a little less than 15 mm per event in their mature stage. This value is relatively homogeneous over the whole Sahelian band, whereas the mean event rainfall in the oceanic regime displays a strong meridional gradient ranging from 18 mm on the coast to 10 mm in the northern Sahel.

[28] The interannual variability of the Sahelian rainfall is largely controlled by the annual fluctuations in the number of these rain efficient convective systems. A composite analysis comparing dry and wet years revealed that the deficit of dry years was essentially concentrated around the core of the continental regime (August). During the dry years, the rainfall during the months of the oceanic regime (April to June) is equal to or even slightly larger than normal. Thus the length of the rainy season is not particularly reduced in dry years, contrary to a common belief.

Also, the mean event rainfall of the large convective systems characterizing the continental regime does not display significant differences between wet and dry years. These results are important in an hydrological perspective because runoff is affected differently by a decrease in the number of large rain events or by a decrease in the overall mean event rainfall.

[29] It was also shown that the raw number of 3–5-day wave is not a good indicator of the number of rain efficient convective systems recorded over the Sahel for a given year. This suggests the distinction between “wet” waves and “dry” waves. This tends to assume the existence of an intraseasonal signal modulating the rainfall during the continental regime. This modulation is currently analyzed using the NCEP/NCAR reanalyses. Phases of stronger AEJ/weaker TEJ, which have been identified in previous studies, might be connected to the existence of dry waves. The question is then to determine the nature of this intraseasonal signal and how it is linked to the interannual variability. Is it dominantly a modulation of the cyclonic activity of the waves or is it related to two different regimes of convection? Improving our understanding of the links between the interannual variability of Sahelian rainfall and its seasonal cycle is thus an important issue for future work on the WAM and its hydrological impact.

[30] **Acknowledgments.** We are grateful to the various national meteorological services which helped IRD (Institut de Recherche pour le Développement, formerly ORSTOM) to build the daily rainfall data base used in this study. This research was funded by IRD.

References

- Burpee, R. W., The origin and structure of easterly waves in the lower troposphere in North Africa, *J. Atmos. Sci.*, **29**, 77–90, 1972.
- Burpee, R. W., Characteristics of North African easterly waves during the summers of 1968 and 1969, *J. Atmos. Sci.*, **31**, 1556–1570, 1974.
- Carlson, T. N., Some remarks on African disturbances and their progress over the tropical Atlantic, *Mon. Weather Rev.*, **97**, 716–726, 1969.
- Charney, J. G., and M. E. Stern, on the stability of internal baroclinic jets in a rotating atmosphere, *J. Atmos. Sci.*, **19**, 159–172, 1962.
- Charney, J. G., W. J. Quirk, S. H. Chow, and J. Kornfield, A comparative study of the effects of albedo change on drought in semi-arid regions, *J. Atmos. Sci.*, **34**, 1366–1385, 1977.
- Cook, K. H., Large scale atmospheric dynamics and Sahelian precipitation, *J. Clim.*, **10**, 1137–1152, 1997.
- D'Amato, N., and T. Lebel, On the characteristics of the rainfall events in the Sahel with a view to the analysis of climatic variability, *Int. J. Climatol.*, **18**, 955–974, 1998.
- Diedhiou, A., S. Janicot, A. Viltard, and P. de Félice, Evidence of two regimes of easterly waves over West Africa and the tropical Atlantic, *Geophys. Res. Lett.*, **25**, 2805–2808, 1998.
- Diedhiou, A., S. Janicot, A. Viltard, P. de Félice, and H. Laurent, Easterly waves regimes and associated convection over West Africa and the tropical Atlantic: Results from the NCEP/NCAR and ECMWF reanalyses, *Clim. Dyn.*, **15**, 795–822, 1999.
- Duvel, J. P., Convection over tropical Africa and the Atlantic ocean during northern summer. part II: Modulations by easterly waves, *Mon. Weather Rev.*, **118**, 1855–1868, 1990.
- Eltahir, E. A. B., and C. Gong, Dynamics of wet and dry years in West Africa, *J. Clim.*, **9**, 1030–1042, 1996.
- Fontaine, B., S. Trazaska, and S. Janicot, Evolution of the relationship between near global and Atlantic SST modes and the rainy season in West Africa: Statistical analyses and sensitivity experiments, *Clim. Dyn.*, **14**, 353–368, 1998.
- Fontaine, B., N. Philippon, and P. Camberlin, An improvement of June–September rainfall forecasting in the Sahel based upon region April–May moist static energy content (1968–1997), *Geophys. Res. Lett.*, **26**, 2041–2044, 1999.
- Janicot, S., V. Moron, and B. Fontaine, Sahel droughts and ENSO dynamics, *Geophys. Res. Lett.*, **23**, 515–518, 1996.
- Janicot, S., S. Trzaska, and I. Poccard, Summer Sahel-ENSO teleconnections and decadal time scale SST variations, *Clim. Dyn.*, **18**, 303–320, 2001.
- Lamb, P. J., and R. A. Peppler, Further case studies of tropical Atlantic surface atmospheric and oceanic patterns associated with sub-Saharan drought, *J. Clim.*, **5**, 476–488, 1992.
- Laing, A. G., J. M. Fritsch, and A. J. Negri, Contribution of mesoscale convective complexes to rainfall in Sahelian Africa: Estimates from geostationary infrared and passive microwave data, *J. Appl. Meteorol.*, **38**, 957–964, 1999.
- Laurent, H., and T. Lebel, How important is the contribution of the mesoscale convective complexes to the Sahelian rainfall?, *Phys. Chem. Earth*, **23**, 629–633, 1998.
- Le Barbé, L., and T. Lebel, Rainfall climatology of the HAPEX-Sahel region during the years 1950–1990, *J. Hydrol.*, **188–189**, 43–73, 1997.
- Le Barbé, L., T. Lebel, and D. Tapsoha, Rainfall variability in West Africa during the years 1950–1990, *J. Clim.*, **15**(2), 187–202, 2002.
- Lebel, T., J. D. Taupin, M. Gréard, Rainfall monitoring: The EPSAT-Niger setup and its use for HAPEX-Sahel, in *Hydrologie et Météorologie de Meso-échelle dans HAPEX-SAHEL: Dispositif de Mesures au Sol et Premiers Résultats*, edited by T. Lebel, pp. 31–68, ORSTOM Editions, Bondy, France, 1995.
- Maddox, R. A., Mesoscale convective complexes, *Bull. Am. Meteorol. Soc.*, **61**, 1374–1387, 1980.
- Mathon, V., Etude climatologique des systèmes convectifs de méso-échelle en Afrique de l'Ouest, 238 pp., Ph.D. thesis, Univ. Paris 7, Paris, 2001.
- Mathon, V., and H. Laurent, Life cycle of the Sahelian mesoscale convective cloud systems, *Q. J. R. Meteorol. Soc.*, **127**, 377–406, 2001.
- Palmer, T. N., Influence of the Atlantic, Pacific and Indian Oceans on Sahel rainfall, *Nature*, **322**, 251–253, 1986.
- Reed, R. J., D. C. Norquist, and E. E. Recker, The structure and properties of African wave disturbances as observed during phase III of GATE, *Mon. Weather Rev.*, **105**, 317–333, 1977.
- Robock, A., R. P. Turco, M. A. Harwell, T. P. Ackerman, R. Andressen, H.-S. Chang, and M. V. K. Sivakumar, Use of general circulation model output in the creation of climate change scenarios for impact analysis, *Clim. Change*, **23**, 293–335, 1993.
- Rowell, D. P., Teleconnections between the tropical Pacific and the Sahel, *Q. J. R. Meteorol. Soc.*, **127**, 1683–1706, 2001.
- Sennazzi, F. H., and L. Sun, The role of orography in determining the Sahelian climate, *Int. J. Climatol.*, **17**, 581–596, 1997.
- Sultan, B., and S. Janicot, Abrupt shift of the ITCZ over West Africa and intra-seasonal variability, *Geophys. Res. Lett.*, **27**, 3353–3356, 2000.
- Thompson, R. M., S. W. Payne, E. E. Recker, and R. J. Reed, Structure and properties of synoptic-scale wave disturbances in the intertropical convergence zone of the eastern Atlantic, *J. Atmos. Sci.*, **36**, 53–72, 1979.
- Thornicroft, C. D., and M. Blackburn, Maintenance of the African easterly jet, *Q. J. R. Meteorol. Soc.*, **125**, 763–786, 1999.
- Wang, G., and E. A. B. Eltahir, Biosphere-atmosphere interactions over West Africa. II: Multiple climate equilibria, *Q. J. R. Meteorol. Soc.*, **126**, 1261–1280, 2000.
- Ward, M. N., Diagnosis and short-lead time prediction of summer rainfall in tropical North Africa at interannual and multi-decadal time scales, *J. Clim.*, **11**, 3167–3191, 1998.
- Zheng, X., and E. A. B. Eltahir, The role of vegetation in the dynamics of West African monsoons, *J. Clim.*, **11**, 2078–2096, 1998.

A. Diedhiou, H. Laurent, and T. Lebel, Laboratoire d'étude des Transferts en Hydrologie et Environnement (UMR 5564), IRD, BP 53, F-38041 Grenoble cedex 9, France. (lebel@hmg.inpg.fr)

Rainfall Estimation in the Sahel. Part II: Evaluation of Rain Gauge Networks in the CILSS Countries and Objective Intercomparison of Rainfall Products

ABDOU ALI

IRD, LTRE, Grenoble, France, and Centre AGRHYMET, Niamey, Niger

ABOU AMANI

Centre AGRHYMET, Niamey, Niger

ARONA DIEDHIOU AND THIERRY LEBEL

IRD, LTRE, Grenoble, France

(Manuscript received 27 January 2005, in final form 14 June 2005)

ABSTRACT

This study investigates the accuracy of various precipitation products for the Sahel. A first set of products is made of three ground-based precipitation estimates elaborated regionally from the gauge data collected by Centre Regional Agrometeorologie-Hydrologie-Meteorologie (AGRHYMET). The second set is made of four global products elaborated by various international data centers. The comparison between these two sets covers the period of 1986–2000. The evaluation of the entire operational network of the Sahelian countries indicates that on average the monthly estimation error for the July–September period is around 12% at a spatial scale of $2.5^\circ \times 2.5^\circ$. The estimation error increases from south to north and remains below 10% for the area south of 15°N and west of 11°E (representing 42% of the region studied). In the southern Sahel (south of 15°N), the rain gauge density needs to be at least 10 gauges per $2.5^\circ \times 2.5^\circ$ grid cell for a monthly error of less than 10%. In the northern Sahel, this density increases to more than 20 gauges because of the large intermittency of rainfall. In contrast, for other continental regions outside Africa, some authors have found that only five gauges per $2.5^\circ \times 2.5^\circ$ grid cell are needed to give a monthly error of less than 10%. The global products considered in this comparison are the Climate Prediction Center (CPC) merged analysis of precipitation (CMAP), Global Precipitation Climatology Project (GPCP), Global Precipitation Climatology Center (GPCC), and Geostationary Operational Environmental Satellite (GOES) precipitation index (GPI). Several methods (scatterplots, distribution comparisons, root-mean-square error, bias, Nash index, significance test for the mean, variance, and distribution function, and the standard deviation approach for the kriging interval) are first used for the intercomparison. All of these methods lead to the same conclusion that CMAP is slightly the better product overall, followed by GPCC, GPCP, and GPI, with large errors for GPI. However, based on the root-mean-square error, it is found that the regional rainfall product obtained from the synoptic network is better than the four global products. Based on the error function developed in a companion paper, an approach is proposed to take into account the uncertainty resulting from the fact that the reference values are not the real ground truth. This method was applied to the most densely sampled region in the Sahel and led to a significant decrease of the raw evaluation errors. The reevaluated error is independent of the gauge references.

1. Introduction

Various rainfall products, widely available through the Internet, are increasingly used as standard input to run hydrological and crop models or to validate atmo-

spheric model outputs. In general, these products combine information from satellites—*infrared imagers* (IR), *microwave imagers* [such as the Special Sensor Microwave Imager (SSM/I)], *radars* [i.e., Tropical Rainfall Measuring Mission (TRMM)]—and/or *rain gauges*. In recognition of the necessity to evaluate these rainfall products as rigorously as possible, several studies (e.g., Morrissey and Greene 1993; Chiu et al. 1993; Xie and Arkin 1995; Ebert and Manton 1998; Bell et al. 2001;

Corresponding author address: Abdou Ali, B.P. 11416, IRD, Niamey, Niger.
E-mail: a.ali@agrhymet.ne

Adler et al. 2001; Ha et al. 2002) have assessed the quality of products from different parts of the world and have shown that the performance of algorithms and the added value of rainfall products may depend on the region concerned (Kummerow et al. 2004).

For at least three main reasons, such a validation is especially needed in West Africa: 1) the severe drought that started in the beginning of the 1970s has made precipitation more irregular and more difficult to estimate, 2) after reaching a peak in the early 1980s, in situ networks are now becoming less dense, and 3) West Africa is one of the world's most sensitive regions in terms of precipitation variability because its economy is still largely dependent on rain-fed agriculture.

Several papers that address rainfall estimation in Africa were published in recent years, such as those of Thorne et al. (2001) for South Africa and McCollum et al. (2000) in equatorial Africa. In West Africa, Laurent et al. (1998) compared and discussed the validation of estimates resulting from five satellite methods, and Ramage et al. (2000) compared rainfall products with different resolutions in Niger. Jobard (2001) reviewed satellite-based rainfall retrieval using multisource data. However, a comprehensive evaluation of various rainfall products remains to be undertaken for Africa. The work presented here may be considered as one step in that direction. Focusing on the Sahel, it adds to previous work in several ways. First, it explicitly addresses the problem that the reference values are not the real ground truth (section 2). Second, as explained in section 3, this study covers a longer period (1986–2000) than any previous work carried out in West Africa and thus addresses a much larger range of climatological conditions. Third, based on the error function developed in a companion paper (Ali et al. 2005), this study examines both regional products—three products elaborated regionally from the gauge data collected by Centre Regional Agrometeorologie–Hydrologie–Météorologie (AGRHYMET)—and global products—elaborated by various international data centers (sections 4 and 5). Last, a way of incorporating the uncertainty associated with reference rain fields into the assessment of the quality of rainfall estimates is tested in section 6.

2. Problem statement and method

a. Generalities

Satellite-based rainfall estimates have been an important research topic since the first operational methods were proposed in the early 1980s [e.g., from the initial review of Barrett and Martin (1981) to the more recent analyses of Petty (1995) that address satellite

rainfall estimation over land and Levizzani et al. (2001) that look at future perspectives]. Two important points must be considered with respect to satellite-based estimate evaluation and intercomparison. First, satellite-based estimates are areal values whereas ground-based references are point values, raising the question of the significance of statistics computed using a reference estimate instead of the unknown true value. The second concern is linked to the objectives of the evaluation and intercomparison, raising the question of which statistics should be used—in other words, which products give the best estimates and in what ways are these estimates better? Several statistics will be used here to substantiate this analysis. Estimate evaluation has traditionally laid emphasis on bias (correspondence between mean values), cofluctuation (the strength of the linear relationship between the estimate and a reference value), and accuracy (the point-by-point level of agreement between the estimate and the reference). However, other performance characteristics are important in assessing the quality of an estimate. For example, a difference in the frequency of low values for two products having similar mean statistics is of great importance for agricultural applications. On the other hand, the high extreme values are of greater importance in hydrology.

b. Relationship between statistics computed using a reference value and those of the unknown true value

The most usual statistics used in rainfall product evaluation relate to the bias b , the root-mean-square error (rmse), and the correlation coefficient r . For more details and discussion of these standard statistics, see, for example, Stanski et al. (1989). These statistics are, in general, computed from an estimated reference value (b_{SR} , rmse_{SR}, and r_{SR}). In the following, the bias and the root-mean-square error are computed using the true reference value (b_{ST} and rmse_{ST}). Because this true reference is unknown, the statistics will be expressed as a function of those derived from the estimated reference value.

Considering that R_S is the estimate under evaluation, R_T is the unknown true reference value, and R_R is the estimated reference value, b_{ST} will be the bias of R_S with respect to R_T , b_{SR} will be the bias of R_S with respect to R_R , and b_{RT} will be the bias of R_R with respect to R_T . Also, rmse_{ST}, rmse_{SR}, and rmse_{RT} will be the respective root-mean-square errors. Thus,

$$\begin{aligned} b_{ST} &= E(R_S - R_T) = E(R_S - R_R) \\ &\quad + E(R_R - R_T) = b_{SR} + b_{RT}. \end{aligned} \quad (1)$$

So, if the reference value is unbiased, the bias of the estimate R_S with respect to this reference value is the true bias. One can denote the following to express rmse_{ST} :

$$\begin{aligned}\Delta_{SR} &= R_S - R_R, \\ \Delta_{ST} &= R_S - R_T, \\ \Delta_{RT} &= R_R - R_T, \\ \sigma_{\Delta SR}^2 &= E(R_S - R_R)^2 = (\text{rmse}_{SR})^2, \\ \sigma_{\Delta ST}^2 &= E(R_S - R_T)^2 = (\text{rmse}_{ST})^2, \quad \text{and} \\ \sigma_{\Delta RT}^2 &= E(R_R - R_T)^2 = (\text{rmse}_{RT})^2.\end{aligned}$$

Also, because $R_S - R_R = (R_S - R_T) - (R_R - R_T)$, we have

$$\begin{aligned}\sigma_{\Delta SR}^2 &= E(R_S - R_T)^2 - 2 \text{Cov}(R_S - R_T, R_R - R_T) \\ &\quad + E(R_R - R_T)^2 - 2E(R_S - R_T)E(R_R - R_T)\end{aligned}\quad (2)$$

or

$$\sigma_{\Delta ST}^2 = \sigma_{\Delta SR}^2 - \sigma_{\Delta RT}^2 + 2 \text{Cov}(\Delta_{ST}, \Delta_{RT}) + 2b_{ST}b_{RT} \quad (3)$$

The relationships above show how the bias and the random error of the reference value can have a significant influence on the computation of the raw statistics. The evaluation of the reference value is thus a crucial part of any objective validation and intercomparison exercise.

Using these relationships, two approaches are possible. First, one can directly base the analysis on the raw statistics computed using the estimated reference values, without taking into account their uncertainty. This means that more confidence is given to the reference value than to the evaluated products. This condition is acceptable if the reference value error is much smaller than the expected error of the evaluated product.

This is, for example, the implicit assumption of Nicholson et al. (2003) in their comparison of rain products, which does not include a quantification of the possible error of the reference. This makes it difficult to assess the degree of significance of the statistics obtained. Thorne et al. (2001), on the other hand, evaluate the reference uncertainty to draw attention to the significance of their statistics but do not use it directly in their calculation.

The second approach is more objective but also more complicated. The statistics (b_{ST} , rmse_{ST}) are related to the true unknown values. With consideration of Eqs. (1) and (3), this approach first requires estimation of

the following associated statistics: b_{RT} , rmse_{RT} , and $\text{Cov}(\Delta_{ST}, \Delta_{RT})$. Correction of the raw rmse (rmse_{SR}) has been attempted by some authors. Barnston (1991), Ciach and Krajewski (1999), and Gebremichael et al. (2003), for instance, have used Eq. (3) in which they assume $\text{Cov}(\Delta_{ST}, \Delta_{RT})$, b_{ST} and b_{RT} to be equal to zero. The method has been called error variance separation (EVS), and Eq. (3) becomes

$$\sigma_{\Delta ST}^2 = \sigma_{\Delta SR}^2 - \sigma_{\Delta RT}^2. \quad (4)$$

In others words, the estimate product errors and reference product errors are assumed to be independent. Because the products under evaluation here often consist of a merging of rain gauge data and satellite information, the reference rain gauge and regional/global products have some common information, which implies that $\text{Cov}(\Delta_{ST}, \Delta_{RT})$ may not be equal to zero and its influence may be significant in Eq. (3). The importance of $\text{Cov}(\Delta_{ST}, \Delta_{RT})$ may depend on the relation between the gauges used for validation and the gauges that are included in the regional and global products. This situation is a critical point for large-scale validation exercises of global products in West Africa, because the available rain gauge network generally used to create the reference value is often not dense and is not very different from the network used to create the global products. Moreover, the non-Gaussianity of rain fields accentuates the effects of the computing bias. The application of the assumption that the error covariance is equal to zero must be considered with much attention. We analyze below how to account for ground-based sampling error in the evaluation error of rainfall products, that is, how rmse_{ST} can be computed by application of Eq. (3) without neglecting the covariance. The results obtained with and without taking into account the reference uncertainty will be compared.

c. Estimation of the terms of Eq. (3)

To assess the rmse_{ST} from Eq. (3), the terms b_{RT} , rmse_{RT} , and $\text{Cov}(\Delta_{ST}, \Delta_{RT})$ are estimated as follows.

1) ESTIMATION OF THE TERM RMSE_{RT}

The question of computing rmse_{RT} has been treated in Ali et al. (2005, hereinafter Part I). A cross-validation procedure has been used to investigate different kriging methods designed to improve the calculation of the ground-based error (rmse_{RT}). A relative error function [Eq. (5) below] has been established and will be used here for the computation of rmse_{RT} :

$$e(A, N_g, K_T, P_T) = \frac{1.05}{\sqrt{N_g} \sqrt{K_T}} \left(\frac{P_T}{K_T} \right)^{-0.2} \times \left[0.28 + 0.17 \log \left(\frac{A}{N_g} \right) \right], \quad (5)$$

where A is the grid area in square kilometers, N_g is the number of rain gauges in A , K_T is the number of events during the considered period, P_T is the cumulative rainfall in millimeters over the same period, and e is the relative estimation error of the mean areal rainfall.

A major variable concerning the error variability in this error model is the number of events, which is the most important explanatory factor of the Sahelian rainfall variability (Le Barbé et al. 2002). Several approaches to determine the number of events on a regional scale, where only daily data are available, are discussed and validated in Part I.

2) ESTIMATION OF THE TERMS b_{RT} AND $\text{Cov}(\Delta_{ST}, \Delta_{RT})$

(i) The bias: b_{RT}

Geostatistical analysis is an unbiased interpolation method. The evaluation procedure in the companion paper shows that the bias is practically equal to zero. So, if the point measurement is assumed to represent the "true" rainfall, the areal rainfall bias can be assumed to be equal to zero. Otherwise the bias of the areal rainfall is equal to the point bias.

(ii) $\text{Cov}(\Delta_{ST}, \Delta_{RT})$

Because a direct computation is not possible here, we analyze on the one hand the possibility of neglecting this term. This option consists of an application of EVS [Eq. (4)]. On the other hand, an area with "dense network" coverage D will be chosen for the assessment of this covariance. The estimation R_D from this dense network can be assimilated to R_T ; then $\text{Cov}(\Delta_{ST}, \Delta_{RT})$ will be estimated as $\text{Cov}(\Delta_{SD}, \Delta_{RD})$. In section 6 the importance of the estimated covariance will be analyzed and the two approaches will be compared.

3. Sahelian rainfall products: Regional and global

a. Regional products

The AGRHYMET rain gauge database (see Part I for details) is used here to study various regional ground-based products. Three kinds of networks (Fig.

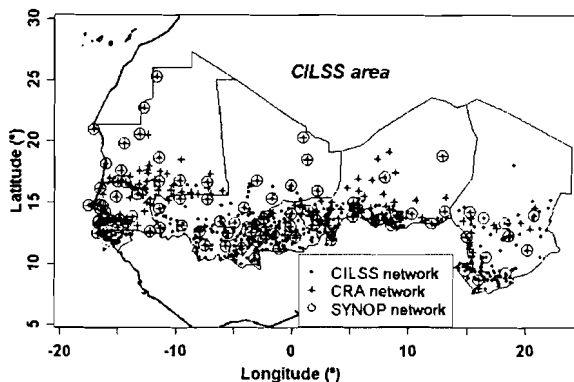


FIG. 1. The operational networks for the Sahelian region. The CILSS network (650 gauges on average) is available at the end of the rainy season at the AGRHYMET Center, the CRA network (280 gauges) is available every 10 days, and the SYNOP network (80 gauges) is available daily.

1) are considered: 1) the whole operational network (Comité Inter-Etats de Lutte Contre la Sécheresse au Sahel; average of 650 rain gauges with data available at the end of the rainy season), hereinafter referred to as "CILSS," 2) the monitoring network (about 250 rain gauges with data available on a 10-day basis at the AGRHYMET Regional Center), hereinafter referred to as "CRA," and 3) the synoptic network [80 rain gauges with data available on a daily basis through the Global Telecommunications System (GTS)], hereinafter referred to as "SYNOP." The CRA network is included in the CILSS network, and the SYNOP network is included in the CRA network. In accordance with the resolution of the global products presented below, regression kriging is used to create a regional rainfall product based on a $2.5^\circ \times 2.5^\circ$ grid for these three networks over the period of 1950–2002.

b. Global products

1) THE GPCC AND GPCP OPERATIONAL DATASETS

The Global Precipitation Climatology Center (GPCC) produces monthly gridded $2.5^\circ \times 2.5^\circ$ rainfall estimates based on gauge-only data from the GTS and other records (Rudolf 1993); this product is referred to as GPCC. The Global Precipitation Climatology Project (GPCP) rainfall product combines different information (gauges and satellite IR and microwave observations). The GPCP product is described in Huffman et al. (1997). The primary GPCP product is a monthly analysis based on a global 2.5° latitude \times 2.5° longitude grid spanning the period from January 1979 up to the present date. A second product is a 5-day global analy-

sis (Xie et al. 2003), and a third is a daily 1° latitude \times 1° longitude analysis from January 1997 to the present date (Huffman et al. 2001).

2) THE CMAP DATASET

The Climate Prediction Center merged analysis of precipitation (CMAP) was constructed by Xie and Arkin (1997). The temporal and spatial scales are similar to those of GPCP, except that there is no daily CMAP product. The first step is to combine the various satellite estimates based on IR, SSM/I, and Microwave Sounding Unit data using a maximum likelihood approach in which weighting coefficients are inversely proportional to the squares of the individual random errors. The resulting satellite-based analyses provide the field shape, which is then adjusted to the rain gauge data (where available).

3) THE GPI

The Geostationary Operational Environmental Satellite precipitation index (GPI; Arkin et al. 1994) assumes that a 3-mm rainfall occurs every hour of cold-cloud duration over a pixel. Because of its simplicity, GPI is still widely used for climatological studies of global precipitation. This is the only *pure* satellite product among the four global products studied here.

4. Evaluation of the CILSS rain gauge networks

a. Sahelian operational network error analysis

Several authors (e.g., Rudolf et al. 1994; Morrissey et al. 1995; Xie and Arkin 1995) suggest that five rain gauges over a $2.5^\circ \times 2.5^\circ$ cell are sufficient to guarantee an estimation error of less than 10% (percentage error is calculated with respect to the mean of the variable considered) for the areal monthly rainfall over the cell. This result does not hold for the Sahelian region, as may be seen from the study of Lebel and Amani (1999). In fact, as clearly shown in Eq. (5), the estimation error depends both on the monthly total and the number of recorded rain events in this total. The greater the number of events for a given total is, the greater is the smoothing of the event-scale spatial variability and, consequently, the smaller is the estimation error.

This is illustrated well in Fig. 2a, showing the dispersion of estimation errors computed for the same number of gauges available over a $2.5^\circ \times 2.5^\circ$ cell using Eq. (5). For five gauges over a $2.5^\circ \times 2.5^\circ$ grid, the error varies from 5% to 30%, depending on the area and month considered. The error is maximum for dry months in the northern part of the domain and is mini-

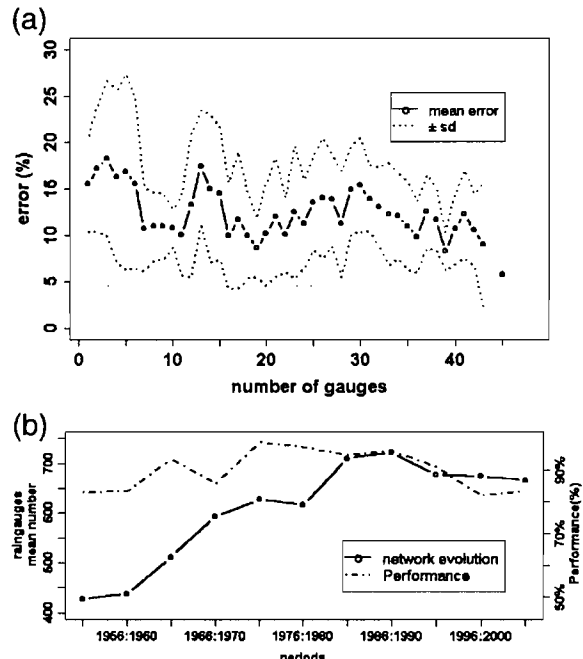


FIG. 2. (a) Relationship between the estimation error and the number of operational gauges. There is a significant dispersion for the same number of gauges (e.g., for five gauges over $2.5^\circ \times 2.5^\circ$, the error varies from 5% to 30%). (b) Mean number of gauges and the performance (percentage of cells for which the monthly estimation error over $2.5^\circ \times 2.5^\circ$ is less than 20%) of the network for the period of 1950–2002. Note that the rapid increase in the number of gauges during the dry period (1970–90) did not involve a better performance (smaller estimation error), because in dry years rainfall is more variable in space and thus requires a comparatively larger number of gauges to guarantee a given level of accuracy.

mum in the south of the domain where, on average, a larger number of rain events are recorded. This dispersion factor is amplified by the fact that, as seen in Fig. 1, the network is far from being homogeneous in terms of density. Even when limiting the computation to the 3 months of the core of the rainy season [July–September (JAS)] so as to obtain a more homogenous sample, the dispersion of errors over a total sample of 1287 values (39 cells \times 3 months \times 11 yr) is still significant, with 80% of the $2.5^\circ \times 2.5^\circ$ errors in the range of 5%–22%. Averaged over the whole period of study and JAS, the mean monthly error is 12% for the entire Sahel but only 9% for latitudes below 15°N . A similar computation performed for $1^\circ \times 1^\circ$ grids shows that 80% of the errors at that resolution range from 8% to 28%.

The overall performance of the CILSS network is presently decreasing, as shown in Fig. 2b. This decrease is the result of both the decrease in the number of

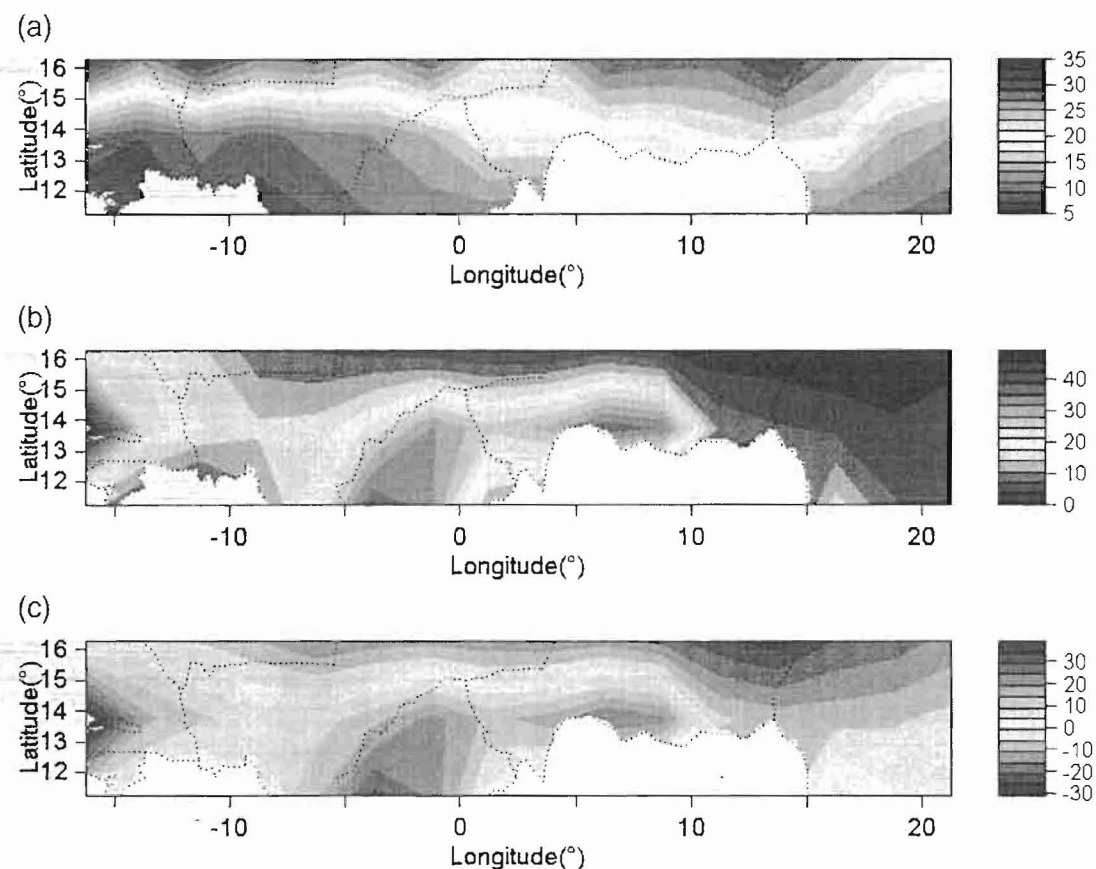


FIG. 3. (a) Mean optimal number of gauges per grid cell ($2.5^\circ \times 2.5^\circ$), which provide the estimation error of less than 10% at the monthly scale for the period 1990–2000. (b) Actual mean number of gauges of the CILSS operational network for the same period. (c) The difference between (a) and (b). The CILSS operational network guarantees a monthly error smaller than 10% for 42% of the grid cells, located south to 15°N and west of 11°E .

gauges since the optimum of the mid-1980s and the decrease in the monthly rainfall of August and September that characterize the drought.

b. Optimal networks

One application of the error function is the determination of optimal networks. The optimal network concept depends on the scale of interest [time K_7 and space A in Eq. (5)]. The criterion of optimality corresponds to the accepted error threshold. For a fixed error, the inversion of Eq. (5) makes it possible to compute the minimum number N_g^* of stations needed to remain below the error threshold. The error threshold e considered here is 10%. The analysis will focus on the $2.5^\circ \times 2.5^\circ$ resolution [$A = 75\,000 \text{ km}^2$ in Eq. (5)] and monthly rainfall corresponding to the resolution of the most widely used operational rainfall products.

For the JAS period, it is found that for the period of

1990–2000 the mean optimal number of rain gauges over a $2.5^\circ \times 2.5^\circ$ cell is 14.6, corresponding to a total of 569 gauges (Fig. 3a). By comparison, the network available over this whole period (shown in Fig. 3b) comprises 561 gauges. However, this rough comparison is not really meaningful given the strong heterogeneity in the statistics. The optimal number of gauges per $2.5^\circ \times 2.5^\circ$ cell is six in the southwest (south of 13°N and west to 5°W), 15 for the central part, and 35 in the north (north of 16°N). This variability in the optimal number of rain gauges is linked to the variability in the number of events \bar{K}_7 as may be seen in Table 1. The network evaluation of Fig. 3c shows that the only area that is in fact optimally covered is the one located south of 15°N and west of 11°E , representing 42% of the CILSS region. For example, at 11°N , the mean optimal number of rain gauges is 8.3, with the actual number being 18.3. At 16°N , the optimal number is 20.6 and the actual number is 5.9.

TABLE 1. Details on the characteristics of optimal networks and the evaluation of the CILSS operational network for different areas and for two scales: monthly values over $2.5^\circ \times 2.5^\circ$ grid cells and 10-day values over $1^\circ \times 1^\circ$ grid cells. The only area over which the CILSS network is optimal everywhere for the $2.5^\circ \times 2.5^\circ$ resolution is the area lying south of 15°N and west of 11°E ; N_g^* is the average number of gauges per cell satisfying the optimality criterion, and N_g^{real} is the average number of gauges per cell of the CILSS network over the subarea. Optimality corresponds to grid cells for which the error is less than 10%. Italics denote values for which the existing network is less than the optimum number of gauges.

Area	\bar{K}_T	N_g^*	N_g^{real}	$(N_g^{\text{real}} - N_g^*) / N_g^*$	No. of optimal cells
Monthly values (JAS) $2.5^\circ \times 2.5^\circ$					
Total	11.8	14.6	14.4	-1%	42%
$10^\circ\text{--}12.5^\circ$ lat	16.3	8.2	18.3	55%	72%
$12.5^\circ\text{--}15^\circ$ lat	12.1	11.2	21.1	47%	69%
$15^\circ\text{--}17.5^\circ$ lat	7	20.6	5.9	-248%	0%
$<15^\circ$ lat and west of 11°E	11.27	9.9	27.1	82%	100%
10-day values $1^\circ \times 1^\circ$					
Total	5.6	16.7	2.6	-538%	1.5%
$10^\circ\text{--}13^\circ$ lat	7.33	11	3.4	-223%	2%
$13^\circ\text{--}15^\circ$ lat	6	14.25	3.6	-296%	2.8%
$15^\circ\text{--}18^\circ$ lat	3.9	23.4	1.2	-1900%	0%
$<15^\circ$ lat and west of 11°E	6.8	12.2	4.5	-169%	3.2%

At the smaller scales of 10 days and $1^\circ \times 1^\circ$, the number of required stations over the whole region increases to 3559. To comply with the 10% error criterion only for the area located south of 15°N , one would need 1736 stations. Only 1.5% of the cells have a number of rain gauges above the optimum number (see also the Table 1 for details).

A rough rule of thumb concerning times scales can be proposed: on average, a network producing a 20% error on a monthly basis provides estimates with a 30% error on a 10-day basis and a 10% error on a seasonal basis at $1^\circ \times 1^\circ$ scale.

5. Global product evaluation: The CILSS product as a reference value

This section uses the classical approach to evaluate global products. The optimal estimates from the CILSS network are used as reference values, not taking into account their uncertainty. The scale considered is monthly and has a $2.5^\circ \times 2.5^\circ$ spatial resolution.

a. Interannual and intraseasonal homogeneity analysis

Before combining any monthly or annual data for global analysis, we carry out a systematic trend analysis

to check for homogeneity. This section aims at determining whether there is a seasonal cycle in the various statistics used for the evaluation and also whether there are systematic differences between wet and dry years. The period of 1986–99 is considered, that is, the period over which the GPCC product was available. Figures 4a(1), 4a(2), and 4a(3) show that there is indeed a seasonal cycle for all three indicators. The rmse and the bias are minimum in the middle of the rainy season and, inversely, the correlation is maximum in the middle of the season. These results show that, for the sake of homogeneity, the core and the margin of the season must be separated. Figures 4a(1), 4a(2), and 4a(3) also show that CMAP has a good score in the core of the season whereas GPCC and GPCP are best in the margins. GPI has the poorest score for the whole season. In view of these results, the analysis will be restricted to the months of JAS. Figures 4b(1), 4b(2), and 4b(3) show that there are no systematic differences between wet and dry years, which indicates that wet and dry years can be mixed in a global analysis covering the whole 1990–99 period. Another result of this analysis is that the rmse has increased in recent years for all products. The nonexistence of this trend for the bias suggests that this deterioration is due to an increased sampling error. The decrease of the network density observed in Fig. 2 for recent years supports this assumption. We can also note a degrading trend in the correlation coefficient after 1992 for all products, which can be explained by the same reason as that for the rmse.

b. Global analysis of the JAS period

1) SCATTERPLOTS AND HISTOGRAMS

Figure 5 is a joint representation of the linear relationship between the global products and the CILSS product and the experimental distribution of monthly areal rainfall for different products. Note that for all products, the regression line is under the bisecting line for high values, suggesting an underestimation with respect to the ground estimate. Also, the regression line tends to be over the bisecting line for low values, suggesting an overestimation. Note that the GPI distribution is far less asymmetric than the other distributions because of the way it is computed.

2) COMPARISON OF DISTRIBUTIONS

Apart from GPI, for which the 25% quartile is roughly equal to the 50% quartile of the other products, the box plots (Fig. 6a) of the different products are

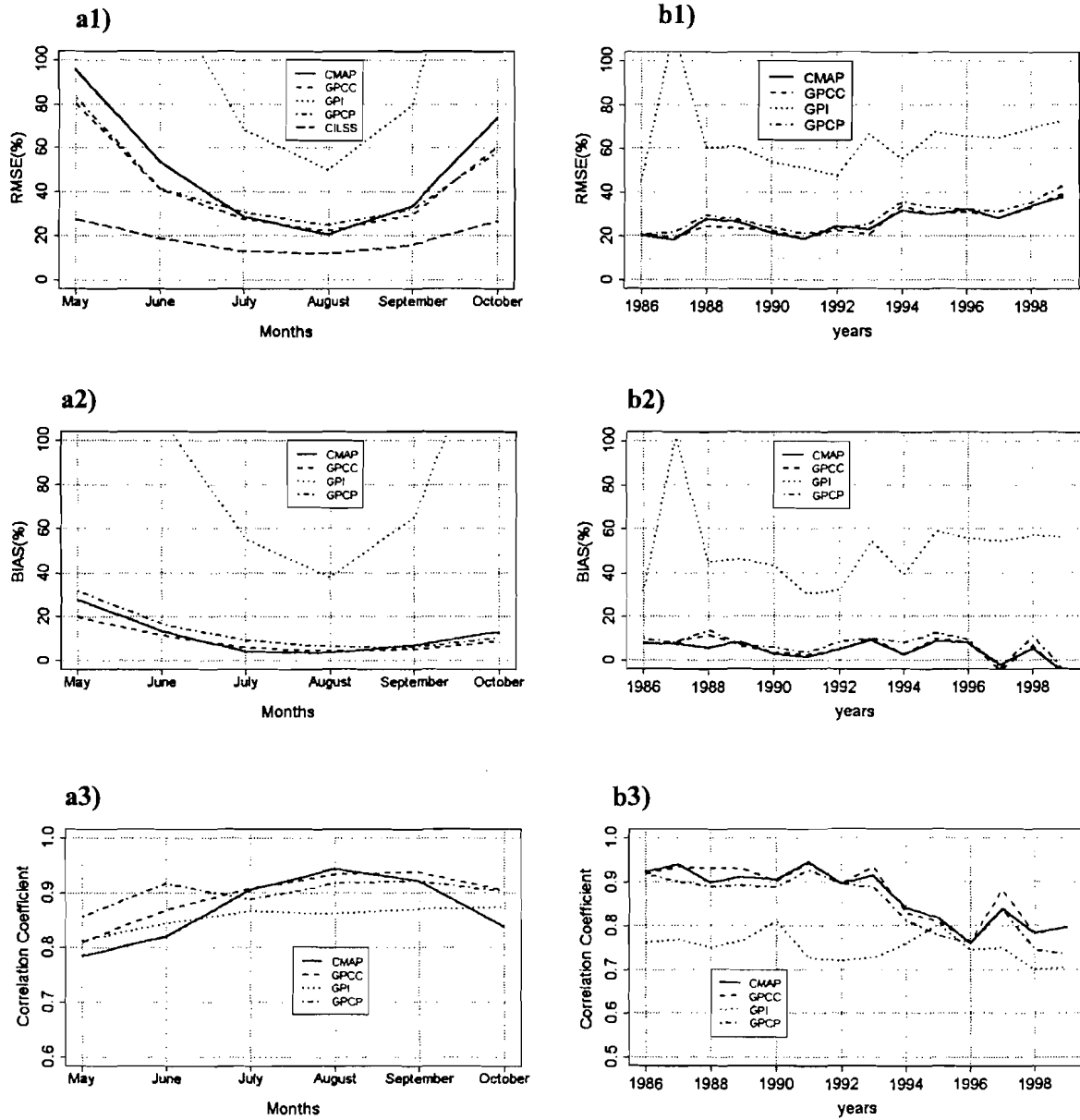


FIG. 4. (a) Monthly mean values for the three statistics used to compare each global product with the CILSS reference [(a1) rmse, (a2) correlation coefficient, and (a3) bias]. The minimum rmse and bias and the maximum correlation occur in the core of the rainy season (i.e., Aug.). All three statistics show a systematic intraseasonal pattern. (b) Annual mean values computed from JAS monthly values only for the three statistics used to compare each global product with the CILSS reference [(b1) rmse, (b2) correlation coefficient, and (b3) bias]. In general, the statistics do not show any systematic difference between wet and dry years. However, the rmse shows an increase in recent years.

similar. However, the 25% quartiles of CMAP, GPCC, and GPCP are slightly higher than that for CILSS. The interquartile intervals (25%-75%) of CILSS and CMAP are very close and that of GPCC is close to that of GPCP. For the empirical distributions (Fig. 6b), all of

the products underestimate the frequency of the low values, as compared with CILSS, and they overestimate the frequency of medium values. The proportion of values below the 25% quartile is 17% for CMAP, 13% for GPCC, 13% for GPCP, and 6% for GPI. This under-

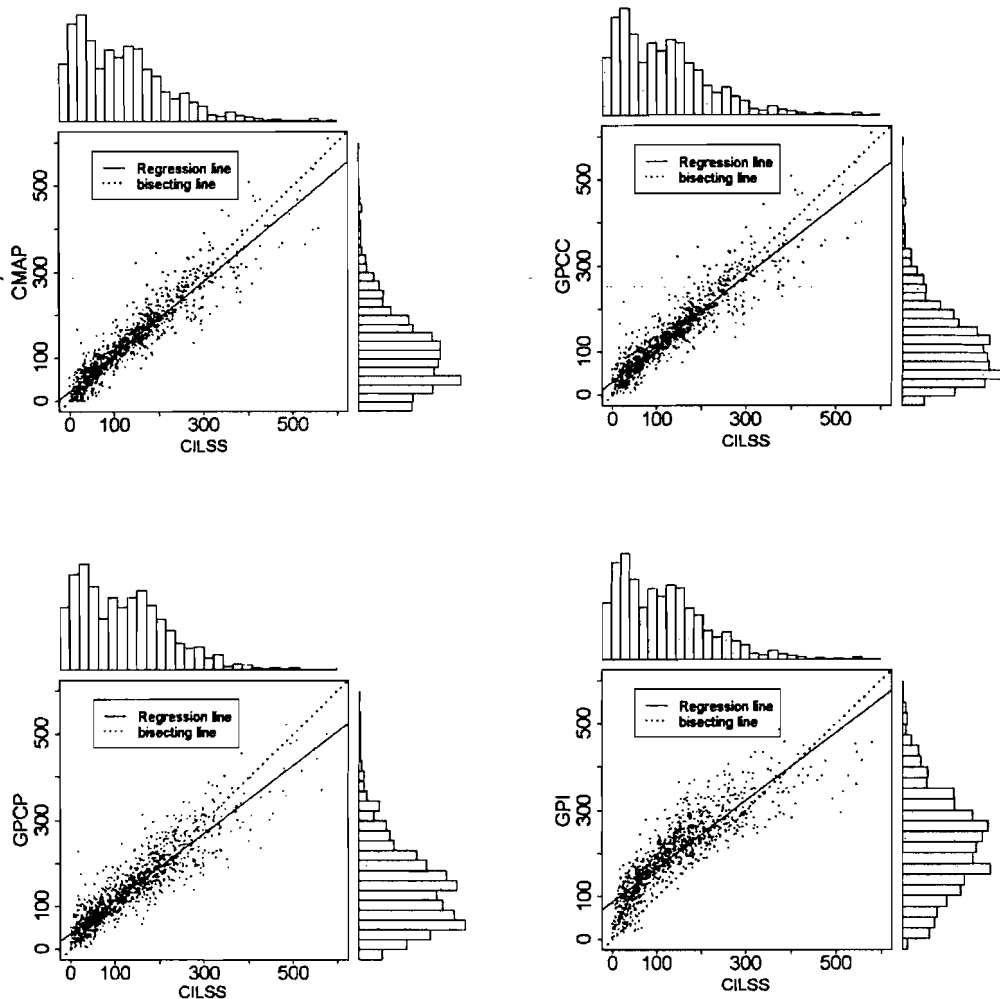


FIG. 5. A joint analysis of scatterplots and histograms for the four global products (CMAP, GPCC, GPCP, GPI) with respect to CILSS. The values represent the JAS monthly rainfall between 1990 and 1999.

estimation of the frequency of low values is due to the inability of satellites to correctly estimate intermittency. For the extremes values, apart from GPI, which continues to be biased, the product distributions are similar. For example, the probability of exceeding 320 mm, which is the CILSS's 95% quartile, is 5%, 4%, 3.7%, and 3.3% for CILSS, CMAP, GPCC, and GPCP, respectively. For GPI, 11% of its values are over the CILSS's 95% quartile.

Figure 7 shows that the major discrepancy between the distribution of the global product and that of the CILSS is observed for the northern part of the domain (north of 15°N), with the GPI distribution being completely unrealistic. In this area the ground-based estimate is also highly uncertain (theoretical kriging error equal to 34%).

3) NUMERICAL CRITERIA: RMSE_{SR}, b_{SR}, AND THE NASH INDEX

For this analysis, the Nash index I_{SR} presented below is considered as an additional statistic to the rmse, bias, and correlation criteria, because it is not influenced by the bias, as is the correlation:

$$I_{SR} = 1 - \frac{\text{rmse}_{SR}^2}{\sigma_R^2}. \quad (6)$$

The Nash index is equal to 1 for a perfect estimate [i.e., $(R_S)_i = (R_R)_i$ for all i] and is equal to 0 if, for all i , $(R_S)_i = \bar{R}_R$.

Table 2 shows that, in fact, CMAP, GPCC, and GPCP have a very low bias (less than 5%), while GPI

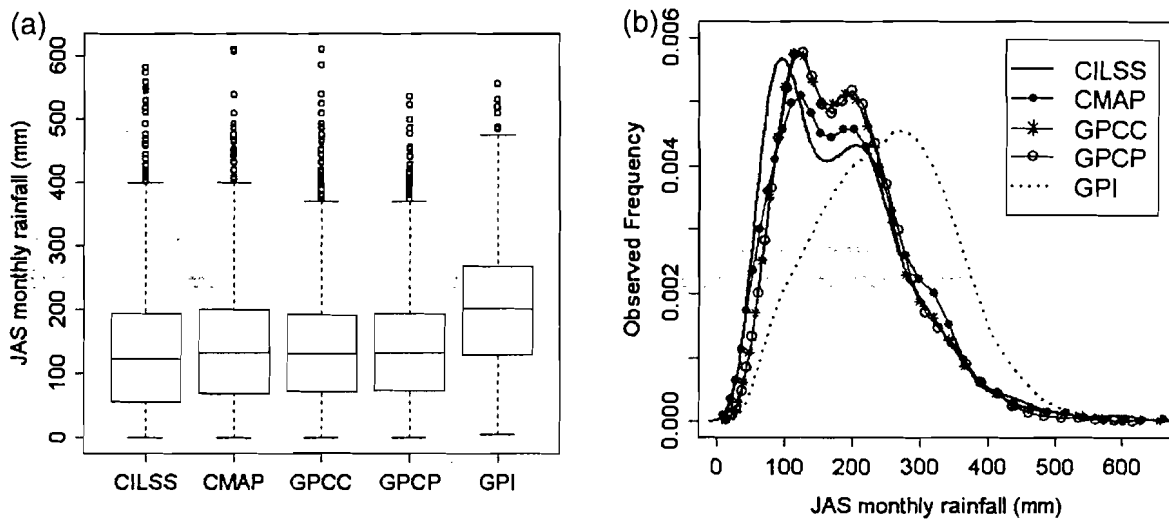


FIG. 6. Comparison of (a) box plots and (b) observed probability distribution function for the CILSS reference and the four global products for the JAS period over the entire CILSS region. The global products overestimate the frequency of the median while the frequency of low values is underestimated.

is highly biased (43%). This, of course, is related to the fact that CMAP, GPCC, and GPCP incorporate ground observations. Because of this low bias the other statistics computed for these products give similar results, with CMAP being slightly better, with 2% and 25% in terms of b_{SR} and rmse_{SR} , followed by GPCC (4% and 27%), GPCP (5% and 28%), and GPI (43% and 55%).

In analyzing these statistics along latitudes, the conclusion is the same as that for the analysis of distributions: the quality of the products is far worse in the northern part of the domain. The minimum errors (rmse_{SR}) are obtained for the medium strip (12.5° – 15°N): 16% for CMAP, 17% for GPCC, 21% for GPCP, and 53% for GPI, against 24%, 22%, 23%, and 44%, respectively, for the southern strip (10° – 12.5°N). For the northern strip (15° – 17.5°N), the errors are very

high: 55%, 69%, and 80% for CMAP, GPCC, and GPCP, respectively, and 130% for GPI.

c. Significance test for the statistics

Because the statistical distribution of rain fields is not Gaussian, nonparametrical statistical tests are used to verify the equality of the means, variances, and cumulative distribution functions (CDF) of global products and the reference regional product (CILSS). The tests are the Wilcoxon U test (abbreviated as W ; Hollander and Wolfe 1973) for the equality of the means, the Ansari–Bradley (Hollander and Wolfe 1973) and Mood (Conover 1971) tests for the equality of the variances, and the Kolmogorov–Smirnov (KS) test for the equality of the CDFs.

A p value of 10% is used to accept or reject the

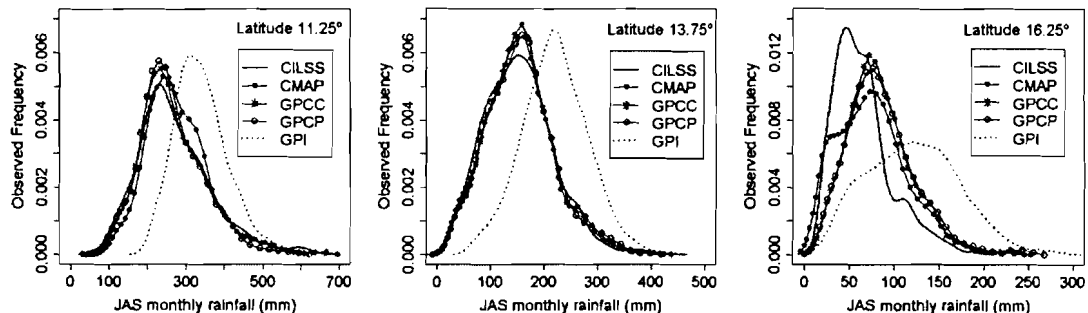


FIG. 7. The observed probability distributions as a function of latitude. At 11.25° and 13.75°N , apart from the GPI product, the other distributions are similar and display the same mode. At 16.25°N all of the distributions become very different from the reference CILSS distribution.

TABLE 2. Average statistics over the entire Sahel when using the CILSS rainfall as a reference, not taking into account its uncertainty.

	CMAP	GPCC	GPCP	GPI
Rmse (%)	25	27	28	55
Bias (%)	2	4	5	43
I	0.88	0.86	0.76	0.42
R^2	0.88	0.86	0.85	0.77

hypothesis tested. The calculations are performed so as to test the homogeneity of statistics with respect to time [the means are computed over 3 (months) \times 14 (years) samples with 39 cells both for CILSS and the product under consideration] and with respect to space [the means are computed over 39 (cells) samples of 3 (months) \times 14 (years)].

The results, summarized in Table 3, show that the temporal fields are more homogeneous than the spatial fields. The percentage of cases accepted is larger for the temporal fields than for the spatial fields, except for the variance. The equality of means and CDFs is accepted for more than 95% of the temporal fields for CMAP, GPCC, and GPCP. CMAP also performs very well for the equality of variances, both in time and space, confirming that it is the closest product to the CILSS reference. Except for the variance, it can be concluded that the global products do a better job in reproducing the seasonal cycle than in accounting for the spatial variability of the monthly rainfall. GPI is an interesting case to analyze because, as already seen previously, its CDF and mean are very different from the CILSS references. However, GPI performs as well as the other products—and even better than GPCC and GPCP—in terms of the equality of the variances. This means that products using only the satellite information may correctly estimate the rain field variances at the scale tested here, confirming the finding of Mathon et al. (2002), that satellite is able to distinguish rain events; because in the Sahelian region the variability of rain fields is mainly due to the variability in the number of events.

d. Interval of kriging standard deviation for performing the analysis: Nonlinear correlation

The computation performed here counts the number of times the estimate of a given rainfall product falls into the theoretical one or two standard deviation interval. The theoretical standard deviation considered is the kriging standard deviation (ksd) of estimation error of the reference. The probability of belonging to this interval must be found experimentally because rain fields are not Gaussian. A cross-validation procedure performed on the reference CILSS fields shows that this probability is 73% on a monthly basis. This approach has already been used by Thorne et al. (2001) and is a useful complement to linear statistics because it makes it possible to quantify the nonlinear fluctuation between the products and the rain gauge-based reference:

$$P = \text{the number of times that } -\text{ksd} \leq R_S - R_R \\ \leq +\text{ksd} \text{ or } -2\text{ksd} \leq R_S - R_R \leq +2\text{ksd}.$$

In accordance with this criterion P , Table 4 shows that CMAP is still the best product, followed by GPCC, GPCP, and GPI. These results indicate some consistency between the different criteria used in this study and show the robustness of the statistics used. Figure 8 also shows that the distribution of the discrepancy between CMAP and CILSS is very close to the discrepancy between GPCC and CILSS.

6. Taking into account the ground-based error in statistics

This section addresses the implementation of a solution to the problem that was theoretically addressed in sections 2b and 2c. The objective is to analyze the degree of uncertainty associated with the classical approach used in section 5 and to obtain a supposedly closer to reality estimation of rmse_{ST} . Three analyses are performed: 1) the whole CILSS network is the reference and the gridded estimates from the two other

TABLE 3. Percentage of null hypothesis H₀ assumption accepted with regard to the tests applied month by month or cell by cell for a 10% acceptance level.

Products	Equality of the variances:							
	Equality of the CDF: KS test		Equality of the means: W test		Ansari–Bradley test		Mood test	
	Months	Cell	Months	Cell	Months	Cell	Months	Cell
CMAP	100	76	100	72	98	98	98	95
GPCC	95	71	100	74	74	93	70	88
GPI	5	9	2	2	90	88	92	90
GPCP	95	67	97	62	74	90	71	90

TABLE 4. The number of times the discrepancy D between the products and CILSS reference is within 1 or 2 times the standard kriging deviation.

P	CMAP	GPCC	GPI	GPCP
Percent ($-ksd \leq \Delta \leq ksd$)	40	38	8	37
Percent ($-2ksd \leq \Delta \leq 2ksd$)	71	69	21	66

networks (CRA, SYNOP) are considered as operational ground-based products to be compared with the global products (CMAP, GPCC, GPI, and GPCP), 2) the CRA and SYNOP networks are considered as possible alternate references and the fluctuation of $rmse_{SR}$ as a function of the reference used is analyzed, and 3), using a densely instrumented subregion, an empirical study is done to estimate the different terms of Eq. (3) to assess $rmse_{ST}$ as compared with $rmse_{SR}$.

a. Comparing regional and global products with respect to CILSS

In this section, for stationarity and homogeneity purposes, only the area south of 15°N (southern Sahel) is considered, representing 23 grid cells with an average density of 19.2 gauges per cell. As may be seen from the CILSS column of Table 5, CRA and SYNOP have a smaller error than the global products when the optimal CILSS rain fields are taken as the references. On the other hand, when neglecting the drift in the computation of the ground products (the "no drift" subcolumn

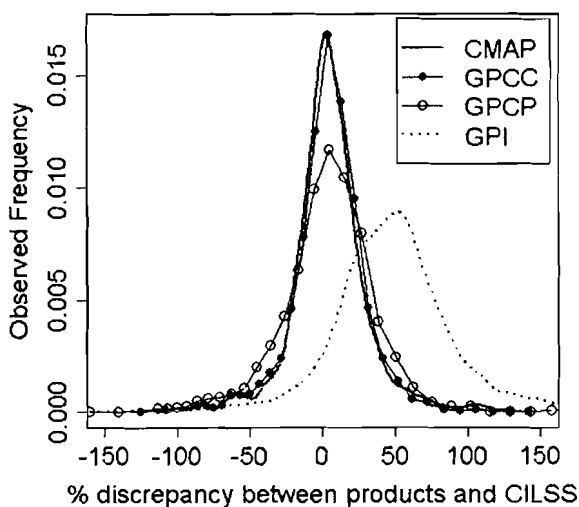


FIG. 8. Probability distributions of the percentage difference between the four global products and the CILSS reference. The distributions for CMAP and GPCC are very similar, whereas the distribution of GPCP is more dispersed. GPI shows significant differences from the other products.

TABLE 5. Estimation errors ($rmse_{SR}$) when using different references for the area lying south to 15°N . Values are in percent. The estimation error associated with each reference ($rmse_R$) is 8.2% for CILSS, 12% for CRA, and 13.6% for SYNOP.

Products	Values of $rmse_{SR}$ for different references			
	CILSS reference	CRA reference	SYNOP reference	No drift
CRA	14.1	18		
SYNOP	14.4	24.5		
CMAP	15.9	21	18	16
GPCC	16	25	18	15.9
GPCP	18	27	19.5	19.1
GPI	42	45	44	44.5

in Table 5), SYNOP performs worse than CMAP. This result means that 1) a blended satellite-ground product, because of the continuous space coverage of the satellite information, is able to constitute better the latitudinal gradients than can a nonoptimally interpolated ground product and 2) it is necessary to use interpolation algorithms incorporating the drift in their interpolation scheme. In terms of the best spatialization method, the ranking of the different products is thus CRA, SYNOP, CMAP, GPCC, GPCP, and GPI.

b. Comparing global products with CRA and SYNOP as references

Changing the reference to either CRA or SYNOP (columns CRA or SYNOP in Table 5) produces contrasted results. On the one hand, the CRA reference is associated with larger $rmse_{SR}$ values of the global products, indicating that references obtained from less dense networks will tend to produce larger values of $rmse_{SR}$. On the other hand, for CMAP and GPCC, the $rmse_{SR}$ values decrease when shifting from the CRA reference to the SYNOP reference (for CMAP, $rmse_{SR} = 15.9\%$ when CILSS is used as reference, 18% when CRA is considered to be the reference, and 16% when the reference is SYNOP). A likely explanation is that CMAP and GPCC include ground data provided by synoptic stations only (not all the synoptic stations, however). This clearly illustrates how the choice of the reference (both the network used and the interpolation algorithm) may influence the results of an intercomparison exercise.

c. Assessment of $rmse_{ST}$

The sensitivity of $rmse_{SR}$ to the reference used underlines the necessity to evaluate the neglected terms of Eq. (3) to obtain a more credible assessment of the

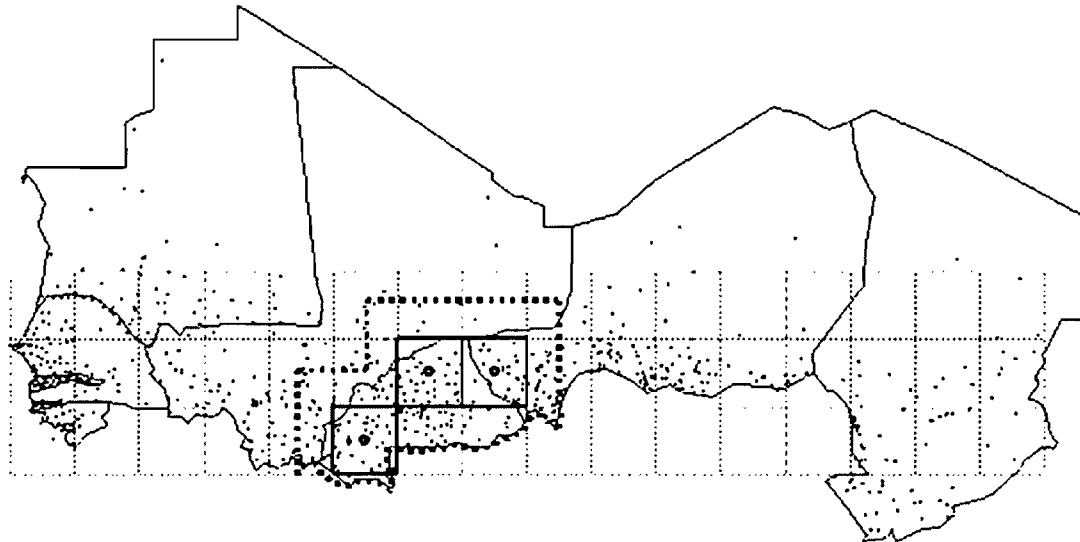


FIG. 9. The target area (thick dashed line) for the subsampling approach in the estimation of the covariance of errors. A total of 217 gauges are covering this area. Various subsampled networks are used to create ground references of varying accuracy over the three central grid meshes (solid line). The objective is to evaluate the influence of the reference on the computation of both the rmse_{SR} and rmse_{ST} .

rainfall product errors. If one assumes that the reference rain fields are unbiased, two terms remain to be evaluated as addressed in section 2c: rmse_{RT} and $\text{Cov}(\Delta_{ST}, \Delta_{RT})$. The theoretical computation of rmse_{RT} is straightforward in the statistical context used here (the results of this computation are given in the caption of Table 5 for the three references tested here). The EVS method presented in Eq. (4) only makes use of rmse_{RS} and rmse_{RT} to compute rmse_{ST} , assuming the covariance to be negligible in comparison of these terms. Because there is no straightforward way to compute $\text{Cov}(\Delta_{ST}, \Delta_{RT})$, this assumption is rarely tested. For the case treated here, the EVS computation leads to surprising results, with a CMAP EVS error equal to 13.6% when CILSS is used as reference and 8.4% when SYNOP is used. There is a clear reference dependency in these results, pointing out the need to assess how the neglected term $\text{Cov}(\Delta_{ST}, \Delta_{RT})$ could influence the value of rmse_{ST} . Because the gauge network used in CMAP is closer to the SYNOP network than to the CILSS network, one can reasonably assume that $\text{Cov}(\Delta_{ST}, \Delta_{RT})$ is larger when SYNOP is the reference than when CILSS is the reference.

A way to test how $\text{Cov}(\Delta_{ST}, \Delta_{RT})$ might influence the overall assessment of rmse_{ST} is to work on a more densely instrumented area where it is possible to build better proxies of R_T than when considering the whole Sahel. Over the target area delimited by the thick dashed line in Fig. 9, a total of 217 gauges is available,

corresponding to 2 times the density of the CILSS network over the southern Sahel (19.2 gauges per $2.5^\circ \times 2.5^\circ$ grid cell). To study the effects of using various references on the computation of rmse_{SR} and rmse_{ST} , a subsampling approach is used to create different reference networks of increasing density, by choosing randomly between 5 and 217 gauges with increments of 10 gauges. For each number of gauges, 21 subsample networks are created. The comparison is then carried out for the three $2.5^\circ \times 2.5^\circ$ cells located at the center of this target area.

As a first step, rmse_{SR} is computed for the different reference networks, leading to the results shown in Fig. 10 [the computations are made with a sample of 14 years (1986–99) \times 3 cells \times 3 months \times 21; i.e., 2646 values]. Except for GPI, which is less dependent on the reference used, rmse_{SR} decreases significantly until reaching a density of approximately 10 gauges over a $2.5^\circ \times 2.5^\circ$ grid cell. This density is one-half of the CILSS density over the southern Sahel.

The second step is to use the denser network of 217 gauges to provide a supposedly better proxy of R_T to estimate the covariance $\text{Cov}(\Delta_{ST}, \Delta_{RT})$ in Eq. (3). It then becomes possible to compute rmse_{ST} for all of the references of step 1. The computation of rmse_{ST} taking into account an estimation of $\text{Cov}(\Delta_{ST}, \Delta_{RT})$ is denoted as $\text{rmse}_{ST}^{\text{COV}}$; when the covariance is neglected it is denoted as $\text{rmse}_{ST}^{\text{EVS}}$. The results of the computation of these two rmse_{ST} are shown in Fig. 11

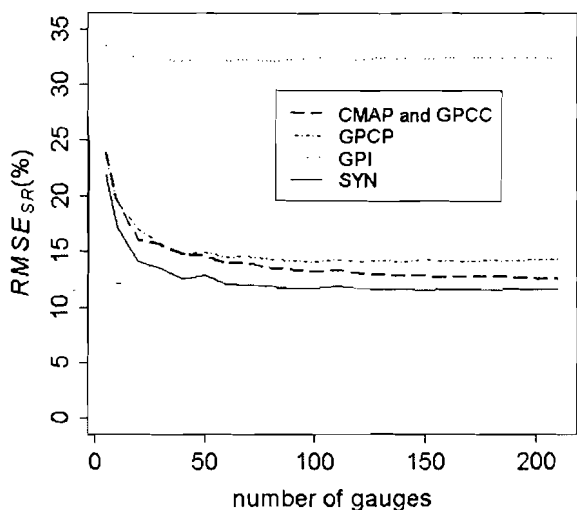


FIG. 10. The raw evaluation error of the global products (rmse_{SR}) as a function of the number of gauges used to compute the reference value in the dense coverage area. There is a decrease of the evaluation error for all products when the number of gauges increases. However, the effect on GPCP and, most notably, on GPI is weaker.

for CMAP, GPCC, GPCP, and SYNOP. The comparison of Fig. 10 and Fig. 11 leads to three main conclusions. 1) The behavior of $\text{rmse}_{ST}^{\text{EVS}}$ depends on the reference and the products under evaluation, whereas the value of $\text{rmse}_{ST}^{\text{COV}}$ does not depend on the gauge

density of the reference and seems to be constant for a given product. 2) For all products, the values of $\text{rmse}_{ST}^{\text{EVS}}$ and $\text{rmse}_{ST}^{\text{COV}}$ are lower than those for rmse_{SR} . For a reference with a density of three gauges per $2.5^\circ \times 2.5^\circ$, rmse_{SR} is approximately 18% and $\text{rmse}_{ST}^{\text{COV}}$ is 11% for CMAP and GPCC. These statistics are, respectively, 15% and 11% for a reference network with a density of 25 gauges per $2.5^\circ \times 2.5^\circ$. 3) The $\text{rmse}_{ST}^{\text{EVS}}$ is highly sensitive to the density of the reference, especially when it is low. This fact leads to some incoherence in the product ranking, which can change with the density of the reference network. For example, the values of $\text{rmse}_{ST}^{\text{EVS}}$ are, respectively, 11.5% and 10% for CMAP and GPCP for a 20-gauge reference network, changing to, respectively, 11% and 12.5% for a 60-gauge reference network. The behavior of $\text{rmse}_{ST}^{\text{COV}}$ is more stable and coherent than that of $\text{rmse}_{ST}^{\text{EVS}}$. For instance, when SYNOP is used as reference in this target area, rmse_{SR} is 12.8%, $\text{rmse}_{ST}^{\text{EVS}}$ is 4.8%, and $\text{rmse}_{ST}^{\text{COV}}$ is 11.4% for CMAP. When CILSS is used as a reference, rmse_{SR} is 15.9%, $\text{rmse}_{ST}^{\text{EVS}}$ is 14%, and $\text{rmse}_{ST}^{\text{COV}}$ is 11% for CMAP. This is just an illustration of how $\text{rmse}_{ST}^{\text{COV}}$ is less sensitive to the density of the reference used than are the two other rmse, as may be seen from Fig. 11.

It is important to note that using $\text{rmse}_{ST}^{\text{COV}}$ does not change the ranking of products obtained from the simple computation of rmse_{SR} but leads to a reevaluation of the estimation error, with $\text{rmse}_{ST}^{\text{COV}}$ being, in our case—and this cannot be extended to other regions without specific studies—significantly lower than rmse_{SR} .

7. Discussion and conclusions

This work presents the use of an error function developed in a companion paper (Part I) to treat three interwoven questions: 1) the definition of an optimal rain gauge network for the ground-based estimation of monthly and 10-day rainfall over the Sahel, optimality being defined as guaranteeing an estimation error below 10% for grid meshes of a given size ($2.5^\circ \times 2.5^\circ$ for monthly rainfall and $1^\circ \times 1^\circ$ for 10-day rainfall), 2) the intercomparison of global products, based on a reference considered as being the ground truth, and 3) the incorporation of the uncertainty of the reference into the quantification of the estimated error of the rainfall products.

Over the Sahel globally (an area of roughly 3 million km^2), the total number of gauges guaranteeing an error smaller than 10% is 568 on the monthly $2.5^\circ \times 2.5^\circ$ scale. This corresponds to a density of 14.5 gauges per $2.5^\circ \times 2.5^\circ$ cell—a number significantly greater than the

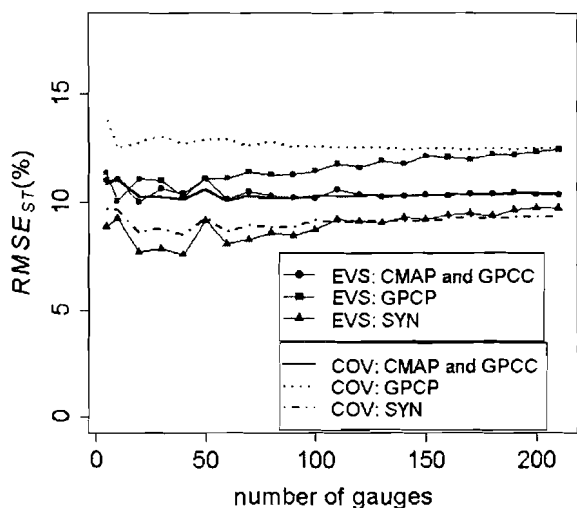


FIG. 11. Correction of the raw evaluation errors shown in Fig. 10. EVS means that the error covariance is neglected ($\text{rmse}_{ST}^{\text{EVS}}$ in the text). COV (solid line) takes into account the estimation of this covariance ($\text{rmse}_{ST}^{\text{COV}}$ in the text). Note that the EVS error displays a much larger sensitivity to the gauge density (oscillations in the curves) than does the COV error.

value of five gauges per $2.5^\circ \times 2.5^\circ$ cell given by several authors for other regions of the world. This number of 568 gauges compares well globally to the 561 gauges available over the region for the period of 1990–2000. However, the density of the optimal network should increase when moving north because of the gradient of the average number of rain events. The distribution of the current network does not conform to this pattern. For instance, the “optimal” network should comprise 238 gauges south of 15°N —or 10.3 gauges per $2.5^\circ \times 2.5^\circ$ cell—whereas the actual network comprises 465 gauges (19.2 per cell), meaning that the south Sahel is covered well. Over the whole region, however, only 42% of the 39 $2.5^\circ \times 2.5^\circ$ meshes satisfy the optimality criterion for monthly rainfall, with the northern and eastern areas being undersampled. North of 15°N , the average estimation error is 34%, which makes the validation of global products very difficult there (the density should be 20.6 gauges per cell in this area). On the 10-day $1^\circ \times 1^\circ$ scale, 1736 gauges would be needed to ensure a good coverage of the area located south of 15°N , as compared with the 465 available. Thus, it is not surprising that the optimality criterion is satisfied for only 3.2% of the 135 cells in this area.

In a second step, four global rainfall products (GPCC, CMAP, GPCP, GPI) were compared, using the rain fields produced by the entire regional rain gauge network (CILSS) as a reference. All of these products (CMAP and GPCP blend satellite and ground information, GPCC is ground-based, and GPI is satellite-based only) highly underestimate the frequency of small rainfall linked to the high spatial intermittency, which is better documented by direct point measurements. Only 17% of the CMAP values, 13% of the GPCC values and GPCP values, and 6% of the GPI values are under the 25% CILSS quantile. Global products also slightly underestimate the frequency of the high values.

Two alternate regional ground-based products were also considered: the CRA monitoring network (about 250 gauges providing data in real time on a 10-day basis) and the synoptic network (about 80 gauges, available daily). Comparison of these two regional ground products with global products has been carried out for the CILSS area with latitudes less than 15°N . At the coarser resolution (1 month, $2.5^\circ \times 2.5^\circ$), the synoptic network performs very well, with its rmse (14.4%) with respect to the CILSS reference being smaller than the rmse of the four global products. CMAP, which performs slightly better than the others global products, has 15.9% rmse. This result is somewhat surprising because, in principle, the mixed global products incorporating ground information make use of the synoptic

information available on the GTS and should therefore perform at least as well as the synoptic-only product. An explanation may reside in the fact that mixed products do not use all of the synoptic stations because not all of them transmit their data on the GTS.

The last part of the paper was devoted to assessing how using a reference value that is not the true value might influence the computation of evaluation errors. This question leads us to take into account two quantities that are usually neglected in the computation: the error of the reference and the covariance between the product-to-truth errors and the reference-to-truth errors. Using a denser instrumented zone, an empirical evaluation of these two quantities was performed, leading to an estimate that the “true” evaluation errors of both the regional and global products might be significantly lower than when these two terms are neglected. For instance, the reevaluated value of rmse for CMAP is around 11%, as compared with the above-mentioned value of 15.9% when the simplified computation is used. This difference is due both to the reference error and to the nonzero covariance existing between the product-to-truth errors and the reference-to-truth errors. Note also that this reevaluation of the rmse does not change the ranking of methods established from the simplified computation. The ground products remain, in this region, superior to the blended products analyzed here.

It is clear that ample room remains for improving the quality of satellite rainfall estimates over the Sahel. The availability of new infrared (e.g., Meteosat Second Generation) and microwave (e.g., TRMM and Global Precipitation Measurement) sensors will undoubtedly lead to more accurate satellite rainfall products. This study shows, however, that a careful and optimal use of ground information is needed to evaluate and intercompare any rainfall products, especially in regions of high rainfall variability.

Acknowledgments. This research was funded by IRD in the framework of the AMMA-CATCH “ORE” program initiated by the French Ministry of Research. Special thanks are given to the Département Soutien et Formation of IRD for the grant allocated to the first author of this paper. We also acknowledge S. Bonaventure for his efforts in the exploitation of the AGRHYMET Center rainfall database and H. Harder for his help in proofreading the article.

REFERENCES

- Adler, R. F., C. Kidd, G. Petty, M. Morissey, and H. M. Goodman, 2001: Intercomparison of global precipitation products:

- The Third Precipitation Intercomparison Project (PIP-3). *Bull. Amer. Meteor. Soc.*, **82**, 1377–1396.
- Ali, A., T. Lebel, and A. Amani, 2005: Rainfall estimation in the Sahel. Part I: Error function. *J. Appl. Meteor.*, **44**, 1691–1706.
- Arkin, P. A., R. Joyce, and J. E. Janowiak, 1994: IR techniques: GOES precipitation index. *Remote Sens. Rev.*, **11**, 107–124.
- Barnston, A. G., 1991: An empirical method of estimating rain-gage and radar rainfall measurement bias and resolution. *J. Appl. Meteor.*, **30**, 282–296.
- Barrett, E. C., and D. W. Martin, 1981: *The Use of Satellite Data in Rainfall Monitoring*. Academic Press, 340 pp.
- Bell, T. L., P. K. Kundu, and C. D. Kummerow, 2001: Sampling errors of SSM/I and TRMM rainfall averages: Comparison with error estimates from surface data and a simple model. *J. Appl. Meteor.*, **40**, 938–954.
- Chiu, L., A. Chang, and J. Janowiak, 1993: Comparison of monthly rain rates derived from GPI and SSM/I using probability distribution functions. *J. Appl. Meteor.*, **32**, 323–334.
- Ciach, J. G., and W. F. Krajewski, 1999: On the estimation of radar rainfall error variance. *Adv. Water Resour.*, **22**, 585–595.
- Conover, W. J., 1971: *Practical Nonparametric Statistics*. John Wiley and Sons, 234 pp.
- Ebert, E. E., and M. J. Manton, 1998: Performance of satellite rainfall estimation algorithms during TOGA COARE. *J. Atmos. Sci.*, **55**, 1537–1557.
- Gebremichael, M., W. F. Krajewski, M. Morrissey, D. Langerud, and G. J. Huffman, 2003: Error uncertainty analysis of GPCP monthly rainfall products: A data-based simulation study. *J. Appl. Meteor.*, **42**, 1837–1848.
- Ha, E., G. R. North, C. Yoo, and K.-J. Ha, 2002: Evaluation of some ground truth designs for satellite estimates of rain rate. *J. Atmos. Oceanic Technol.*, **19**, 65–73.
- Hollander, M., and D. A. Wolfe, 1973: *Nonparametric Statistical Inference*. John Wiley and Sons, 250 pp.
- Huffman, G. J., and Coauthors, 1997: The Global Precipitation Climatology Project (GPCP) Combined Precipitation Data Set. *Bull. Amer. Meteor. Soc.*, **78**, 5–20.
- , M. Morrissey, D. T. Bolvin, S. Curtis, R. Joyce, B. McGavock, and J. Susskind, 2001: Global precipitation at one-degree daily resolution from multisatellite observations. *J. Hydrometeor.*, **2**, 36–50.
- Jobard, I., 2001: Status of satellite retrieval of rainfall at different scales using multi-source data. *Proc. Second MEGHATROPPIQUES Scientific Workshop*, Paris, France, ISRO-CNRS, 10 pp. [Available online at http://meghatropiques.ipsl.polytechnique.fr/documents/workshop2/proc_s4p03.pdf.]
- Kummerow, C., P. Poyner, W. Berg, and J. Thomas-Stahle, 2004: The effects of rainfall inhomogeneity on climate variability of rainfall estimated from passive microwave sensors. *J. Atmos. Oceanic Technol.*, **21**, 624–638.
- Laurent, H., I. Jobard, and A. Toma, 1998: Validation of satellite and ground-based estimates of precipitation over the Sahel. *Atmos. Res.*, **47–48**, 651–670.
- Le Barbé, L., T. Lebel, and D. Tapsoba, 2002: Rainfall variability in West Africa during the years 1950–1990. *J. Climate*, **15**, 187–202.
- Lebel, T., and A. Amani, 1999: Rainfall estimation in the Sahel: What is the ground truth? *J. Appl. Meteor.*, **38**, 555–568.
- Levizzani, V., and Coauthors, 2001: EURAINSAT—Looking into the future of satellite rainfall estimations. *Proc. 2001 EUMETSAT Meteorological Satellite Data Users' Conf.*, Antalya, Turkey, EUMETSAT, 375–384.
- Mathon, V., H. Laurent, and T. Lebel, 2002: Mesoscale convective system rainfall in the Sahel. *J. Appl. Meteor.*, **41**, 1081–1092.
- McCollum, J. R., A. Gruber, and M. B. Ba, 2000: Discrepancy between gauges and satellite estimates of rainfall in equatorial Africa. *J. Appl. Meteor.*, **39**, 666–679.
- Morrissey, M. L., and J. S. Greene, 1993: Comparison of two satellite based rainfall algorithms using atoll rain gauge data. *J. Appl. Meteor.*, **32**, 411–425.
- , J. A. Malikekal, J. S. Greene, and J. Wang, 1995: The uncertainty in spatial averages using raingauge networks. *Water Resour. Res.*, **31**, 2011–2017.
- Nicholson, S. E., and Coauthors, 2003: Validation of TRMM and other rainfall estimates with a high-density gauge dataset for West Africa. Part I: Validation of GPCC rainfall product and pre-TRMM satellite and blended products. *J. Appl. Meteor.*, **42**, 1337–1354.
- Petty, G. W., 1995: The status of satellite-based rainfall estimation over land. *Remote Sens. Environ.*, **51**, 125–137.
- Ramage, K., I. Jobard, T. Lebel, and M. Desbois, 2000: Satellite estimation of 1-day to 10-day precipitation: Comparison and validation over tropical Africa of TRMM, Meteosat and GPCP products. *Proc. 2000 EUMETSAT Meteorological Satellite Data User's Conf.*, Bologna, Italy, EUMETSAT, 363–369.
- Rudolf, B., 1993: Management and analysis of precipitation data on a routine basis. *Proc. Int. WMO/IAHS/ETH Symp. on Precipitation and Evaporation*, Bratislava, Slovakia, Slovak Hydrometeorology Institute, 69–76.
- , H. Hauschild, W. Rüth, and U. Schneider, 1994: Terrestrial precipitation analysis: Operational method and required density of point measurements. *Global Precipitations and Climate Change*, M. Dubois and F. Desalmand, Eds., Springer Verlag, 173–186.
- Stanski, H. R., L. J. Wilson, and W. R. Burrows, 1989: Survey of common verification methods in meteorology. Tech. Doc. WMO/TD-No. 358, 114 pp.
- Thorne, V., P. Coakeley, D. Grimes, and G. Dugdale, 2001: Comparison of TAMSAT and CPC rainfall estimates with rain-gauges, for southern Africa. *Int. J. Remote Sens.*, **22**, 1951–1974.
- Xie, P., and P. A. Arkin, 1995: An intercomparison of gauge observations and satellite estimates of monthly precipitation. *J. Appl. Meteor.*, **34**, 1143–1160.
- , and —, 1997: Global precipitation: A 17-year monthly analysis based on gauge observations, satellite estimates, and numerical model outputs. *Bull. Amer. Meteor. Soc.*, **78**, 2539–2558.
- , J. E. Janowiak, P. A. Arkin, R. F. Adler, A. Gruber, R. Ferraro, G. J. Huffman, and S. Curtis, 2003: GPCP pentad precipitation analyses: An experimental dataset based on gauge observations and satellite estimates. *J. Climate*, **16**, 2197–2214.

AFRICAN MONSOON MULTIDISCIPLINARY ANALYSIS

An International Research Project and Field Campaign

BY JEAN-LUC REDELSPERGER, CHRIS D. THORNCROFT, ARONA DIEDHIOU,
THIERRY LEBEL, DOUGLAS J. PARKER, AND JAN POLCHER

AMMA strives to improve our understanding of the West African Monsoon system and will facilitate the multidisciplinary analysis needed to improve prediction of its variability and its associated societal impacts.

African Monsoon Multidisciplinary Analysis (AMMA) is an international project to improve our knowledge and understanding of the West African monsoon (WAM) and its variability with an emphasis on daily-to-interannual time scales. AMMA is motivated by an interest in fundamental scientific issues and by the societal need for improved prediction of the WAM and its impacts on West African nations. Vulnerability of West African societies to climate variability is likely to increase in the next

decades as demands on resources increase in association with one of the world's most rapidly growing populations. Vulnerability may be further increased in association with the effects of climate change and other factors linked to the fast-growing population, such as land degradation and water pollution.

Recognizing the societal need to develop strategies that reduce the socioeconomic impacts of the variability of the WAM, AMMA will facilitate the multidisciplinary research required to provide improved predictions of the WAM and its impacts. The international AMMA project has three overarching aims:

- 1) To improve our understanding of the WAM and its influence on the physical, chemical and biological environment regionally and globally;
- 2) To provide the underpinning science that relates variability of the WAM to issues of health, water resources, food security and demography for West African nations and defining and implementing relevant monitoring and prediction strategies; and
- 3) To ensure that the multidisciplinary research carried out in AMMA is effectively integrated with prediction and decision making activity.

AFFILIATIONS: REDELSPERGER—CNRM/GAME CNRS and Meteo-France, Toulouse, France; THORNCROFT—State University of New York at Albany, Albany, New York; DIEDHIOU AND LEBEL—LTHE, IRD, Niamey, Niger; PARKER—University of Leeds, Leeds, United Kingdom; POLCHER—LMD, CNRS, Paris, France

CORRESPONDING AUTHOR: Chris Thorncroft, Department of Earth and Atmospheric Sciences, University at Albany, SUNY, Albany, NY 12222

E-mail: chris@atmos.albany.edu

The abstract for this article can be found in this issue, following the table of contents.

DOI:10.1175/BAMS-87-12-1739

In final form 7 July 2006
©2006 American Meteorological Society

AMMA is endorsed by the World Climate Research Programme (WCRP) and continues to develop in association with the Climate Variability and Predictability (CLIVAR) and Global Energy and Water Cycle Experiment (GEWEX). AMMA has also been endorsed by two projects within the International Geosphere–Biosphere Programme (IGBP): International Global Atmospheric Chemistry (IGAC) and Integrated Land Ecosystem–Atmosphere Processes Study (ILEAPS). AMMA is working with other international projects and programs to achieve its aims, including the Global Climate Observing System (GCOS), Global Ocean Observing System (GOOS), and The Observing System Research and Predictability Experiment (THORPEX).

MOTIVATION AND MAJOR ISSUES. The interannual and interdecadal variability of WAM is well documented and has motivated considerable research efforts (e.g., Nicholson 1981; Lamb 1983; Folland et al. 1986; Fontaine and Janicot 1996; Le Barbé et al. 2002). The dramatic change from wet conditions in the 1950s and 1960s to much drier conditions in the 1970s, 1980s, and 1990s over the whole region represents one of the strongest interdecadal signals on the planet in the twentieth century. Superimposed on this, marked interannual variations in recent decades have resulted in extremely dry years with devastating environmental and socioeconomic impacts. Such variability has raised important issues related to

sustainability, land degradation, and food and water security in the region.

We are currently hindered in providing skillful predictions of WAM variability and its impacts. There are still fundamental gaps in our knowledge of the coupled atmosphere–land–ocean system at least partly arising from a lack of appropriate observational datasets, but also because of the complex scale interactions between the atmosphere, biosphere, and hydrosphere, which ultimately determine the nature of the WAM. The monitoring system for WAM and its variability are inadequate, with many gaps in the standard routine network and a lack of routine monitoring of some key variables. While the next generation of satellites will undoubtedly help with routine monitoring and prediction efforts, more research is required to validate and exploit these data streams. Dynamical models used for prediction suffer from large systematic errors in the West African and tropical Atlantic regions (e.g., WCRP 2000; Davey et al. 2002). Finally, there is a lack of integrative science linking the work on WAM variability with work on food, water, and health impacts.

The WAM system provides an ideal framework for considering scale interactions in a monsoon system: it possesses pronounced zonal symmetry with characteristic jets and associated well-defined weather systems. Research on such scale interactions, and in particular those linking dynamics and convection with the land surface, will be relevant

to other monsoon systems and is needed in order to improve the coupled atmosphere–ocean–land models used for weather and climate prediction. In order to carry out this research extra observations are needed.

Further motivation for a research project concerned with WAM variability and predictability comes from recognizing the role West African weather and climate has on the rest of the world. Latent heat release in deep cumulonimbus clouds in the ITCZ over Africa represents one of the major heat sources on the planet. Its meridional migration and associated

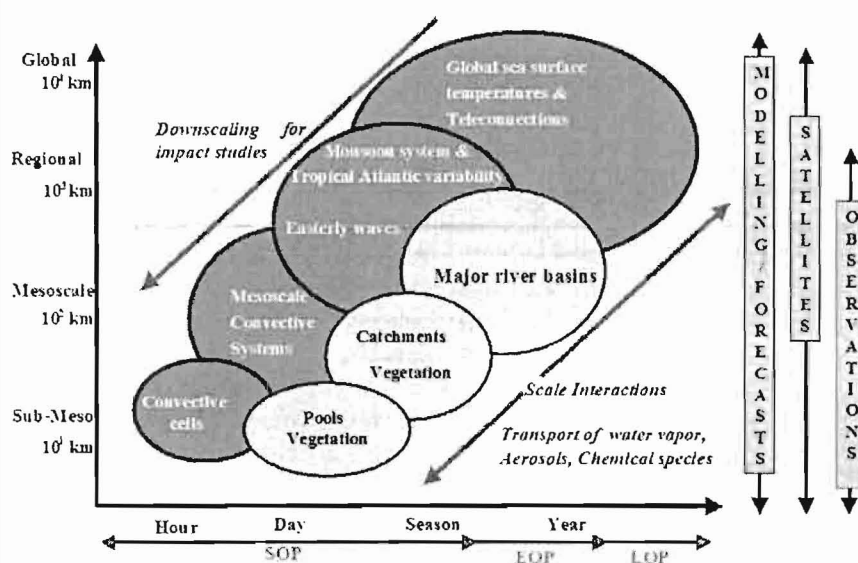


FIG. 1. Simplified schematic of key phenomena together with their associated space and time scales. The arrow is included to highlight the importance of scale interactions and transport processes in the WAM. SOP, EOP and LOP refer to the AMMA observing periods, Special Observing Period, Enhanced Observing Period and Long-term Observing Period respectively.

regional circulation impact other tropical and mid-latitude regions, as exemplified in the known correlation between West African rainfall and Atlantic hurricane frequency (e.g., Landsea and Gray 1992). In addition to the large-scale interactions, we know that a majority of hurricanes that form in the Atlantic originate from weather systems over West Africa (e.g., Avila and Pasch 1992); however, we know little about the processes that influence this and why only a small fraction of these "seedlings" actually become hurricanes. Tropical Africa is also the world's largest source of atmospheric dust. Both the fire aerosols and dust play a major role in radiative forcing and in cloud microphysics, and thus are an important part of the WAM system that require study.

Finally, West Africa is also an important source region for natural and anthropogenic emissions of precursors to key greenhouse forcing agents (e.g., ozone, aerosols). For example, Africa contributes around 20% to the global biomass-burning fires. Long-range transport of trace gases out of West Africa has important implications for the global oxidizing capacity of the atmosphere (which controls the level of many greenhouse gases), global climate change, and the transport of key constituents (e.g., water vapor, ozone-depleting substances) into the stratosphere.

A review of the present state of knowledge on the West African monsoon and the related scientific questions to be addressed by AMMA are described in the International Science Plan (ISP). The ISP also includes a description of the strategy proposed to tackle these questions. The ISP is available on the international AMMA Web site (online at www.amma-international.org/science/docs/AMMA_ISP_May2005.pdf).

THE AMMA PROGRAMME. A *multiscale approach*. To address the multiple scales that characterize WAM, the AMMA program is structured around the following four interacting spatial scales (Fig. 1): i) global scale: the scale at which WAM interacts with the rest of the globe (Emphasis is given to improving our understanding of the role of global SST patterns on WAM variability; seasonal-to-decadal variability is the main time scale of interest.); ii) regional scale: the scale at which we consider monsoon processes and scale interactions [Emphasis is given to improving our understanding of the interactions between the atmosphere, land, and tropical Atlantic ocean (especially the Gulf of Guinea). It is important to study the role of land-surface feedbacks on variability of the WAM at this scale, including the key roles of vegetation and soil

moisture. The annual cycle and seasonal-to-interannual variability are the main time scales of interest.]; iii) mesoscale: the scale of the typical rain-producing weather systems [This scale is central to the understanding of scale interactions in the WAM system (e.g., through interactions with synoptic easterly waves and the African easterly jet), and the coupling between hydrology and the atmosphere at the catchment scale.]; iv) local or submesoscale: from an atmospheric point of view, this is the convective rain scale (It is central to the hydrology of the Sahel and of small watersheds to the south; it is the main scale of interest for agriculture and for human impact studies in general).

AMMA emphasizes the importance of an improved understanding of how these scales interact and combine to characterize the WAM and its variability, including how these interactions impact the sources and transport of water vapor, aerosol, and key chemical species (e.g., key greenhouse gases, ozone, and aerosol precursors) in the West African region and globally.

Integrative science. While it is convenient and appropriate to describe the research plans in terms of the different spatial scales for an improved understanding, it is essential to study the scale and process interactions. The implementation of AMMA is designed in this spirit (Fig. 2). The AMMA project integrates the scales at which the geophysical and human processes interact. Furthermore, the various disciplines involved in the study of WAM need to be integrated to achieve the three overarching aims. This approach has guided the structuring of the scientific objectives.

From the geophysical perspective, the fundamental science underpinning the AMMA project can be viewed as the various disciplines coming together within broader integrative science topics: i) the interactions between WAM and global climate from a physical as well as a chemical perspective, ii) the water cycle of WAM from the regional to the local scale, and iii) the coupled atmosphere–land–ocean system and its multiple scales. To feed these integrative topics with sound disciplinary knowledge of the processes and their scale dependence detailed studies of the following processes are needed: i) atmospheric processes, with a focus on the convective processes that are key to the rainfall production; ii) oceanic processes, because they contribute to and depend on WAM; iii) biophysical processes over the continent from the regional to the local scale; and iv) aerosol and chemical processes in the atmosphere.

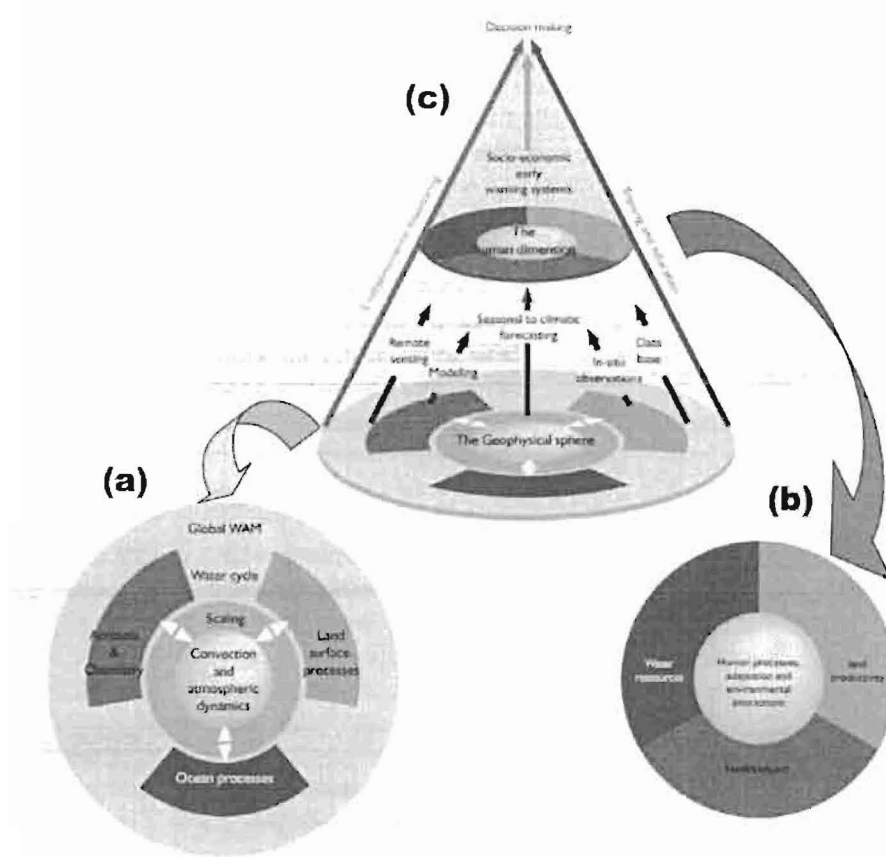


FIG. 2. Implementation of AMMA: (a) Integrative science for the geophysical and (b) human dimension. (c) Integration from this knowledge through various tools and for the exploitation by impact studies.

To study the human dimension of the variability and possible trends in the West African monsoon, AMMA aims to address the direct impact of the environmental conditions on the following three limiting conditions for African societies: i) land productivity, ii) water resources, and iii) health impacts. This activity will be coordinated to achieve a better understanding of how weather and climate variability impact food security and human processes in the region.

To achieve the AMMA scientific objectives and master the challenge of multiscale and multidisciplinary aspects, the following consistent set of tools and methods adapted to the problem of the West African monsoon will be used: i) models and data assimilation; ii) field campaigns; iii) satellite remote sensing and long-term atmosphere, and ocean data collection; and iv) database creation. These activities are key to transferring knowledge from the geophysical community in AMMA to the activities in the human dimension. AMMA will strive to use the above tools and activities to collect and consolidate knowledge, integrate the knowledge, and materialize

the predictive skill gained with this knowledge.

The field program. AMMA is a multiyear project and involves three nested observation periods. The enhancement of observations during these periods will provide a unique opportunity to determine the future operational monitoring necessary to improve weather and climate forecasts over the West African region. More than this, a high priority for AMMA is to establish this operational network of observations, providing a visible legacy useful for society from the international AMMA program.

- The Long term Observing Period (LOP) is concerned with observations of two types: (i) historical observations to study interannual-to-decadal variability of the WAM (including

currently unarchived observations) and (ii) additional long term observations (2002–2010) to document and analyse the interannual variability of the WAM.

- The Enhanced Observing Period (EOP) is designed to serve as a link between the LOP and the SOP (below). Its main objective is to document over a climatic transect the annual cycle of the surface conditions and atmosphere and to study the surface memory effects at the seasonal scale. The EOP will be 2–3 year duration (2005–2007).
- The Special Observing Period (SOP) focused on detailed observations of specific processes and weather systems at various key stages of the rainy season during three periods in the summer of 2006: (i) the dry season (Jan–Feb), (ii) Monsoon onset (15 May–30 June), (iii) Peak monsoon (1 July–14 August) and (iv) Late monsoon (15 August–15 September).

More detailed information regarding the different field phases, including this year's special observing period (SOP), is available in the ISP and in the

AMMA implementation (see the AMMA Web site online at www.amma-international.org). Here we only briefly describe the different periods.

Central to the observing strategy for AMMA is the Coupling of the Tropical Atmosphere and the Hydrological Cycle (CATCH) hydrology project. CATCH has established enhanced observations in the "CATCH window" depicted in Fig. 3 to support the long-term monitoring of the surface component of the continental water cycle. It includes three mesosites that sample different environments along a climate transect. The observing strategy for the EOP is to enhance the observations of the atmosphere, land, and ocean along the "climate transect," which includes the CATCH hydrology project. These enhancements include i) extra radiosoundings, ii) new surface flux measurements along the climate transect, iii) ground-based remotely sensed observations (e.g., radars, profilers), iv) enhanced hydrological observations (underground water fluxes, soil moisture), and vegetation, aerosol, and trace gas monitoring, and v) ocean observations in the tropical Atlantic, including the Gulf of Guinea, to extend the climate transect into the ocean key for understanding the coupled WAM system.

Embedded within the multiyear framework provided by the long-term observing period (LOP)/EOP is the SOP. Detailed studies of key processes,

impractical to study in a multiyear framework, will be carried out within the SOP and are focused on enhancing the observations along the climate transect through the provision of additional ground-based instruments (e.g., radars, lidars, sodars, high-frequency radiosoundings, etc.), research aircraft, and other platforms (e.g., driftsonde, tethered balloons, etc.). A considerable effort was made to ensure that all relevant data (e.g., extra radiosondes, dropsondes) were broadcast to the Global Telecommunication System (GTS) to support operational forecasting and to facilitate future observing system experiments (see working group 5 below). The special measurements proposed during the SOP, combined with those established through the LOP/EOP, will provide the international community with an invaluable set of observations to investigate the multiple-scale interactions and processes that determine the nature of WAM and its variability.

Modeling studies in AMMA. AMMA will coordinate various modeling activities and will ensure that the benefits of this work are communicated to the operational prediction centers. The datasets obtained in AMMA provide a unique opportunity to assess the ability of models to predict WAM and its impacts at daily-to-interannual time scales, to evaluate and improve key parameterizations, and to recommend a sustained

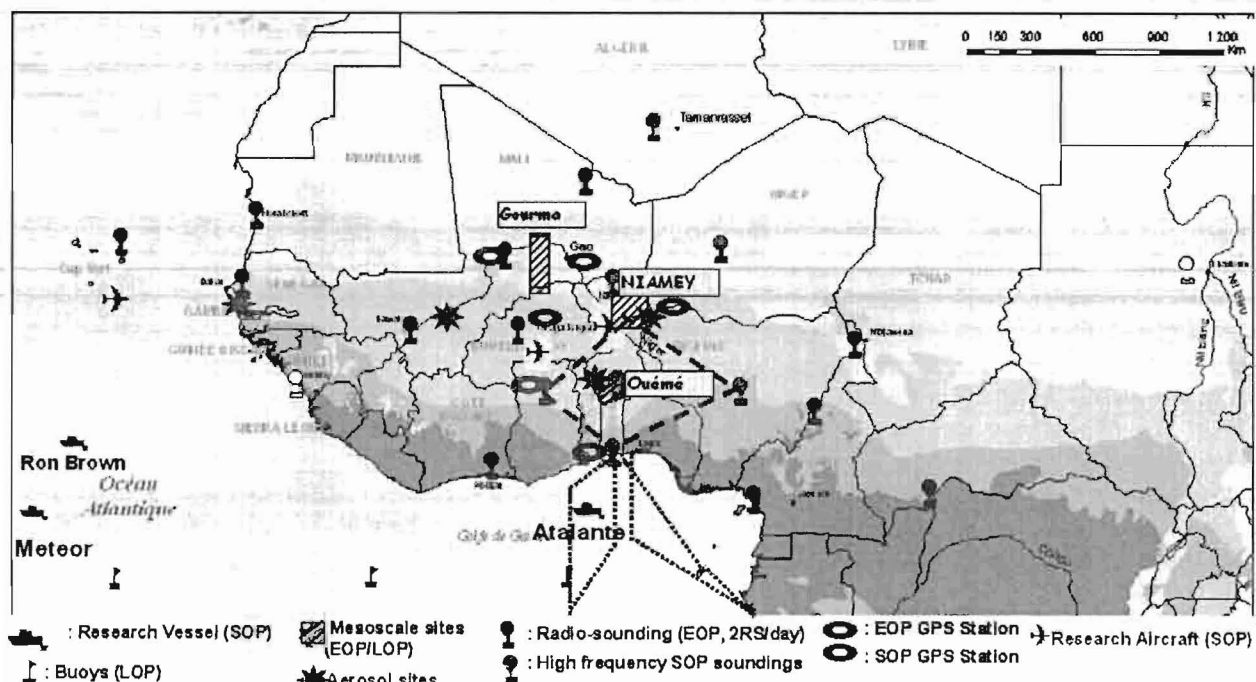


FIG. 3. Field implementation of AMMA observations based on nested networks. Circles indicated the atmospheric sounding network activated during the SOP.

observing system necessary for further research and prediction at these time scales. The following are several foci for modeling studies in AMMA:

- State-of-the-art general circulation models (GCMs) used for weather and climate prediction have difficulty simulating the annual cycle of rainfall and associated regional circulations. AMMA observations along the climate transect, including the extension into the ocean, will be especially useful for exploring the interactions between the heat low and the ITCZ and investigating how well these are represented in dynamical models.
- The zonal symmetry of the low-level thermodynamic contrasts, well-defined jets, and associated weather systems make this an ideal natural laboratory for investigating scale interaction issues in monsoon systems (Redelsperger et al. 2002). Together with analysis of the intense diurnal cycle (see Parker et al. 2005), such investigations are central for improving the GCMs used for weather and climate prediction in West Africa and tropical Atlantic regions.
- Recent modeling studies (e.g., Koster et al. 2004) suggest that land surface-atmosphere feedbacks are particularly strong in the West African region. However, observations are currently lacking in order to evaluate these studies. AMMA will provide new observations to explore land surface-atmosphere interactions and associated feedbacks, including how these are modeled at a range of spatial scales.
- The large amounts of dust present in the vicinity of WAM makes this region ideal for investigating aerosol issues and assessing their impact on regional weather (including downstream hurricanes) and climate. AMMA is providing new observations and coordinating various modeling efforts to investigate the role of aerosol in influencing WAM and its variability.
- AMMA is taking advantage of the observations made during the LOP/EOP and the SOP to carry out a suite of observing system experiments. These are needed to recommend the future sustained observing system for supporting weather and climate prediction.

IMPLEMENTATION OF AMMA. *National and pan-national projects.* The international AMMA program benefits from several national and pan-national projects (see information online at www.amma-international.org/projects/index). AMMA-Africa brings together scientists from many African nations and coordinates their contribution to AMMA. It is based on

proposals made by teams in universities and operational and research centers. Compared to the other components of AMMA, the emphasis in AMMA-Africa is more on impact studies. AMMA-EU is an integrated project funded by the European Union. It federates most of the national activities in Europe and brings together the geophysical and socioeconomic communities working in Africa. AMMA-France, which initiated AMMA, is a project supported by all French research organizations involved in environmental sciences and covers most aspects of AMMA. AMMA-UK is the sum of various projects associated with a Natural Environmental Research Council (NERC)-funded consortium, bringing together the British AMMA community. AMMA-US gathered a number of American scientists to prepare a U.S. proposal for AMMA. While this was not supported as a unified program, the Department of Energy (DOE), National Aeronautics and Space Administration (NASA), and National Oceanic and Atmospheric Administration (NOAA) are supporting several projects that incorporate some subprojects that arose from this proposal.

International coordination. AMMA aims to strengthen the international framework needed to facilitate interactions between researchers working in the different national and pan-national projects and to ensure that the field campaigns are well coordinated to optimize the scientific impact of the observations. An international structure has been established to oversee and coordinate these efforts (see Fig. 4). The International Scientific Steering Committee (ISSC) will ensure the scientific integrity and coherency of the scientific objectives of AMMA and the fulfillment of the three overarching aims. The ISSC is under the control of the International Governing Board (IGB) to ensure that it fulfills its coordination role for AMMA. Implementation of the multiyear field campaign is the responsibility of the International Implementation and Coordination Group (ICIG). In addition, a permanent Project Office (PO) assists the ISSC and ICIG.

SCIENTIFIC WORKING GROUPS. For scientific coordination the work of the ISSC is structured by five integrative science working groups (WGs) (Fig. 4), which take up five topics central to the aims of AMMA. WG1, "West African monsoon and global climate," is concerned with the two-way interactions between WAM and the rest of the globe, especially as they relate to and influence the variability of WAM and its global impacts. It includes aerosol and chemistry aspects. WG2, "Water cycle," is concerned with the processes in-

volved in the water budget occurring through all scales (i.e., regional scale, mesoscale, and local scale; see Fig. 1). WG3, "Surface-atmosphere feedbacks," is concerned with providing increased knowledge and understanding of the coupling between atmosphere and continental surfaces at the regional scale and mesoscale and, separately, the coupling between the atmosphere and ocean (the coupled atmosphere–land–ocean system is addressed in WG1). WG4, "Prediction of climate impacts," is concerned with the second major aim of AMMA and will provide strong linkages between the work taking place on impacts and that taking place on observed variability and predictability of WAM in WG1. WG5, "High-impact weather prediction and predictability," is a joint WG with THORPEX and is concerned with improving our knowledge and understanding of high-impact weather over the West African continent, and its impacts on the tropical Atlantic and extratropics. Operational activities will be promoted, including the tailoring of forecast products for users, and data impact and targeting studies.

IMPLEMENTATION OF FIELD OBSERVATIONS. The implementation of the field program is carried out through the establishment of task teams (TTs) and support teams (STs). The TT responsibilities are i) to design an observational strategy for a given subset of scales/variables of interest that addresses the scientific objectives presented in the ISP, and ii) to monitor and have final responsibility for deployment of relevant instrumentation. The TTs are composed of the Principal Investigators (PIs) of the instruments planned to be deployed in the framework of the space/time scale covered by the TTs. The ST responsibilities are i) to act in support of TTs, ii) to look in more detail into operational matters, and iii) to propose a scheme of operations to be agreed upon by TT leaders and to be submitted to the ISSC to verify that these schemes satisfy the needs of AMMA.

The AMMA Operations Centre (managed by ST2) was particularly important for facilitating the

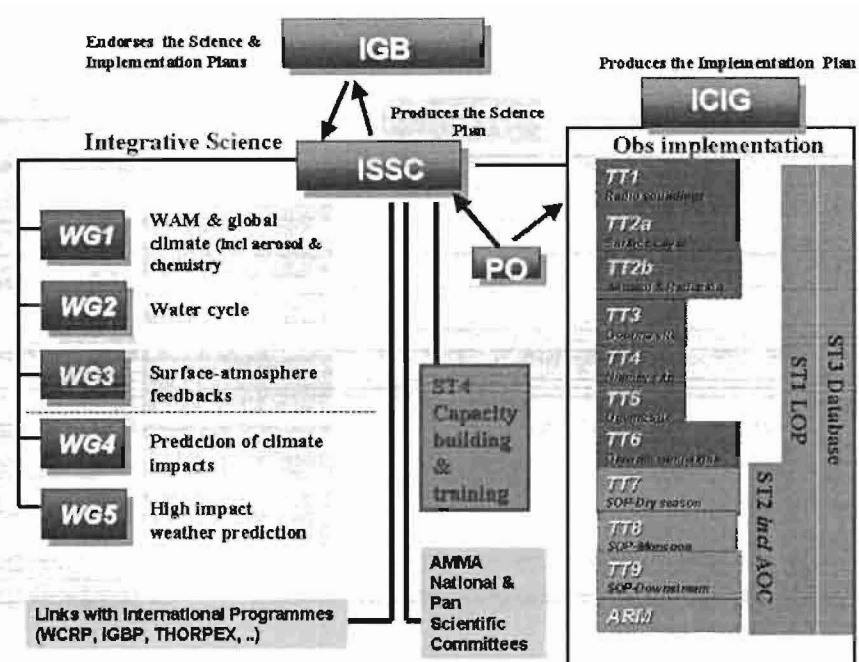


FIG. 4. International organization of AMMA.

smooth running of the field program during the SOP. A crucial component of this was the forecasting activity to support in-the-field decision making. The AMMA forecasting team represented a successful collaboration between numerical weather prediction centers [the European Centre for Medium-Range Weather Forecasts (ECMWF), Météo-France, National Centers for Environmental Prediction (NCEP), and the Met Office], together with the African Centre of Meteorological Application for Development (ACMAD) and African Weather Services. The AMMA forecasting team was responsible for the development of a comprehensive set of Web pages to support forecasting in the West African region (see information online at <http://aoc.amma-international.org>), which will be maintained as far as possible after the SOP to support future operational forecasting. AMMA is also establishing several training activities for African forecasters, including coordinating visits to ECMWF and NCEP (Africa desk) and also a series of training workshops in collaboration with ACMAD in Niamey, Niger. The aim of these workshops is to discuss forecasting strategies and to help familiarize forecasters with new forecasting products (before the SOP), and to evaluate these products and debrief the forecasting activity (after the SOP).

FINAL COMMENTS. AMMA has been carefully conceived to improve our fundamental understanding of the West African monsoon and its societal impacts,

and to make sustainable improvements to monitoring and predicting the West African environment. Our activities are embedded within a “long-term observing period” (“LOP”) structure, which will ensure that our intensive activities are directed toward systematic improvements in monitoring and predicting over the coming decades. We will develop and upgrade two important land-based atmospheric monitoring systems (for the upper-air and surface fluxes), and over the LOP we will transfer responsibility for these networks to the local African agencies. In addition, ocean-monitoring systems in the tropical Atlantic, including the Gulf of Guinea, that have been shown to improve both weather and climate forecasts will continue to provide data to these groups. These networks of observations are of enormous value both to global prediction systems and to local forecasting systems based in Africa.

ACKNOWLEDGMENTS. Based on an French initiative, AMMA was built by an international scientific group and is currently funded by a large number of agencies, especially from France, the United Kingdom, the United States, and Africa. It has been the beneficiary of a major financial contribution from the European Community’s Sixth Framework Research Programme. Detailed information on scientific coordination and funding is available on the AMMA International Web site at www.amma-international.org.

AMMA relies on the inputs and help of many people. We would also like to give special thanks to the members of the AMMA Project Office: Elisabeth van der Akker, Isabelle Genau, Karine Ginoux, and Cheikh Kane. We would like to acknowledge all other members of the International Scientific Steering Committee: Ernest Afiesimama, Abel Afouda, Abou Amani, Anton Beljaars, Benrard Bourles, Andreas Fink, Amadou Gaye, Jim Haywood, Paul Houser, Peter Lamb, Bob Molinari, Joe Prospero, Claire Reeves, and Madeleine Thomson. We would like to thank also other people helping to lead WGs, TTs, and STs, especially Peter Brandt, Bernard Cappelaere, Lassine Dairra, Luc Descroix, Laurence Eymard, Michel Desbois, Cyrille Flamant, Laurence Fleury, Sylvie Galle, Serge Janicot, Greg Jenkins, Sarah Jones, Jean-Philippe Lafore, Colin Lloyd, Celine Mari, Béatrice Marticorena, Andy Morse, Eric Mougin, Jacques Pelon, Alain Protat, Christophe Peugeot, Florence Rabier,

Frank Roux, Paulo Ruti, Josiane Seghieri, Chris Taylor, and Zoltan Toth.

REFERENCES

- Avila, L. A., and R. J. Pasch, 1992: Atlantic tropical systems of 1991. *Mon. Wea. Rev.*, **120**, 2688–2696.
- Davey, M. K., and Coauthors, 2002: STOIC: A study of coupled model climatology and variability in tropical ocean regions. *Climate Dyn.*, **18**, 403–420.
- Folland, C. K., T. N. Palmer, and D. E. Parker, 1986: Sahel rainfall and worldwide sea temperature 1901–1985. *Nature*, **320**, 602–607.
- Fontaine, B., and S. Janicot, 1996: Sea surface temperature fields associated with West African rainfall anomaly types. *J. Climate*, **9**, 2935–2940.
- Koster, R. D., and Coauthors, 2004: Regions of strong coupling between soil moisture and precipitation. *Science*, **305**, 1138–1140.
- Lamb, P. J., 1983: West African water variations between recent contrasting Subsaharan droughts. *Tellus*, **35A**, 198–212.
- Landsea, C. W., and W. M. Gray, 1992: The strong association between Western Sahel monsoon rainfall and intense Atlantic hurricanes. *J. Climate*, **5**, 435–453.
- Le Barbé, L., T. Lebel, and D. Tapsoba, 2002: Rainfall variability in West Africa during the years 1950–90. *J. Climate*, **15**, 187–202.
- Nicholson, S. E., 1981: The nature of rainfall fluctuations in subtropical West Africa. *Mon. Wea. Rev.*, **108**, 473–487.
- Parker, D. J., R. Burton, A. Diongue, R. J. Ellis, M. Felton, C. M. Taylor, C. D. Thorncroft, and P. Bessemoulin, 2005: The diurnal cycle of the west African monsoon circulation. *Quart. J. Roy. Meteor. Soc.*, **131**, 2839–2860.
- Redelsperger, J. L., A. Diongue, A. Diedhiou, J. P. Ceron, M. Diop, J. F. Gueremy, and J. P. Lafore, 2002: Multi-scale description of a Sahelian synoptic weather system representative of the West African monsoon. *Quart. J. Roy. Meteor. Soc.*, **128**, 1229–1257.
- WCRP, 2000: CLIVAR Africa implementation plan. Informal Rep. 5/2000, ICPO Publication Series 35, 35 pp. [Available online at www.clivar.org/organization/vacs/clivar_africa_iplan.htm.]